University of Massachusetts Amherst
ScholarWorks@UMass Amherst

Doctoral Dissertations 1896 - February 2014

1-1-2005

Surface chemistry of poly (p-xylylene) and nylon.

Margarita Herrera-Alonso
University of Massachusetts Amherst

Follow this and additional works at: https://scholarworks.umass.edu/dissertations_1

Recommended Citation

Herrera-Alonso, Margarita, "Surface chemistry of poly (p-xylylene) and nylon." (2005). *Doctoral Dissertations 1896 - February 2014*. 1068.
https://doi.org/10.7275/zzbc-7v48 https://scholarworks.umass.edu/dissertations_1/1068

This Open Access Dissertation is brought to you for free and open access by ScholarWorks@UMass Amherst. It has been accepted for inclusion in Doctoral Dissertations 1896 - February 2014 by an authorized administrator of ScholarWorks@UMass Amherst. For more information, please contact scholarworks@library.umass.edu.

UMASS/AMHERST
3 1206b 0288 8687 1

SURFACE CHEMISTRY OF POLY (*p*-XYLYLENE) AND NYLON

A Dissertation Presented

by

MARGARITA HERRERA-ALONSO

Submitted to the Graduate School of the
University of Massachusetts Amherst in partial fulfillment
of the requirements for the degree of

DOCTOR OF PHILOSOPHY

February 2005

Polymer Science and Engineering

© Copyright by Margarita Herrera-Alonso 2005

All Rights Reserved

SURFACE CHEMISTRY OF POLY(*p*-XYLYLENE) AND NYLON

A Dissertation Presented

by

MARGARITA HERRERA-ALONSO

Approved as to style and content by:

Thomas J. McCarthy, Chair

E. Bryan Coughlin, Member

Seshu B. Desu, Member

Shaw Ling Hsu, Department Head
Polymer Science and Engineering

DEDICATION

Para ustedes, mamá y papá.

Por ser mis ejemplos y fuentes de inspiración.

Por inculcar en mi, el aprecio al valor del conocimiento y a la belleza de la humanidad.

Y sobre todo, por su inmensurable y desprendido amor que me ha llevado tan lejos.

Las palabras me son insuficientes para agradecerles y explicarles lo mucho que los quiero.

ACKNOWLEDGEMENTS

I would like to acknowledge my advisor, Professor Tom McCarthy, for conveying his enthusiasm and interest in science to me. I am grateful for his confidence and "benign neglect", which helped to shape my future. Thanks Tom for allowing me to work for you, it was an honor. I also thank my Committee members, Professors Bryan Coughlin and Seshu Desu, for their valuable suggestions regarding my work, and their advice on the life after finishing a Ph.D. I am most sincerely grateful and indebted to Professors Tom Russell and Alan Lesser for their support and confidence in me.

Life in Amherst was fantastic in every sense. I owe part of that to the Faculty and Staff of PSE. Special thanks to Lou Raboin, Eileen Besse, and Joann Chauvin. Some of the my happiest times were in the lab, thanks to past and present McCarthy Group members. Thanks to Jack, Chris, Xinqiao, Jeff, Didem, Chuntao, Misha, Taryn, Wei, Ebru, Jay, Kevin, Taehyung, Zhixiang, and Sung In, and most especially to Ilke and Jung Ah. I will always remember with great affection the time we spent together. I also want to thank Raji, Serkan, Matt, Amanda, Sterling, and César, and my 'Amherst Family': Bhavini, Angelo, and Kishore for all the fun times.

I could not have made it this far without the support of many people back home, especially my aunts Nena and Chivis, and the Garcia-Leiner Family. Finally I want to thank my Family: my parents, Margarita and Rafael, whose love and faith carried me throughout this journey; and my by brothers, Rafa and Manolo, for their incomparable friendship and encouragement. Most importantly I thank Manuel, for believing in me, and for his endless love and understanding. His friendship and companionship have been, by far, the most rewarding experiences of all. Gracias, corazón.

ABSTRACT

SURFACE CHEMISTRY OF POLY(*p*-XYLYLENE) AND NYLON

FEBRUARY 2005

MARGARITA HERRERA-ALONSO, B.S.,
UNIVERSIDAD NACIONAL AUTONOMA DE MEXICO

M.S., UNIVERSIDAD NACIONAL AUTONOMA DE MEXICO

M.S., UNIVERSITY OF MASSACHUSETTS AMHERST

Ph.D., UNIVERSITY OF MASSACHUSETTS AMHERST

Directed by: Professor Thomas J. McCarthy

The interaction of a material with its surroundings occurs at the material-environment interface, therefore, the chemical and physical characteristics of the material's surface plays a fundamental role in determining its properties, such as its biocompatibility, adhesion, and wettability, and ultimately, its technological applicability. This dissertation discusses aspects of the chemical surface modification of two polymers, poly(*p*-xylylene) and nylon.

Chapter 2 focuses on the synthesis and wet-chemistry surface modification of poly(*p*-xylylene) (PPX) thin films. A series of electrophilic aromatic substitutions were studied including chlorosulfonation, chloroamidomethylation, and Friedel-Crafts catalyzed reactions. It was found that the yields and surface selectivity of the reactions studied were highly dependent on the interaction of the polymer with the reaction medium.

Chapter 3 describes the use of vapor deposition polymerization in template-assisted synthesis. Poly(*p*-xylylene) nanotubes were synthesized by template assisted methods using porous aluminum oxide membranes as the templating material. The pore diameter showed a linear dependence with respect to the deposition time. FESEM analysis showed that PPX was deposited along the pores of the membranes. Exposure of the membranes to a reactive solution resulted in chemical functionalization of the inner walls of the nanotubes, confirmed by XPS.

Chapter 4 discusses the chemical reduction of nylon film surfaces by reaction with a borane-tetrahydrofuran complex. It was observed that, while the reaction occurs in high yields, its surface-confinement is highly dependent on the segmental mobility of the polymer. The amine-rich surfaces were further used as templates for the synthesis of composite films by electrostatic adsorption of polyanions.

Chapter 5 deals with the synthesis of linear polyalkyleneimines of different hydrocarbon lengths by the surface-mediated reduction of nylons. These polyalkyleneimines were further used as compatibilizers for the melt intercalation of montmorillonite clays, modified and unmodified, with polypropylene. The polyamines were found to interact favorably with the clays, leading to intercalated and exfoliated systems. The determining factor in controlling the degree of dispersion of the clays, was the enthalpic interaction between the clay and the compatibilizer.

TABLE OF CONTENTS

LIST OF TABLES

LIST OF FIGURES

CHAPTER 1

OVERVIEW

The interaction of a material with its surroundings occurs at the material-environment interface, therefore, its chemical and physical characteristics are fundamental in determining its properties. A constant challenge for surface chemists has been to establish the conditions under which surface modification reactions occur and the effect of the reaction conditions on their extent. It is important to emphasize that the extent of reaction entails both the yield and the penetration depth, parameters that are important for achieving surface selectivity. Knowledge of the surface chemistry of a polymer will ultimately allow fine-tuning of its properties.

The unifying theme of the chapters that form this dissertation is the utilization of surface chemistry for the synthesis of novel materials. Aspects of the chemical surface modification of two polymers, poly(*p*-xylylene) and nylon, are discussed. In the first part, the surface chemistry of poly(*p*-xylylene) is studied for the first time, and then used to produce PPX nanotubes with functionality on the inner walls. The second part begins by exploring the surface chemistry of nylon, to later provide an explanation for the surface-mediated synthesis of polyamines derived from nylon precursors.

The second chapter deals with the synthesis and chemical surface modification of poly(*p*-xylylene) (PPX) thin films. Several electrophilic aromatic substitution reactions were surveyed with regard to the extent to which they occurred on the surface of PPX. The effect of the interaction between the polymer and the reagents was determinant on the degrees of substitution and depths of penetration observed.

The third chapter focuses on the fabrication of functionalized poly(*p*-xylylene) nanotubes by a template-assisted method. Anodized aluminum membranes were used as templates for the vapor deposition polymerization of [2.2] paracyclophane. As determined by spectroscopic measurements, the inner diameter of the PPX nanotubes was a determinant of the polymerization conditions. Knowledge of the surface chemistry of PPX allowed for chemical modification of the inner walls of the nanotubes.

The fourth chapter involves a study on the chemical reduction of nylon film surfaces by reaction with a borane-tetrahydrofuran complex to generate amine-rich surfaces. The reaction occurred in high yield and its confinement to the outermost surface was dependent on the glass-transition temperature and crystallinity of the polymer. The reduced nylon substrates were further modified through electrostatic adsorption of poly(4-sodium styrenesulfonate) or alginate.

The last chapter discusses the synthesis of linear polyalkyleneimines by the surface-mediated reduction of nylons. The first objective of this work was to study the conditions under which the chemical reduction of nylon surfaces, discussed in the preceding chapter, could be driven to occur in the bulk. The polyamines synthesized were then used as compatibilizers for polypropylene/montmorillonite clay nanocomposites. The formation of intercalated and exfoliated systems suggests a favorable enthalpic interaction between the clay and the polyamines.

CHAPTER 2

SURFACE MODIFICATION OF POLY(*p*-XYLYLENE) THIN FILMS

2.1. Introduction

Polymeric thin film coatings represent a practical alternative to surface modification since they preserve the properties of the underlying material while allowing, through a judicious choice of the coating method and polymer, control over macroscopic surface properties such as biocompatibility, wettability, and adhesion. In the past, the McCarthy group has studied the surface modification of a wide variety of polymers with particular interest in the introduction of functional groups that allow the build-up of polyelectrolyte multilayers in a layer-by-layer assembly, thus affecting the surface properties.[1,2,3,4] Currently we are interested in using polymeric thin film coatings as surface modification elements due to their chemical, electrical, and optical versatility. We are also interested in building up multilayer films using several film growth strategies; the first example is the use of the spontaneous adsorption of poly(vinyl alcohol) to hydrophobic substrates to increase their wettability and serve as a platform for further chemistries,[5] the second example is the chemical vapor deposition polymerization of poly(ethyl cyanoacrylate) coatings to form nanometer scale thick coatings.[6] In this sense, polymeric thin film coatings, as surface modification elements, are interesting due to their chemical, electrical, and optical versatility.

Among the coating techniques, vapor deposition polymerization (VDP) has gained substantial interest in recent years since it proceeds in the absence of solvents, thus avoiding problems associated with dewetting phenomena, and produces conformal

pinhole-free coatings, regardless of the geometric complexity of the substrate.[7,8] VDP is a particular case of chemical vapor deposition (CVD); what differentiates it from traditional CVD is that the reaction is a polymerization, which can proceed through free-radical, ionic, or step-growth mechanisms. One of the early examples of VDP was reported in 1932 for the synthesis of polyoxomethylene from the ring-opening polymerization of trioxymethylene in the presence of formaldehyde.[9] Other examples of VDP are the synthesis of polydiacetylenes, poly(vinylidene fluoride), polysiloxanes, phtalocyanine derivatives, polyimides, poly(ethyl cyanoacrylate), and N-containing heterophanes.[10]

One of the most widely studied chemical vapor deposited polymers is poly(*p*-xylylene) (PPX). Due to its excellent barrier properties, low dielectric constant, and high solvent resistance has found application in circuit boards, semiconductors, hybrid circuits, corrosion resistant coatings, and biocompatible coatings.[11] PPX is highly resistant to most organic solvents and inorganic reagents. The substrate-dependent polymerization of *p*-xylylene is another interesting property that has been used for the selective growth of films with potential applications in surface patterning.[12,13] CVD polymerization of [2.2]paracyclophane to yield PPX is an inherently clean process since the monomer gas is directly converted to polymer without the need for initiator or catalysts and produces linear high molecular weight polymer with approximately 2000 to 3000 repeat units per polymer molecule, resulting in molecular weights of 200,000-300,000 g/mol (eq. 1).[14] PPX is a semicrystalline polymer with degrees of crystallinity and crystalline modifications that are dependent on the deposition conditions;[15,16] the

crystalline domains of PPX are embedded in an amorphous matrix and are responsible for its chemical and solvent resistance.

Although poly(*p*-xylylene) and its family of polymers have interesting properties, the polymers bear no reactive functional groups, making them essentially inert. Functionalization of poly(*p*-xylylene), either in bulk or on the surface, broadens the applications of these polymers, for example by enhancing their adhesion, improving their haemocompatibility, and finely tuning their optical properties. Poly(*p*-xylylene)s with reactive functional groups have been obtained by post-deposition "dry" and "wet" treatments, and by chemical modification of the precursor. The objective of the first two methods is to engineer the surface and interface of the coatings, while the modification of the precursor will in turn modify the bulk properties of the deposited films. The advantage of post-deposition "dry" treatments is that they maintain the inherent cleanliness of the reaction and preferentially alter the surface, leaving the bulk properties unchanged. This has been accomplished by exposing poly(*p*-xylylene) films (fluorinated and chlorinated analogs also) or coated substrates to plasmas including SO_2, O_2, N_2, Ar, and He.[17,18,19,20] In general, this procedure has proven to incorporate various functional groups that enhance the reactivity of the modified films and their wettability, however problems associated with roughening and identification of the functionalities are criticisms of these experiments.

Modified poly(*p*-xylylene)s have been obtained through "wet" chemistry by taking advantage of the "living" nature of the polymerization. Studies of thick poly(*p*-xylylene) films report the molecular weight of the polymer to be relatively high (on the order of 10^5), however for thinner films (< 32 Å), oligomeric species are obtained. The

oligomers have a higher concentration of end groups, with respect to the thick films, and these radicals have been used for reaction with aqueous ammonium sulfide to incorporate hydroxyl functionalities.[21,22]

Finally, chemical modification of the precursor has proven to be a very useful method to generate functionalized poly(*p*-xylylene)s.[23] Similar to the post-deposition "dry" treatments, it also preserves the cleanliness of the process and allows for a wide variety of chemical functionalities to be incorporated, such as alcohol, acetate, anhydride, amine, and triflate, to name a few. Studies of the optical properties of the functionalized films conclude that substitution of the benzene rings in the main chain alters the electronic properties, thus influencing their optical properties.[24] This method has also been used for patterning proteins and mammalian cells, which could potentially serve as a platform to produce biosensors.[25,26,27] While modification of the precursor proves to be a useful method, the reaction conditions, namely the pyrolysis temperature and the inert gas flow rate, must be carefully adjusted in order to minimize decomposition of the functional group, particularly during pyrolysis; oxidation and secondary reactions are not uncommon in these systems.

This chapter focuses on the chemical surface modification of poly(*p*-xylylene) films as an alternative method for the production of functionalized PPX coatings. Functionalization of PPX was studed by reactions at the aromatic ring using electrophilic aromatic substitution. We focused on preparing positive (PPX-NH_3^+) and negative (PPX-SO_3^-) surfaces so that PPX films could be incorporated into polyelectrolyte multilayer assemblies. Additionally, Friedel-Crafts catalyzed

chemistries were also studied on PPX film surfaces as alternatives to alkylated and acylated precursors.

2.2. Background

2.2.1. Poly(*p*-xylylene)

Poly(*p*-xylylene) is synthesized by two methods. The first involves the Wurtz-type coupling reaction of 1,4-bis(halomethyl)benzenes and different coupling reagents in solution.[28] The second method, by far the most important, is by VDP of [2.2] paracyclophane. The chemical deposition of thin poly(*p*-xylylene) films was first observed by Szwarc in 1947 after reduced-pressure pyrolysis of p-xylene.[29] The reaction conditions required very high pyrolysis temperatures (700 to 900 °C) and only moderate yields of the polymer were obtained. Gorham in the 1960s found that vapor deposition polymerization of [2.2] paracyclophane produced poly(*p*-xylylene) (Equation 2.1) in higher yields compared to the Szwarc method, and that the temperature necessary for the reaction to occur was considerably lower by starting from [2.2] paracyclophane (550 °C).[30] In both cases, the synthesis involved a system consisting of three sections: sublimation, pyrolysis, and deposition.

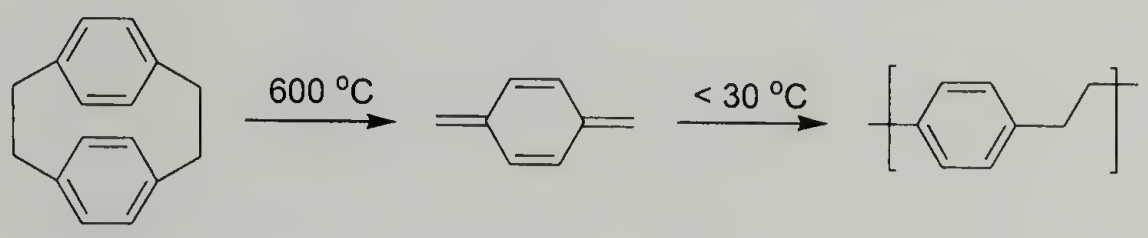

Equation 2.1. Synthesis of poly(p-xylylene) by VDP of [2.2]paracyclophane.

In the first stage of the polymerization, [2.2] paracyclophane, also referred to as the dimer or precursor, is sublimed at moderate temperatures (60 to 140 °C). The rate of

sublimation is dictated by the pressure, temperature, and surface area of the solid. Once the dimer is in the vapor phase, it is carried through a pyrolysis oven where it is thermally cleaved to form two *p*-xylylene molecules. The facile conversion of the dimer to p-xylylene is a result of its considerable ring strain.[11,31] Formation of the monomer occurs by cleavage of the two $-CH_2-CH_2-$ bonds, to produce the conjugated olefin rather than the aromatic biradical. This mechanism was confirmed by the pyrolysis of acetyl di-p-xylylene, where deposition at different temperatures resulted in two different polymers: poly(*p*-xylylene) and poly(acetyl *p*-xylylene), and in another experiment in which *p*-xylylene vapors were exposed to iodine and the diiodo product was recovered.[11,31]

A vapor deposition polymerization apparatus, like a CVD apparatus, consists of the following three sections – precursor feed, reactor, and exhaust. While the three sections must be arranged in this particular order, the geometric design of the reactor will strongly affect the characteristics of the film.[32,33] Once the monomer exits the pyrolysis oven it enters the reactor and the following deposition sequence takes place:

1. Bulk transport of *p*-xylylene from the inlet of the reactor to the deposition zone
2. Adsorption of precursor onto the growth surface
3. Diffusion to growth sites
4. Reaction at the growing film
5. Transport of unreacted monomer to the reactor exit

The net flux of monomer molecules that strike the growth surface greatly exceeds the number of monomer molecules that actually participate in either initiation or propagation reactions therefore, desorption of monomer occurs at any moment

throughout the polymerization. Also it is important to note that, unlike many CVD processes, VDP of [2.2] paracyclophane proceeds without the formation of byproducts.

The first step of the polymerization is the initiation. Initiation occurs by coupling of two monomer molecules to form the dimer diradical, an energetically unfavorable reaction in which the rate of formation of the diradical is greatly exceeded by its rate of destruction (Equation 2.2). Further reaction with a third monomer molecule produces the trimer diradical, which is energetically more stable and considered the initiator.[11] The proximity of the monomer molecules is higher at the surface than in the vapor phase, therefore it is assumed that initiation and propagation will preferentially occur in the adsorbed phase rather than in the vapor phase. This may not be the case for reactions at high pressures, where polymerization in the gas phase is observed by the formation of "dust" or "snow".

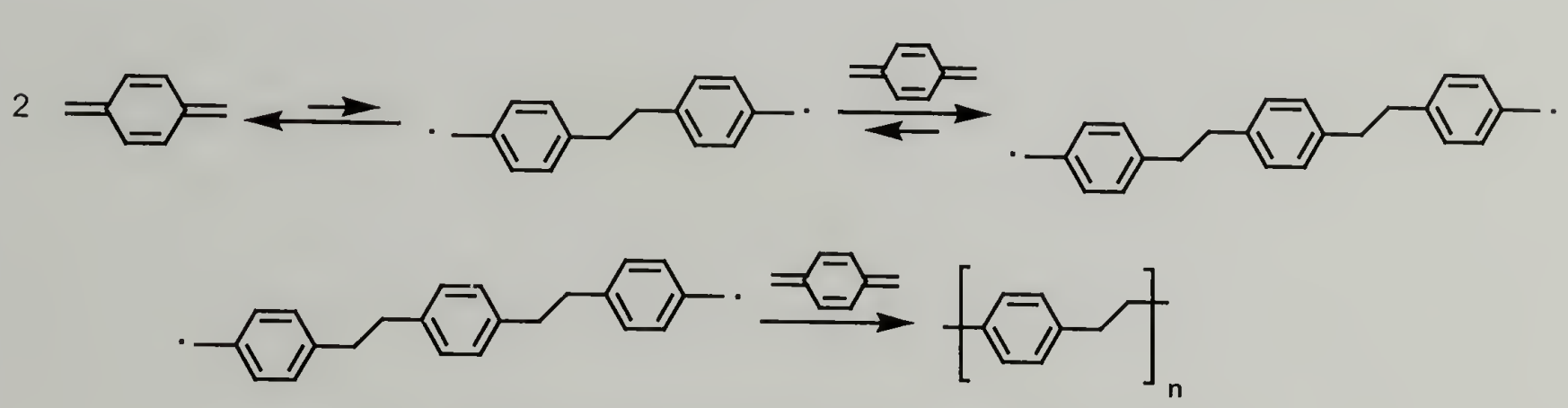

Equation 2.2. Initiation and propagation reactions of *p*-xylylene

Propagation proceeds by further reaction of monomer molecules at the chain ends of the polymer. Polymers with molecular weights ranging from 200,000 to 500,000 g/mol have been obtained by this method.[15] Termination by coupling of active chain ends does not occur because of their limited mobility; rather, the polymer ceases to grow because of the decreasing diffusivity of the monomer in the solid film.

The monomer deposits and spontaneously polymerizes on any surface, regardless of its geometric complexity, when the substrate is below a threshold temperature. Above this temperature the growth rate of the film is practically zero; for the particular case of the unsubstituted di-p-xylylene, the threshold temperature is in the range of 30 °C. Another case of polymerization inhibition was observed by Vaeth and Jensen, and used for the fabrication of patterned surfaces.[12] They found that certain metals, metal salts, and their organometallic complexes (Ru, Fe, Pt, Ag, Cu, Pd, Ag, and Ta) inhibit *p*-xylylene from participating in initiation and propagation reactions, possibly due to binding and complexation with the metal, or conversion of the *p*-xylylene to [2.2]paracyclophane derivatives. This phenomenon occurs until the concentration of "deactivated" monomer on the inhibiting surface reaches a critical value above which the incoming monomer can no longer "complex" with the underlying metal and is free to polymerize.

Poly(*p*-xylylene) is a semi-crystalline polymer with micron crystalline domains embedded in an amorphous matrix.[16] The degree of crystallinity (30% to 50%) varies depending on the sublimation and deposition rates.[15] The polymer has at least two crystalline modifications – the α form which is stable at higher deposition temperatures (26 °C to –17 °C), and the β form, stable at lower deposition temperatures (-78 °C); transition from the α to the β form occurs around 220 °C. The α polymorph is monoclinic ($a = 0.592$ nm, $b = 1.064$ nm, $c = 0.655$ nm, $\beta = 134.7°$) and the β form is hexagonal ($a = 2.052$ nm, $c = 0.655$ nm, $\gamma = 120°$). Wunderlich proposed that competing propagation and crystallization explain the polymorphism.[15]

As mentioned previously, the characteristics of the poly(*p*-xylylene) films obtained by VDP are highly dependent on the process parameters such as the sublimation, deposition and pyrolysis temperatures, and inert gas pressure. An increased partial pressure of the monomer with sublimation temperature results in an increased deposition rate as well as increased roughness.[34] On the other hand, lower pyrolysis temperatures or low residence times in the pyrolysis oven resulted in the incomplete cleavage of [2.2] paracyclophane to di-*p*-xylylene.[35]

A number of models have been developed to describe the chemical vapor deposition of poly(*p*-xylylene). The models that consider the reaction as the controlling mechanism assume that reaction occurs either exclusively on the surface or on the surface and in the bulk, and they differ in the method used to estimate the monomer concentration at the surface of the growing film. Although they correctly predict the growth rate as a function of system pressure, they all fail to model the decrease in deposition rate with higher deposition temperatures. On the other hand, the model proposed recently by Fortin and Lu,[36] based on the kinetics of the adsorption process, accounts for physisorption followed by chemisorption and considers both the rate at which the monomer impinges on the surface as well as the rate at which it reacts with existing radical chain-ends. While this model is not useful at high temperature and pressure, it correctly predicts the increase in growth rate with pressure as well as the decrease in the deposition rate with increasing temperature. The rate of deposition is estimated with the following equation:

$$R_d = \frac{S_o(1-\theta)P N_a V_m \left(60\times 10^{10}\right)}{\left(2\pi m_r R T_o\right)^{0.5}} \qquad S_o = \frac{1}{\left(1 + V e^{-(E_d - E_a)/RT}\right)}$$

where (1-θ) is the fraction of the surface sites that are reactive (radical chain ends), P is the system pressure, N_a is Avogadro's number, V_m is the volume of one molecule, m_r is the molecular mass, R is the Rydberg gas constant, T_o is the temperature of the gas, E_a and E_d are the activation energies for chemisorption and desorption, and V is a preexponential constant. From these equations it is clear that the rate of deposition will increase linearly with the system pressure, and that it has an exponential decay dependence with respect to the deposition temperature.

2.3. Experimental

2.3.1. Materials

Reagents were supplied by Aldrich and used without further purification. [2.2]paracyclophane was also obtained from Aldrich and purified by sublimation prior to polymerization. Dichloromethane and 1,2-dichloroethane (Fisher) were distilled from calcium hydride onto 3 Å molecular sieves.

2.3.2. Vapor Deposition Polymerization

Poly(*p*-xylylene) (PPX) was synthesized by chemical vapor deposition of [2.2]paracyclophane (eq. 1) using a home-built system modeled after one reported by Gorham.[30] The reactor consists of three sections: sublimation, pyrolysis, and deposition. The temperature in each section was maintained constant throughout the reaction and the base pressure was kept below 60 mTorr to prevent polymerization in the vapor phase.[37] [2.2]paracyclophane was sublimed at 110 °C (±2 °C), followed by pyrolysis at 650 °C and deposition at 10 °C (±0.5 °C). Free standing polymer film samples were obtained by peeling the poly(*p*-xylylene) film off the walls of the

deposition chamber after the reaction. PPX film samples of thickness ranging from 4-8 μm were extracted (Soxhlet) with dichloromethane for 8 - 12 h and dried under reduced pressure (<100 mTorr) at room temperature for 12 h. Film samples of 1.5 x 1.5 cm^2 were then cut and stored in scintillation vials for later use.

2.3.3. Characterization

X-ray photoelectron spectra (XPS) were recorded on a Perkin-Elmer-Physical Electronics 5100 spectrometer with Mg K_α excitation at 400 W and 15 kV. Depth profiling was done by collecting spectra at 15° and 75° take-off angles with respect to the plane of the sample surface; the analysis at 15° has a penetration depth of ~10 Å and that at 75° corresponds to a penetration depth of ~40 Å.[38] Infrared spectroscopy was performed both in transmission and attenuated total reflectance (ATR) modes on a Bio Rad FTS 175C FT-IR spectrometer. ATR IR spectra were recorded using Germanium crystals (45° and 60°) as internal reflection elements. Assuming the refractive index of PPX in the wavelength range examined by ATR IR (4000-700 cm^{-1}) is constant and has an approximate value of 1.661,[10,33] the penetration depths observed by this technique are: 0.17-0.99 μm for Ge-45° and 0.13-0.75 μm for Ge-60°.[39] Contact angle measurements were performed using a Ramè-Hart telescopic goniometer and a Gilmont syringe with a 24-gauge flat tipped needle. Water purified by reverse osmosis, ion-exchange and filtration (Milli-Q water) served as the probe-fluid. Advancing and receding contact angles were measured while the probe fluid was added to and withdrawn from the drop, respectively. Differential scanning calorimetry (DSC) analysis was performed on a TA Instruments 2100 DSC. The experiments were conducted in the temperature range of 25 °C to 450 °C with a heating rate of 10 °C/min.

The samples were only subjected to one heating cycle as PPX decomposes at temperatures very close to its melting temperature (~ 420 °C). Wide-angle X-ray scattering (WAXS) experiments were carried out using a Statton camera device with an operating voltage of 40 kV and a total current of 30 mA under vacuum; single films (4-8 μm thick) were exposed for 12 h. Gravimetric analyses were performed on a Cahn 29 automatic electromicrobalance. Field emission scanning electron micrographs were obtained using a JEOL JSM 6320F instrument.

2.3.4. General Procedures

All reactions (Fig. 1) were carried out with continuous stirring under a nitrogen atmosphere. Unless otherwise specified, after each reaction, the samples were isolated and rinsed separately with 5 x 10 mL of each solvent, extracted (Soxhlet), dried under vacuum at room temperature for 12 h and stored in scintillation vials prior to characterization.

2.3.5. Chlorosulfonation/Sulfonation

Concentrated chlorosulfonic acid, or a solution of chlorosulfonic acid in 1,2-dichloroethane (2.5% - 75% vol.) was added to PPX film samples and allowed to react at 5 °C or 20 °C. The samples were then thoroughly rinsed with 1,2-dichloroethane and dried at 100 °C for 4 h under reduced pressure (<100 mTorr). Sulfonated PPX was obtained by treating these films with a 1.5 N sodium hydroxide solution at 110 °C for 3 h and rinsing with hydrochloric acid (1 N) and distilled water in copious amounts.

2.3.6. Chloroamidomethylation

N-methylol-2-chloroacetamide (NMCA) (2.0 g) was dissolved in 20 mL of a sulfuric acid/1-nitropropane mixture (1:1 wt%).[40] The NMCA solution was added to

PPX film samples and allowed to react at room temperature. The film samples were rinsed with methanol and distilled water, and extracted with methanol (Soxhlet) for 4 h.

2.3.7. Aminomethylation

Aminomethylated films were prepared by reaction of chloroamidomethylated films with a 1:1 (vol.) solution of 37% hydrochloric acid and ethanol under reflux.[41] Film samples were rinsed in ethanol, ethanol/distilled water (1:1 vol.) and distilled water. A derivatization reaction was performed to label the amine functional group.[42] Pentafluorobenzaldehyde (PFB, 0.5 mL) was added to the bottom of a Schlenk tube containing the aminomethylated samples suspended in a specially built glass holder. The tube was capped and the reaction was carried out at 45 °C for 6 h. The reaction was carried out as a vapor/solid reaction and the film samples did not contact liquid PFB. Film samples were then rinsed and extracted (Soxhlet) with THF for 2 h.

2.3.8. Alkylation with propylene oxide[43]

Stannic chloride (5 eq. with respect to PPX) was added to a flask containing PPX films and 20 mL of anhydrous dichloromethane. Propylene oxide was added drop-wise to the mixture (1:1 molar with respect $SnCl_4$) during 1 min and under continuous stirring. The reaction was allowed to proceed at 20 °C for 5 h, after which time it was terminated by addition of methanol. The films were rinsed with ethanol, hydrochloric acid (0.1 N), methanol, and distilled water in this order. Alkylated PPX films were further reacted with trifluoroacetic anhydride.[44] The vapor phase reaction was carried out by addition of 0.5 mL of the anhydride to the bottom of a Schlenk tube containing the polymer films (suspended in a glass holder) and allowed to react at room

temperature and atmospheric pressure for 1 h. Rinsing with THF was followed by extraction with THF (Soxhlet) for 4 h.

2.3.9. Acylation with trifluoroacetic anhydride[45]

Dichloromethane (20 mL) was added to PPX film samples in the presence of aluminum chloride (10 eq. with respect to PPX). The solution was stirred for 5 min at room temperature and trifluoroacetic anhydride (TFAA) was then added drop-wise over 1 min (1:1 molar with respect $AlCl_3$). After various reaction times, methanol was added to quench the reaction and the films were rinsed with methanol, water, and THF (in this order) and extracted (Soxhlet) with THF for 4 h.

2.3.10. Acylation with succinic anhydride

Anhydrous 1,2-dichloroethane (25 mL) was added to a flask containing PPX films and aluminum chloride (10 eq. with respect to PPX). Succinic anhydride (0.66 M in 1,2-dichloroethane) was added (1:1 molar with respect to $AlCl_3$) and allowed to react at room temperature. After the desired time, 10 mL of ice water was added to the solution and left overnight to complete the hydrolysis. The films were then rinsed with HCl (37%) and distilled water. The resulting carboxylic acid was labeled with trifluoroethanol (TFE).[46] TFE (0.9 mL) was added to the bottom of a Schlenk tube with the samples suspended. After 10 min, 0.4 mL of pyridine and 0.3 mL of di-t-butylcarbodiimide were added. After 12 h the film samples were rinsed and extracted (Soxhlet) with THF for 4 h.

2.3.11. Acylation with 3-chloropropionylchloride

Acylation with 3-chloropropionylchloride.[47] This reaction was carried out following the same protocol as for the acylation with trifluoroacetic anhydride. A 1.45

M solution of 3-chloropropionylchloride in anhydrous dichloromethane was used and added in excess with respect to the PPX repeat units (10 eq.). The reaction was quenched by addition of methanol and the samples were rinsed with methanol, and distilled water, and then extracted (Soxhlet) with methanol for 4 h.

2.4. Results and Discussion

2.4.1 Poly(*p*-xylylene) films

PPX film samples were prepared as described in the Experimental Section. A schematic of the reactor setup is presented in Figure 2.1. As mentioned previously, the temperature in each of the three sections of the reactor was independently controlled and monitored. The dimer was loaded to the system by using a boat inserted through an open-end quartz tube. The temperature of the sublimation section was controlled with a heating tape attached to a temperature controller. Pyrolysis was carried out using a tube furnace maintained at ~ 675 °C, equipped with a temperature controller. The deposition chamber was a jacketed glass tube, the temperature of which was controlled by continuous feed from a recirculator. A liquid nitrogen trap was placed at the end of the reactor, and before the vacuum manifold, to trap the unreacted monomer. The pressure of the system was measured from the vacuum manifold.

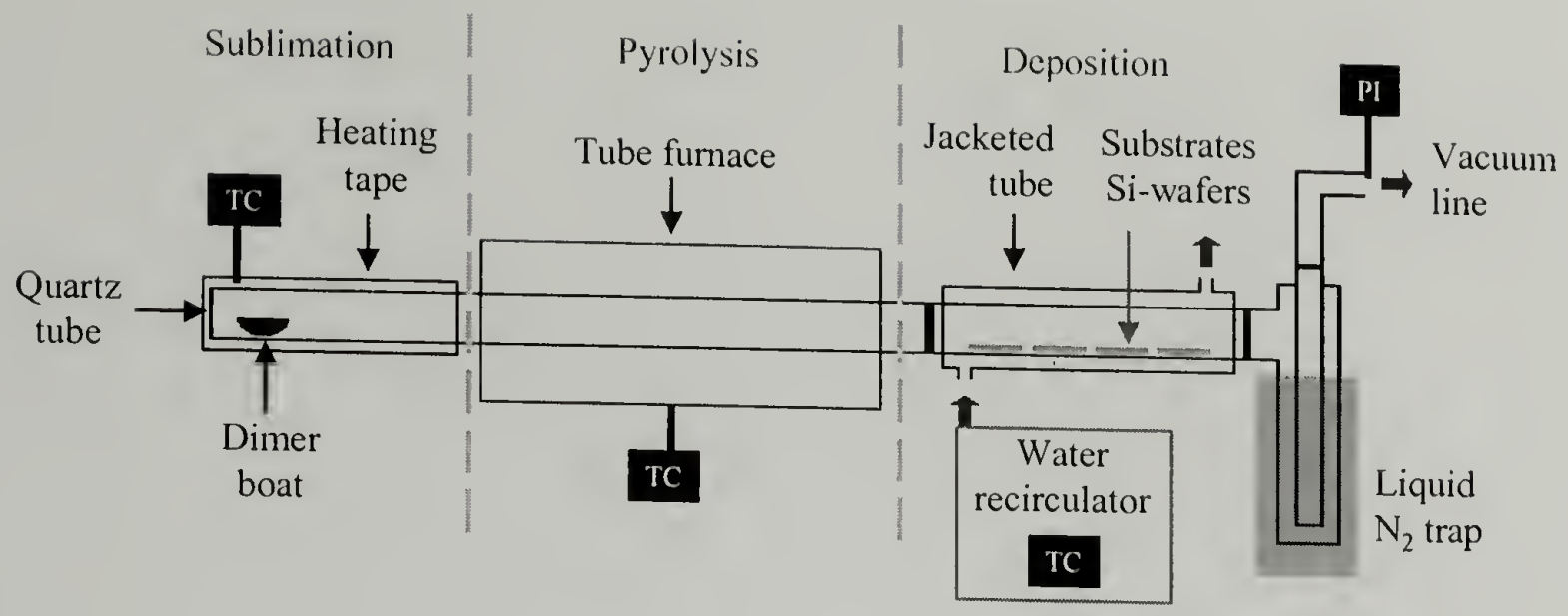

Figure 2.1. Vapor deposition polymerization apparatus.

Three of the most important process parameters are the sublimation and deposition temperatures, and the system pressure. As observed in Figure 2.2 an increase in the sublimation temperature produces an increase in the partial pressure of the precursor, which in turn results in an increased deposition rate. The film thickness varies linearly with time, and the deposition rate has an exponential dependence on sublimation temperature: 0.13 nm/min, 0.37 nm/min, and 1.26 nm/min at 55 °C, 63 °C, and 70 °C, respectively.

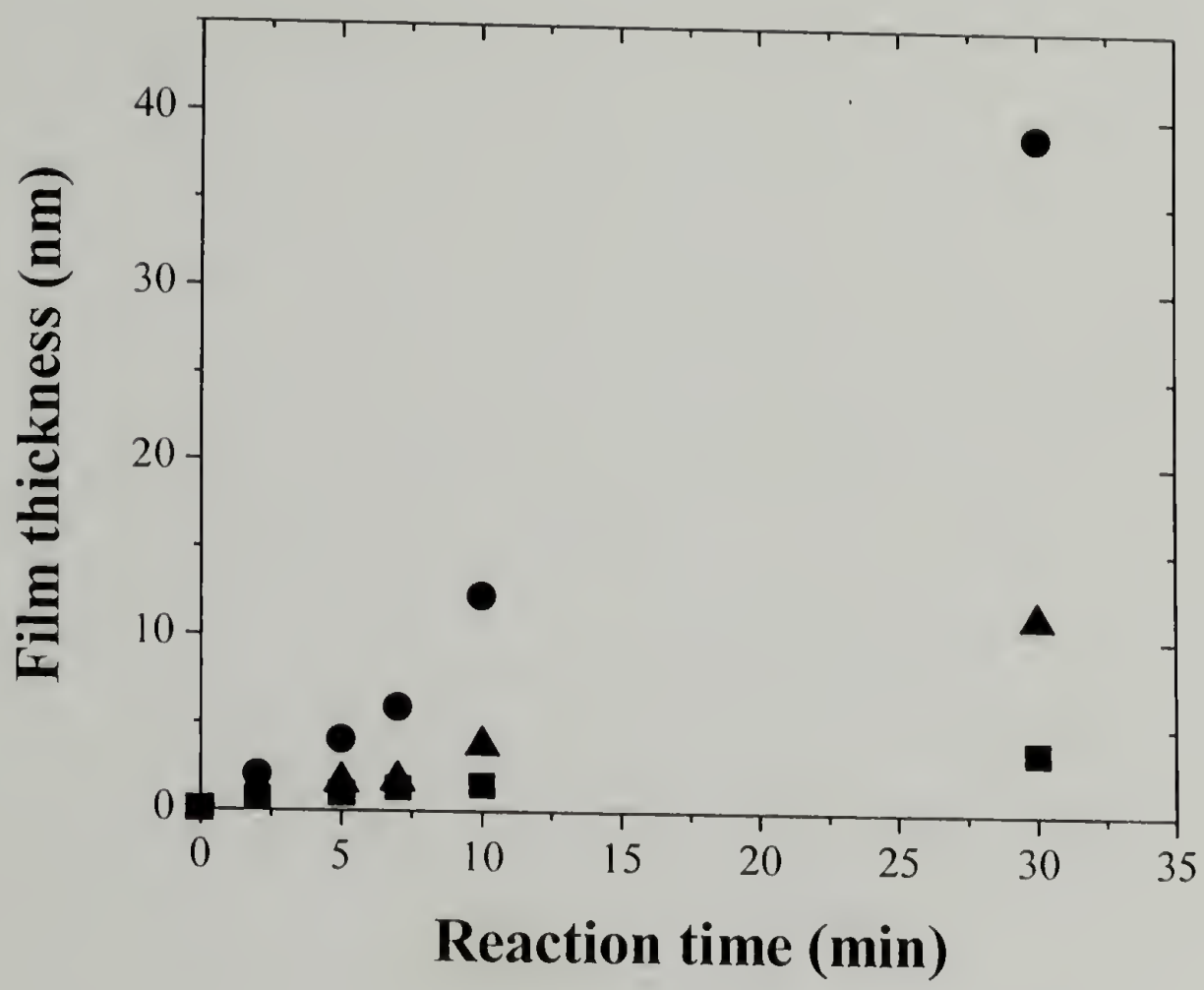

Figure 2.2. Effect of sublimation temperature on deposition rate, determined by ellipsometry. Reaction conditions: $T_{pyrolysis}$ = 675 °C, $T_{deposition}$ = 20 °C, system pressure = 85 mTorr. Sublimation temperatures are 55 °C (■), 63 °C (▲) and 70 °C (●).

Unlike most chemical vapor deposition processes where the film growth rate increases with deposition temperature, VDP of poly(*p*-xylylene) shows the opposite behavior, as presented in Figure 2.3. In this case, increasing the deposition temperature produces a decrease in the growth rate. Although an exponential dependence has been previously reported, the data presented here do not allow this trend to be confirmed.

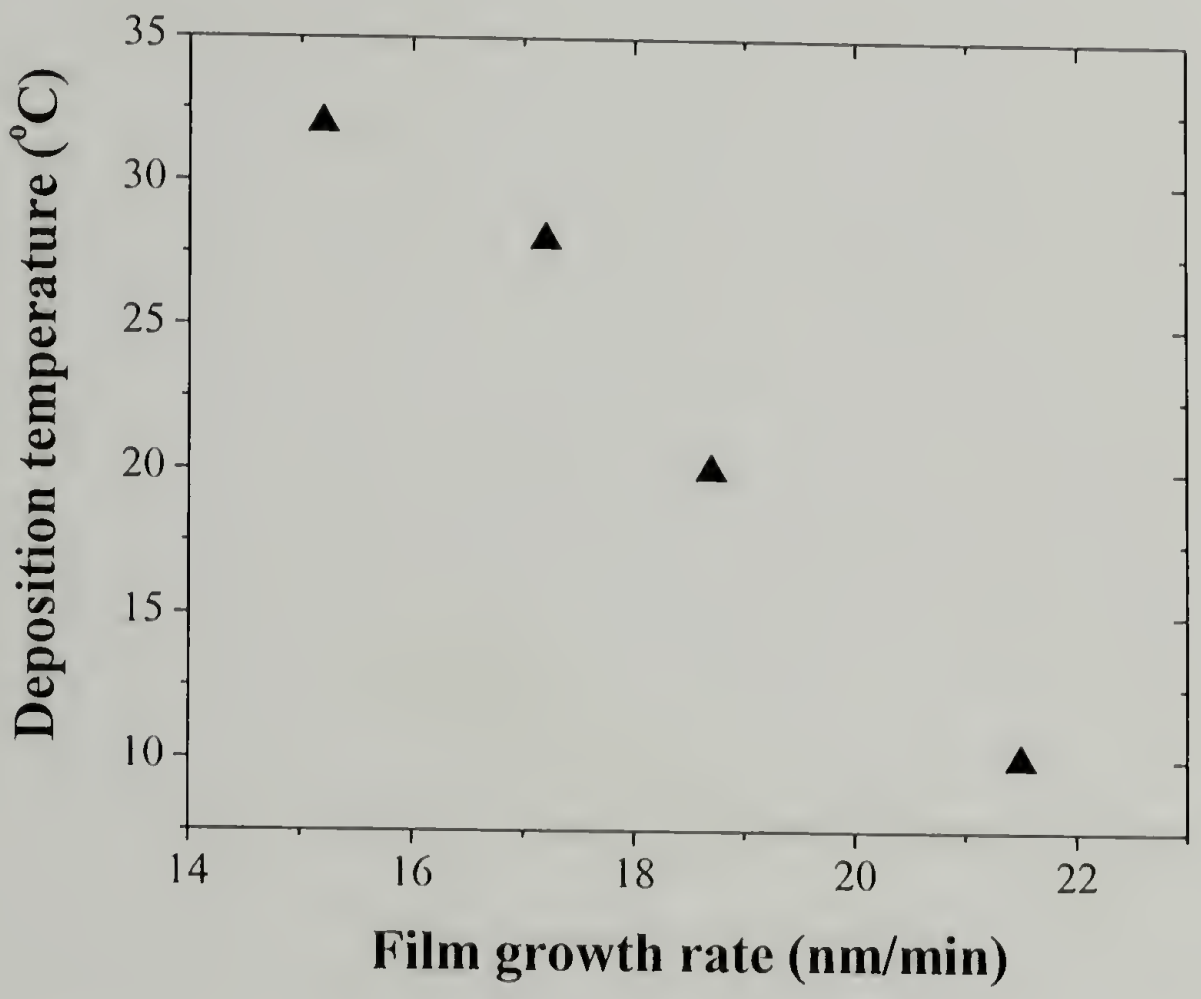

Figure 2.3. Effect of deposition temperature on film growth rate for poly(*p*-xylylene). Reaction conditions: $T_{sublimation}$ = 110 °C, $T_{pyrolysis}$ = 685 °C, system pressure = 95 mTorr.

After deposition, the films were extracted for 12 h with dichloromethane to ensure complete removal of unreacted dimer[48] and characterized by XPS, IR, DSC, and WAXS. As assessed by WAXS and DSC, the crystallinity of the as-deposited and extracted films was approximately 50%, indicating that solvent annealing did not occur during extraction. The DSC thermogram (Figure 2.4) presents three endothermic transitions at 210 °C, 270 °C, and 430 °C, attributed to melting of oligomers, $\beta_1 \rightarrow \beta_2$ transition, and melting of polymer crystals, respectively.[16] WAXS results (Figure 2.5) also reveal that both the deposited and extracted films exist in the α-crystalline form of PPX, with strong reflections at the (020) and (110) planes,[16] corresponding to d-spacings of 0.51 nm and 0.39 nm, respectively.

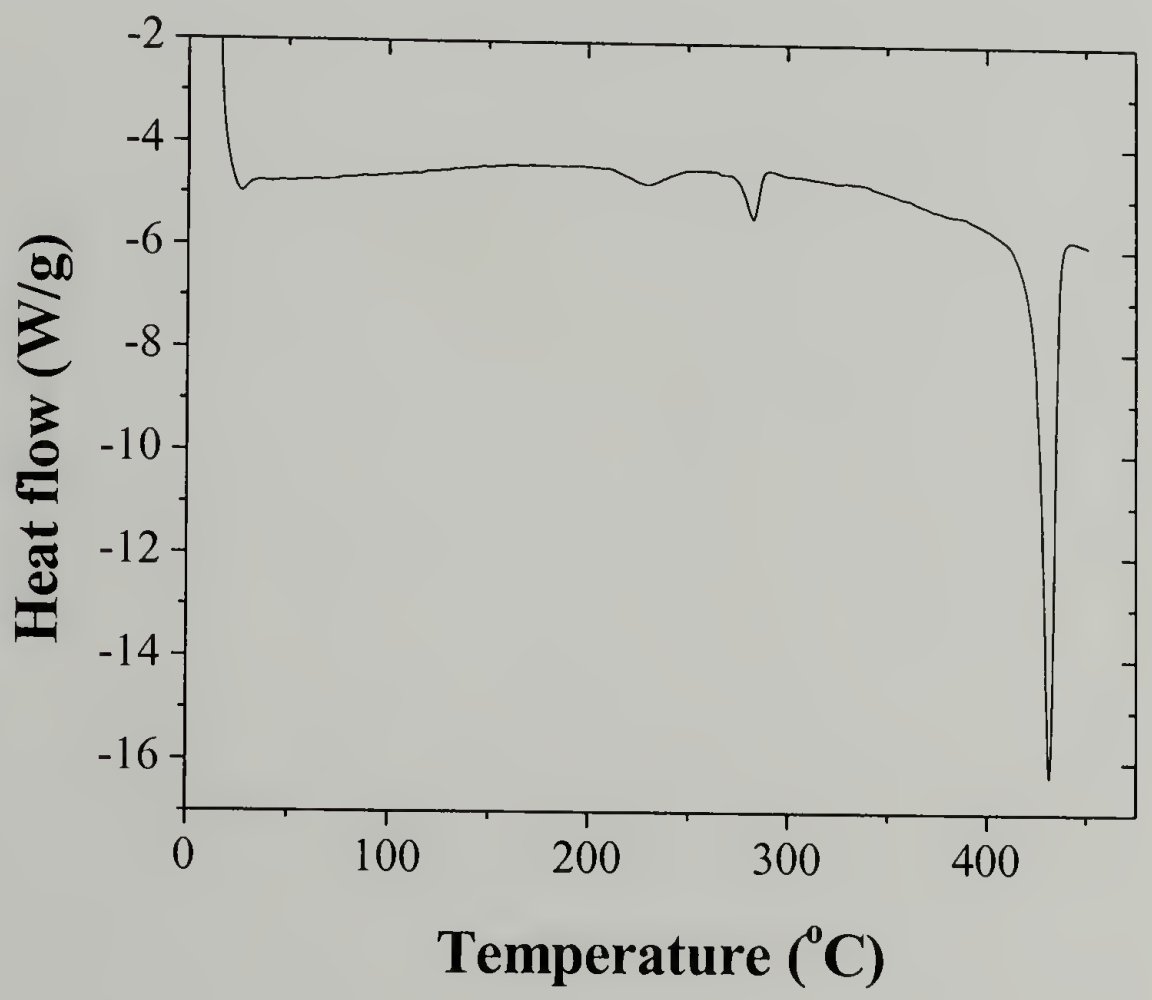

Figure 2.4. DSC thermogram of as-deposited poly(*p*-xylylene).

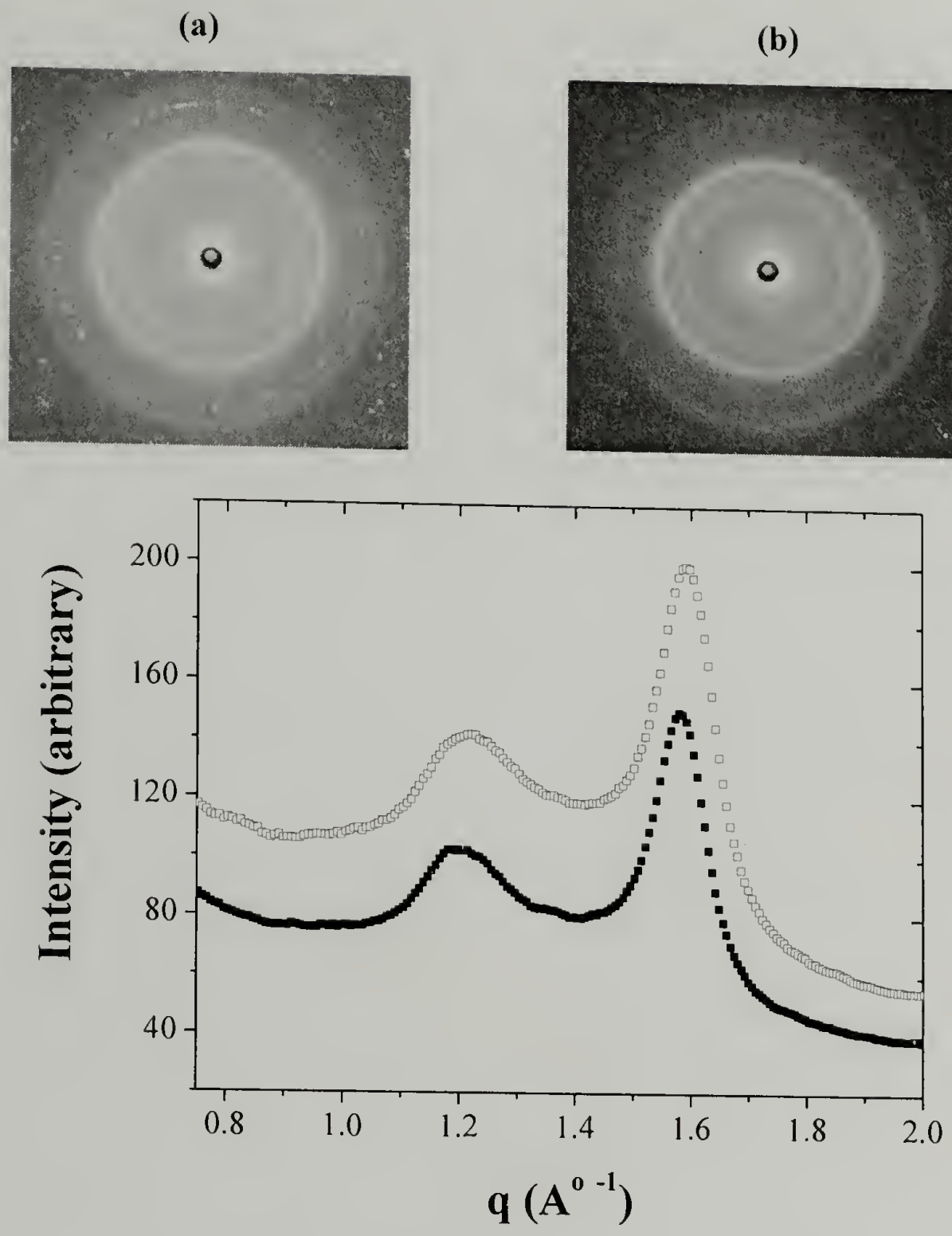

Figure 2.5. X-Ray diffraction patterns of poly(*p*-xylylene) free-standing films illustrating the effect of dichloromethane extraction on crystallinity and crystalline modification. As deposited (a and ■), and solvent-extracted films (b and □).

The surface chemical composition of extracted PPX was determined by XPS; the only two elements present in the outermost ~10 Å of the surface are carbon (97.93%) and oxygen (2.07%), and the concentration of the latter decreases within the film (1.17% at ~ 40 Å analysis depth). The presence of oxygen is believed to be a consequence of the benzylic radical chain ends, which react with oxygen when exposed to air after deposition or with adventitious oxygen present in the reactor, however the low oxygen content reveals the high purity of the samples. IR analysis of the films (Figure 2.7) shows absorption signals at ~3000 cm^{-1} corresponding to CH_2 and =C-H stretching, at 1513 cm^{-1} and 1453 cm^{-1} indicative of the aromatic stretching and deformation, and an intense signal at 821 cm^{-1} due to C-H out-of-plane deformation. Contact angle measurements indicate that PPX is a hydrophobic polymer, with advancing and receding water contact angles of 95° and 75°, respectively.

2.4.2. Modification Reactions

The modification reactions on PPX film surfaces that were studied in this work are presented in Figure 2.6. Sulfonation and aminomethylation reactions were studied in detail, while Fridel-Crafts catalyzed alkylation and acylations were not optimized.

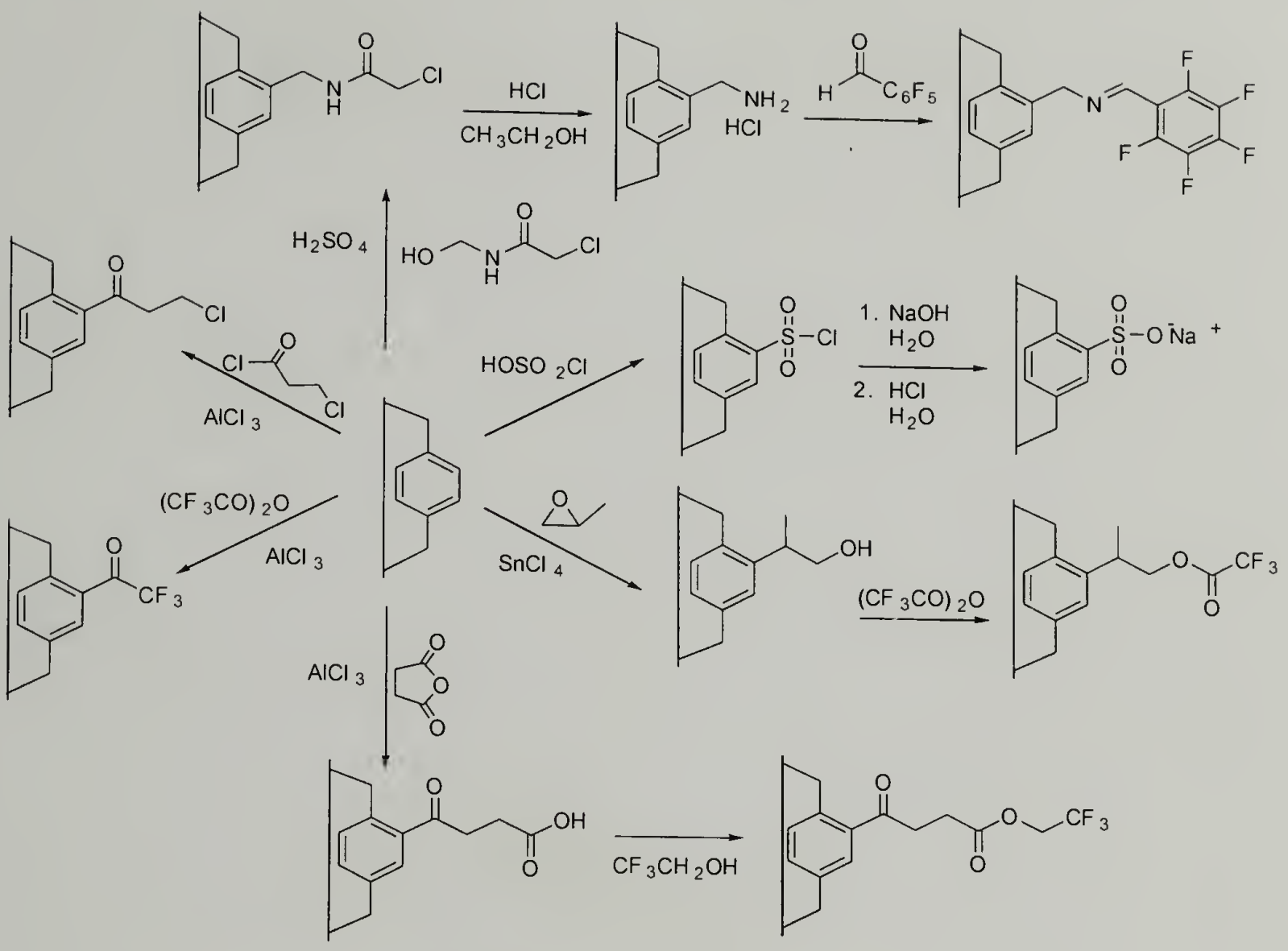

Figure 2.6. Functionalization reactions on poly(*p*-xylylene) film surfaces.

2.4.3. Sulfonation

Poly(*p*-xylylene) films were chlorosulfonated by reaction with concentrated chlorosulfonic acid or with a solution of the acid in 1,2-dichloroethane. The effect of reaction time, temperature, and acid concentration on the degree of substitution of PPX were studied by XPS and IR spectroscopies and gravimetric analysis.

An important characteristic of PPX is that it presents low degrees of swelling in common organic solvents and inorganic reagents (i.e. strong acids such as sulfuric, nitric, etc.), which in turn determines its chemical and solvent resistance. Therefore it is surprising that reaction with chlorosulfonic acid occurred readily with high penetration depths, observable both by ATR (Figures 1.8 and 1.9) and transmission IR. While the absorption signals at ~3000 cm^{-1} decrease in intensity after reaction, new signals appear in the region from 1470 to 850 cm^{-1}. The most predominant are those present at 1368 cm^{-1} and 1174 cm^{-1}, characteristic of the S=O asymmetric and symmetric stretch of the chlorosulfonyl group. Signals denoting a 1,2,4-trisubstituted benzene ring also appear at 1491 cm^{-1} and 850 cm^{-1}, accompanied by a decreased intensity of the signals corresponding to a 1,4-disubstituted species (1513 cm^{-1} and 821 cm^{-1}). Also, the band present at 1320 cm^{-1} is indicative of the formation of sulfone bonds, which has been observed in similar systems upon reaction with chlorosulfonic acid.[49]

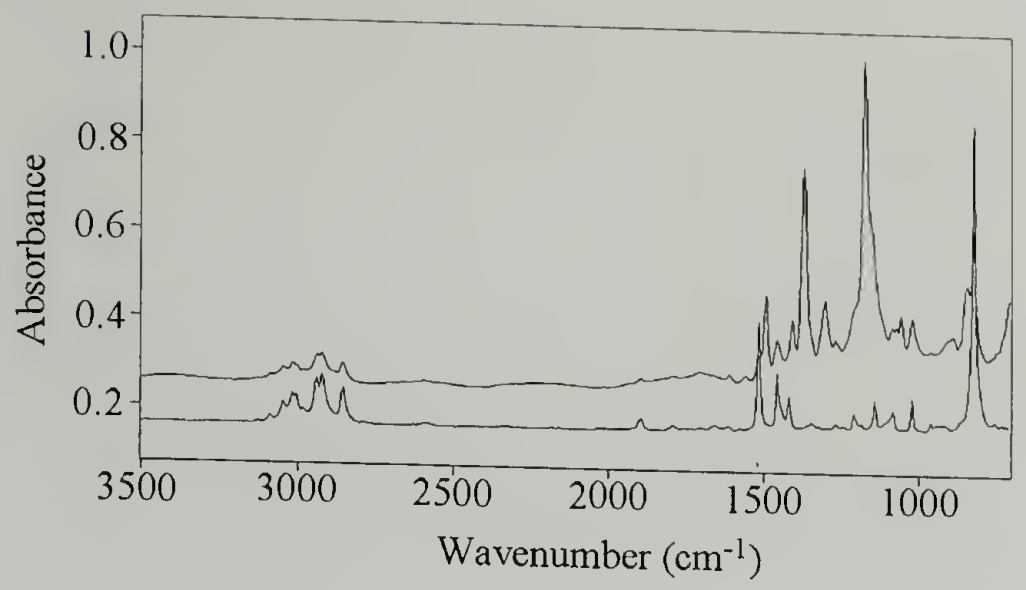

Figure 2.7. ATR IR spectra of poly(*p*-xylylene) (lower spectrum) and chlorosulfonated poly(*p*-xylylene) (upper spectrum).

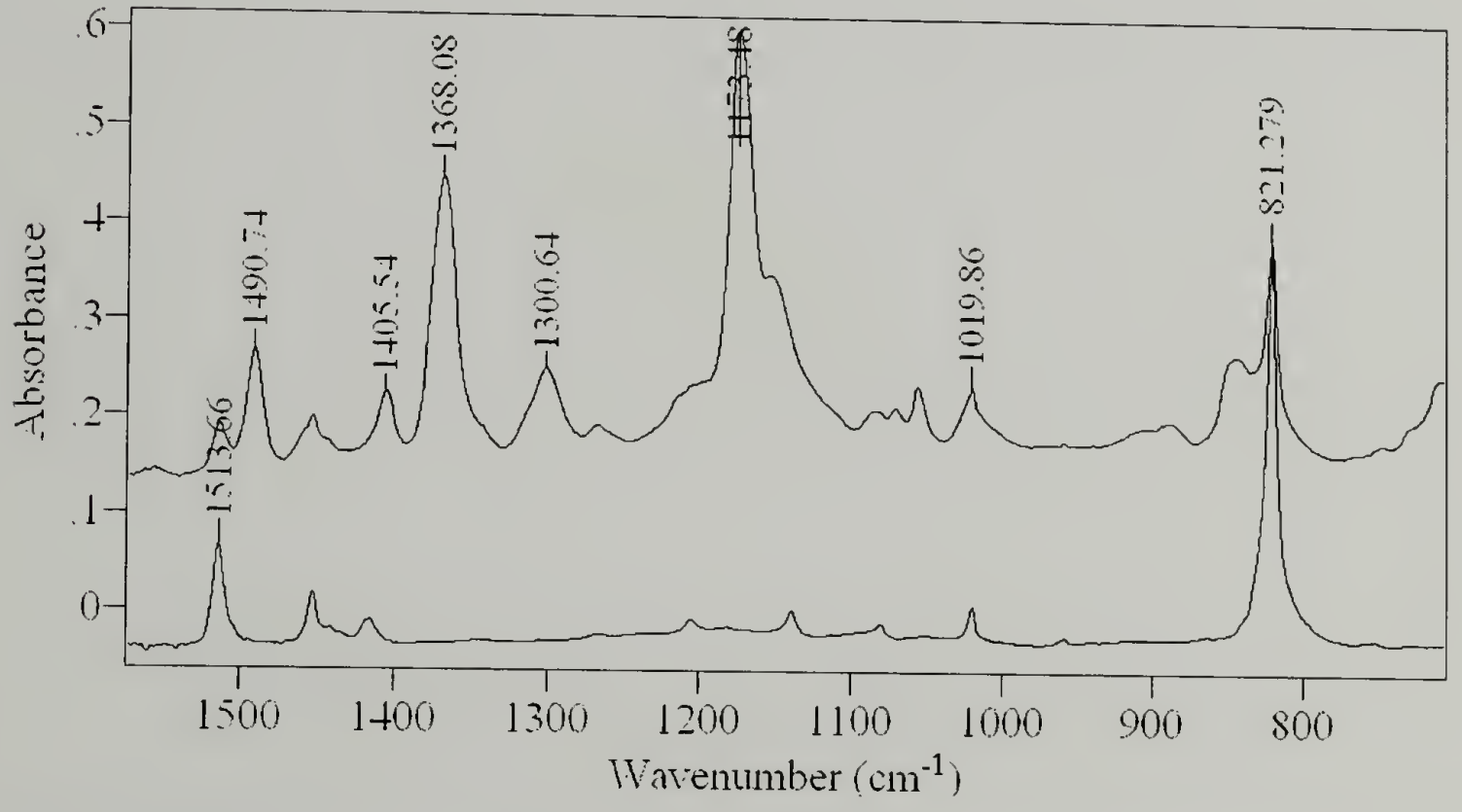

Figure 2.8. ATR IR spectra of poly(*p*-xylylene) (lower spectrum) and chlorosulfonated poly(*p*-xylylene) (upper spectrum).

ATR IR analysis was used to study the kinetics of the reaction near the surface region and different internal reflection elements were used to estimate the dependence of time on the penetration depth. The results, however, show discrepancies, possibly due to high reaction rates or to differences in contact of the film samples with the internal reflection elements, and thus could not be used for quantitative analysis. The degree of substitution, therefore, was estimated based on the intensities of the signals characteristic of 1,4-disubstituted (1513 cm^{-1}) and 1,2,4-trisubstituted (1419 cm^{-1}) species by transmission IR.[50] The degree of substitution was calculated according to: $A_{1491}/(A_{1513}+A_{1491})$, where A_{1491} and A_{1513} represent the absorbance at the corresponding wavenumbers. Figure 2.9 presents the kinetics of the reaction as observed by transmission IR at two different temperatures (5 °C and 20 °C). The strong effect of temperature on the yield of the reaction is apparent. A maximum yield of 65% was obtained under the conditions studied.

Since PPX is a semicrystalline polymer, it is presumed that reaction with chlorosulfonic acid will occur preferentially in the amorphous regions, with formation of the monosubstituted species. As estimated by DSC and WAXS, the degree of crystallinity is approximately 50%, while the maximum degree of substitution estimated by IR is 65%. The infrared results must be regarded as estimates. Although they are similar to the DSC and WAXS data, they may suggest that a fraction of the polymer larger than that corresponding to the amorphous phase undergoes reaction. This could be explained assuming that chlorosulfonic acid swells PPX and produces a decrease in crystallinity (not assessed). Initial reaction at the outermost surface of the polymer may

render it more permeable to the acid, facilitating its diffusion and reaction inside the film.

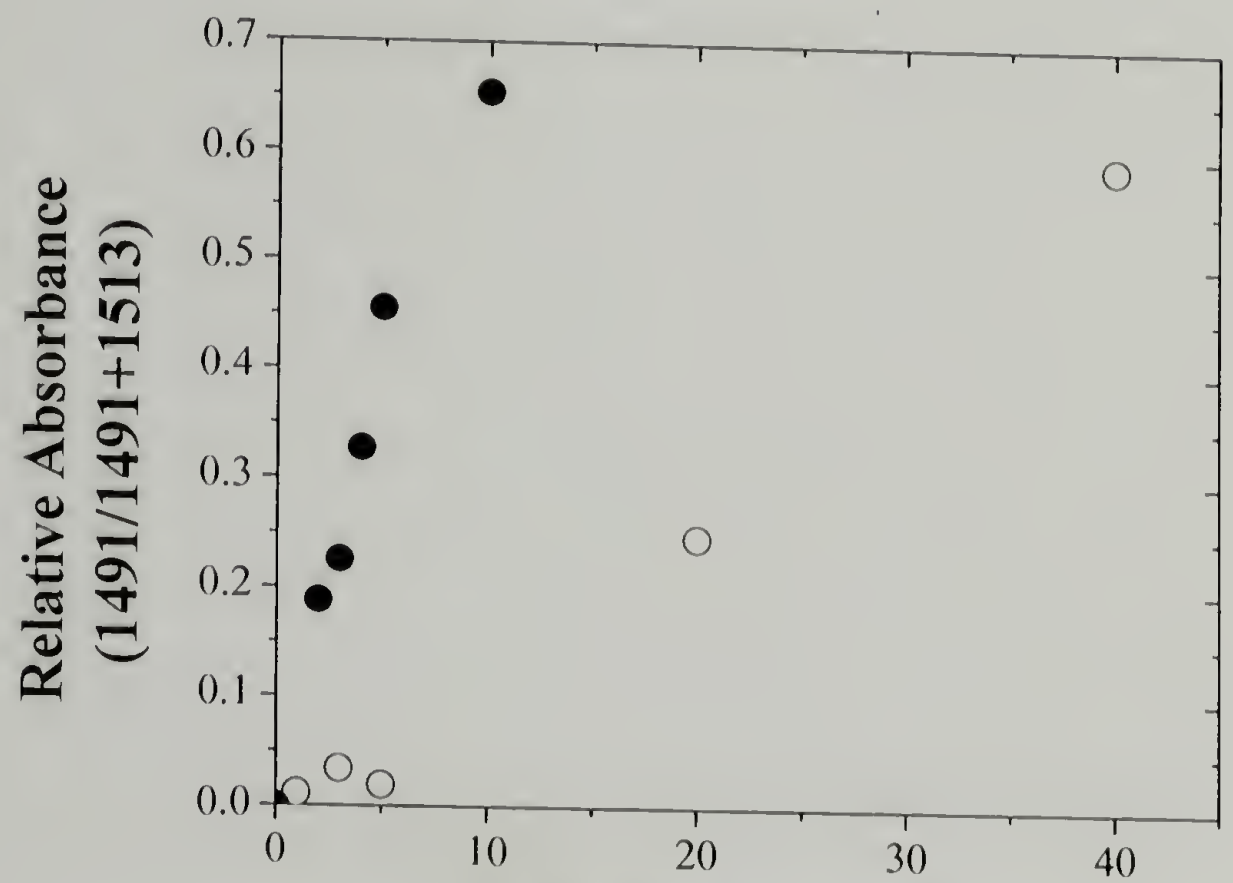

Figure 2.9. Kinetics of chlorosulfonation determined by IR spectroscopy for reactions conducted at 5 °C (○) and 20 °C (●).

Gravimetric analyses indicate an increase in mass with chlorosulfonation time; the values of mass gain obtained by this method (Figure 2.10) also show a tendency of increasing mass with reaction time. The yield was estimated considering that the only substituent is SO_2Cl, which is a rough approximation since sulfone and sulfonic acid groups are also present after chlorosulfonation.

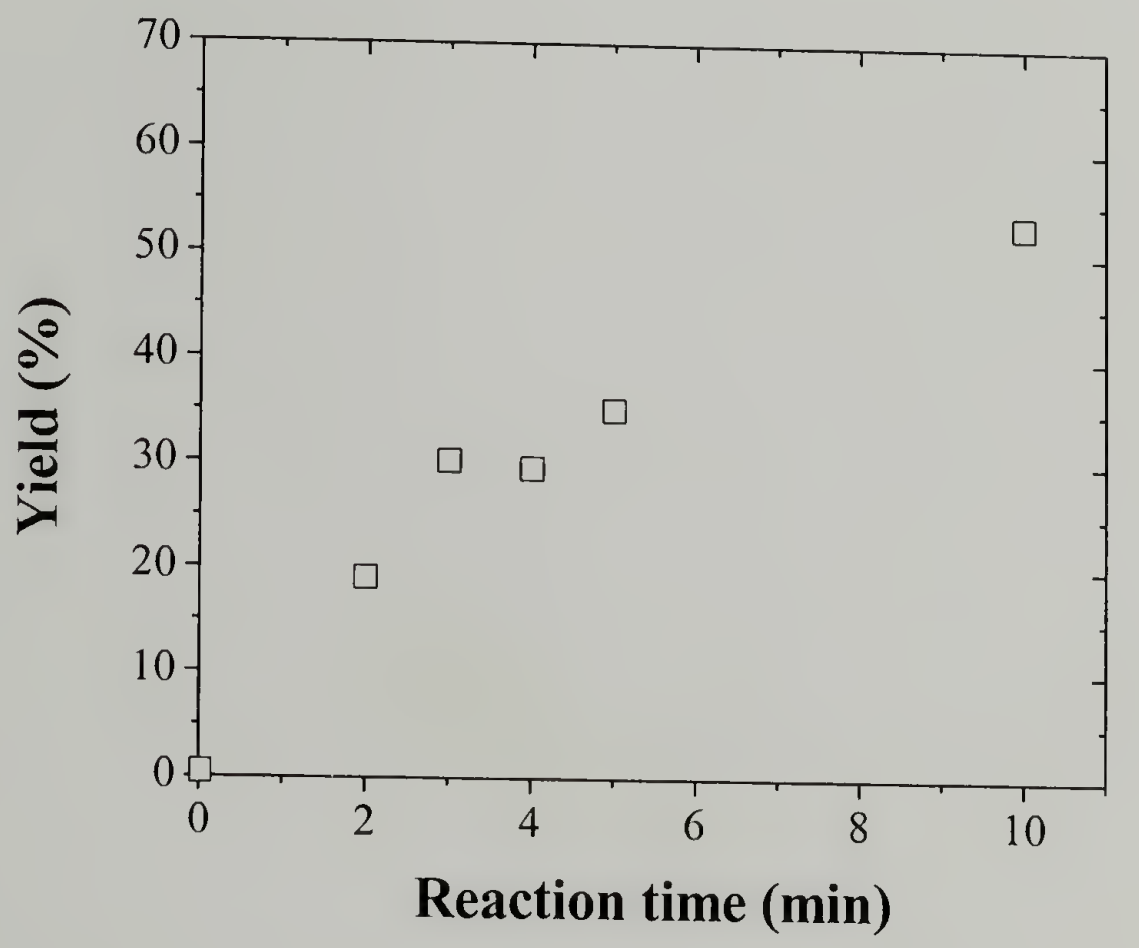

Figure 2.10. Degree of substitution for chlorosulfonation at 20 °C estimated by gravimetry (□).

The morphology of the films was determined by SEM (Figure 2.11) and, roughening of the samples is observed upon reaction. This effect can be attributed both to the increase in mass and to increased mobility of the polymer chains in chlorosulfonic acid. At long reaction times and high temperatures, severe deformation and loss of transparency of the films occurs. Coloration of the films also occurs at long reaction times and high temperatures and is likely a consequence of the formation of olefins.[50]

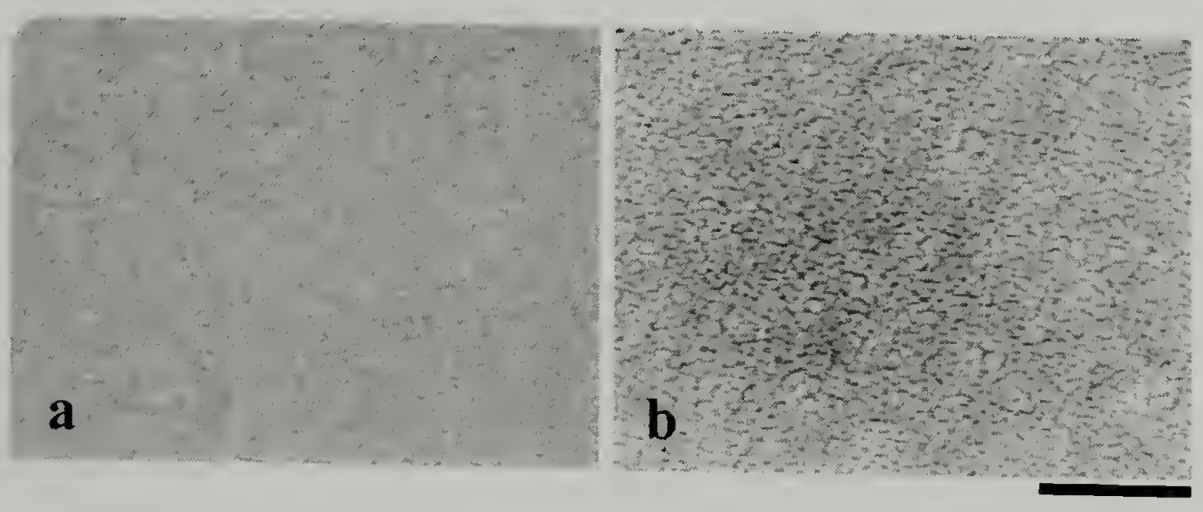

Figure 2.11. FESEM images of PPX before (a) and after (b) chlorosulfonation.

The outermost surface of the film samples after chlorosulfonation was analyzed by XPS. Kinetics of the reaction indicates rapid reaction in the XPS sampling depth. After short times in chlorosulfonic acid at both 5 and 20 °C the surface composition indicates that ~50% of the repeat units of PPX are substituted (Table 2.1) and that the sulfonyl chloride group accounts for 66% of the substituents. Dilution of the chlorosulfonic acid with dichloroethane does not slow the reaction as observed by XPS and increases the yield of sulfone. Infrared studies, however, indicate that under these conditions the reaction is surface-selective (no non-PPX absorbances are observed).

Table 2.1. XPS atomic composition and water contact angles for PPX derivatives.

Sample (PPX-)	Atomic composition (15° take-off angle data)						Water contact angle (degrees)
	C	O	S	N	Cl	F	
$-SO_2Cl$ [a]	78.79	12.40	5.24		3.57		65/15
$-SO_2Cl$ [b]	78.10	13.12	5.32		3.45		68/17
$-SO_2Cl$ [c] (dilute)	72.64	20.24	5.55		1.57		-
$-CH_2NHCOCH_2Cl$ [d]	74.93	10.64		8.38	6.05		60/15
$-CH_2NH_2$ [e]	81.22	10.93		6.35	1.5		70/25
$-CH_2NHCOC_6F_5$	73.04	10.00		5.06	0.35	11.54	-
$-CO(CH_2)_2Cl$	85.42	12.48			2.10		82/57
$-COCF_3$	84.43	11.88				3.69	80/32
$-CO(CH)_2COOCH_2CF_3$	81.80	14.24				3.96	-
$-(CH)CH_3CH_2OCOCF_3$	92.48	5.01				2.52	92/50

Reaction Conditions: [a]20 min at 5 °C in 100% $ClSO_3H$; [b]20 min at 20 °C in 100% $ClSO_3H$; [c]2min at 20 °C in 5% $ClSO_3H/C_2H_4Cl_2$; [d]69 h at 20 °C; [e]4 h under reflux.

Chlorosulfonated films were hydrolyzed by reaction with aqueous sodium hydroxide. XPS analysis of these films shows a decrease in the intensity of the chlorine signal and an increase in the oxygen content. PPX films sulfonated by this two-step reaction were compared to samples synthesized by sulfonation with concentrated sulfuric acid and silver sulfate.[31] While their IR spectra show similarities (Figure 2.12), in the presence of water, the samples obtained by direct sulfonation swell considerably while those prepared by the two-step process do not. This difference is attributed to the formation of sulfone bonds during chlorosulfonation, which form crosslinks and prevent swelling.

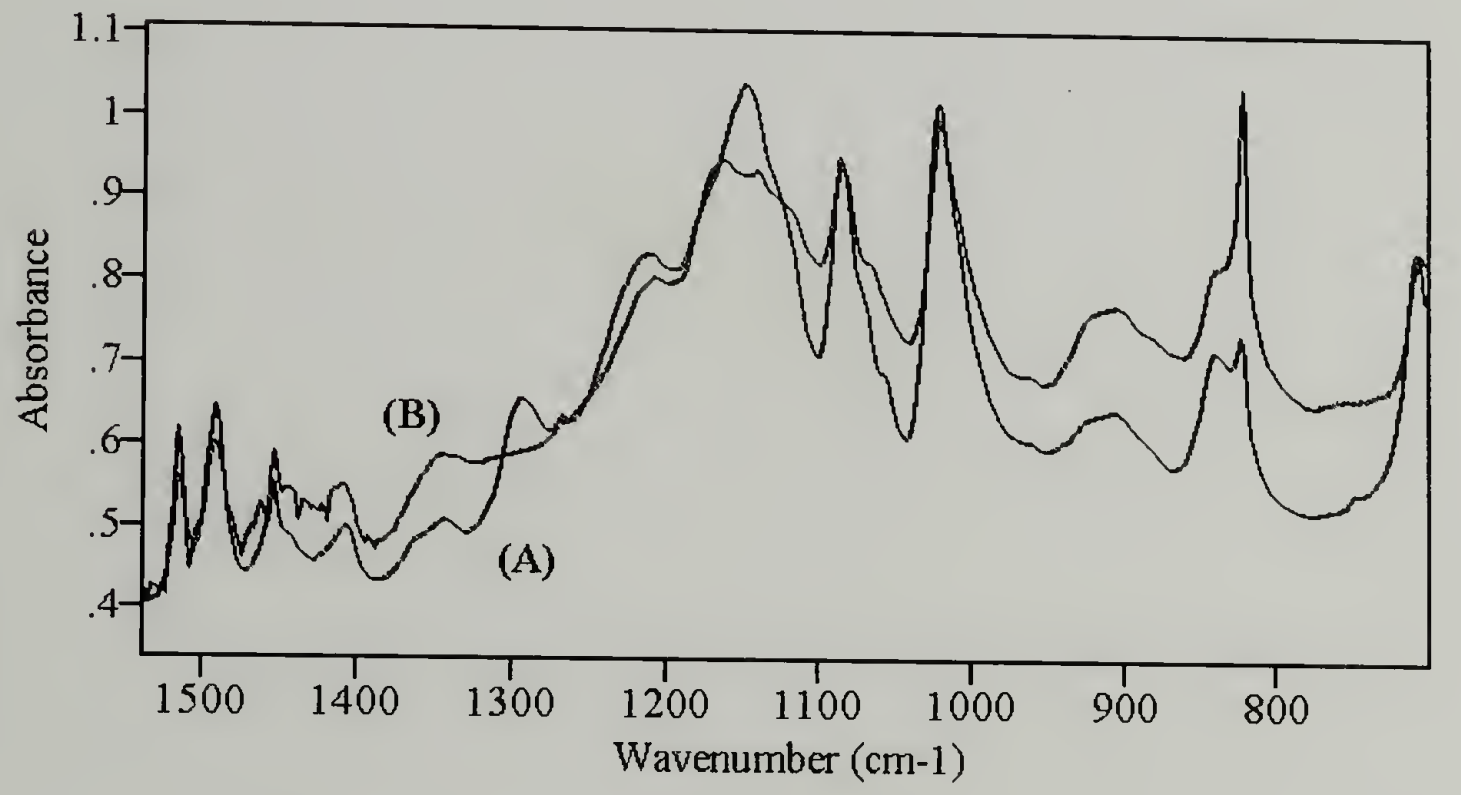

Figure 2.12. ATR IR spectra of sulfonated poly(*p*-xylylene) obtained by catalyzed sulfonation (A) and chlorosulfonation followed by hydrolysis (B).

2.4.4. Chloroamidomethylation

PPX films were chloroamidomethylated using the Tscherniac-Einhorn reaction,[51] according to the procedure established by Teramoto for functionalization of polystyrene surfaces.[40] XPS survey spectra of chloroamidomethylated PPX (PPX-$CH_2NHC(O)CH_2Cl$) films indicate incorporation of chlorine and nitrogen and an increase in the intensity of the O_{1s} signal. High-resolution spectra of the C_{1s} signal before and after reaction are presented in Figure 2.13. The most predominant peak, at 286 eV, corresponds to methylene and aromatic carbons of PPX; the shake-up satellite signal (π-π^* transition) is clearly observed at 292.7 eV. After chloroamidomethylation, broadening of the carbon signal to higher binding energy is observed and is attributed to the carbon species associated with the chloroamidomethyl group (-$\underline{C}H_2$-NH-$\underline{C}O$-$\underline{C}H_2$-Cl). Binding energy values are not charge-corrected.

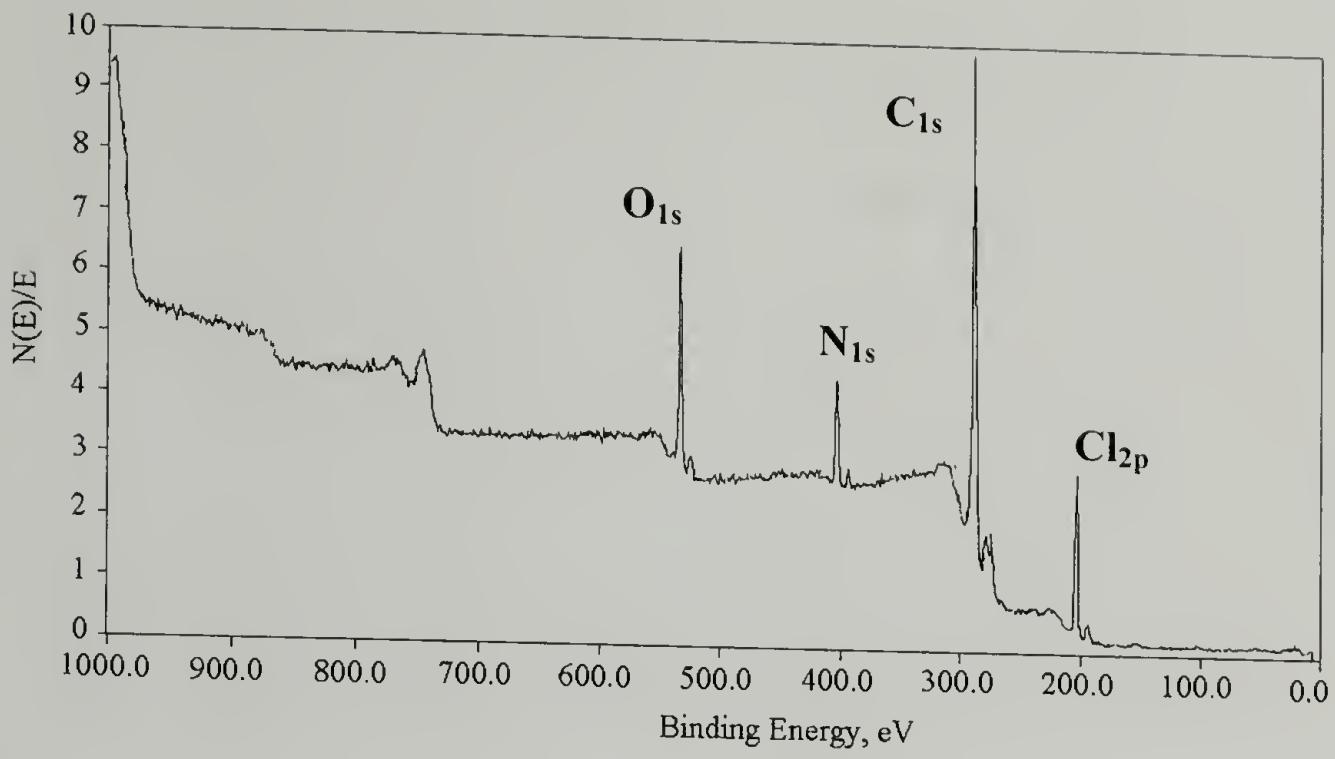

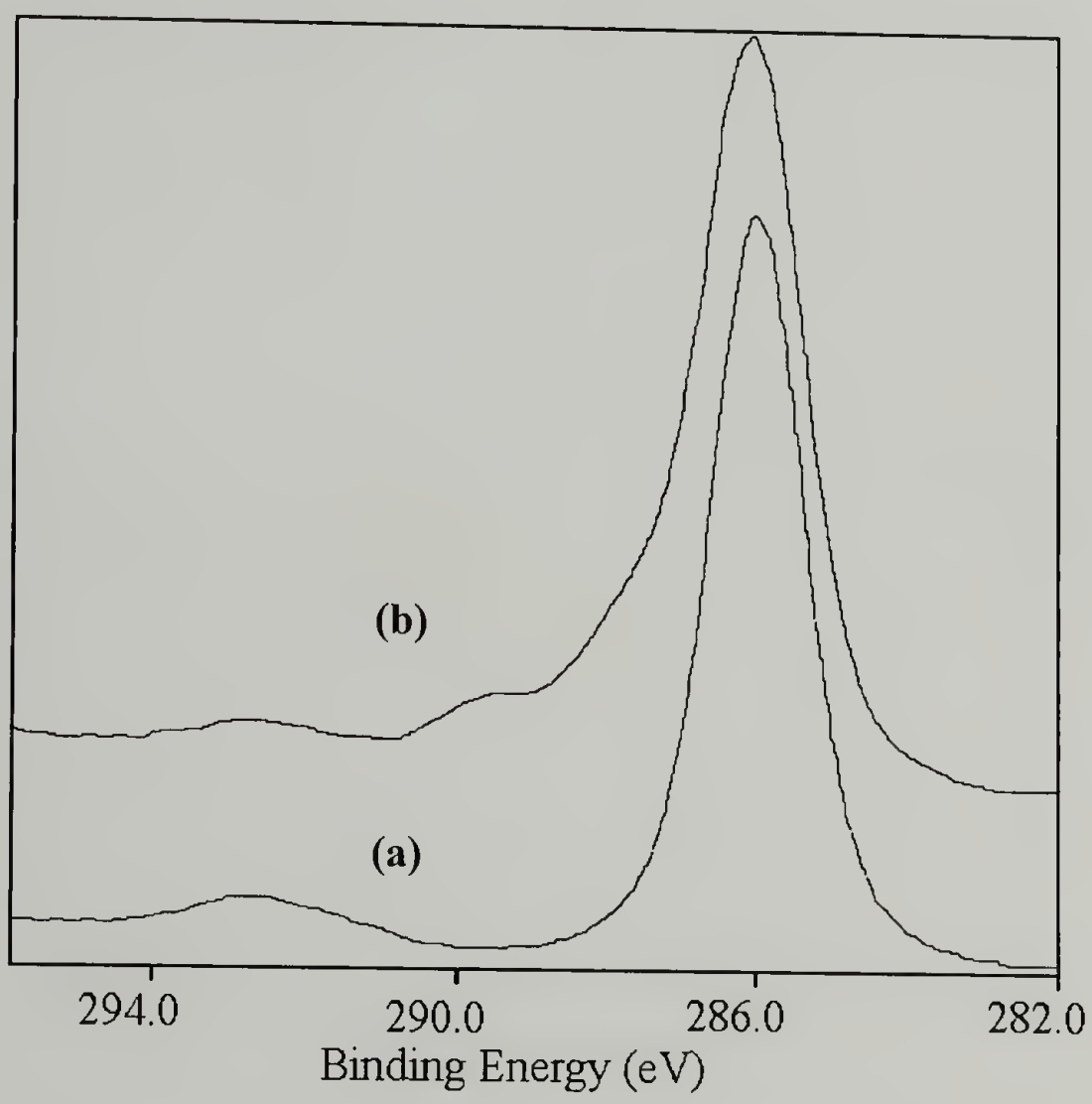

Figure 2.13. Top: XPS survey spectrum of chloroamidomethylated-PPX. Bottom: high-resolution XPS spectrum of the carbon C_{1s} signal for PPX (a) and PPX-$CH_2NHC(O)CH_2Cl$ (b).

The kinetics of reaction, monitored by XPS and contact angle are presented in Figure 2.14. XPS data are presented for a 75° take-off angle since these results were more reproducible than the data obtained at a 15° take-off angle. A limiting yield, as assessed by these techniques, is obtained after approximately 4 h. The composition at this plateau (Table 2.1), $C_{11}O_{1.4}N_{1.1}Cl_{1.0}$, is very similar to the theoretical value if mono-substitution occurs ($C_{11}ONCl$). This would require reaction of crystalline domains or a lack of crystallinity in the surface region. We cannot discount disubstitution of the aromatic rings in the amorphous regions. Sulfonation, a possible side reaction, occurs to a small extent compared to chloroamidomethylation; the concentration of sulfur, as determined by XPS, was below 1% in all cases. The introduction of the polar amide groups produces a decrease in both the advancing and receding water contact angles from 95°/75° to 60°/15° after 4 h of reaction.

AFM and SEM analyses revealed that the topography of the sample remained unchanged, which is expected since sulfuric acid has a small effect on the swelling of PPX (0.2% at 20 °C).[11] PPX-$CH_2NHC(O)CH_2Cl$ films were also characterized by ATR IR. Weak signals attributed to the amide group were observed at 3290 cm^{-1}, 1660 cm^{-1}, and a small shoulder at 1535 cm^{-1}; the signals characteristic of a 1,2,4-trisubstituted species were not apparent. Although XPS analysis of these films reveals that the degree of substitution on the surface is high, the intensity of the signals observed by ATR IR is low, suggesting that the reaction is confined to the near surface region. These results are very different than those of the chlorosulfonation reaction.

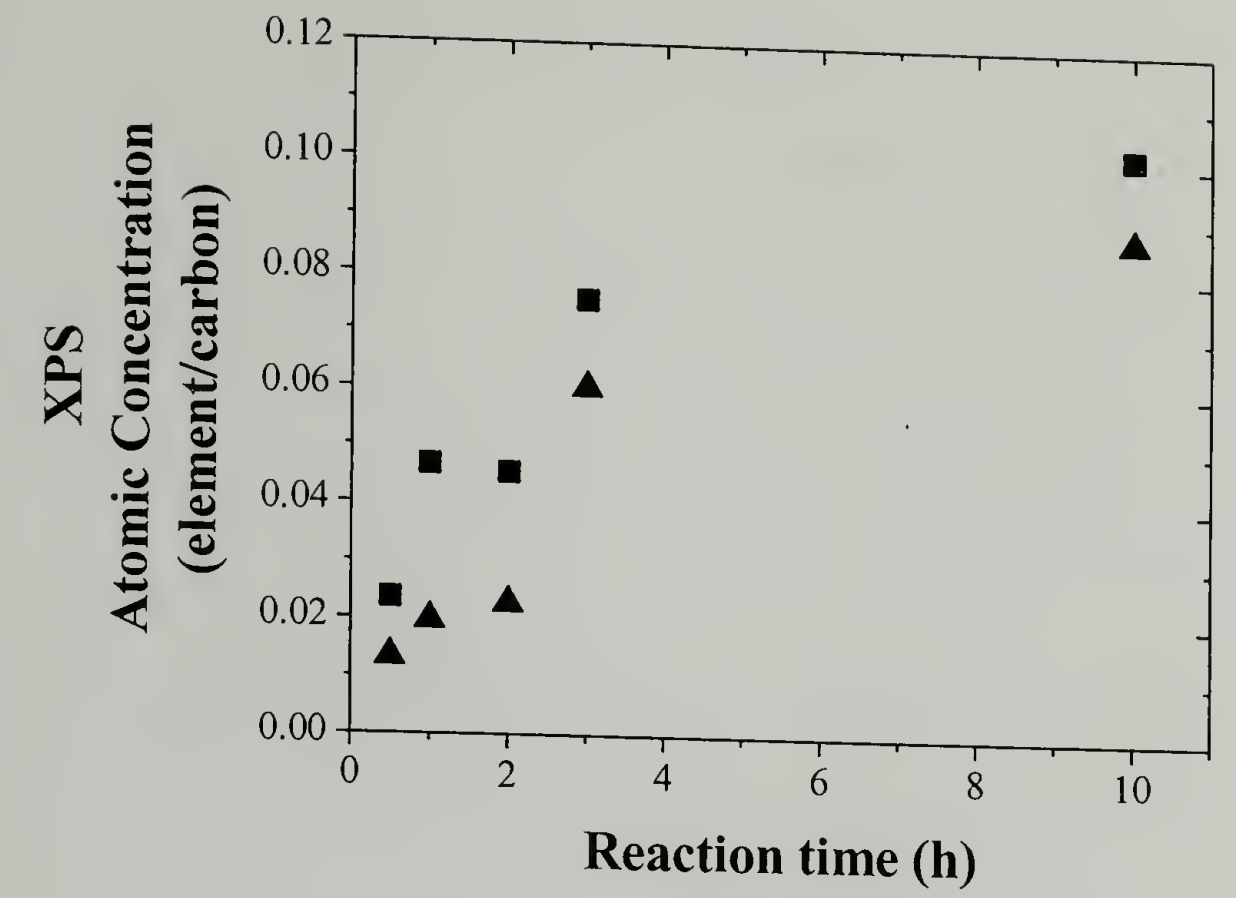

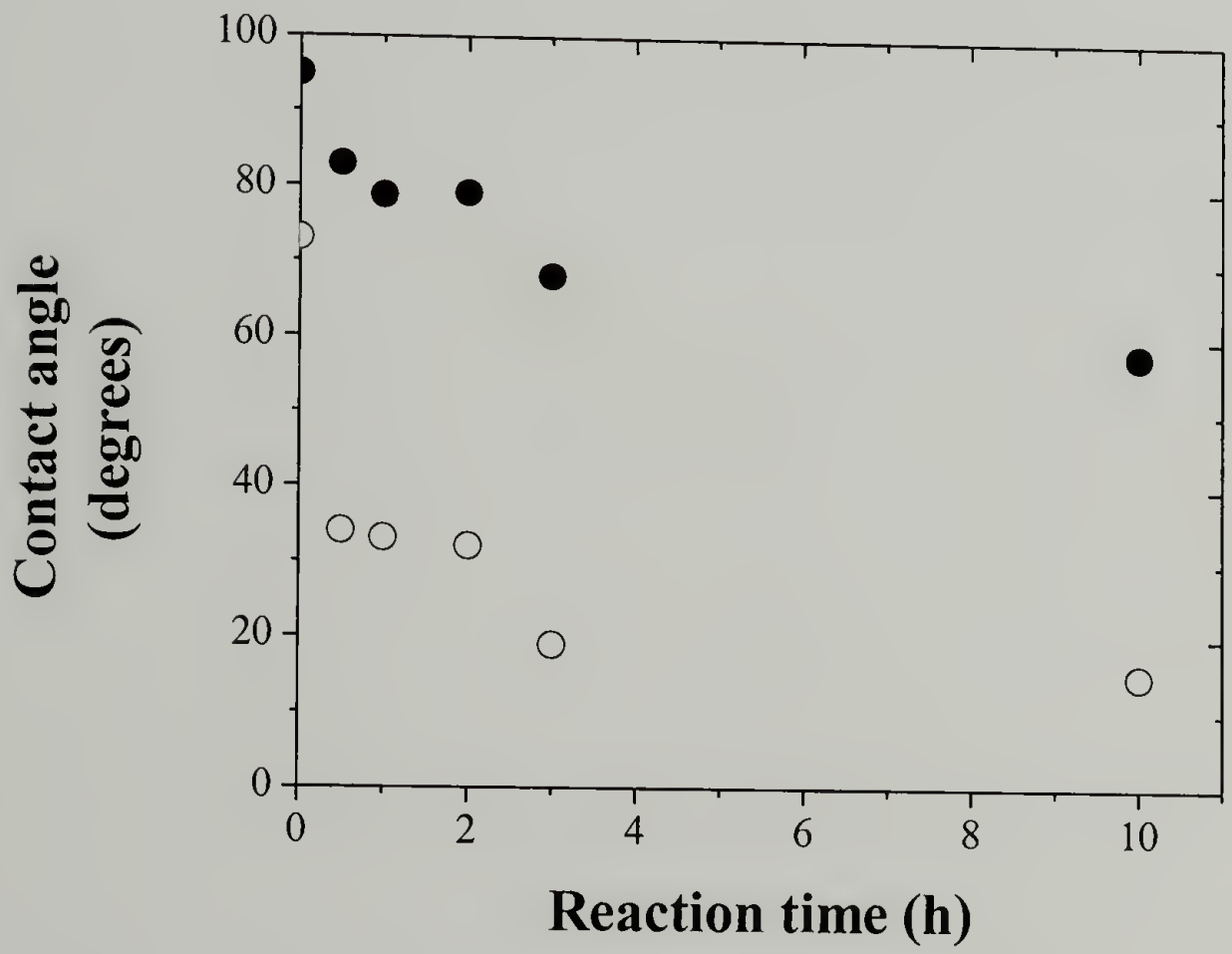

Figure 2.14. Top: atomic ratios determined by XPS for 75° take-off angle during chloroamidomethylation, N/C (■) and Cl/C (▲). Bottom: advancing (●) and receding (○) water contact angles during chloroamidomethylation.

PPX-$CH_2NHC(O)CH_2Cl$ films were subsequently hydrolyzed in ethanol and hydrochloric acid to produce aminomethylated PPX (PPX-CH_2NH_2). A decrease in the concentration of chlorine with reaction time was observed (Figure 2.15, Table 2.1). As observed in Figure 2.16, the C_{1s} signal narrows upon reaction, indicating that the carbonyl and chloromethyl carbons are removed upon hydrolysis. The N_{1s} peak broadens, indicating that nitrogen is present as more than one species (PPX-$\underline{N}H_2$, PPX-$\underline{N}H_3^+Cl^-$ and residual amide PPX-$\underline{N}H_2C(O)CH_2Cl$). The intensity of the chlorine signal decreases and shifts to lower binding energy indicating that it is present as the chloride or that charging of the sample is occuring. The topography of the surface, as assessed by SEM, showed no change after hydrolysis.

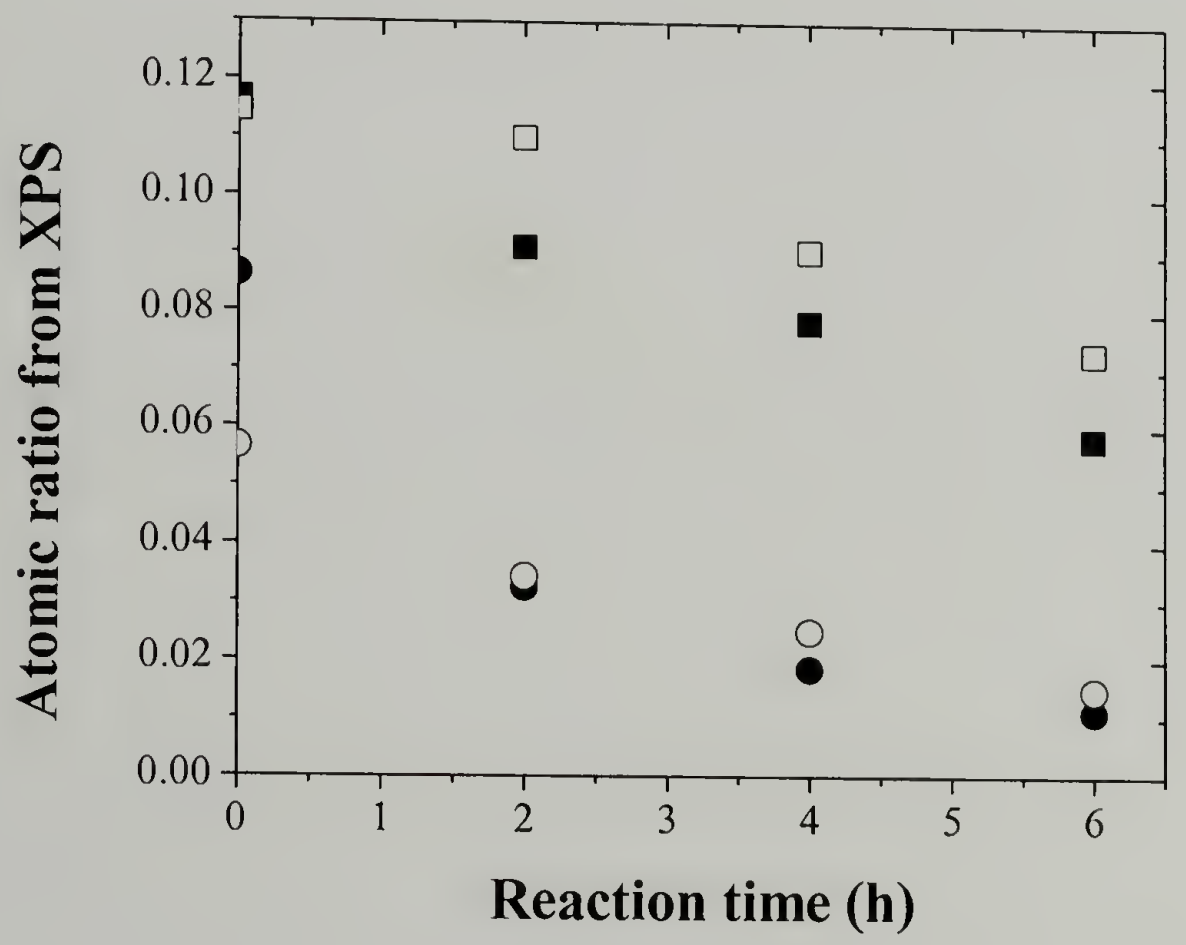

Figure 2.15. Atomic ratios for hydrolysis of the chloroamidomethyl group, determined by XPS for different take-off angles: Cl/C-15° (●), Cl/C-75° (○), N/C-15° (■), and N/C-75° (□).

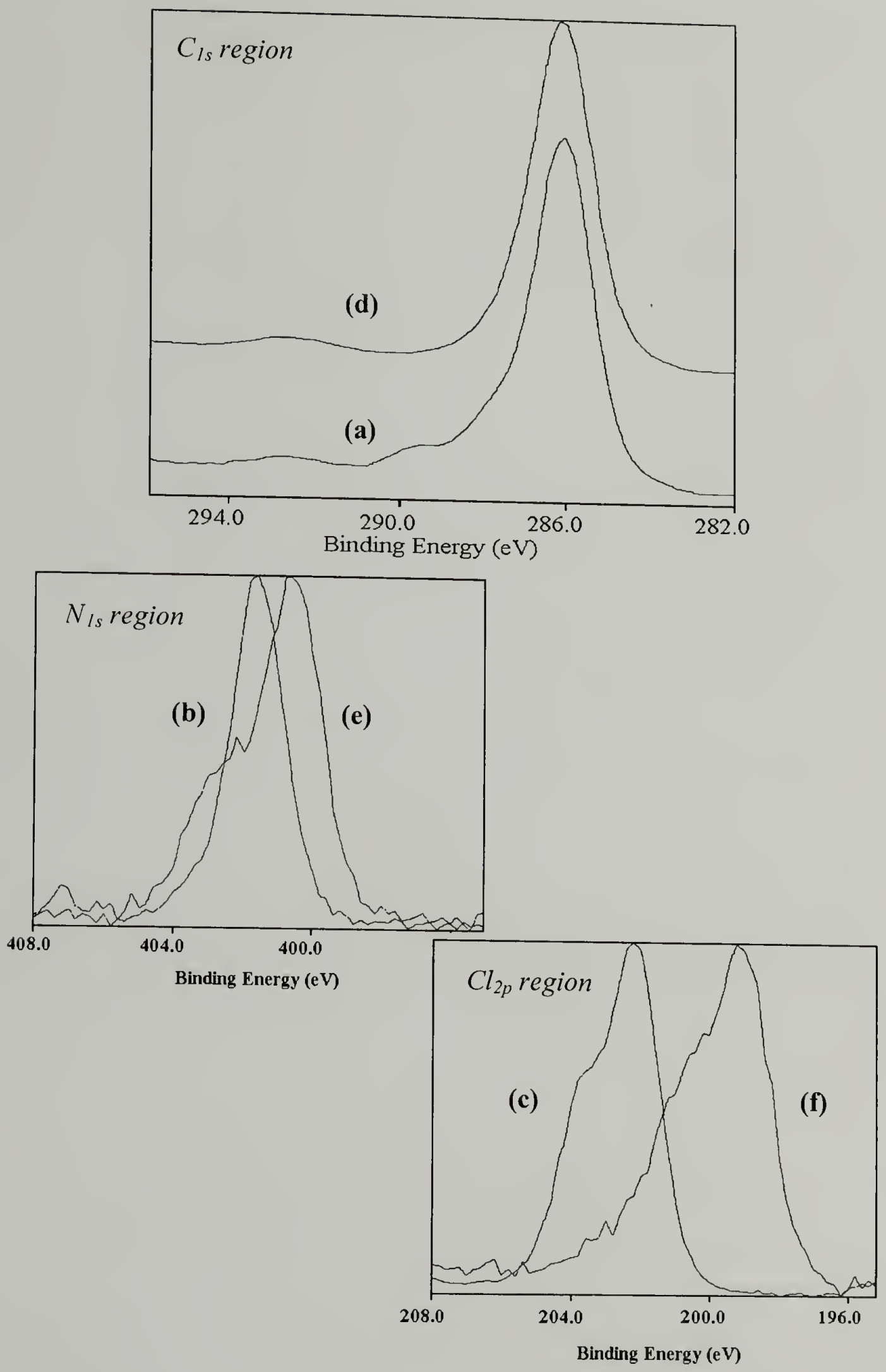

Figure 2.16. High-resolution XPS spectra of the C_{1s}, N_{1s}, and Cl_{2p} signals of PPX-$CH_2NHC(O)CH_2Cl$ (a, b, c) and PPX-CH_2NH_2 (d, e, f).

To further confirm aminomethylation, the films were derivatized with pentafluorobenzaldehyde (PFB). Film samples were thoroughly rinsed with sodium hydroxide and reverse osmosis-treated water before derivatization; PPX and PPX-$CH_2NHC(O)CH_2Cl$ were also reacted under the same conditions and served as references. The F_{1s} signal that appears after reaction and increases considerably with hydrolysis time (Table 2.1) is attributed to the presence of primary amine groups; the reaction of PFB with PPX and PPX-$CH_2NHC(O)CH_2Cl$ was negligible (F < 0.3%).

2.4.5. Alkylation and acylations of PPX

PPX film samples were modified through Lewis acid catalyzed chemistry using aluminum chloride and tin (IV) chloride. This type of chemistry has been widely studied for the synthesis of poly(styrene-divinylbenzene) cation exchange resins, the production of functionalized [2.2] paracyclophanes for use as chiral reagents,[52] and for the synthesis of modified poly(*p*-xylylene)s by direct pyrolysis of the paracyclophanes and polymerization of *p*-xylene.[24,27]

ATR IR analysis of the films confirmed that the reactions were strictly confined to the outermost surface of the sample since the characteristic signals of PPX remained unchanged and new signals were not observed. This was expected based on the high impermeability of PPX with respect to the organic solvents used. As assessed by XPS, an increase in the concentration of oxygen with reaction time was observed for all of the reactions. The presence of chlorine and fluorine for the reactions with 3-chloropropionyl chloride (CPC) and trifluoroacetic anhydride (TFAA), respectively, were further evidence of the reaction with PPX.

To estimate the degree of substitution for the reactions with succinic anhydride and propylene oxide, vapor phase derivatization of the films was carried out. Carboxylic acid groups were labeled with trifluoroethanol and hydroxylated-PPX was derivatized with trifluoroacetic anhydride. Fluorine, present in the XPS spectra of the derivatized films, confirmed that carboxylation and hydroxylation had been successful.

Surface compositions of the films showed that lower degrees of substitution had been obtained for acylations and alkylation compared to chlorosulfonation and chloroamidomethylation (Table 2.1). The highest yield was obtained when CPC was used ($C_{11}O_{1.6}Cl_{0.3}$ vs. $C_{11}OCl$) and the lowest corresponded to the reaction with propylene oxide ($C_{13}O_{0.7}F_{0.4}$ vs. $C_{13}O_2F_3$). This difference could be attributed to the higher reactivity of acyl chlorides to substitution and the lower reactivity of tin chloride compared to aluminum chloride as Friedel-Crafts catalyst.[53] Kinetics were studied for the acylation reactions and the results are presented in Figure 2.17. In general, an increase in the yield was observed with reaction time.

Regarding the effect of substitution on wettability, incorporation of polar groups (hydroxyl, carboxylic acid, and carbonyl) produced a decrease in water contact angle for all of the reactions (Table 2.1), the magnitude of which was dependent on the yield of the reaction and the substituent.

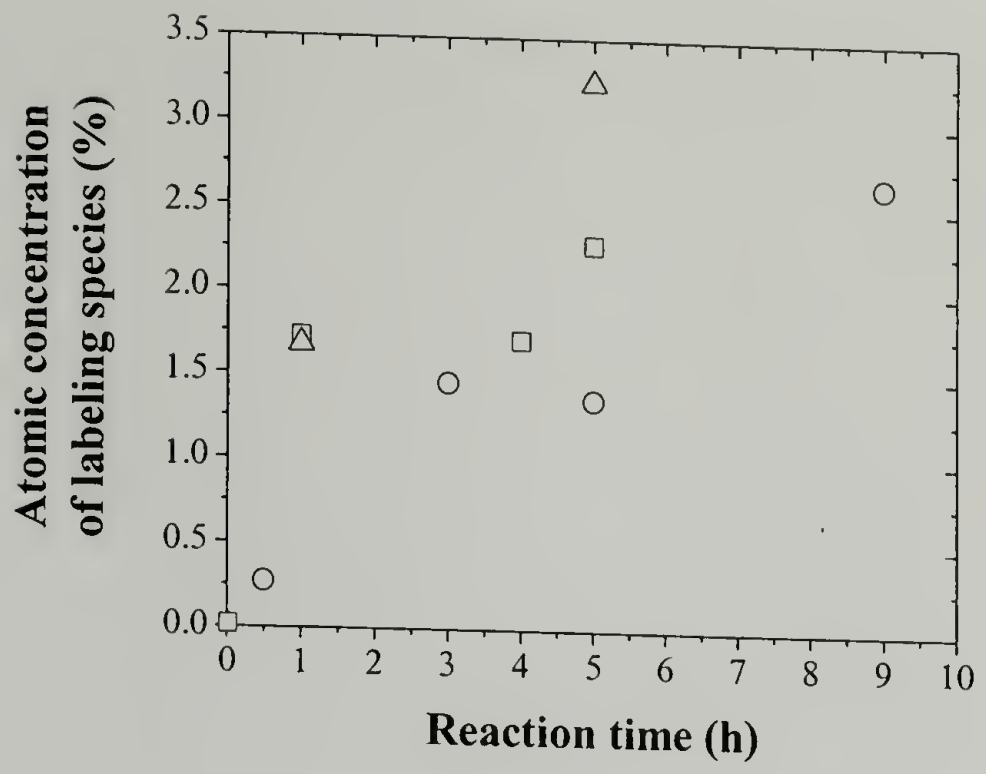

Figure 2.17. Kinetics of Fridel-Crafts acylations on poly(*p*-xylylene) film sufaces, determined by XPS. Acylations with trifluoroacetic anhydride (□, labeling species is F), 3-chloropropionylchloride (○, labeling species is Cl), and succinic anhydride (△, labeling species is F).

2.5. Conclusions

Free-standing poly(*p*-xylylene) thin films were functionalized through wet chemistry to introduce a variety of reactive groups to the aromatic ring. The yields and surface selectivity of the reactions were dependent on the interaction of the polymer with the reaction medium. Chlorosulfonation occurred readily in the bulk to produce sulfonyl chloride and sulfone functionalities. Chloroamidomethylation occurred to high yields at the near surface region; the extent of the reaction was time-dependent and presented a limiting behavior at approximately 4 h. Aminomethylated films were prepared by subsequent hydrolysis of the amide. Acylation and alkylation reactions were performed and incorporation of functional groups was evidenced by derivatization reactions. The yields were low due mainly to the lack of permeability of PPX by the organic solvents used, limiting the reactions to the surface.

2.6. References

1. Chen, W.; McCarthy, T. J. *Macromolecules* **1997**, *30*, 78.

2. Leväsalmi, J.-M.; McCarthy, T. J. *Macromolecules* **1997**, *30*, 1752.

3. Hsieh, M. C.; Farris, R. J.; McCarthy, T. J. *Macromolecules* **1997**, *30*, 8453.

4. Hsieh, M. C.; Farris, R. J.; McCarthy, T. J. *Macromolecules* **1997**, *30*, 8453.

5. Kozlov, M.; Quarmyne, M.; Chen, W.; McCarthy, T. J. *Macromolecules* **2003**, *36*, 6054.

6. Lu, Z.; McCarthy, T. J. *Polym. Prepr. (Am. Chem. Soc. Div. Polym. Chem.)* **2004**, *45*, 1051.

7. Kubono, A.; Okui, N. *Prog. Polym. Sci.* **1994**, *19*, 389.

8. Polymeric Materials Encyclopedia, CRC Press: New York, 1996; p 7171.

9. Kohlschütter, H. W.; Sprenger, L. *Z. Phys. Chem.* **1932**, *B16*, 284.

10. Kubono, A.; Okui, N. *Prog. Polym. Sci.* **1994**, *19*, 389.

11. Encyclopedia of Polymer Science and Engineering, John Wiley and Sons Inc.: New York, 1989; Vol. 17, p 990.

12. Vaeth, K. M.; Jensen, K. F. *Chem. Mater.* **2000**, *12*, 1305.

13 . Duffy, D. C.; Jackman, R. J.; Vaeth, K. M.; Jensen, K. F.; Whitesides, G. M. *Adv. Mater.* **1999**, *11*, 546.

14. Gorham, W. F. *J. Polym. Sci., Part A-1* **1966**, *4*, 3027. Beach, W. F. *Macromolecules* 1978, 11, 72. Errede, L. A.; Gregorian, R. S.; Hoyt, J. M. *J. Am. Chem. Soc.* **1960**, *82*, 5218.

15. Surendran, G.; Gazicki, M.; James, W.J.; Yasuda, H. *J. Polym. Sci., Part A: Polym. Chem.* **1987**, *25*, 1481.

16. Iwamoto, R.; Bopp, R.C.; Wunderlich, B. *J. Polym. Sci., Polym. Phys. Ed.* **1975**, *13*, 1925.

17. Nowlin, T. E.; Smith, D. F. *J. Appl. Polym. Sci.* **1980**, *25*, 1619.

18. Lahann, J.; Klee, D.; Thelen, H.; Bienert, H.; Vorwerk, D.; Hcker, H. *J. Mater. Sci.-Mater. Med.* **1999**, *10*, 443.

19. Yu, Q.; Deffeyes, J.; Yasuda, H. *Prog. Org. Coatings* **2001**, *41*, 247.

20. Martini, D.; Shepherd, K.; Sutcliffe, R.; Kelber, J.; Edwards, H.; San Martin, R. *Appl. Surf. Sci.* **1999**, *141*, 89.

21. Senkevich, J. J.; Yang, G.-R.; Lu, T.-M. *Colloids and surfaces A* **2003**, *216*, 167.

22. Senkevich, J. J.; Yang, G.-R.; Lu, T.-M. *Colloids and surfaces A* **2003**, *214*, 119.

23. Waters, J. F.; Sutter, J. K.; Meador, M. A. B.; Baldwin, L. J.; Meador, M. A. *J. Polym. Sci. Polym. Chem.* **1991**, *29*, 1917. Reich, H. J.; Cram, D. J. *J. Am. Chem. Soc.* **1969**, *13*, 3505. Reich, H. J.; Cram, D. J. *J. Am. Chem. Soc.* **1969**, *91*, 3527. Reich, H. J.; Cram, D. J. *J. Am. Chem. Soc.* **1969**, *91*, 3505. Guest, A.; Hoffman, P. H.; Nugent, M. J. *J. Am. Chem. Soc.* **1972**, *94*, 4241. Hopf, H.; Grahn, W.; Barret, D. G.; Gerdes, A.; Hilmer, J.; Hucker, J.; Okamoto, Y.; Kaida, Y. *Chem. Ber.* **1990**, *123*, 841. Pelter, A.; Crump, R. A. N. C.; Kidwell, H. *Tetrahedron Lett.* **1996**, *37*, 1273. Kane, V. K.; Gerdes, A.; Grhan, W.; Ernst, L.; Dix, I.; Jones, P. G., Hopf, H. *Tetrahedron Lett.* **2001**, *42*, 373.

24. Lahann, J.; Langer, R. *Macromolecules* **2002**,*35*, 4380.

25. Lahann J.; Höcker, H.; Langer, R. Angew. *Chem. Int. Ed.* **2001**, *40*, 726.

26. Lahann J.; Choi, I. S.; Lee, J.; Jensen, K. F.; Langer, R. *Angew. Chem. Int. Ed.* **2001**, *40*, 3166.

27. Lahann, J.; Balcells, M.; Rodon, T.; Lee, J.; Choi, I. S.; Jensen, K. F.; Langer, R. *Langmuir* **2002**, *18*, 3632.

28. Grenier, A.; Mang, S.; Schäfer, O.; Simon, P. *Acta Polymer.* **1997**, *48*, 1.

29. Szwarc, M. *Discuss. Faraday Soc.* **1947**, *2*, 46.

30. Gorham, W. F. *J. Polym. Sci. A-1* **1966,** *4*, 3027.

31. Itoh, T. Prog. *Polym. Sci.* **2001**, *26*, 1019.

32. Hitchman, M. L.; Jensen, K. F. Chemical Vapor Deposition: Principles and Applications; Academic Press: London, 1993.

33. Pierson, H. O. Handbook of Chemical Vapor Deposition, Noyes Publications: New York, 1992.

34. Göschel, U.; Walter, H. *Langmuir* **2000**, *16*, 2887.

35. Schmidt, C.; Stümpflen, V.; Wendorff, J. H.; Hasenhindl, A.; Gronski, W.; Ishaque, M.; Grenier, A. *Acta Polymer.* **1998**, *49*, 232.

36. Fortin, J. B.; Lu, T.-M. *Chem. Mater.* **2002**, *14*, 1945.

37. Ganguli, S.; Agrawal H.; Wang, B.; McDonald, J. F.; Lu, T.; Yang, G.-R.; Gill, W. N. *J. Vac. Sci. Technol. A* **1997**, *15*, 3138.

38. Clark, D. T.; Thomas, H. R. *J. Polym. Sci. Polym. Chem. Ed.* **1977**, *15*, 2843.

39. Harrick, N. J. Internal Reflection Spectroscopy John Wiley and Sons: New York, 1967.

40. Teramoto, K. *Reactive Polymers* **1991**, *15*, 89.

41. Plattner, J. J.; Martin Y. C.; Smital, J. R.; Lee, C-M.; Fung, A. K.; Horrom, B. W.; Crowley, S. R.; Pernet, A. G.; Bunnell, P. R.; Kim K. H. *J. Med. Chem.* **1985**, *28*, 79.

42. Nakayama, Y.; Takahagi, T.; Soeda, F.; Hatada, K.; Nagaoka, S.; Suzuki, J.; Ishitani, A. *J. Polym. Sci. A* **1998**, *26*, 559.

43. Park, B. D.; Lee, H. I.; Ryoo, S. J.; Lee, Y. S. *Tetrahedron Letters* **1997**, *38*, 591.

44. Hutt, D. A.; Leggett, G. J. *Langmuir* **1997**, *13*, 2740.

45. Waters, J.F.; Sutter, J.K.; Meador, M.A.; Baldwin, L.J.; Meador, M.A. *J. Polym. Sci., Part A: Polym. Chem.* **1991**, *27*, 1917.

46. Chilkoti, A.; Ratner, B. D.; Briggs, D. *Chem. Mater.*, **1991**, *3*, 51.

47. Schaverien, C.J.; Ernst, R.; Schut, P.; Skiff, W.M. *J. Am. Chem. Soc.* **1998**, *120*, 9945.

48. Surendran, G.; Gazicki, M.; James, W.J.; Yasuda, H. *J. Polym. Sci., Part A: Polym. Chem.* **1987**, *25*, 1481.

49. Bogoczek, R.; Kociolek-Balawedjer, E. *Reactive Polymers* **1986**, *4*, 311.

50. Sochilin, V. A.; Pebalk, A. V.; Semenov, V. I.; Kardash, I. Ye. *Polymer Science* **1991**, *33*, 1426.

51. For reviews see: Zaugg, H. E.; Martin, W. B. Org. React. 1965, 14, 52. van Bommel, K. J. C.; Westerhof, F.; Verboom, W.; Reinhoudt, D. N. *J. Prakt. Chem.* **1999**, *341*, 284. Pastushok, V. N.; Hu, K.; Bradshaw, J. S.; Dalley, N. K.; Bordunov, A. V.; Lukyanenko, N. G. *J. Org. Chem.* **1997**, *62*, 212.

52. Reich, H. J.; Cram, D. J. *J. Am. Chem. Soc.* **1969**, *91*, 3527. Reich, H. J.; Cram, D. J. *J. Am. Chem. Soc.* **1969,** *91*, 3505. Guest, A.; Hoffman, P. H.; Nugent, M. J. *J. Am. Chem. Soc.* **1972**, *94*, 4241. Hopf, H.; Grahn, W.; Barret, D. G.; Gerdes, A.; Hilmer, J.; Hucker, J.; Okamoto, Y.; Kaida, Y. *Chem. Ber.* **1990**, *123*, 841. Pelter, A.; Crump, R. A. N. C.; Kidwell, H. *Tetrahedron Lett.* **1996**, *37*, 1273. Kane, V. K.; Gerdes, A.; Grhan, W.; Ernst, L.; Dix, I.; Jones, P. G., Hopf, H. *Tetrahedron Lett.* **2001**, *42*, 373.

53. Olah, G. "Friedel-Crafts and related reactions", John Wiley and Sons: London, 1963; Vol. 1.

CHAPTER 3

FABRICATION OF POLY(*p*-XYLYLENE) NANOTUBES BY A TEMPLATE-ASSISTED METHOD

3.1 Introduction

In recent years there has been enormous interest in reducing the dimensions of objects, both from scientific and technological perspectives. This miniaturization has lead to increasing research towards the fabrication of nanostructures, or structures with one of their dimensions on a length scale of less than 100 nm. For example, polymer nanoparticles have found potential applications in biomedical sciences as vehicles for enzyme encapsulation, DNA transfection, biosensors, and drug delivery;[54] conducting polymer nanotubes and nanowires can be used in nanosized transistors, displays, sensors, or molecular wires; chemically-modified silica nanotubes have been applied for the enantiomeric separation of drugs.[55] Because of their ease of fabrication, spherical nanoparticles are most commonly used for such applications, however tubular structures represent an important alternative, since, compared to nanospheres, they possess larger inner volumes, distinct inner and outer surfaces that can be independently modified to impart different functionalities at both surfaces, and open ends. Encapsulation by the use of nanotubes could potentially be achieved by filling the tubes with the desired substance and capping the open ends, an easier method would be to fabricate nanotubes open only at one end.[56]

Undoubtedly, the most common method of fabrication of organic (polymeric) and inorganic nanotubes and nanofibers is by template-assisted methods, also known as template synthesis, where tubes of the desired material are deposited along the walls of

a porous template. The dimensions of the tubes are limited by the pore size (diameter and length) of the template. Due to their availability and precise control over pore dimensions, the most widely studied templates have been anodized aluminum membranes, although zeolite nanochannels, MCM mesoporous materials, and polymeric membranes have also been used. Fabrication of inorganic nanotubes or nanowires by templating with porous aluminum oxide membranes has been accomplished through sol-gel chemistry to produce silica[56] and zinc oxide nanotubes[57] and by electrodeposition of gold.[58] On the other hand, polymeric nanotubes or nanofibrils have been obtained by wetting the pores with a polymer melt or solution,[59,60] and by vapor deposition polymerization.[63-67] Fabrication of polymeric nanotubes is of particular interest since these can be used to produce carbon nanotubes with controlled dimensions and aligned in regular patterns.[61,62]

The fabrication of polymer nanotubes by vapor deposition polymerization has been accomplished using two different templating approaches. In the first method, poly(*p*-xylylene) nanotubes were fabricated by using polymer nanofibers as templates, a method referred to as TUFT (tubes by filler templates).[63] The templating materials consisted of electrospun nylon 4/6 and poly(L-lactide) fibers with diameters of tens of nanometers. Removal of the template by thermal degradation or solvent extraction produced poly(*p*-xylylene) nanotubes, whose internal diameter was limited by the external diameter of the fibers. When electrospinning was done in the presence of palladium (II) diacetate as a conductivity modifier, subsequent removal of the template by heat treatment produced PPXN/Pd hybrid tubes.

The second approach is by vapor deposition polymerization on porous templates. Conversely to the previous method, in this case the outer diameter of the nanotubes is fixed by the inner diameter of the template. Poly(phenylene vinylene) (PPV) nanotubes were prepared by a two step process consisting of the polymerization of α, α'-dichloro-*p*-xylenc insidc the pores of alumina (200 nm pore size) or polycarbonate filters (100 nm and 10 nm pore sizes), followed by dehydrochlorination by heat treatment under vacuum.[64] This method provided tubular or rod-like PPV structures. Compared with PPV bulk films, these nano-objects exhibited longer photoluminescence decay times and higher photoluminescencc efficiencies. The same approach was used to synthesize polypyrrole[65] and poly(furfuryl alcohol)[66,67] nanotubes and thermally convert them to carbon nanotubes. In thesc cases, the template was impregnated with ferric chloride or *p*-toluenesulfonic acid that served as initiator for the polymerization of pyrrole or furfuryl alcohol, respcctively. Wall thickness, or the inner diameter of the tubes, was controlled by varying the concentration of monomer and polymerization conditions. In addition to the production of nanotubes, vapor deposition polymerization on porous substrates can also be used to modify the surface energy of pore walls. Recent studies on the confinement of block copolymers inside cylindrical pores have found that the morphologies observed are strongly influenced by the copolymer period and the imposed curvature, but also by the surface energy of the pore walls,[68] which can be modified through chemistry to preferentially segregate one phase of the block copolymer to the walls.

While vapor deposition polymcrization has certain advantagcs over other tcmplate-synthcsis techniques, such as the absencc of solvents and problems associated

with dewetting phenomena, its major drawback is the fact that the rates of deposition are, on occasions, too fast to allow film thickness uniformity to be achieved along the length of the templates; the tubes essentially become blocked at their ends (membrane surface) with a lower amount of material deposited within.[69] The thickness uniformity is dependent on the 'sticking coefficient' of a particle, which is defined as the probability of a particle to fix onto a solid surface at a single collision. Its value ranges between one and zero and species with low sticking coefficients are able to form more uniform coatings on substrates with complex geometry. *P*-xylylene is reported to have a low sticking coefficient (2.0×10^{-5} at 60 °C to 1.4×10^{-3} at -60 °C),[70] which allows the monomer to penetrate into small pores and confined spaces, hence its applicability in the coating industry.

Several models have been proposed to explain the effect of the variables that determine the thickness uniformity of poly(*p*-xylylene) films. Tolstopyatov[71] and Broer and Luijks[72] have used macroscopic conservation equations of momentum and mass to explain the influence of deposition temperature and partial pressure of the monomer, on the thickness profile in long but narrow channels of aspect ratios (height/width) on the order of $1x10^3$ to $1x10^4$. In both approaches, it was assumed that the length of the molecule mean free path exceeds the channel cross-section, limiting the flow inside the channels by molecular collisions (molecular flow). In Tolstopyatov's model the relative coating thickness or the ratio of the absolute film thickness at a given point x to that at the open surface, δ/δ_o, is dependent on the temperature, pressure, and the order of the deposition process (n). As observed in Figure 3.1, decreasing the monomer pressure will improve the thickness uniformity, however it will also decrease the rate of

deposition. Broer and Luijks also eonelude that deereasing monomer pressures with corresponding low deposition rates, results in inereasing penetration properties.

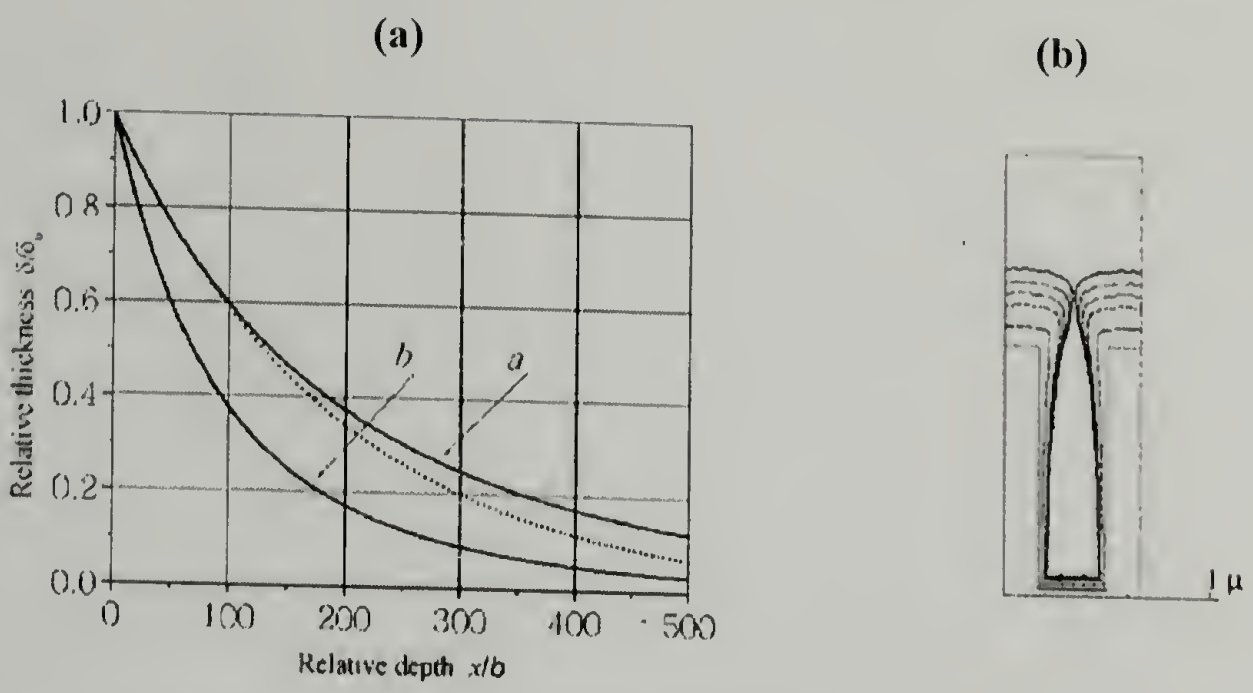

Figure 3.1. (a) PPXN eoating thiekness distribution in ehannel (flat elearanee, room temperature).[71] Broken eurve: $n = 1$, $k = 1\times10\text{-}7$ kg $m^{-2}s^{-1}Pa^{-1}$; full eurves: $n = 2$, $k = 2 \times 10\text{-}8$ $kgm^{-2}s^{-1}Pa^{-1}$. (a) $Po = 2$ Pa; (b) $Po = 8$ Pa. (b) Caleulated feature profiles at the end of deposition (inner field).[73] Film thiekness at field edges is roughly 115% of that at the field eenter. Figure eorresponds to an aspeet ratio of 3.

However, when the dimensions of the features approaeh the mean-free path of the monomer, these eontinuum models are no longer valid. Rodgers and Jensen[73] proposed instead simultaneous solutions of reaetor seale and feature seale environments using a linking method, based on the average number of eneounters that moleeules entering from the maeroseopie environment have with the substrate surfaee. A hybrid Monte Carlo approaeh was used, whieh ineluded the effeets of feature size heterogeneity and transport resistanee, and the reaetor seale problem was solved with a finite element method. The results are then matehed to ensure eontinuity aeross the maero-miero interfaee. The system studied eonsisted of 0.33 μm wide trenehes with aspeet ratios of 2 and 3. They found that film uniformity suffers eonsiderably with the introduetion of

microscale heterogeneity and that the growth of the entire surface is depressed. As presented in Figure 2, during deposition the features are filled thus changing the effective area presented to the macroscopic environment. Eventually, the features begin to close rapidly, causing the exposed surface to resemble a featureless flat substrate; their profile shows limited deposition on the bottom and side walls.

This chapter describes the fabrication of poly(*p*-xylylene) nanotubes, prepared by the template synthesis method, using commercial aluminum oxide membranes as the templating material. The nanotubes prepared, open either at both or only on one end, were functionalized by a chloroamidomethylation reaction to hydrophilize the inner walls of the nanotubes. The results obtained from this study prove that this method can be used not only to fabricate nanostructures with well-defined chemical characteristics, but also, as a method to control the surface energy of porous materials.

3.2. Experimental

3.2.1 Materials

All reagents were used as received, unless otherwise indicated. [2.2]paracyclophane, N-methylol-2-chloroacetamide, 1-nitropropane, polystyrene (Mw = 280,000 g/mol), sodium hydroxide, ethanol, and methanol were purchased from Aldrich. Sulfuric acid, hydrochloric acid (37%), xylenes, and aluminum oxide membranes (Whatman Anodisc, 200 nm nominal pore diameter) were obtained from Fisher. [2.2] paracyclophane was sublimed prior to vapor deposition polymerization. Silicon wafers were supplied by International Wafer Service (100 mm diameter, 100 orientation, P/B doped, 20-40 ohm-cm resistivity). Wafers were cut into 1 cm × 0.5 cm

pieces, rinsed with reverse osmosis treated water, dried at 125 °C for 20 min, and cleaned by exposure to oxygen plasma for 5 min immediately prior to deposition experiments.

3.2.2 Methods

Scanning electron microscopy (SEM) images were acquired on a JEOL JSM 6320 F instrument; a thin layer of gold was sputtered on the samples prior to characterization. Ellipsometric measurements were made using a Rudolph Research SL-II ellipsometer with a He-Ne laser light source (λ = 632.8 nm). The angle of incidence used was 70°. Film thickness was measured at three different spots for each sample and calculated using a DafIBM software from the ellipsometric parameters Δ and ψ. The refractive indices used were 1.462 for SiO_2 and 1.661 for poly(*p*-xylylene). X-ray photoelectron spectroscopy (XPS) spectra were recorded on a Physical Electronics Quantum 2000 Scanning ESCA Microprobe with MgK_α excitation at 15 kV and 5 W for a probing size of 20 μm. All spectra were acquired at a 45° take-off angle with respect to the plane of the sample surface. Transmission electron microscopy (TEM) images were obtained on a JEOL 100CX instrument, using Electronic Microscopy Systems carbon-coated copper grids with a mesh size of 400. Sample preparation was done by dispersing the nanotubes in ethanol and placing a drop of the suspension on a carbon-coated grid. Reactive-ion etching (RIE) was done on a South Bay Technology Inc. RIE-200.

3.2.3 Fabrication of closed-end templates

The procedure followed for the fabrication of the closed-end templates is similar to the one used for fabricating polymer "pencils", recently reported by our group.[74] A

30% wt solution of polystyrene (PS) in xylene was prepared and cast onto a clean glass slide with the aid of a 125 μm gap applicator. The film was allowed to dry for 3 days at room temperature. The supported PS film was heated to 200 °C on a hot-plate for 5 min, after which aluminum oxide membranes were placed on top of the molten film and a small amount of pressure was applied to ensure adequate contact between the membrane and the polymer. The side of the membrane in contact with the polystyrene melt is the top one (see Figure 3.2). After 1 h, the supported film/membrane was slowly cooled to room temperature and subsequently peeled-off the glass slide. These composite templates will be referred to as PS/Al_2O_3 membranes.

3.2.4 Vapor Deposition Polymerization

Polymerization of [2.2]paracyclophane was carried out in a home-built reactor modeled after the one reported by Gorham. [2.2]paracylophane was sublimed at 75 °C (± 2 °C), followed by pyrolysis at 675 °C, and deposition at 21 °C (±0.5 °C); the system pressure was maintained between 35 mTorr and 40 mTorr. In a typical experiment, 0.1 g of [2.2] paracyclophane was loaded into the sublimation section with the aid of a glass boat, and the membranes were placed inside the deposition chamber, along with clean silicon wafers. The system was evacuated to the base pressure (35-40 mTorr) for 3 h prior to deposition, during which time both the pyrolysis oven and the deposition section were allowed to equilibrate at their operating temperatures. The sublimation section was then heated and the 'deposition time' was considered once the temperature in this section reached 75 °C. Once polymerization time had elapsed, sublimation and pyrolysis sections were cooled to room temperature and the system was back-filled with air. The samples were removed from the reactor and placed in clean scintillation vials

for further modification or characterization. To be consistent with the nomenclature, the alumina templates coated with poly(*p*-xylylene) will be identified as Al_2O_3/PPX, while the coated composite templates will be referred to as PS/Al_2O_3/PPX.

3.2.5. Chloroamidomethylation

Functionalization of PPX-coated alumina or alumina/PS membranes was done following the procedure established previously for the chemical surface modification of free-standing poly(*p*-xylylene) films.[75] 1 g of N-methylol-2-chloroacetamide was dissolved in a mixture of sulfuric acid (3.5 mL) and 1-nitropropane (7.5 mL). PPX-coated membranes were immersed in the solution and allowed to react for 4 h. After this time, the membranes were rinsed with 2 × 10 mL of methanol and immersed into 20 mL of clean methanol for 12 h. Samples were dried under a delicate stream of nitrogen and stored in clean glass scintillation vials for characterization.

Chloroamidomethylated-PPX samples will be referred to as PPX-$CH_2NHC(O)CH_2Cl$.

3.2.6. Template removal and isolation of individual nanotubes

Al_2O_3/PPX membranes were broken in half (along the diameter of the membrane) to expose the underlying alumina template. Samples were then immersed in an ethanolic solution of hydrochloric acid (1:1 vol.), and maintained at constant temperature (50 °C) for 12 h. The same procedure was followed for the functionalized membranes. For the case of PS/Al_2O_3/PPX membranes, removal of the alumina template preceded removal of the polystyrene template, which was done by immersion in xylene for 24 followed by drying under a gentle stream of nitrogen.

3.3. Results and Discussion

The membranes used in this study were commercially available alumina membranes with a nominal pore size of 200 nm, produced by anodization of aluminum. The process of anodization creates a growing front of hexagonally packed pores (ideally) in an alumina matrix with an oxide/metal interface at the base of the pores. In order to cleave this interface and detach a porous film of alumina open on both ends, the anodization voltage is gradually decreased; chemical attack at the oxide/metal interface occurs, causing the pores to divide into smaller pores, thus producing asymmetric structures open on both ends.[76] The asymmetry of the pores along the longitudinal direction, with respect to their size and density, is observed from the SEM images and illustrations presented in Figure 3.2. The side of the membranes with smaller pores (diameter ~168 nm) and with a honeycomb structure will be identified as the 'top' side, while the side with the larger pores (diameter ~258 nm) will be referred to as the 'bottom' side. Coating with poly(*p*-xylylene) was done by exposing the membranes to *p*-xylylene vapor for varying periods of time. A schematic of the reactor setup is presented in Figure 3.3. Clean silicon wafers also served as substrates for polymerization since a precise value of the film thickness can be obtained from ellipsometric measurements on these substrates. The membranes were placed inside the deposition reactor with their longitudinal direction parallel or perpendicular to the flow of monomer. No noticeable differences, in terms of film thickness, were observed from preliminary experiments so further depositions were carried out using the former orientation.

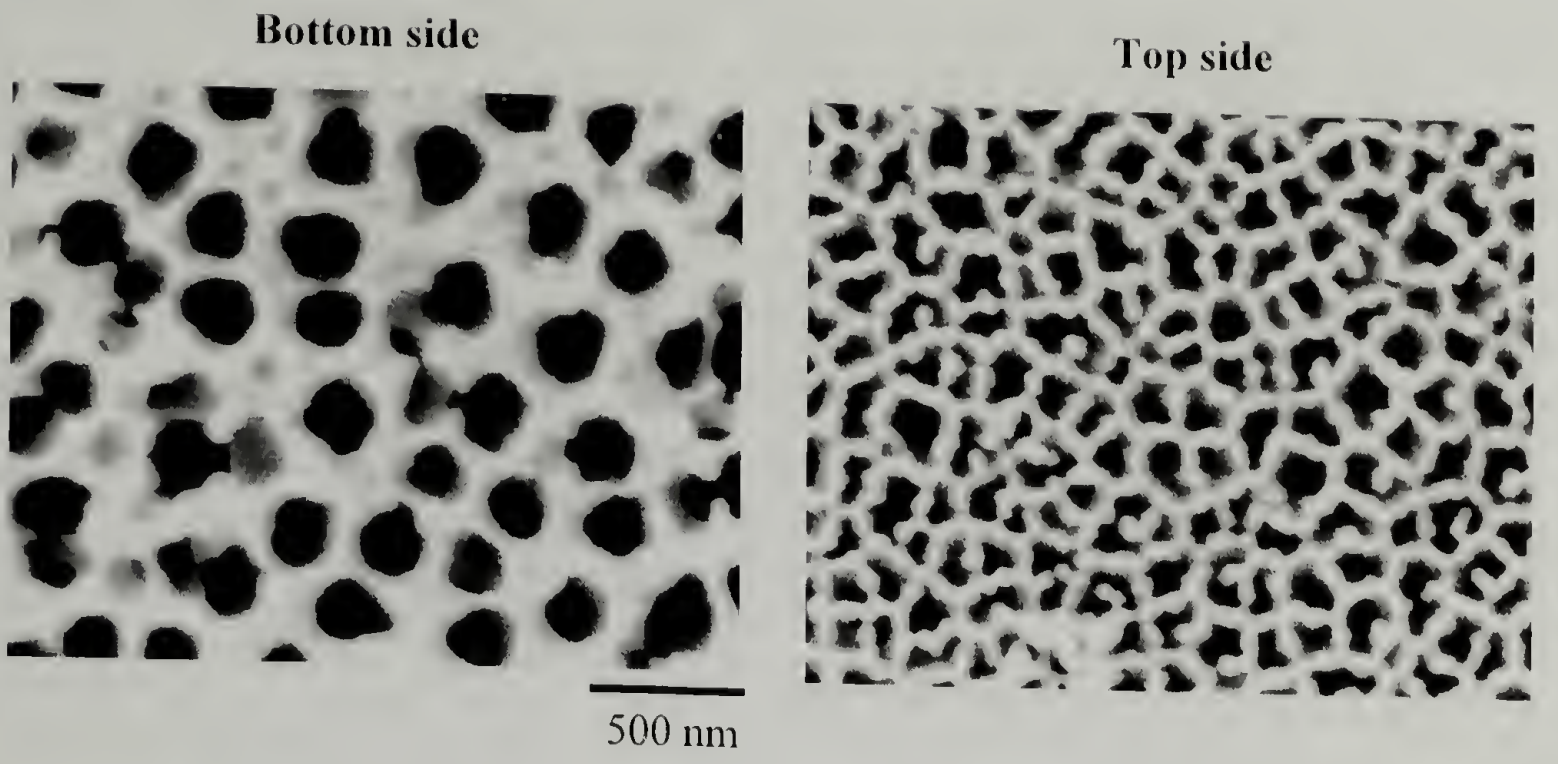

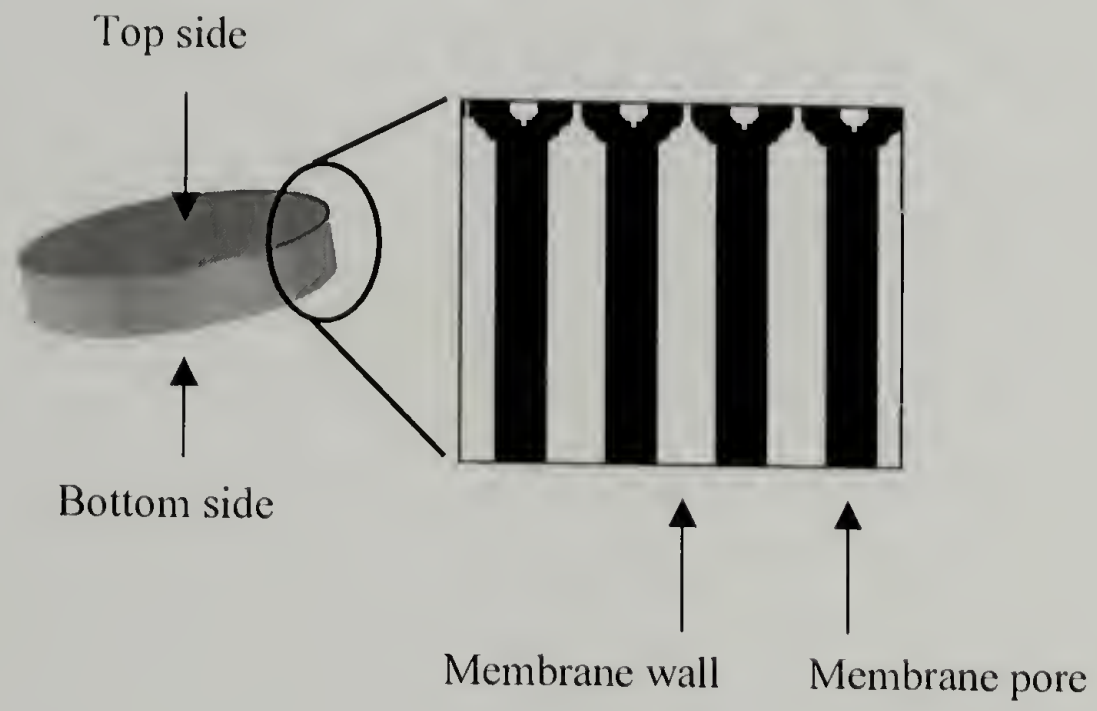

Figure 3.2. FESEM images and schematic of commercial alumina membranes, illustrating the asymmetry of the pores.

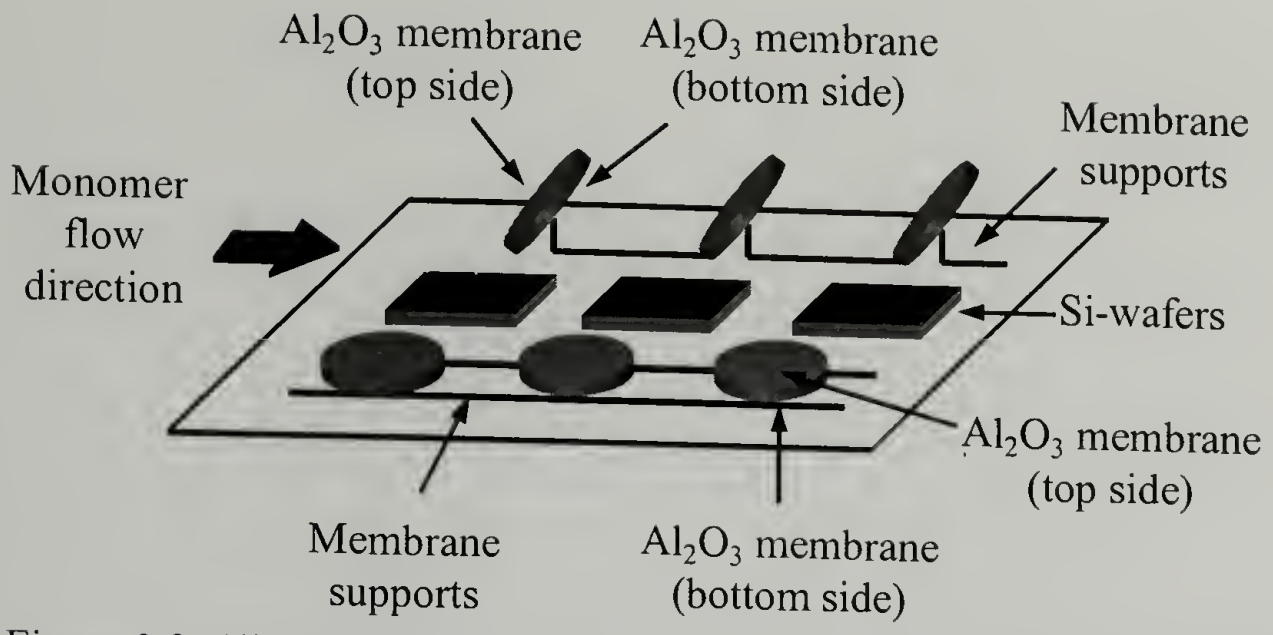

Figure 3.3. Illustration of the sample setup inside the deposition chamber.

As mentioned previously, one of the difficulties of using chemical vapor deposition techniques in the template synthesis approach for the fabrication of nanostructures is the thickness uniformity of the films along the pores of the membranes. Experimental and modeling results show that the thickness distribution of a chemical vapor deposited film is inversely proportional to the deposition rate; therefore low partial pressures and high deposition temperatures are favored. The effect of deposition time on the pore diameter of the membranes, or poly(*p*-xylylene) film thickness, was determined by FESEM and TEM of the coated membranes, and by ellipsometry measurements on reference silicon wafers. FESEM images of Al_2O_3/PPX membranes are presented in Figures 3.4 and 3.5, where a considerable decrease in pore diameter is observed with deposition time. The roughness of the coating is attributed to the inherent roughness of the membrane surface, as observed in Figure 3.4 (a), where depressions on the walls in between the pores are observed.

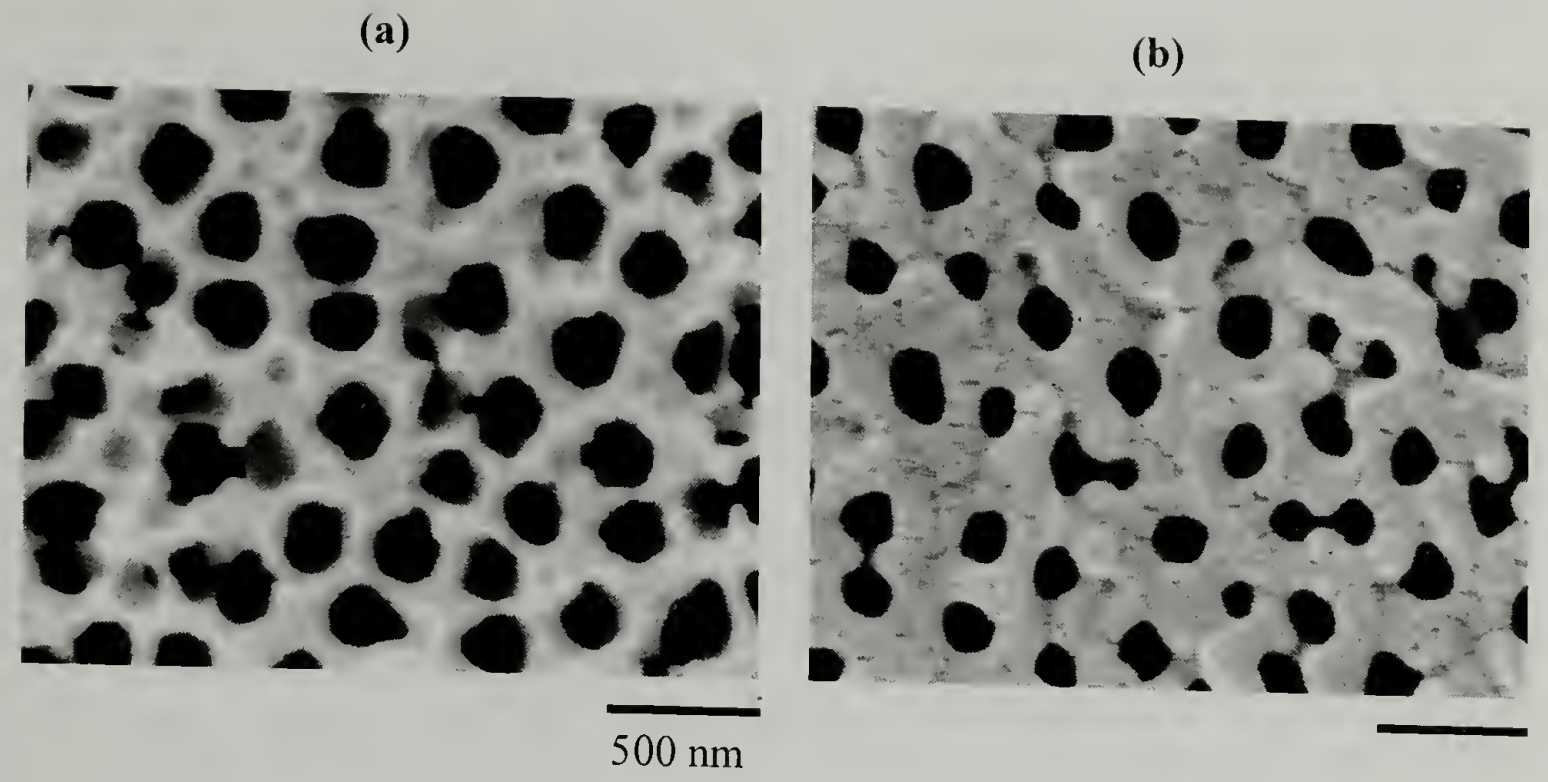

Figure 3.4. FESEM images of poly(*p*-xylylene)-coated aluminum oxide membranes (bottom side of the membrane). Reaction conditions: $T_{sublimation}$ = 75 °C, $T_{pyrolysis}$ = 675 °C, $T_{deposition}$ = 21 °C, system pressure = 35 mTorr. Deposition times are 0 min (a), 100 min (b), 130 min (c), and 170 min (d). Scale bar corresponds to 500 nm for all cases.

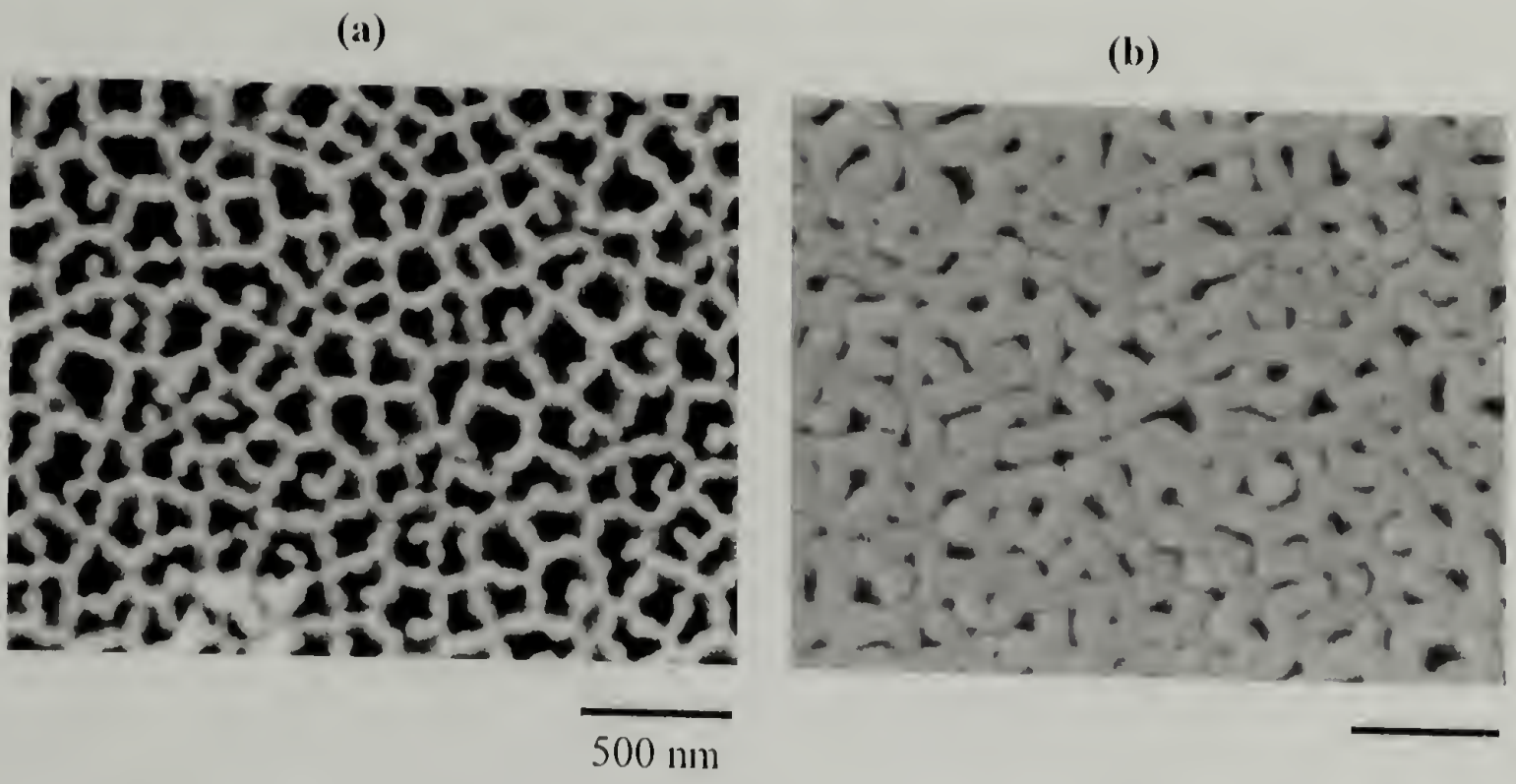

Figure 3.5. FESEM images of poly(*p*-xylylene)-coated aluminum oxide membranes (top side of the membrane). Reaction conditions: $T_{sublimation}$ = 75 °C, $T_{pyrolysis}$ = 675 °C, $T_{deposition}$ = 21 °C, system pressure = 35 mTorr. Deposition times are 0 min (a) and 100 min (b). Scale bar corresponds to 500 nm for both cases.

The pore diameter, measured from the 'bottom' surface of the membranes, was plotted as a function of deposition time and the results are presented in Figure 3.6; the data points correspond to the average pore diameter measured for 25 pores, the error bars are the standard deviation. As is the case for deposition on a flat, featureless surface, the data can be correlated by a linear function. The rate of deposition, determined from the slope, is approximately 0.57 nm/min. More precise measurements were obtained from ellipsometric measurements on silicon substrates, as presented in Figure 3.7. The film thickness from FESEM measurements was calculated with the final diameter at a given time referenced to the initial pore diameter. The difference between the ellipsometric thickness and that determined from FESEM is attributed to the lack of precision of the latter measurement and is not specific to the chemical nature

of the substrate since aluminum and silicon are both non-inhibitors of poly(*p*-xylylene) growth.[77] Measured by ellipsometry, the rate of deposition was estimated to be 0.50 nm/min, similar to the result obtained from FESEM.

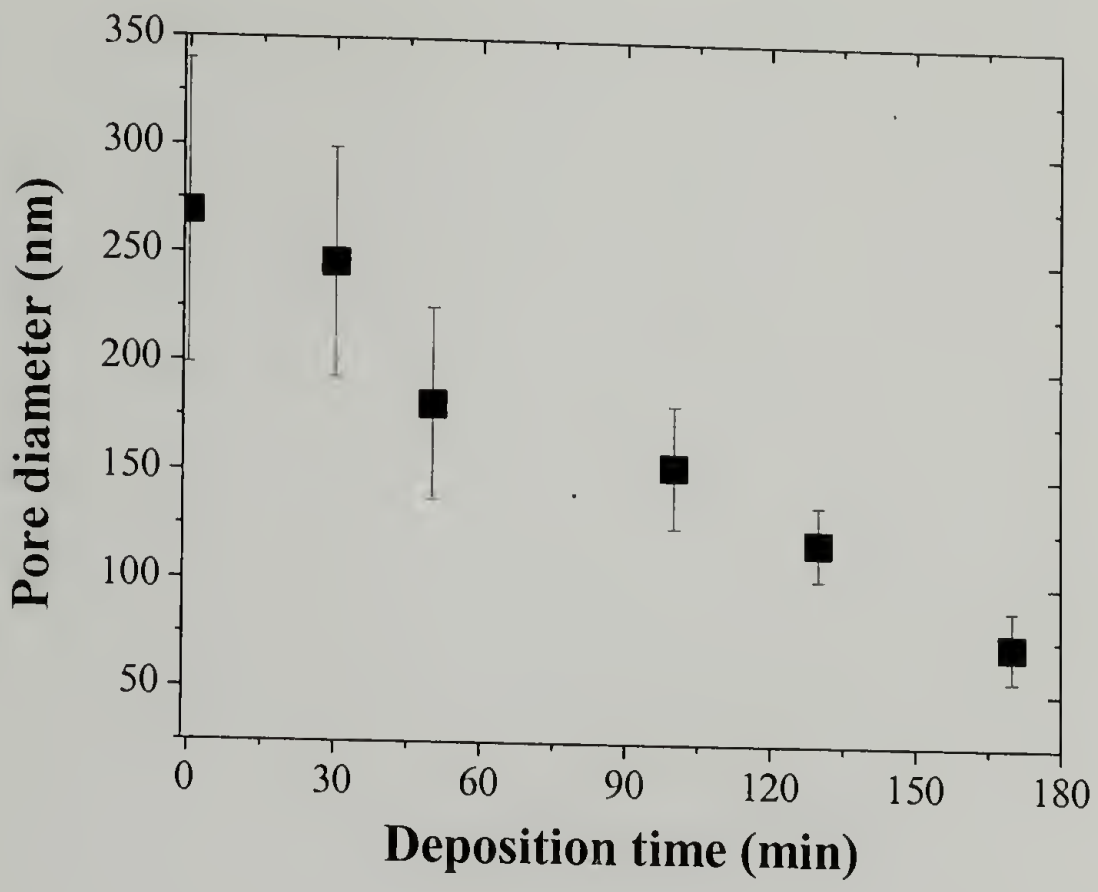

Figure 3.6. Pore diameter of Al_2O_3/PPXN membranes as a function of the deposition time, measured from FESEM images. Reaction conditions: $T_{sublimation}$ = 75 °C, $T_{pyrolysis}$ = 675 °C, $T_{deposition}$ = 21 °C, system pressure = 35 mTorr.

Film uniformity along the longitudinal direction was determined by dissolving the alumina template. This was accomplished by cutting the membrane along its diameter to expose the underlying alumina, followed by immersion in an ethanolic hydrochloric acid solution for 24 h at 55 °C. Figure 3.8 shows the PPX nanotubes formed inside the pores. The surface layers, present at the top and bottom sides of the membrane, maintain the nanotubes joined and the length of the nanotubes (~ 58 μm) agrees well with the thickness of the membranes (60 μm). In absence of the underlying

template, collapsing of the nanotubes is observed and attributed to their lack of structural stability at high aspect ratios (L/D = 60 μm/0.2 μm = 300). The outer diameter of the nanotubes (~ 280-300 nm) is similar to that measured from the membrane surface (270 nm) and the asymmetry along the longitudinal direction is also well replicated. The pores are believed to be smooth since no defects were observed on the nanotube surface, however the poly(*p*-xylylene) replica showed that the pores along the alumina membrane are not perfect and show the structural defects of the membranes near the top (honeycomb-structure) side of the membrane.

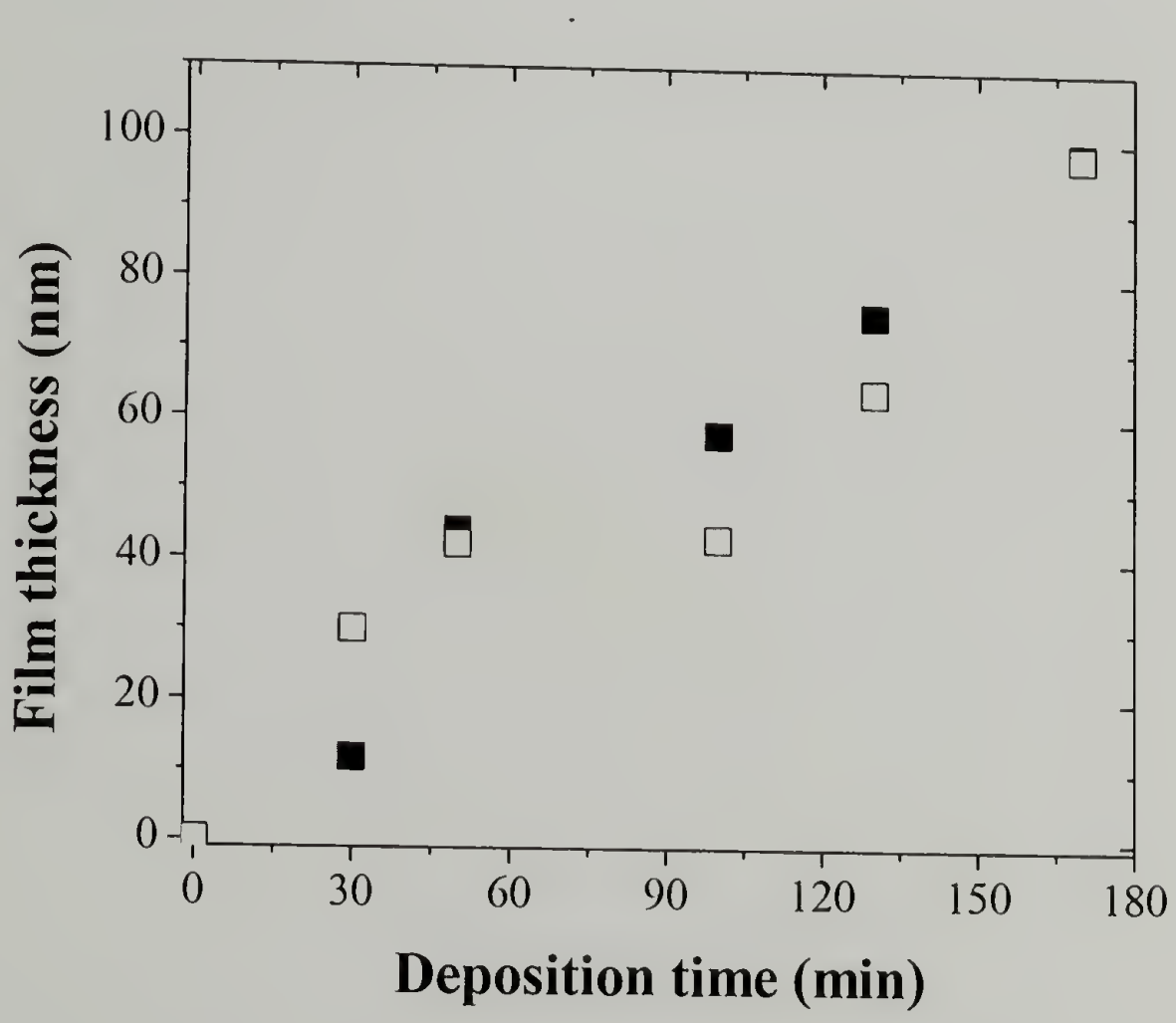

Figure 3.7. PPX film thickness as a function of the deposition time, measured by ellipsometry on reference Si-wafers (□) and calculated from FESEM images of Al_2O_3/PPXN membranes (■). Reaction conditions: $T_{sublimation}$ = 75 °C, $T_{pyrolysis}$ = 675 °C, $T_{deposition}$ = 21 °C, system pressure = 35 mTorr.

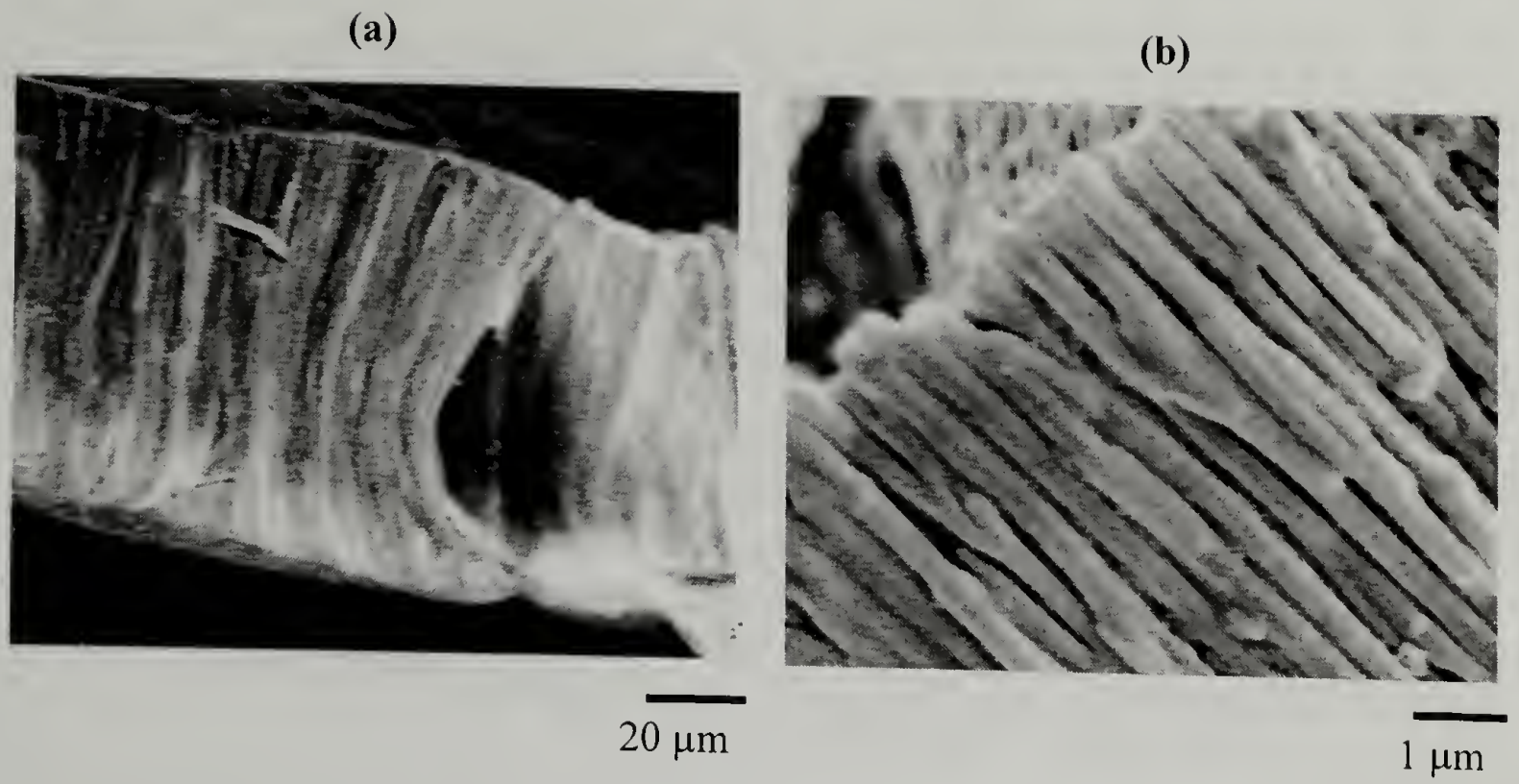

Figure 3.8. FESEM cross-section images of PPX nanotubes after removal of the template.

While FESEM analysis revealed information regarding the outer surface of the nanotubes, TEM analysis was used to determine the thickness uniformity of the film inside the pores. Isolation of individual nanotubes was done by removal of the template followed by sonication in ethanol, to separate the nanotubes from the surface layer. Sonication resulted in a suspension of aggregates of different sizes. Drops of the suspension were placed on a carbon-coated grid for TEM analysis; FESEM analysis was done by filtering the suspension through a nucleopore membrane with 0.02 μm pores.

FESEM analysis revealed that two different morphologies were observed after sonication, depending on sonication time. As observed in Figure 3.9, both individual nanotubes and joined nanotubes were obtained. The measured diameter in both cases was approximately 280 nm, regardless of the polymerization time, which is expected since the outer diameter is dictated by the inner diameter of the template. The individual nanotubes (Figure 3.9, b) show that sonication has a detrimental effect on the structure of the nanotubes. While they can be separated from the surface layer, bending and breaking of the nanotubes also occurs. As image (c) shows, either during drying or filtering, some nanotubes flatten out, forming what appear to be ribbons. The measured thickness of the ribbons is approximately 450 nm, which agrees well with one-half the length of the circumference of the tubes, considering an external diameter of 280 nm. This morphology indicates that in FESEM measurements, the diameter of the nanotubes can vary between approximately 280 nm, when they maintain their original shape, to 450 nm, when they have collapsed to form ribbons.

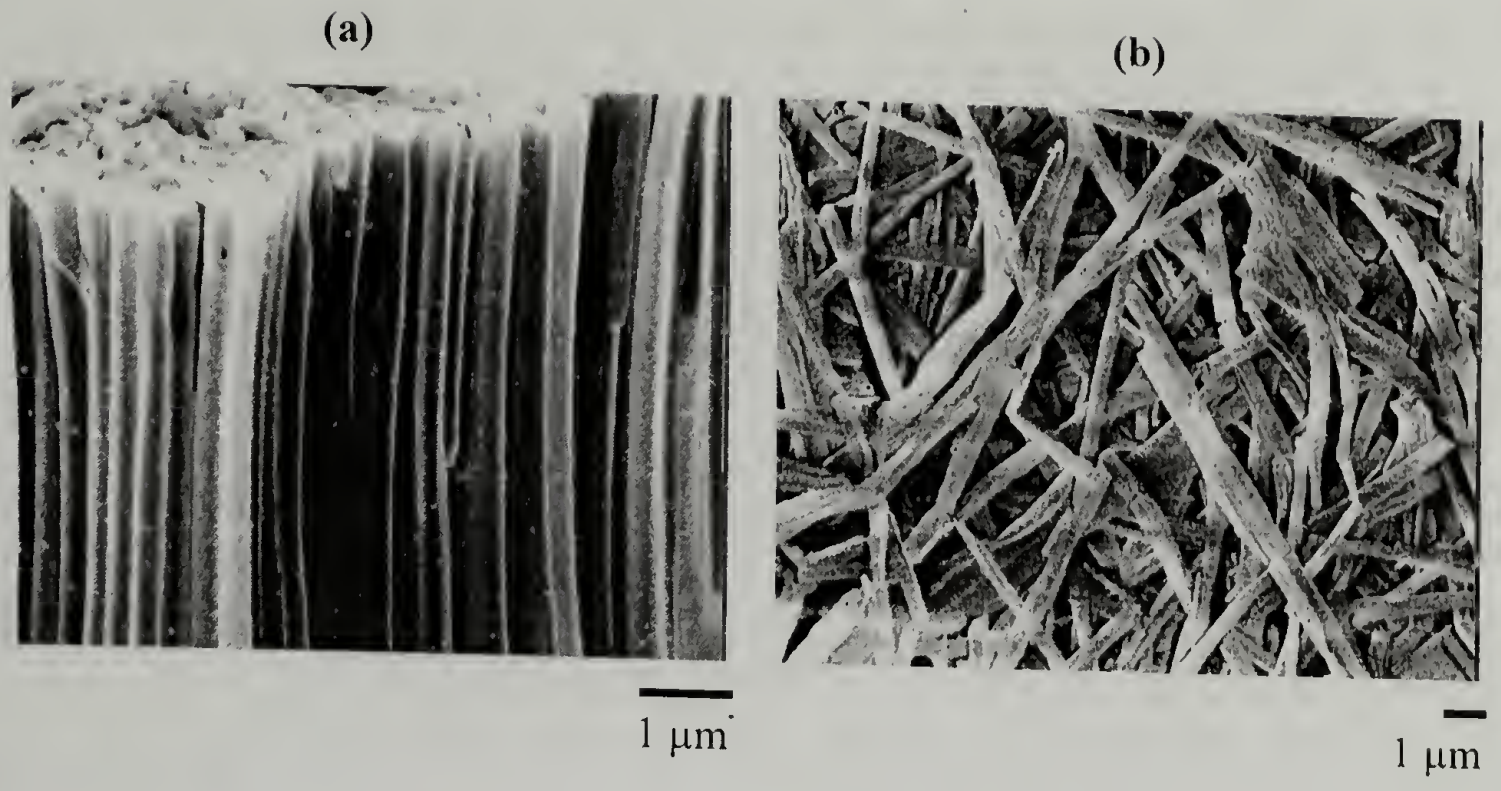

Figure 3.9. FESEM images of PPX nanotubes obtained after removal of the template, followed by sonication in ethanol. The inner diameter of the nanotubes, estimated by FESEM measurements, is 65 nm.

TEM analysis did not provide additional information regarding the inner diameter of the nanotubes, regardless of the thickness of the poly(*p*-xylylene) coating. As shown in Figure 3.10, nanotubes of different diameters were observed. This difference is attributed to folding, which occurs predominantly at the edges of the tubes, and is identified as the darker regions along the length of the tubular structures. Due to the thickness of the poly(*p*-xylylene) walls (ranging 30 nm to 100 nm, approximately) it was not possible to look through the tubes to determine film uniformity.

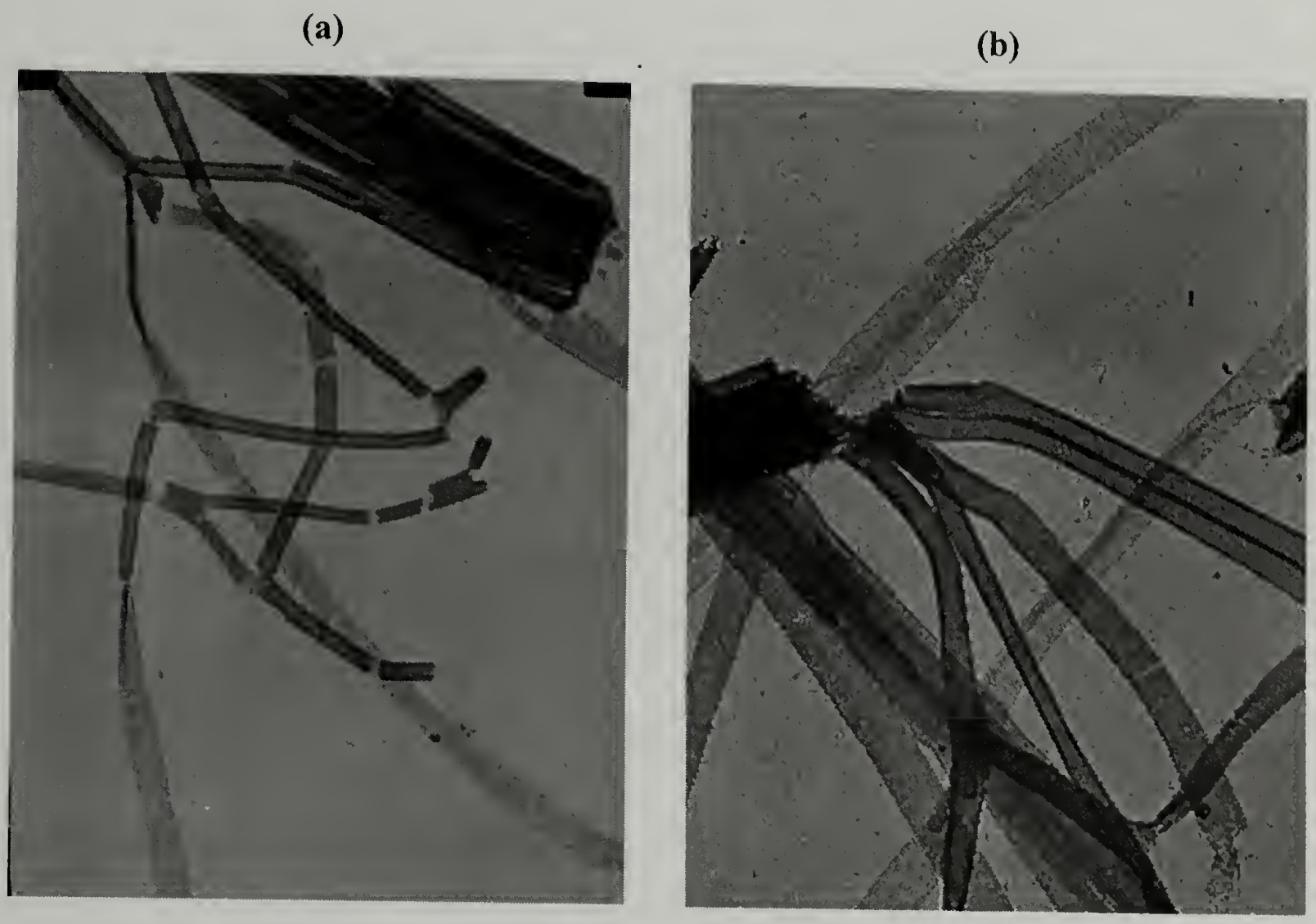

Figure 3.10. TEM images of PPX nanotubes obtained after removal of the template, followed by sonication in ethanol. The inner diameter, determined by FESEM, was 65 nm (a) and 113 nm (b).

Deposition of poly(*p*-xylylene) along the pore walls of the membranes allows not only control over the pore diameter, but also control over the pore's surface energy. We have shown that post-deposition chemical surface modification of poly(*p*-xylylene) is possible and that the extent of reaction strongly depends on the interaction of the medium with the polymer. We chose the chloroamidomethylation reaction for surface modification of the inner walls of the poly(*p*-xylylene) nanotubes since we are interested in hydrophilizing the inside of the tubes. Al_2O_3/PPX membranes were functionalized by reaction with N-methylol-2-chloroacetamide at atmospheric pressure followed by rinsing with methanol; the functionalized membranes will be referred to as Al_2O_3/PPX-$CH_2NHC(O)CH_2Cl$. The chemical composition of the two functionalized surfaces was analyzed. The first consists of an Al_2O_3/PPX membrane that was functionalized and then cut along its diameter to expose the inside of the nanotubes; the second is an Al_2O_3/PPX membrane that was cut along its diameter to expose the nanotubes and then functionalized. XPS analysis of these surfaces was done by probing sections with a 20 μm spot size and the results are presented in Tables 3.1 and 3.2. The membrane that was cut after functionalization shows aluminum and oxygen signals that are ascribed to the alumina template; an excess of oxygen, with respect to the theoretical composition of Al_2O_3, is observed for all cases, and is attributed to the creation of new and very rough surfaces. The presence of sulfur suggests that unreacted sulfuric acid remains after washing, or/and that sulfonation of poly(*p*-xylylene) occurred. In previous studies on free-standing poly(*p*-xylylene) films we found that sulfonation occurred to a negligible degree with respect to chloroamidomethylation, resulting in concentrations of sulfur considerably lower than those of nitrogen and chlorine (<1% S vs. 6.05% Cl,

8.38% N), so the former hypothesis seems to be correct. Also, as mentioned in the previous chapter, the radical chain ends, when in contact with air, form peroxides leading to an increased concentration of oxygen-containing species. The presence of nitrogen and chlorine suggest that chloroamidomethylation did occur inside the poly(*p*-xylylene) nanotubes. The relative concentration of nitrogen and chlorine varies depending on pore size, however more important is their composition relative to carbon. The yield, estimated considering a composition of $C_{11}NOCl$ for monosubstitution, was approximately 89%, which is slightly lower than the degree of substitution obtained for free-standing films under analogous reaction conditions. The second type of surface analyzed was that where the reaction occurred after exposing the inside of the nanotubes (Table 3.1). Chloroamidomethylation is confirmed by the presence of nitrogen and chlorine, however, aluminum was not observed and a lower concentration of oxygen was obtained, suggesting that the reaction medium, mainly concentrated sulfuric acid, dissolves the alumina template. Also, sulfur was not present, confirming the hypothesis that rinsing by immersion in methanol was insufficient to remove the sulfuric acid.

Table 3.1. Surface atomic composition of the cross-section of Al_2O_3/PPX-$CH_2NHC(O)CH_2Cl$ membranes (cleaved prior to reaction).

C	O	N	Cl
73.2	16.0	6.6	4.2
69.5	16.7	7.8	6.0
79.3	9.4	6.9	4.3

Membrane pore size was 96 nm. [a] Determined by FESEM measurements. [b] Spectra acquired at a 45° take-off angle with a 20 μm spot size; top and bottom lines are two different data points on each sample.

Table 3.2. Surface atomic composition of the cross-section of Al_2O_3/PPX-$CH_2NHC(O)CH_2Cl$ membranes (reaction prior to cleaving).

Al_2O_3/PPX membrane pore size (nm) [a]	XPS Atomic composition (%) [b]					
	C	O	N	Cl	S	Al
65	11.7	60.7	0.9	0.6	1.5	24.7
	11.3	59.7	0.8	0.9	1.8	25.5
96	19.5	54.6	1.5	1.1	1.2	22.1
	19.4	55.0	1.6	1.3	1.1	21.7
113	34.4	48.7	2.5	1.1	1.9	11.4
	32.3	42.5	3.5	2.1	2.4	17.3

[a] Determined by FESEM measurements. [b] Spectra acquired at a 45° take-off angle with a 20 μm spot size; top and bottom lines for each diameter are two different data points on each sample.

After chloroamidomethylation the membranes were treated with an ethanolic solution of hydrochloric acid at 55 °C, which dissolves the alumina template, but can also lead to hydrolysis of the amide functionality, although this reaction is favored at higher temperatures (ethanol reflux, 78 °C) and prolonged periods of time (see Chapter 1). After removal of the template, the morphology of the membranes was analyzed by FESEM. As observed in Figure 3.11, SEM images show that the dimensions of the functionalized nanotubes did not change upon reaction, which is expected since poly(*p*-xylylene) does not swell in any of the solvents used for reaction or rinsing. Isolation of individual functionalized nanotubes was also attempted by sonication in ethanol. As for the non-functionalized nanotubes, longer sonication times resulted in larger amounts of dispersed nanotubes. Figure 3.12 presents the two typical morphologies observed after sonication, which are the same as for the non-functionalized nanotubes. As before,

some samples were damaged either due to handling or sonication and breaking of the nanotubes is observed (b), along with flattened nanotubes (c).

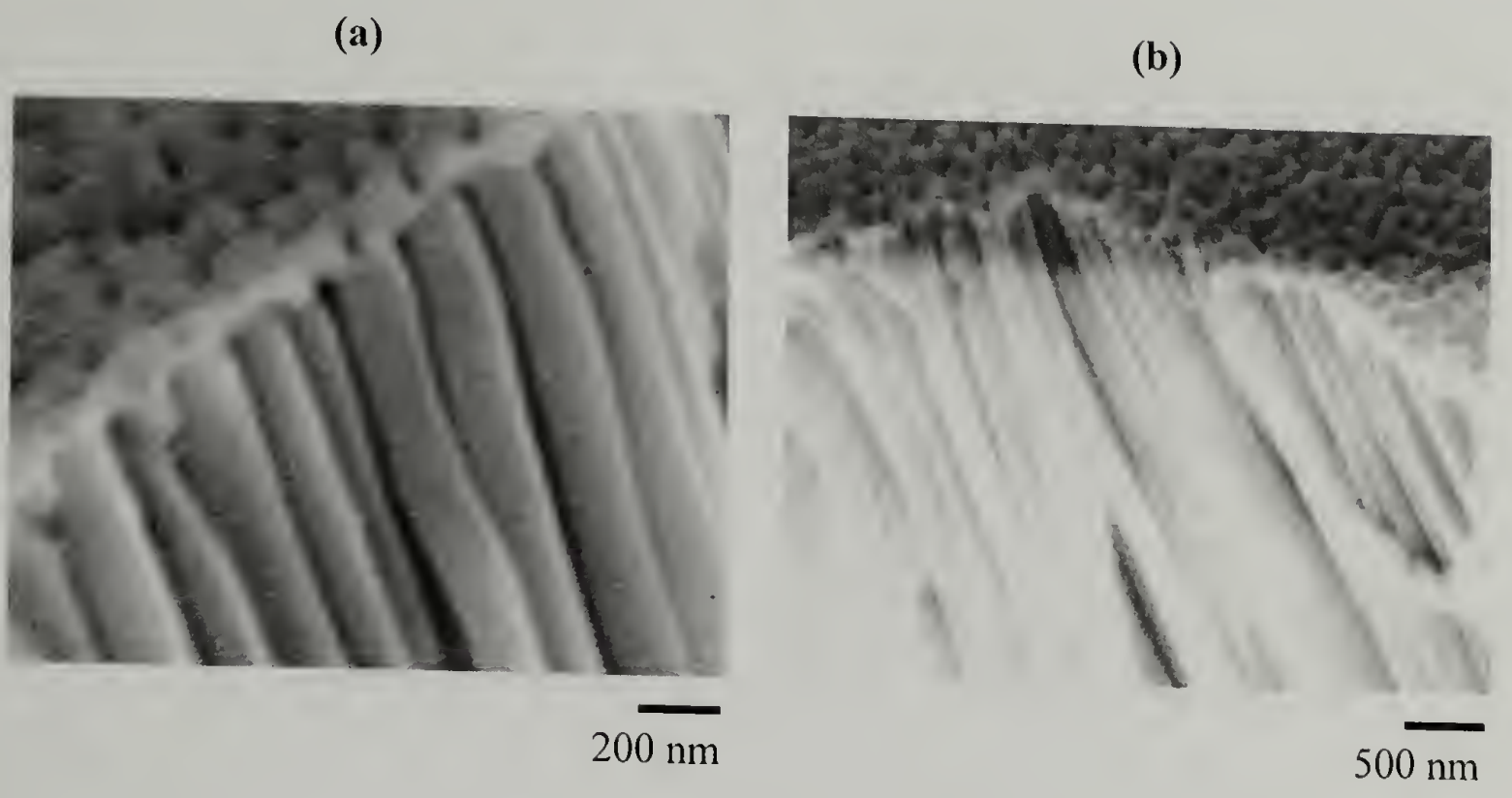

Figure 3.11. FESEM images of Al_2O_3/PPX-$CH_2NHC(O)CH_2Cl$ nanotubes after removal of the template. Images (a) and (b) correspond to a view of the cross-section, and image (c) is a view from the top. The pore diameter of the sample, estimated by FESEM measurements prior to modification, is 65 nm.

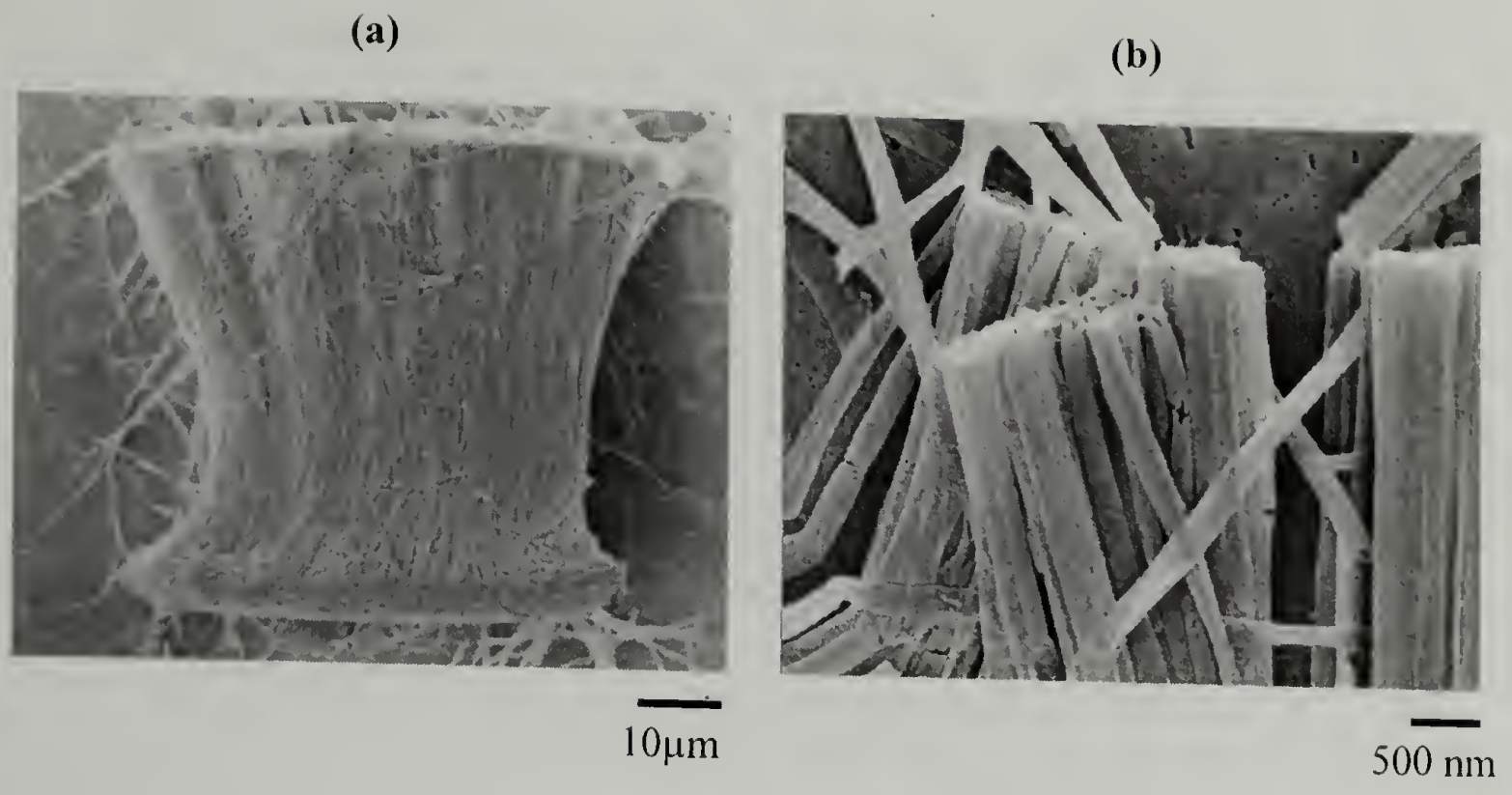

Figure 3.12. FESEM images of Al2O3/PPX-$CH_2NHC(O)CH_2Cl$ nanotubes after removal of the template and sonication for 2 min. The resulting suspensions were filtered through nucleopore membranes (pore diameter = 100 nm).

A second approach to isolating individual nanotubes was by removing the surface layers of PPX by reactive ion etching (RIE). Al_2O_3/PPX membranes (functionalized or not) were etched for 5 min. Discoloration of the polymer, due to oxidation, was observed after etching. The nanotubes remained joined upon removal of the template, indicating that the surface layer was not completely removed. Sonication of the membranes resulted in a suspension that was filtered to determine the effectiveness of this process. FESEM images of the nanotubes (functionalized and not) after removal of the template are presented in Figure 3.13. As before, the nanotubes were either joined at their ends by the surface layer or dispersed in the suspension, however, unlike the previous approach, severely damaged structures were also observed.

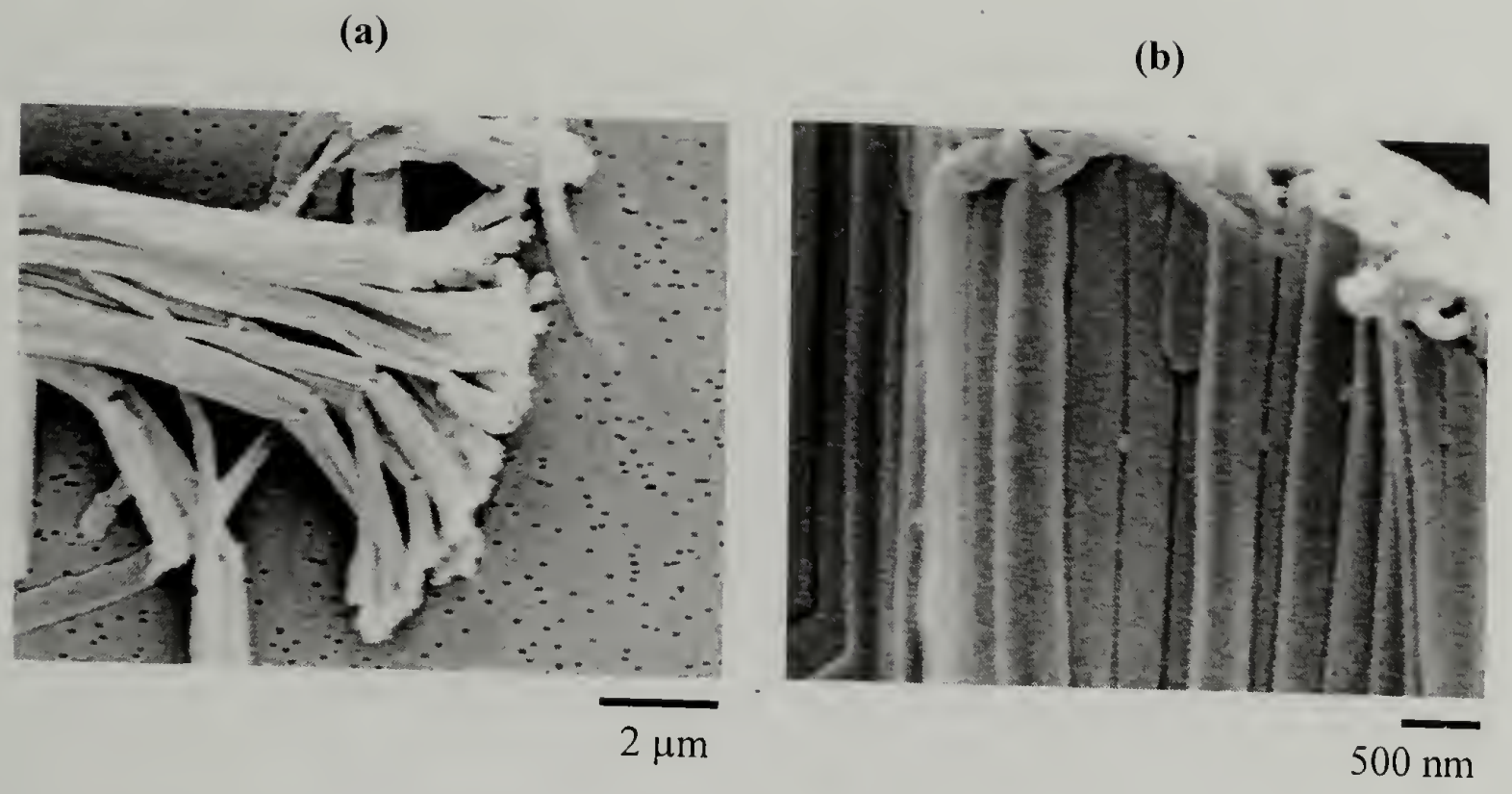

Figure 3.13. FESEM images showing the different morphologies observed during the isolation of individual Al_2O_3/PPX-$CH_2NHC(O)CH_2Cl$ nanotubes by RIE followed by sonication in ethanol.

Recently there have been great efforts in fabricating nanotubes closed at one end for potential applications as encapsulation media. The original idea proposed by Mirkin and collaborators, is based on the use of alumina/aluminum templates produced by the anodization of aluminum, followed by sol-gel chemistry to produce a replica of the closed-end tubes. Our approach to this end was the fabrication of poly (*p*-xylylene) nanotubes closed at one end using alumina/polystyrene templates. Polystyrene rods were grown inside alumina membranes by contacting the membrane with a supported polystyrene film at 200 °C; capillary action drives the polymer inside the pores where, once cooled, forms solid polymer rods. The temperature, degree of contact between the alumina template and the underlying polystyrene melt, and contact time will determine the length of the rods. Figure 3.9 shows the polystyrene rods formed inside the alumina membrane. The polystyrene rods bundle up after removal of the template as observed in Figure 3.9 (a), and their length, estimated from cross-section analysis was approximately 20 μm. As observed previously, the capillary forces that drive the molten polystyrene into the pores produce menisci at the ends of the rods.[74]

After exposure to *p*-xylylene vapor and removal of the templates, the nanotubes were analyzed by FESEM. Figure 3.13 (a) and (b) show the closed ends of the tubes. The measured diameter is approximately 610 nm, which is larger than the diameter of the nanotubes observed before, and also larger than the thickness of the nanotubes assuming that they had collapsed to form ribbons. Since the alumina template was removed prior to the polystyrene template, this increase in diameter can only be attributed to swelling of poly(*p*-xylylene) by xylene during removal of PS, producing an

irreversible change in dimensions, however mixed xylenes swell high molecular weight poly(*p*-xylylene) in a minor extent (< 2.1%).

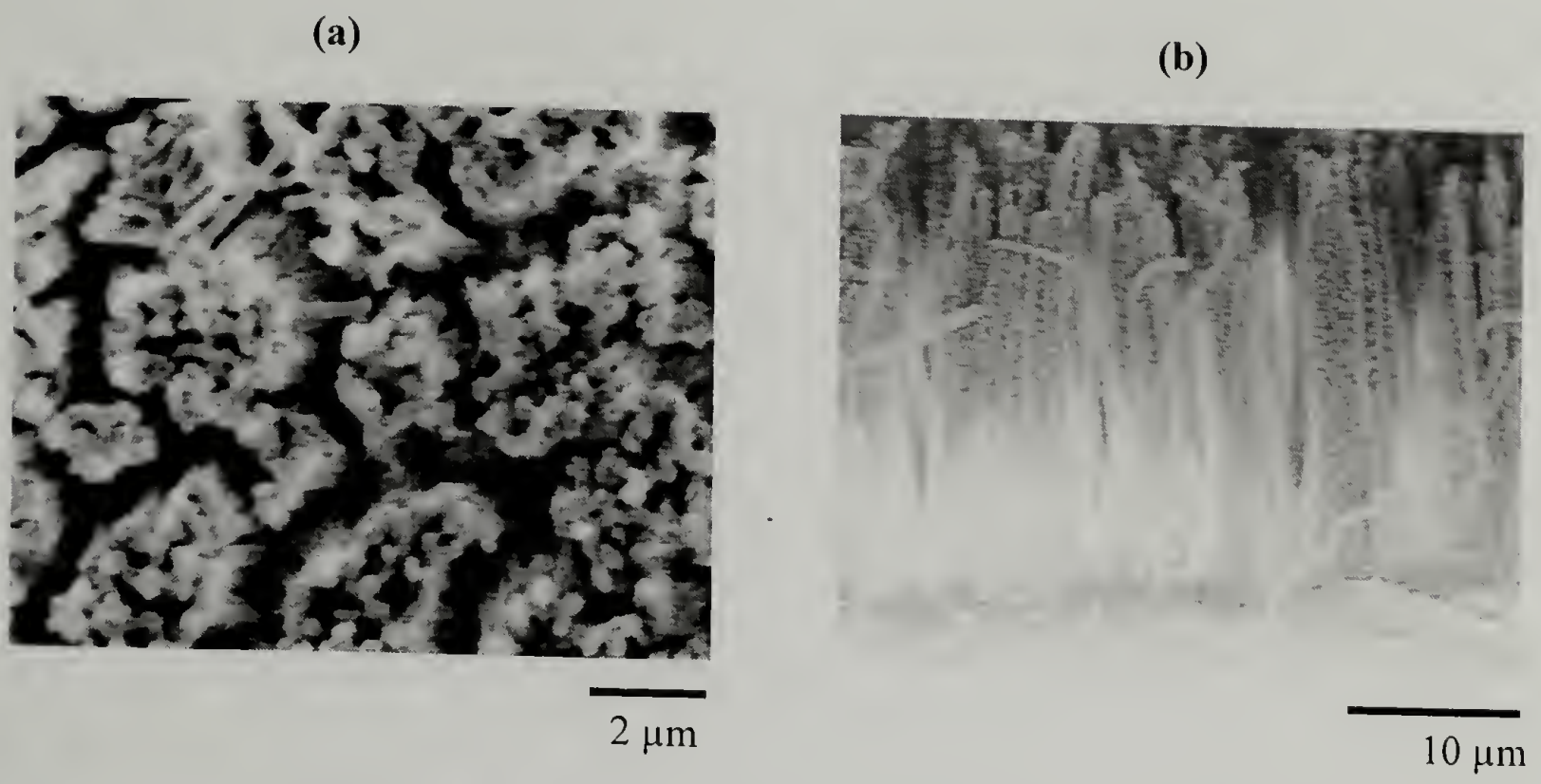

Figure 3.14. FESEM images of polystyrene (PS) nanorods grown inside an aluminum oxide membrane by melt flow. Image (a) shows bundled PS nanorods from a top view, while image (b) corresponds to the cross-section.

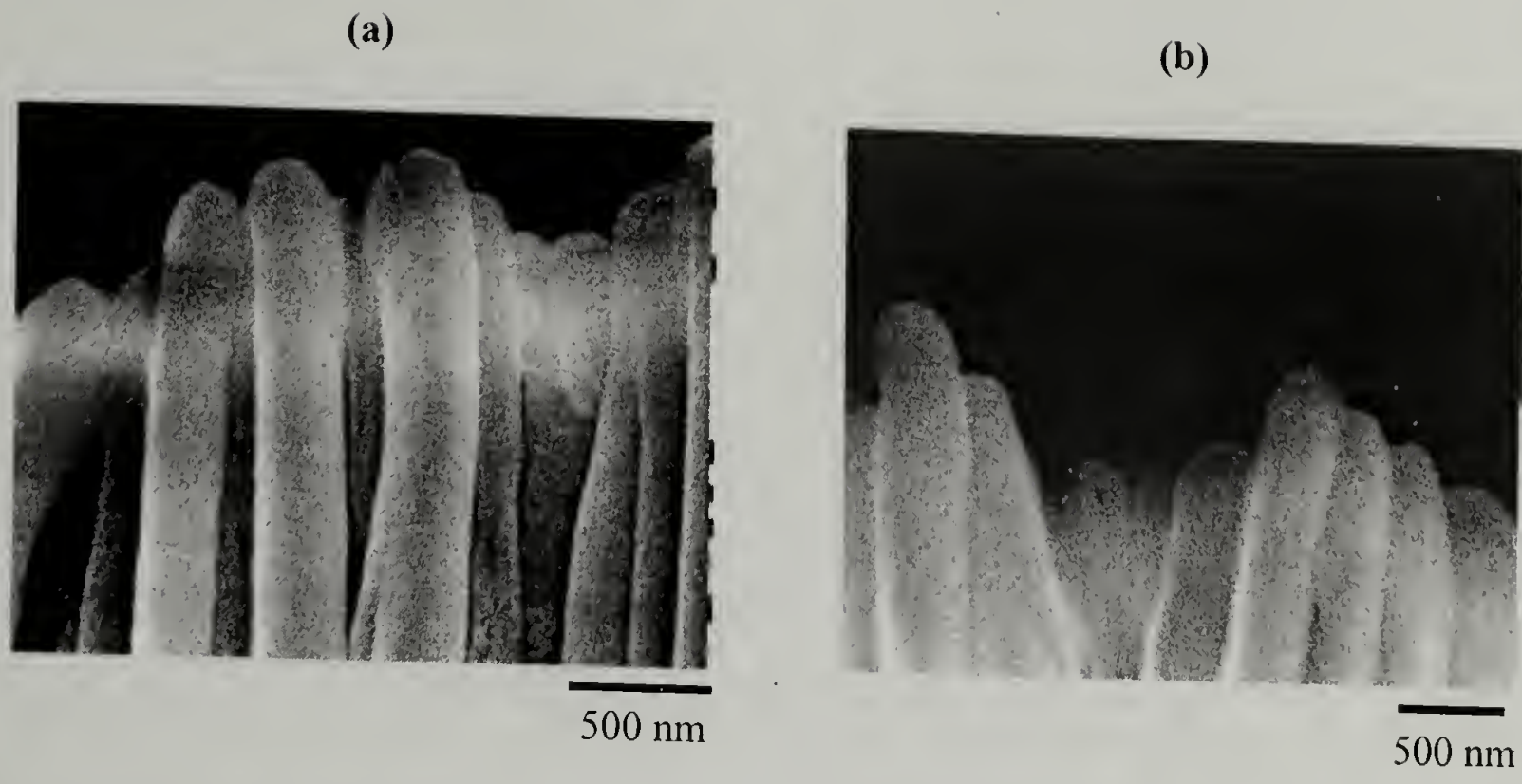

Figure 3.15. FESEM images of closed-end PPX nanotubes. Images (a) and (b) correspond to cross-sectional views of the closed ends of the tubes, while image (c) is a view from the top of showing the nanotube bundles formed after removal of the template.

3.4. Conclusions

Poly(*p*-xylylene) nanotubes, open on one or both ends, were synthesized by template assisted methods using porous aluminum oxide membranes as the templating material. A linear dependenee of the pore diameter with respeet to the deposition time was observed for the surfaces of the membranes, however it was not possible to prove that the eoating thiekness along the longitudinal direetion of the pores was uniform. FESEM images showed that PPX was deposited along the pores of the membranes and the outer diameter of the PPX nanotubes is in good correspondence with the diameter measured from the membrane surfaee. Exposure of the membranes to a reactive solution resulted in ehemieal functionalization of the inner walls of the nanotubes, whieh was confirmed by XPS analysis. These functionalized nanotubes can potentially be used for the eneapsulation of a broad series of substances, ranging from something as simple as water, to something as complex as drugs.

54. Martin, C. R.; Kohli, P. *Nature Rev.* **2003,** *2*, 29.

55. Lee, S. B.; Mitchell, D. T.; Trofin, L.; Nevanen, T. K.; Söderlund, H.; Martin, C. R. *Science* **2002**, *296*, 2198.

56. Gasparac, R.; Kohli, P.; Mota, M. O.; Trofin, L.; Martin, C. R. *Nano Lett.* **2004**, *4*, 513.

57. Wang, Z.; Li, H. L. *Appl. Phys. A* **2002**, *74*, 201.

58. Wang, Z.; Su, Y.-K.; Li, H.-L. *Appl. Phys. A* **2002**, *74*, 563.

59. Steinhart, M.; Wendorff, J. H.; Grenier, A.; Wehrspohn, R. B.; Nielsch, K.; Schilling, J.; Choi, J.; Gösele, U. *Science* **2002**, *296*, 1997.

60. Cepak, V. M.; Martin, C. R. *Chem. Mater.* **1999**, *11*, 1363.

61. Wu, C.-G.; Bein, T. *Science* **1994**, *266*, 1013.

62. Parthasarthy, R. V.; Phani, K. L. N.; Martin, C. R. *Adv. Mater.* **1995**, *7*, 896.

63. Hou, H.; Jun, Z.; Reuning, A.; Shaper, A.; Wendorff, J. H.; Greiner, A. *Macromolecules*, **2002,** *35*, 2429.

64. Kim, K.; Jin, J.-I. *Nano Lett.* **2001**, *1*, 631.

65. Jang, J.; Oh, J. H. *Chem. Commun.* **2004**, 882.

66. Kruk, M; Jaroniec, M.; Kim, T.-W.; Ryoo, R. *Chem. Mater.* **2003**, *15*, 2815.

67. Fuertes, A. B. *Carbon* **2002**, *40*, 1597.

68. Xiang, H.; Shin, K.; Kim, T.; Moon, S. I.; McCarthy, T. J.; Russell, T. P. *Macromolecules* **2004**, *37*, 5660.

69. Hulteen, J. C.; Martin, C. R. *J. Mater. Chem.* **1997**, *7*, 1075.

70. Fortin, J. B.; Lu, T.-M. *Chem. Mater.* **2002**, *14*, 1945.

71. Tolstopyatov, E. M. *J. Phys. D. Appl. Phys.* **2002**, *35*, 1516.

72. Broer, D. J.; Luijks, W. *J. Appl. Polym. Sci.* **1981**, *26*, 2415.

73. Rodgers, S. T.; Jensen, K. F. *J. Appl. Phys.* **1998**, *83*, 524.

74. Moon, S. I.; McCarthy, T. J. *Macromolecules* **2003**, *36*, 4253.

75. Herrera-Alonso, M.; McCarthy, T.J. *Langmuir* **2004**, in print.

76. Furneaux, R. C.; Rigby, W. R.; Davidson, A. P. *Nature* **1989**, *337*, 147

77. Vaeth, K. M.; Jensen, K. F. *Chem. Mater.* **2000**, *12*, 1305.

CHAPTER 4

CHEMICAL REDUCTION OF NYLON SURFACES

4.1. Introduction

Nylons are among the most important commercial thermoplastics. Depending on their molecular characteristics, particularly their hydrocarbon segment length, nylons vary in their physical properties, but in general they possesses a good combination of high strength, flexibility, toughness, abrasion resistance, dyeability, low coefficient of friction, low creep, and resistance to solvents, oils, bases, fungi, and body fluids.[78] Some of their applications include fibers for apparel, carpets, tire reinforcements, surgical sutures, and most importantly, in automotive and electrical applications.[78,79] The commercial relevance of nylons merits a careful study of the effect of their surface characteristics (physical and chemical) on their macroscopic properties.

Nylon surfaces have been previously modified by methods that can be grouped into two categories. The first category includes the chemical modification of nylon surfaces by exposure to plasma,[80,81] and modification by plasma polymerization of monomers.[82] While these methods are efficient at introducing a variety of functional groups, they have also been observed to produce changes in the surface morphology, and ultimately, lead to surface destruction. The second approach to controlling the macroscopic properties of nylons includes their surface modification by "wet" chemistry. This has been accomplished by reaction at the terminal amine groups or by reaction with the amide functionality. Since the concentration of terminal amine groups on the surface is relatively low (0.011 amine ends/nm^2 for the case of nylon 6/6

fibers),[83] high coverage is achieved only when the size and the number of reactive sites of the grafted species are high, which is the case when grafting polymers, for example grafting polyethylene and polydimethylsiloxane containing reactive groups onto nylon 6/6 fibers reduces boundary friction.[83] On the other hand, reactions at the naturally abundant amide group include N-alkylation, O-alkylation,[84,85,86] and partial hydrolysis.[87] Examples of N-alkylation include cross-linking of nylon 6/6 yarn by reaction with diisocyanates and diacid chlorides;[88] O-alkylation was achieved by reaction with dimethylsulfonate, producing imidoester groups.[86] Partial hydrolysis of the amide resulted in increased concentrations of amine and carboxylic acids, which have been used for the immobilization of enzymes by using carbodiimide or dialdehyde chemistries.[86,87]

Another potentially useful reaction at the amide group is reduction, and although this reaction has not been exploited for nylons, amine-functionalized substrates play an important role in processes such as the removal of heavy metal ions from aqueous solutions,[89] for biofouling prevention,[90] in microelectromechanical systems,[91] and for the covalent and electrostatic immobilization of biomolecules such as DNA and polysaccharides. Reduction of carboxylic acid amides to the corresponding amines can be achieved by a variety of complex metal hydrides, metal hydrides, and borane complexes. The most common reagent is lithium aluminum hydride ($LiAlH_4$), however its yields are generally low due to cleavage of the C-N bond, leading to the formation of alcohols. On the other hand, reactions with borane complexes (either as dimethysulfide or tetrahydrofuran adducts) occur faster than with $LiAlH_4$ and the reaction is compatible

with many functional groups (for example nitro, halogen, ester, sulfone, carbamate, etc.).[92]

An important application of the chemical surface modification of nylon substrates is in the production of affinity membranes, used in the biotechnological industry. Ultrafiltration membranes are used for the recovery of biological material in diafiltration of protein solutions prior to separation, and final concentration.[93] One of the problems associated with these membranes is biofouling, or adsorption of biological solutes, which produces a decrease in the permeation flux and is manifested in longer filtration times and shorter membrane lives because of the harsh conditions necessary for cleaning. These membranes, commonly polypropylene, poly(sulfone), or nylon, are surface-modified to enhance their protein-resistance and also to act as templates for the immobilization of biological ligands. To improve their performance properties, the membranes are commonly treated with a plasma which induces the formation of radical or ionic species that are then used for grafting monomers that will enhance the hydrophilicity of the membranes, and in turn, improve their protein-resistance.

Some examples of polymers which have been successful in controlling protein-adsorption include poly(hydroxyethyl methacrylate) hydrogel coatings,[94] poly(acrylamide),[95] poly(acrylic acid),[96,97] poly(1-vinyl-2-pyrrolidinone),[98] poly(vinyl alcohol),[99] and hydrophilic polysaccharide coatings.[100,101,102,103,104,105] While controversy exists regarding the exact mechanisms that prevent adsorption from occurring, some suggest that it is a consequence of the ability of the polymer to provide a steric and entropic barrier to adsorption and also due to the high hydrophilicity of the surfaces where displacement of water for proteins is an energetically unfavorable

process. Among the polysaccharides that have been studied for their low-biofouling properties in both *in vivo* and *in vitro* applications are dextrans, carbomethoxylated dextrans, hyaluronic acid, and alginic acid. Immobilization of these polysaccharides is achieved either by covalent binding or by electrostatic interaction with amine-rich substrates, and in all cases, a high density of functional groups is required in order to obtain stable coatings. Covalent attachment, the most prevalent form of coating, is generally based on carbodiimide chemistry, and surface coverage is dependent on the charge densities of the substrate and adsorbate. For the particular case of nylon substrates, covalent coating is based on amidation reactions through the terminal amine groups with bis-epoxides, or by activation of the amide group with formaldehyde.[99-101] Alternately, polysaccharide coatings can be produced by electrostatic adsorption onto oppositely charged substrates,[90,103] and in this case the coverage is sensitive to the pH of the adsorbing solution as well as to the concentration of the adsorbate. Since most substrates, generally polystyrene, polypropylene, or silica, lack functional groups reactive toward covalent or electrostatic binding, it is common practice to modify their surface through a combination of plasma treatment and/or polyamine adsorption. Due to its high concentration of primary, secondary, and tertiary amine groups, poly(ethyleneimine) (PEI), is commonly used as the interlayer. Its high charge density allows it to irreversibly adsorb onto oxidized and negatively charged surfaces, and at the same time, provide a surface with a high concentration of amine groups to allow immobilization of the polysaccharides.

In this chapter, the chemical reduction of nylon surfaces with borane chemistry is described in detail. The amine-enriched surfaces produced, of controlled surface

charge density, were further used to study the electrostatic adsorption of alginate, in an attempt to improve the protein-resistance of nylons.

4.2. Experimental

4.2.1. Materials

All chemicals were used as received. Nylon 6/6 film, Dartek ® C-101, was obtained from DuPont, Canada. Nylon 4/6 and nylon 6/12 films were prepared by melt-pressing from the respective pellets, purchased from Aldrich. Borane-tetrahydrofuran (BH_3·THF) complex (1 M in tetrahydrofuran), anhydrous tetrahydrofuran (THF), sodium hydroxide, pentafluorobenzaldehyde, poly(sodium 4-styrenesulfonate), alginate (sodium salt), and lysozyme were purchased from Aldrich. Hydrochloric acid (1 N aqueous solution) was obtained from Fisher. House-purified reverse-osmosis water was treated using a Milli-Q system that involves ion exchange and filtration steps (18×10^6 Ωcm). Water obtained with this purification method will be referred to as Milli-Q water.

4.2.2. Pretreatment of nylon films

As obtained from DuPont, nylon 6/6 samples contain a slip agent on one side of the film. The slip agent was removed by wiping the film first with an acetone-soaked Kimwipe, followed by a dry Kimwipe. The side of the film that contained the slip agent was identified and was not used for analysis. Film samples were cut to approximate dimensions of 1.2 cm × 1.8 cm. Prior to modification, film samples were rinsed with reverse osmosis-purified water (RO water), ethanol, acetone, tetrahydrofuran, and hexanes, and were dried at 50 °C under reduced pressure (50 mTorr) for 12 h.

Modifications were done immediately after drying the samples, to prevent absorption of moisture. Nylon 4/6 and 6/12 pellets were rinsed following the same sequence as described above for nylon 6/6 films and dried under reduced pressure (50 mTorr, 50 °C, 12 h) prior to melt-pressing. The pellets were melt-pressed at 300 °C (nylon 4/6) and 190 °C (nylon 6/12) between a silicon wafer and a polyimide film to an approximate thickness of 200 μm. The side of the film that was in contact with the silicon wafer during melt-pressing was used for further analysis, the other side of the films was wiped with an acetone-soaked Kimwipe. Film samples were cut to approximate dimensions of 1.2 cm × 1.8 cm, rinsed, and dried in the same manner as described above for nylon 6/6 films.

4.2.3. Characterization

X-ray photoelectron spectra (XPS) were recorded on a Perkin-Elmer-Physical Electronics 5100 spectrometer with Mg K_α excitation at 400 W and 15 kV. Depth profiling was done by collecting spectra at 15° and 75° take-off angles with respect to the plane of the sample surface; the analysis at 15° has a penetration depth of ~ 10 Å and that at 75° corresponds to a penetration depth of ~ 40 Å.[106] For the adsorption of alginate and lysozyme, and for analyses that required a small probing size, spectra were acquired on a Physical Electronics Quantum 2000 Scanning ESCA Microprobe with MgK_α excitation at 15 kV and 50 W and 5 W for probing sizes of 200 μm and 20 μm, respectively. Attenuated total reflectance infrared spectroscopy (ATR IR) was performed on a Bio Rad FTS 175C FT-IR spectrometer with a germanium crystal (45°) as internal reflection element. Considering a refractive index of n_D=1.53 for nylon 6/6,[79] the penetration depths observed by this technique, in the range from 4000 cm^{-1} to

700 cm^{-1} are 0.96-0.17 μm. Dynamic water contact angles were measured using a Ramè-Hart telescopic goniometer and a Gilmont syringe with a 24-gauge flat tipped needle; milli-Q water served as the probe fluid. Advancing and receding contact angles were measured while the probe fluid was added to and withdrawn from the drop, respectively. Differential scanning calorimetry (DSC) analysis was performed on a TA Instruments 2910 DSC. Experiments were conducted under nitrogen in the temperature range of 25 °C to 320 °C with a heating rate of 10 °C/min. Atomic force microscopy (AFM) images were acquired with a Digital Instruments NanoScope III AFM, operated in tapping mode.

4.2.4. Reduction with BH_3·THF[93,107]

Dry nylon film samples were supported on a specially built glass holder with the side that previously contained the slip agent in contact with the glassware. The glass holder was placed inside a Schlenk tube, which contained a magnetic stirbar. Anhydrous THF (20 mL) was cannulated into the reaction tube and the system was allowed to equilibrate at 0 °C under a nitrogen atmosphere. A 1 M solution of BH_3·THF (4 mL) was then slowly added. The system was allowed to equilibrate at room temperature for 1 h, after which period of time the reaction tube was placed inside an oil bath at 50 °C and maintained at that temperature for varying periods of time (1-24 h). Samples were then removed from the reaction solution and were thoroughly rinsed with THF, HCl (1.0 N), RO water, NaOH (1.0 M), and RO water, and dried (50 °C, 50 mTorr) for 12 h prior to further modification or characterization. The surface-reduced samples will be abbreviated as follows: nylon $4/6^{red}$, nylon $6/6^{red}$, and nylon $6/9^{red}$.

4.2.5. Labeling

Amine funetionalities (primary or seeondary) were labeled by reaetion with pentafluorobenzoylehloride.[108] Film samples were plaeed on a glass holder inside a Sehlenk tube that eontained a magnetie stirbar. Anhydrous THF (20 mL) was eannulated into the reaetion tube. Pentafluorobenzoyl ehloride (0.72 mL) and triethylamine (0.28 mL) were sequentially added via syringe. The reaetion proeeeded for 4 h at room temperature, after whieh the samples were removed from the solution and rinsed with THF, ethanol, diehloromethane, aeetone, and hexane. Films were dried at 50 °C under redueed pressure (50 mTorr) for 12 h prior to eharaeterization.

4.2.6. Polyeleetrolyte adsorption

Adsorption of poly(4-sodium styrenesulfonate)[109] and alginate[103] were performed at room temperature in unstirred solutions and with no added salt. Solutions of alginate in Milli-Q water, of eoneentrations ranging from 0.01% to 0.5% (w/v), were prepared 12 h prior to adsorption. Adsorption was studied at pH=6 without added salt. Nylon film samples were plaeed inside elean glass seintillation vials and 5 mL of the alginate solution were added. After a given period of time (0.5 h to 10 h), the alginate solution was removed by dilution through the sequential addition of Milli-Q water (3 mL) and removal of solution (3 mL), over five eyeles. Film samples were then removed from the vial, further rinsed with eopious amounts of Milli-Q water, and left overnight in Milli-Q water (15 mL) to ensure desorption of the non-speeifieally adsorbed alginate. After a final rinse with elean water, the samples were dried under a gentle nitrogen stream and plaeed under redueed pressure at room temperature for 2 h prior to analysis.

A 0.02 M (in repeat units) solution of poly(4-sodium styrenesulfonate) (PSS) in Milli-Q water at pH = 2.26 was prepared 12 h prior to adsorption. The solution pH was adjusted by using dilute (0.01 M) aqueous solutions of hydrochloric acid and sodium hydroxide. Nylon film samples were placed inside clean glass scintillation vials and 5 mL of the PSS solution were added. After 1 h, the PSS solution was removed by dilution with Milli-Q water, as explained for the adsorption of alginate. The film samples were thoroughly rinsed with Milli-Q water and dried under a gentle nitrogen stream before characterization.

4.2.7. Crosslinking reactions

A 0.01 M solution of alginate in Milli-Q water was prepared 12 h prior to crosslinking. Calcium sulfate dihydrate (1% molar with respect to the moles of alginate) was weighed in a beaker containing a magnetic stirbar. 25 mL of the alginate solution were then added and the solution was stirred overnight. Adsorption experiments were carried out by submerging the film samples in the crosslinked-alginate solution. The samples were rinsed and dried following the procedure established previously for the adsorption of non-crosslinked alginate.

4.3. Results and Discussion

4.3.1. Chemical Reduction of Nylons

The reduction of secondary amides by diborane, in solution, is believed to proceed as depicted in Figure 4.1.[107] The first step is the acid-base reaction between the first equivalent of borane and three amidic hydrogens, followed by addition of two hydride equivalents per amide leading to the triaminoborane intermediate. Excess borane is required to complete the reduction, such that six equivalent hydrides, per amide, are necessary.

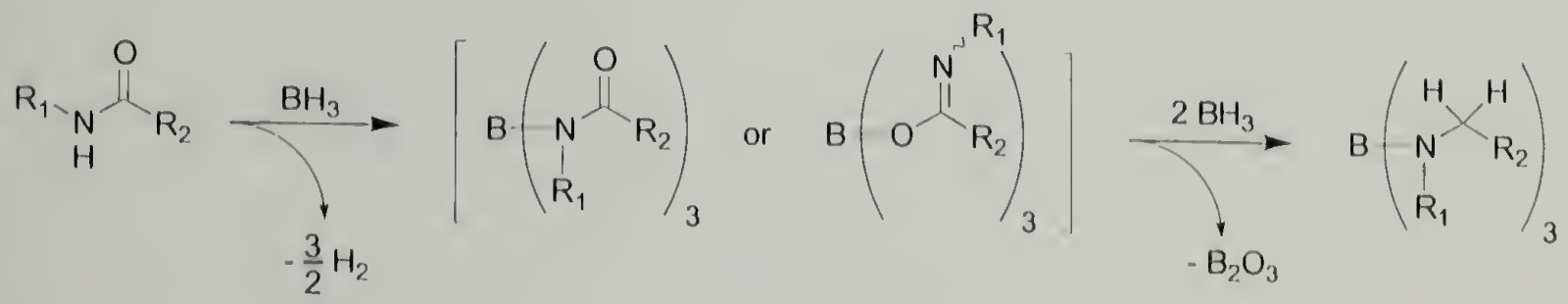

Figure 4.1. Reduction mechanism of amides with borane and isolation of the free amine by treatment in acidic media.

Reductions of nylon films were carried out by reaction with a borane-tetrahydrofuran complex, with THF as the solvent. Since the nylons studied are insoluble and do not swell in the presence of THF, the polyamides lack the mobility required for the formation of the triaminoborane intermediate, requiring a greater molar excess of borane than the reaction in solution. This condition is ensured since a large

excess of borane was added to the rcaction flask. The mechanism proposcd for thc reaction at the surfacc is depicted in Figure 4.2.

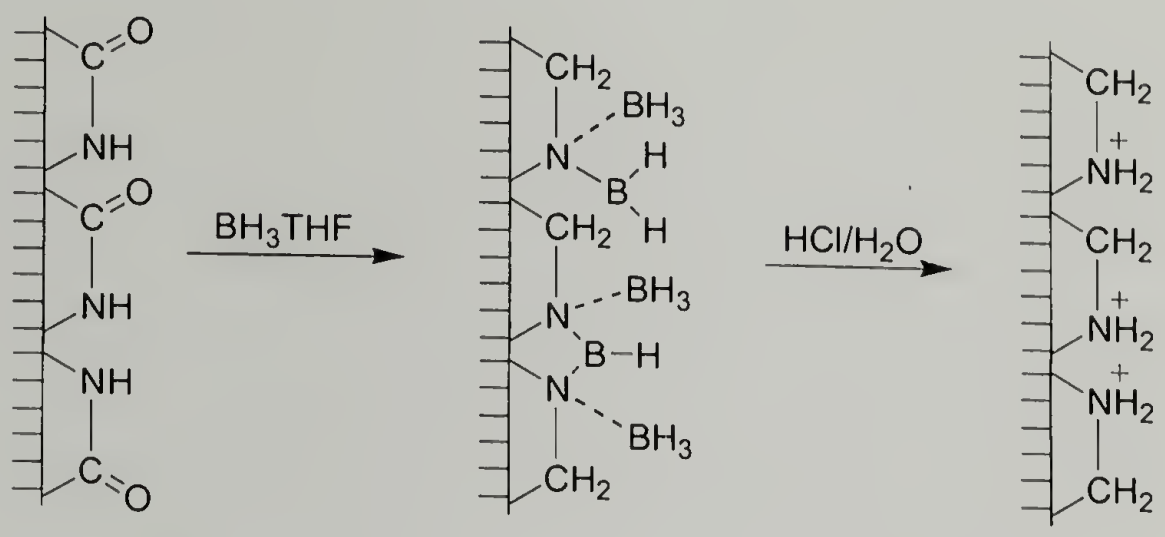

Figure 4.2. Mechanism proposed for the heterogeneous reduction of nylon film surfaces.

Preliminary studies on the chemical reduction of nylon surfaces provided information regarding the effect of the solvent propertics on the yield of the rcaction.[110] For the same reaction conditions (temperature and time), reduction with a borane-tetrahydrofuran complex in THF resulted in higher yicld than thc reaction with a borane-dimethylsulfide complex in toluene (69% vs. 27%). The high yield observed for the reduction with BH_3·THF was interesting and warranted further investigation in regard to the kinetics of the reaction and the morphology of the films, and also their potential applications as amine-rich surfaces of controlled charge density. For this study, three types of nylons that differ in their amide/methylene ratios were chosen: nylon 4/6, nylon 6/6, and nylon 6/12. The crystallinity, watcr contact angle, and surface atomic composition of the virgin films were determined and are presented in Table 4.1.

Table 4.1. Physical and chemical properties of nylons.

Sample	XPS Atomic Composition (%) [a]			Contact Angle (°) [b]		Crystallinity (%) [c]	Tg (°C) [d]
	C	N	O	θ_A	θ_R		
nylon 4/6	79.66 74.00	8.37 13.18	11.97 12.82	57	20	44	78
nylon 6/6	77.75 76.04	11.52 12.50	10.74 11.46	69	20	27	60-80
nylon 6/12	86.83 84.67	6.48 7.47	6.69 7.86	78	13	18	50-60

[a] upper rows correspond to 15° take-off angle data and lower rows are 75° take-off angle data. [b] advancing and receding water contact angles. [c] determined by DSC of film samples. [d] glass transition temperatures taken from Williams, J. C. L. In *Nylon Plastics Handbook*; Kohan, M. I.; Ed.; Hansen Publishers: New York, NY, 1995; p. 294.

As previously reported for modification of nylon 6/6,[110] the penetration depth of reduction is smaller than the probing depth of ATR IR since the spectra of reduced samples, regardless of the type of nylon, remain unchanged after reaction (data not shown). Therefore, the surface chemical reduction was studied by XPS. Figure 4.3 (a-f) shows the high-resolution C_{1s} peak of virgin and reduced nylon samples. Visual inspection of the spectra clearly indicate that the reactions proceeded to high extent, since the signals attributed to the amide group, present at high binding energy ($\underline{C}H_2C{=}O$ at 289.49 eV and $CH_2\underline{C}{=}O$ at 292.02 eV) essentially disappear upon reaction. Water contact angle and surface atomic composition data after reduction are presented in Table 4.2. A large decrease in the water contact angle was observed after reduction, indicating a high conversion of amide to amine groups. The disappearance of the signals associated with the amide group is in agreement with the water contact angle and atomic composition data. The C_{1s} region was curve-fitted with four peaks, as shown in Figure

4.4, with binding energies at 289.01 eV ($\underline{C}H_2$), 289.49 eV ($\underline{C}H_2C{=}O$), 290.08 eV ($\underline{C}H_2NH$), and 292.01 eV ($CH_2\underline{C}{=}O$).[111] The higher binding energies of these signals compared to values previously reported were attributed to charging of the sample during analysis, however curve-fitting was performed maintaining their difference in binding energies constant. An example of the change in the composition of the carbon signal as a function of reaction time for nylon 6/6 is presented in Figure 4.5. The decrease in the intensity of the signals associated with the carbonyl group ($\underline{C}H_2C{=}O$ and $CH_2\underline{C}{=}O$) was accompanied by an increase of the signals attributed to the amine ($\underline{C}H_2$ and $\underline{C}H_2NH$). The theoretical composition of the carbon signal for 100% reduced nylon 6/6 is also included in Figure 4.5 (dashed lines); assuming complete conversion of the amide groups, the concentration of $\underline{C}H_2$ and $\underline{C}H_2NH$ species should correspond to 66.66% and 33.33%, respectively, while that of the $\underline{C}H_2C{=}O$ and $CH_2\underline{C}{=}O$ species should approach zero. If the reaction were confined to the surface, the take-off angle dependence should be such that a lower concentration of amide-related signals and a higher concentration of amine-related signals should be observed closer to the film-solution interface (lower take-off angles). The data presented in Figure 4.5 show that this is not the case; the discrepancy in the data suggest mobility of the surface during reduction since no clear take-off angle dependent behavior is observed, however the results obtained from the curve-fitting analysis approach the values theoretically predicted at long reaction times (24 h).

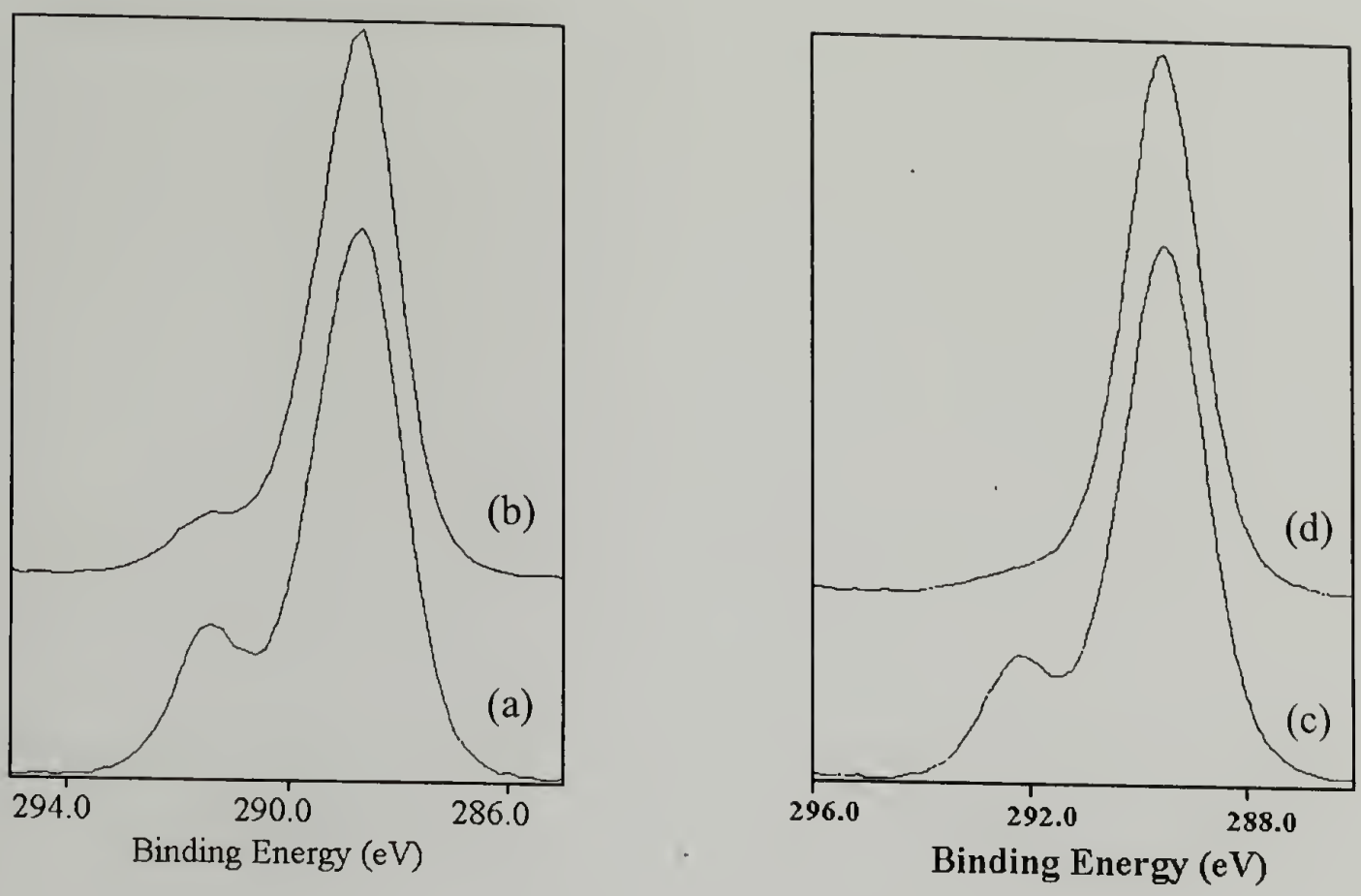

Figure 4.3. High-resolution XPS spectra of the C_{1s} region of nylons. (a) virgin nylon 4/6, (b) nylon 4/6 ^{red}, (c) virgin nylon 6/6, (d) nylon 6/6 ^{red}, (e) virgin nylon 6/12, (f) nylon 6/12 ^{red}.

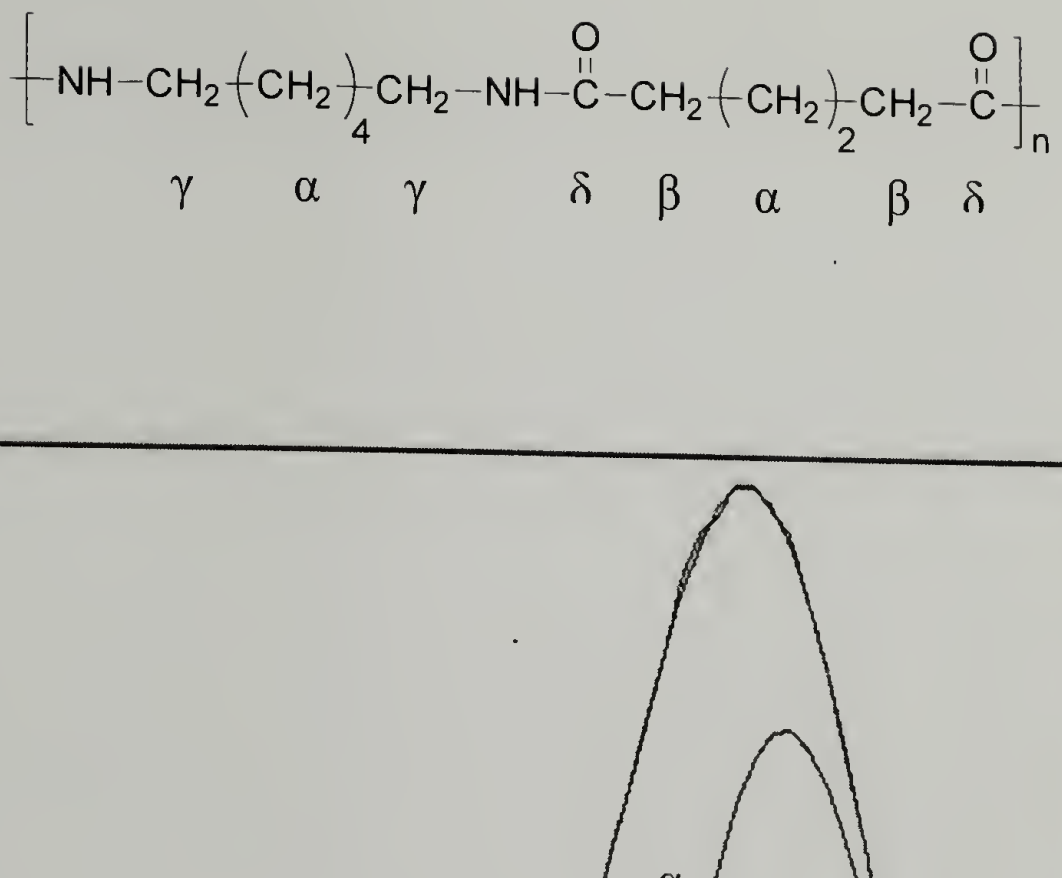

Figure 4.4. Curve-fitting analysis for nylon 6/6 illustrating the deconvolution of the C_{1s} signal.

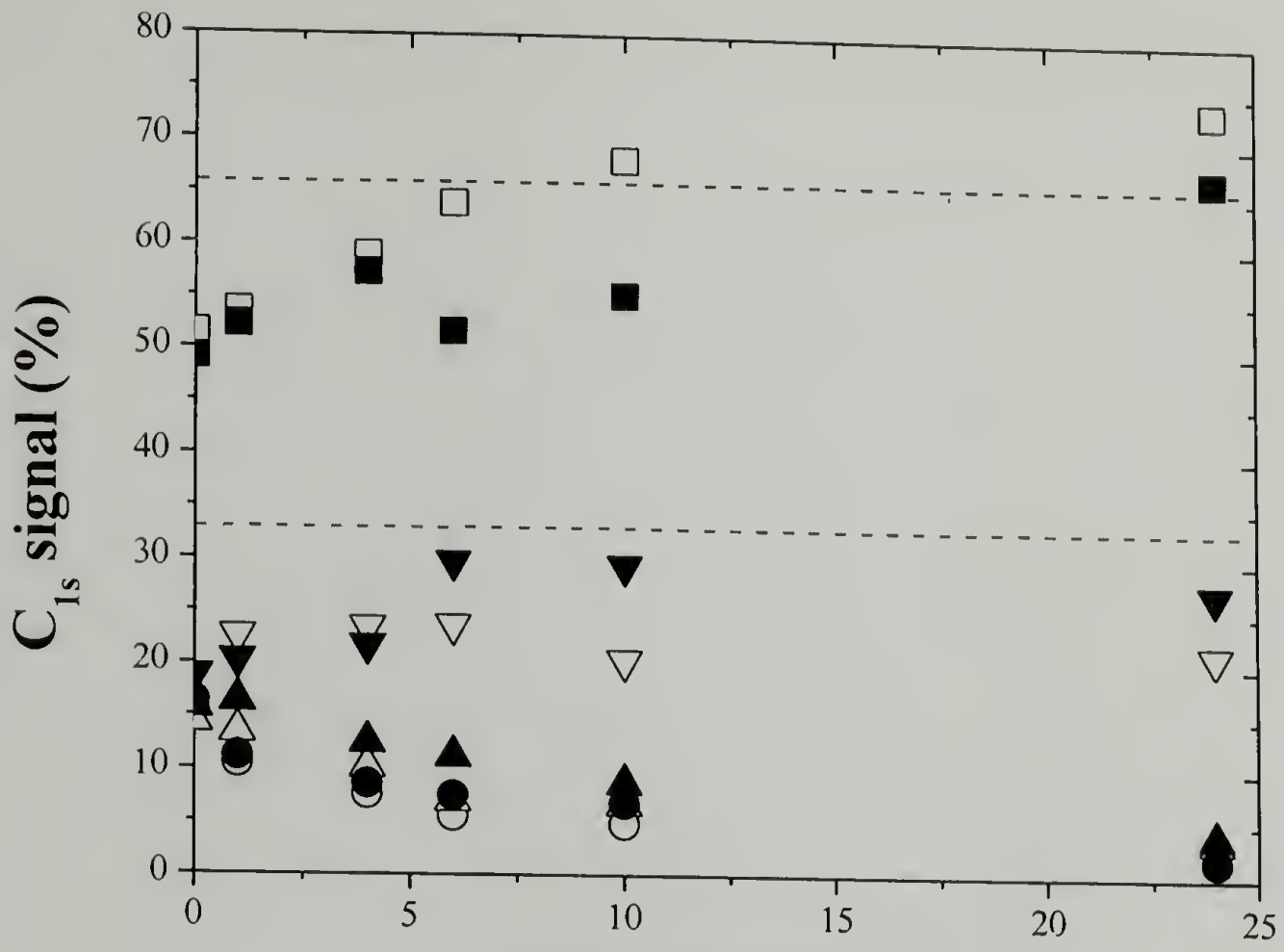

Figure 4.5. XPS curve-fitting analysis of the C_{1s} region of nylon 6/6 ^{red}. Closed and open signals correspond to data acquired at 15° and 75° take-off angles, respectively. $\underline{C}H_2$ (■,□); $\underline{C}H_2NH$ (▼,▽); $\underline{C}H_2C{=}O$ (▲,△); $\underline{C}{=}O$ (●,○). Dashed lines correspond to the composition for a theoretical yield of 100%.

Table 4.2. XPS atomic composition and water contact angle data for the chemical reduction of nylon film surfaces.

Sample	XPS Atomic composition (%) [a]				Contact angle (°) [b]	
	C	N	O	Other	θ_A	θ_R
Nylon 6/6	77.75 76.04	11.52 12.50	10.74 11.46		69	20
Nylon 6/6 ^{red}	83.6 80.9	10.4 12.2	5.5 6.5	0.5 ^{Cl} 0.4 ^{Cl}	30	15
Nylon 6/6 ^{red} $(R_2NH_2^+Cl^-)^c$	81.80 78.40	8.70 11.1	3.40 3.40	6.20 ^{Cl} 7.20 ^{Cl}	20	5
Nylon 6/6 + $ClCOC_6F_5$	85.60 78.09	5.91 10.72	6.92 10.08	1.58 ^{F} 1.11 ^{F}		
Nylon 6/6 ^{red} + $ClCOC_6F_5$	59.45 57.40	5.07 5.56	6.11 5.18	29.37 ^{F} 31.86 ^{F}	87	36
Nylon 4/6	79.66 74.00	8.37 13.18	11.97 12.82		57	20
Nylon 4/6 ^{red}	90.27 81.91	3.76 9.92	5.55 7.01	0.43 ^{Cl} 1.16 ^{Cl}	28	16
Nylon 6/12	86.83 84.67	6.48 7.47	6.69 7.86		78	13
Nylon 6/12 ^{red}	81.61 83.41	4.78 6.50	12.90 8.89	0.71 ^{Cl} 1.11 ^{Cl}	65	16

[a] upper rows correspond to 15° take-off angle data and lower rows are 75° take-off angle data. [b] advancing and receding contact angles. [c] Sample rinsed with HCl without neutralization.

The change in the chemical nature of the surface is also manifested in the water contact angles, as presented in Figure 4.6. Upon reduction, a gradual decrease in both the advancing and receding water contact angles is observed, indicating that the polyamine resulting from the reduction is more wettable than the parent polyamide.

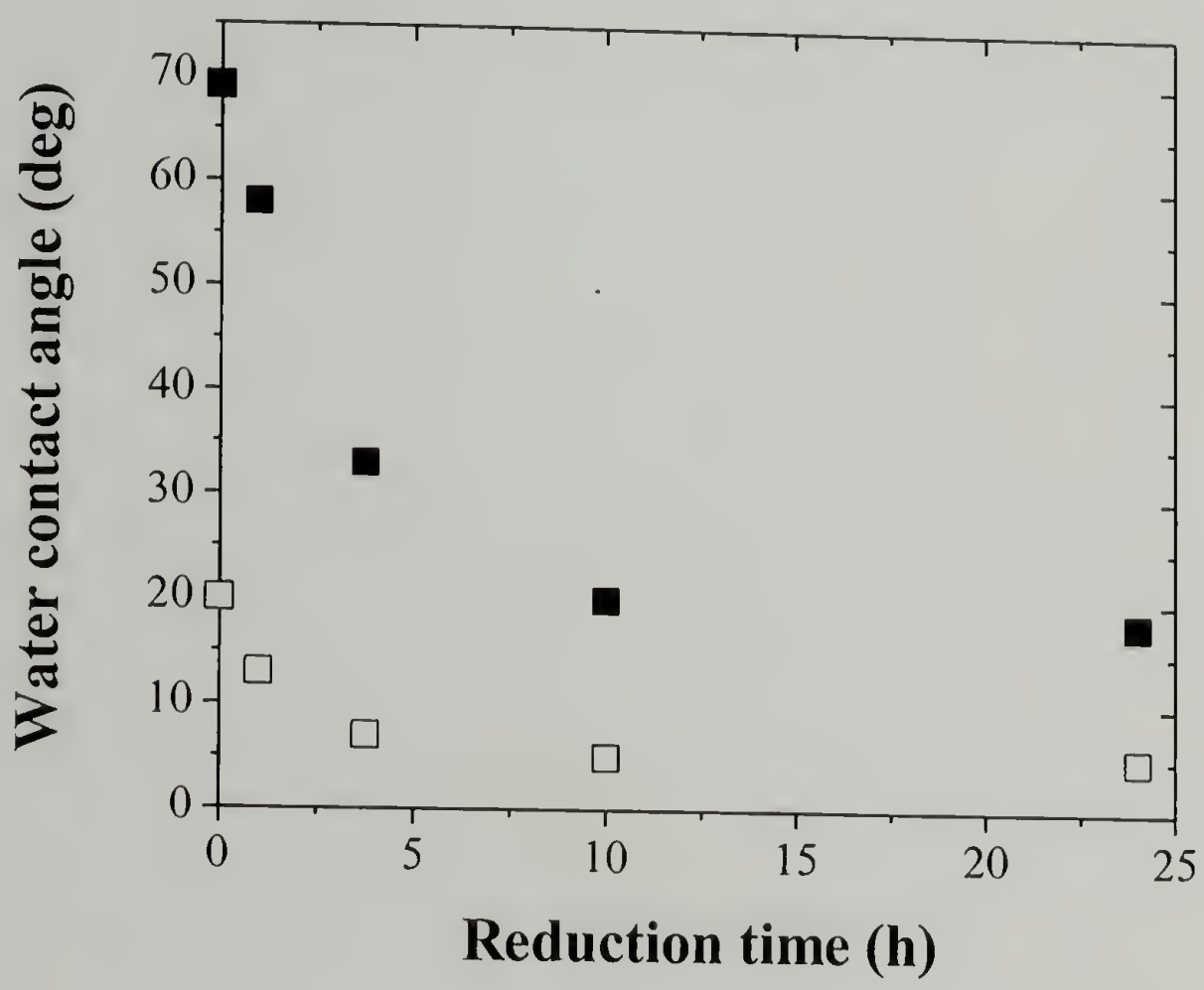

Figure 4.6. Advancing (■) and receding (□) water contact angles during reduction of nylon 6/6.

Because of its ease of identification, the signal characteristic of the carbonyl carbon was chosen to quantify the degree of reduction. Yields were estimated by comparing the area of this signal at a given time $(A^{C=O})_t$, referenced to its value for virgin nylon $(A^{C=O})_{to}$ as: $Yield\ (\%) = [(A^{C=O})_t - (A^{C=O})_{to}] / (A^{C=O})_{to}$. Kinetics of the chemical reduction for the nylons studied are presented in Figures 4.7 to 4.9, in terms of the yield as a function of reaction time and penetration depth.

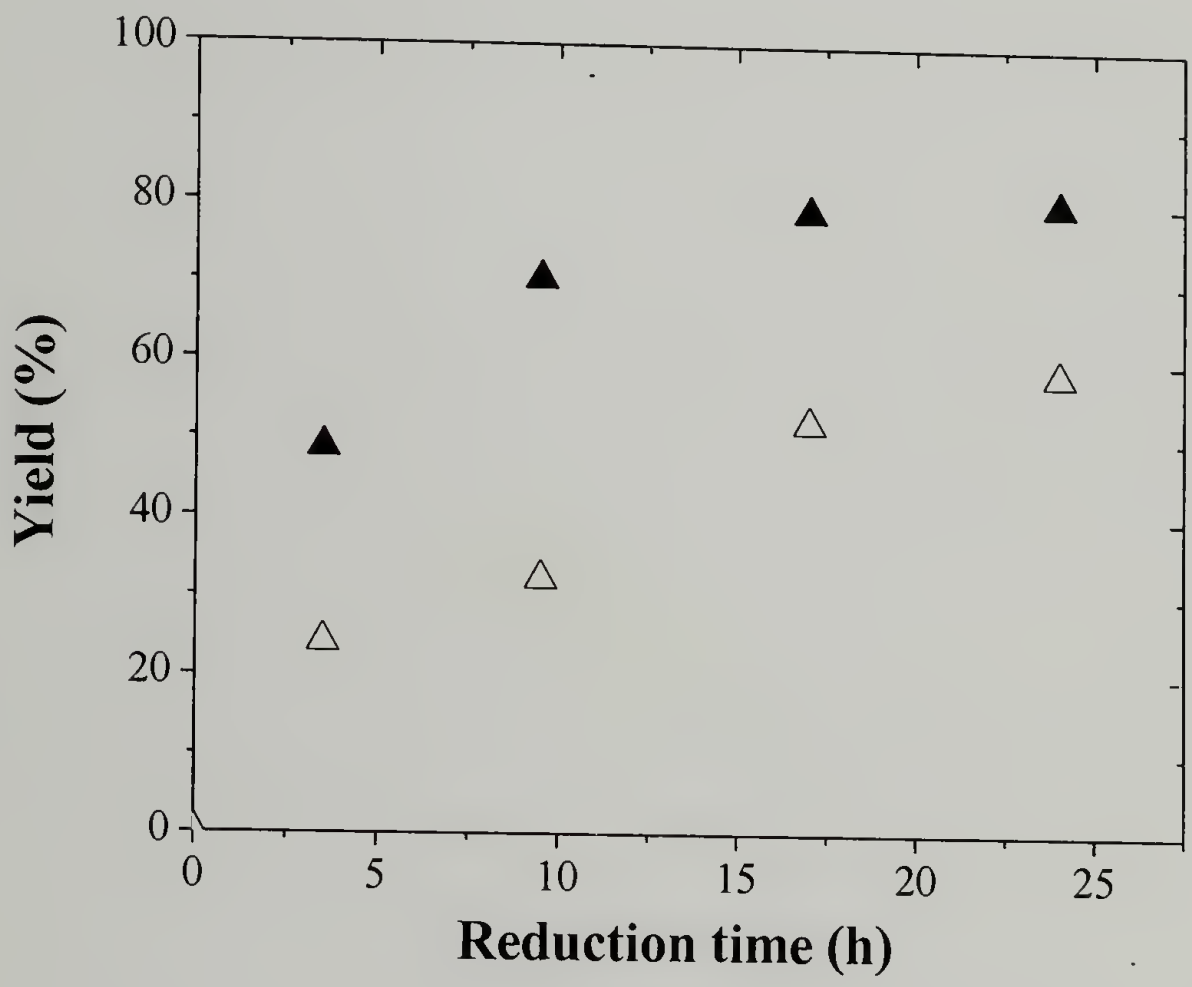

Figure 4.7. Kinetics of reduction of nylon 4/6 determined by XPS at 15° (closed symbols) and 75° (open symbols) take-off angles.

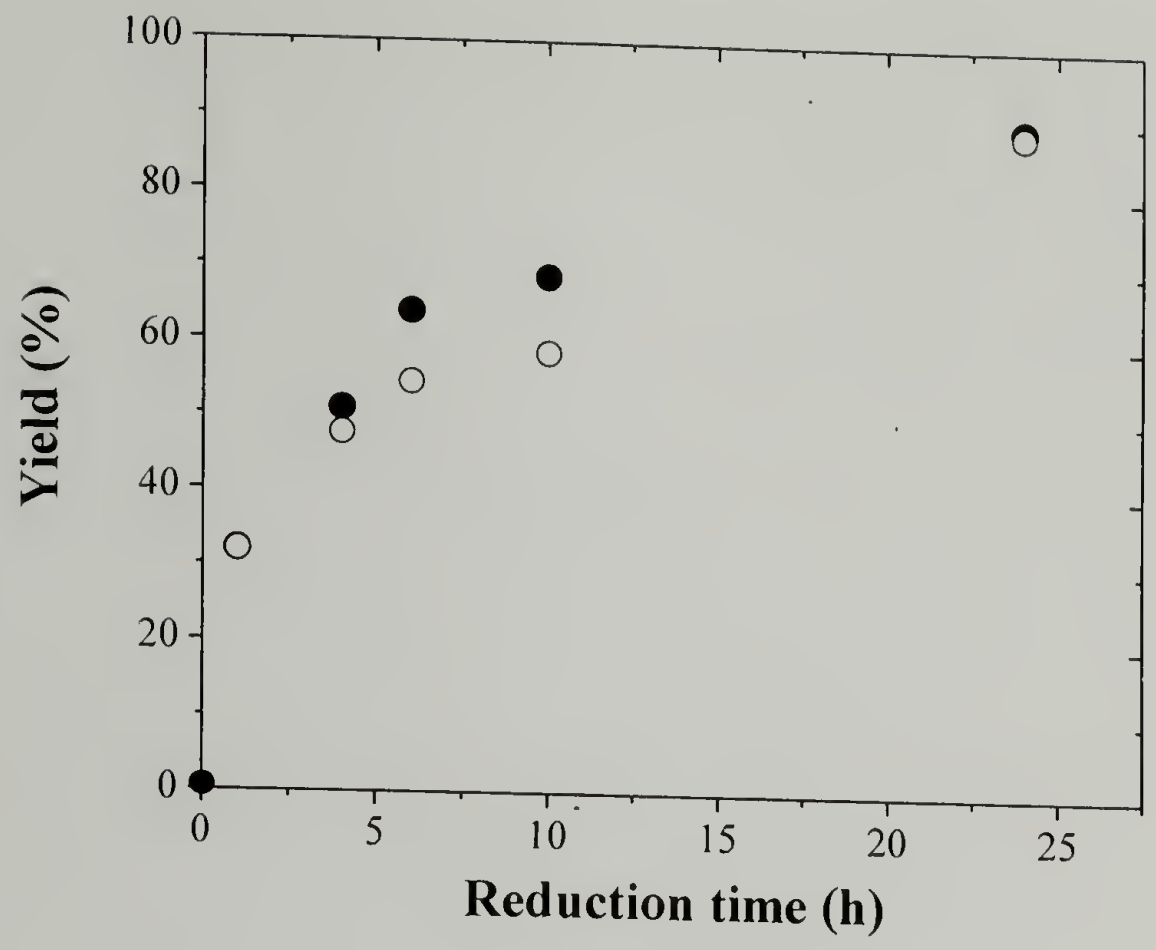

(a)

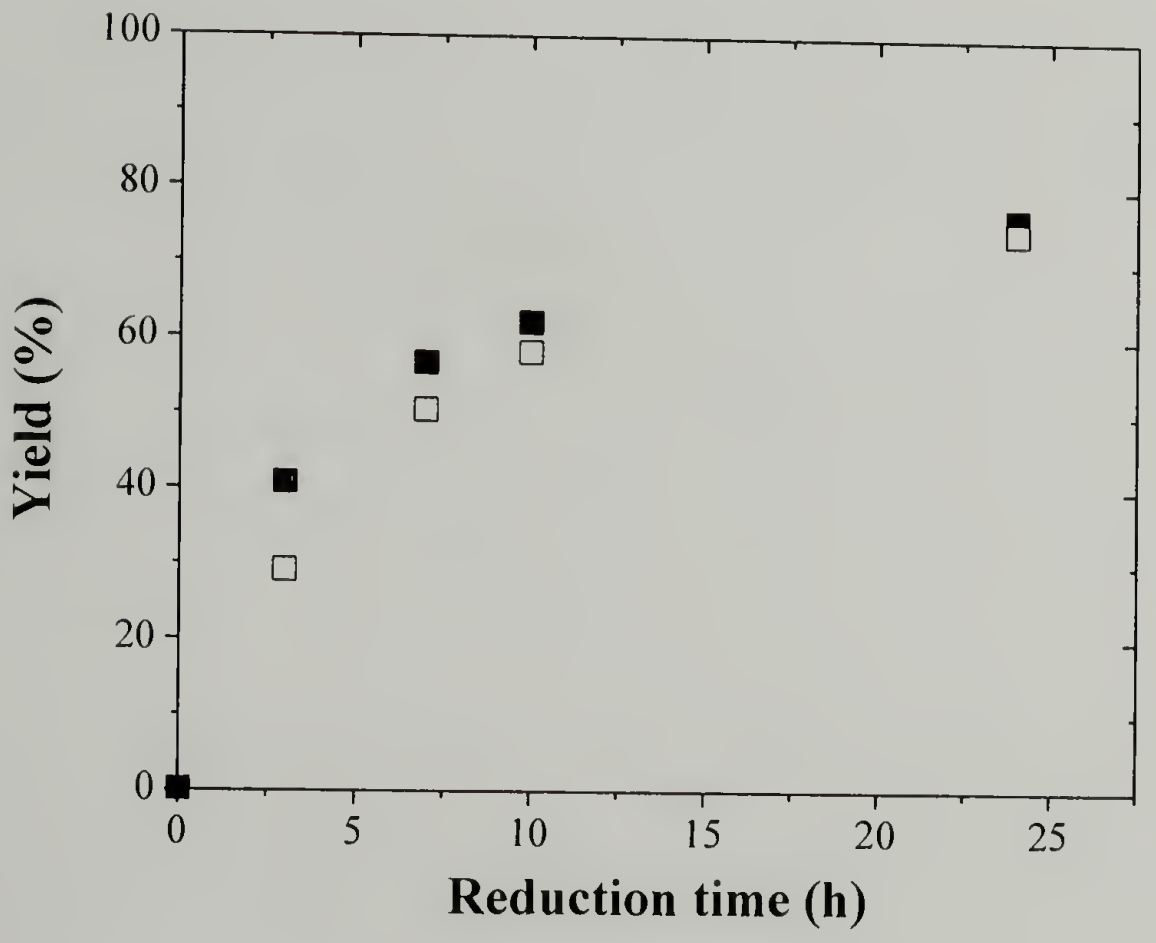

(b)

Figure 4.8. Kinetics of reduction of nylon 6/6 (a) and nylon 6/12 (b) determined by XPS at 15° (closed symbols) and 75° (open symbols) take-off angles.

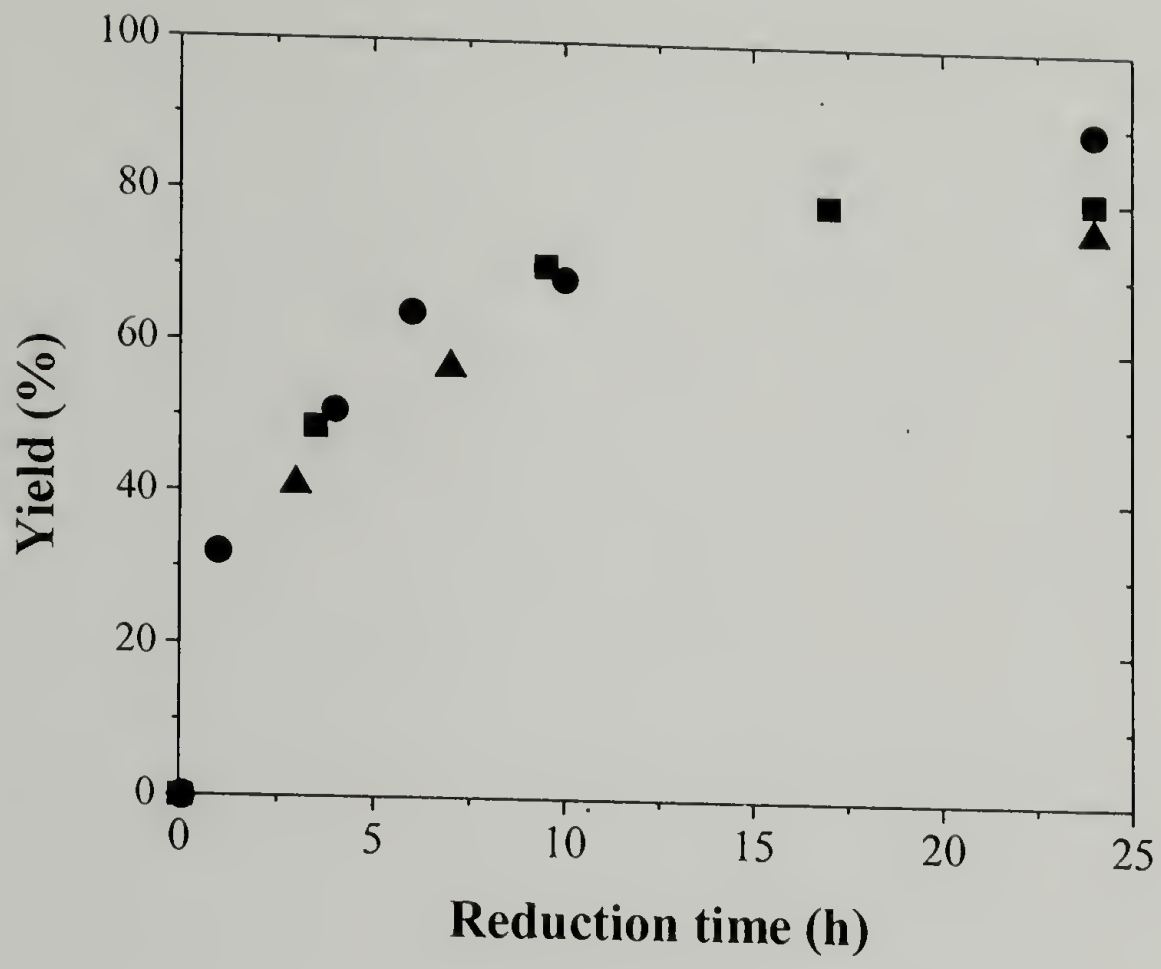

Figure 4.9. Comparison of the kinetics data for the reduction of nylons, determined by XPS at a 15° take-off angle. Nylon 4/6 (▲); nylon 6/6 (●); nylon 6/12 (■).

The similarity of the data for all three nylons at the outer 10 Å of the surface (15° take-off angle, Figure 4.9) shows that at this penetration depth, the yield is independent of the characteristics (Tg or crystallinity) of the nylon, and that their reactivity is similar, however at higher penetration depths (40 Å or 75° take-off angle), differences in segmental mobility begin to gain importance. The data for nylon 6/6 and 6/12 at the outermost 10 Å and 40 Å indicate that the reaction occurs to comparable extents throughout this depth (Figure 4.8). This behavior contrasts with that of nylon 4/6, for which stronger penetration-depth dependence was observed (Figure 4.7). These results can be explained in terms of the segmental mobility of the three different nylons during

reaction, a concept that has been used previously to explain the surface modification of poly(propylene) and linear low density polyethylene by a Mercat reaction with aqueous ammonia.[112] Polymer surface modification reactions are commonly carried out at temperatures below their glass transition to limit the segmental motion of the polymer and therefore confine the reaction to the outer surface. It is expected that reactions conducted at temperatures closer to the Tg of the polymer would have higher penetration depths. Assuming that the drying conditions employed (50 °C, 20 mTorr, 24 h) are effective in removing absorbed water, the glass transition temperatures of the nylons studied decrease in the order nylon 4/6 > nylon 6/6 > nylon 6/12, as presented in Table 4.1. The slightly higher Tg of nylon 4/6 explains its lower degree of functionalization at higher penetration depths. The same argument would predict a higher take-off angle dependence of nylon 6/6 compared to nylon 6/12, however the data show a similar behavior for both systems. On the other hand, reaction of a semi-crystalline polymer is expected to occur preferentially at the amorphous regions since diffusion of reagents inside the crystalline regions is highly limited and unlikely. Although crystallization of a semi-crystalline polymer at the surface occurs under different conditions and rates than in the bulk and assuming that the degree of crystallinity of the bulk, if not equal to, is proportional to the crystallinity in the outer 40 Å of the surface, the take-off angle dependence would decrease as: nylon 4/6 > nylon 6/6 > nylon 6/12, analogous to the segmental mobility (Tg) argument. The difference in the degree of crystallinity, however, is larger for nylon 4/6 (18% with nylon 6/6 and 26% with nylon 6/12) compared to the other two nylons (8% difference), which could explain the weaker penetration depth dependence observed for both nylon 6/6 and 6/12.

In the synthesis of small-molecule amines by the chemical reduction of amides, one of the most important steps of the reaction is the isolation of the free amine from the borane-amine adduct, which is commonly accomplished by basic hydrolysis, treatment in protolytic conditions (for example, hydrochloric acid), or by amine-interchange reactions.[107] To achieve complete dissociation of the borane-amine complex, long reaction times and elevated temperatures are generally required. As presented in Figure 4.10, in the surface-reduction with BH_3·THF, we observed that hydrolysis times close to 1 h were necessary in order to ensure complete cleavage of the amino-borane complex to generate the free amine. Chlorine is observed because of incomplete neutralization of the protonated amine.

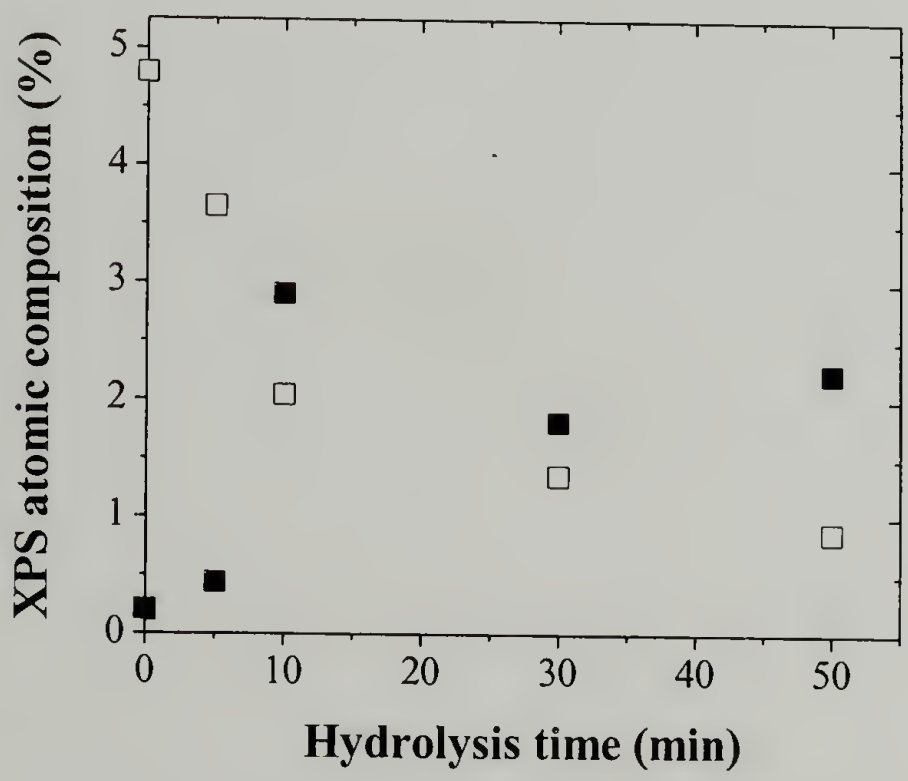

Figure 4.10. Surface atomic composition during cleavage of the amino-borane complex of nylon 6/6 ^{red}. Chlorine (■) and boron (□) at 15° take-off angle.

The third entry in Table 4.2 corresponds to the atomic composition of the protonated amine surface; a high concentration of chlorine is observed and it is assumed to be in its ionized form, acting as the counterion of the ammonium ion. The higher concentration of chlorine observed at 75° (7.20%) compared to that at 15° (6.20%) is indicative of the non-surface specificity of the reaction with BH_3THF. In its protonated form, the amine surface has very low water contact angles (θ_A/θ_R=20°/5°), which is expected since ionizable surfaces have higher wettability when they are present in their ionized form.[113] As a control, virgin nylon was also subjected to the same acidic treatment and no changes were observed with regard to its atomic composition and wettability. Neutralization of the amine surfaces with 1 M NaOH and subsequent rinsing in water produced a decrease in the concentration of chlorine along with a slight increase in the water contact angle (Table 4.2, entry 2). The fourth entry in Table 4.2 corresponds to a surface-reduced nylon 6/6 sample, whose amine groups had been labeled with a fluorine-containing label (pentafluorobenzoyl chloride). The high concentration of fluorine (29.37% and 31.86% at 15° and 75° take-off angles) is indicative of reduction having occurred.

The morphology of the films was determined by AFM. While, macroscopically the samples remained unchanged after reduction, the data previously discussed would predict a change in the surface morphology upon reaction. Height-image micrographs corresponding to the reduction of nylon 6/6 at different reaction times are presented in Figure 4.11. The AFM images reveal that the original well-defined, spherulitic morphology of virgin nylon 6/6 is gradually lost upon reaction, and after 10 h the morphology has changed considerably. This result can be explained in terms of the

change in the solvent properties of the medium with respect to nylon, resulting in relatively high reaction penetration depths and increased mobility of the chains on the surface, allowing chain reorientation to occur. Although THF is neither a plasticizer nor a solvent for the nylons studied, the amino-borane complex formed in the reaction of polyamides with BH_3 is soluble in THF,[114,115] resulting thus in modified films with little surface specificity. However, the fact that the structure of the polyamine can be inferred by XPS analysis, both in the atomic composition as well as in the shape of the C_{1s} peak, suggests that under the reaction conditions studied, not all the chains that reacted dissolved into the solution, despite their favorable interaction with the medium.

The polyamines derived from the bulk reduction of nylons are soluble in water under acidic conditions, as will be discussed in the next chapter.[115] To determine the stability of the polyamine layer resulting from the surface-reduction, nylon 6/6 film samples reduced for 24 h were submerged in water for 24 and dried under a gentle stream of nitrogen prior to analysis by optical microscopy, AFM, and XPS. The favorable interaction of water with the polyamine produced a dewetting pattern upon drying, observable by optical microscopy (Figure 4.12). The fact that the polyamine layer did not dissolve off the underlying nylon is a consequence of the insolubility of the polyamide in water, pinning down the polyamine layer. XPS analysis of the dewetted regions of the film samples was done using a probe size of 20 μm. The composition of the surface at these points is similar to nylon 6/6, and careful examination of the carbon signal shows that the characteristic carbonyl signal of the polyamide is once again present (Table 4.3 and Figure 4.13). This dewetting behavior was not observed for

samples with reduction times shorter than 5 h, such that reductions with yields lower than 50% produce stable amine-rich surfaces.

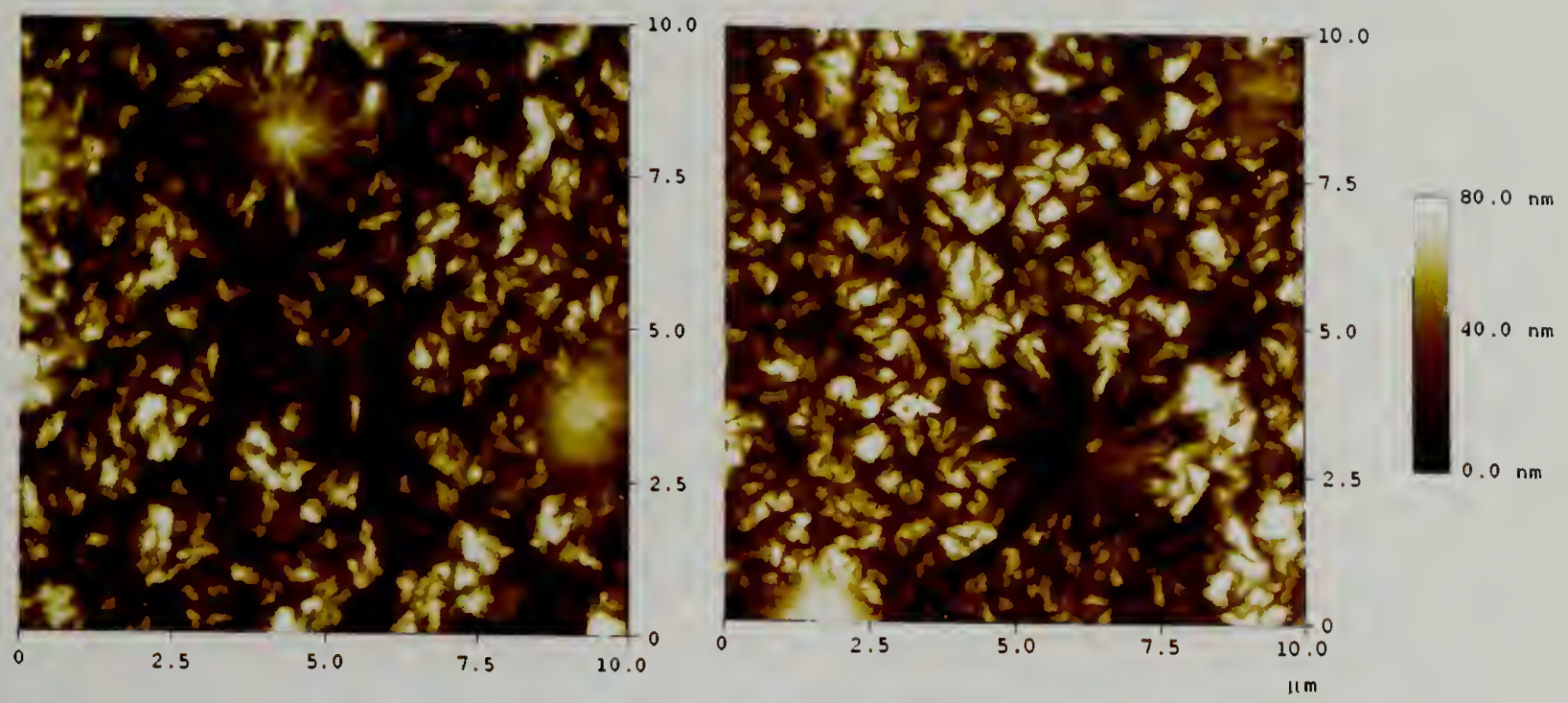

Figure 4.11. AFM images obtained in tapping mode of nylon 6/6 ^{red} at different reduction times: 0 h (a), 1 h (b), 4 h (c), and 10 h (d). Images correspond to height plots of a 10 µm × 10 µm sampling area.

Figure 4.12. Optical micrograph of the surface of nylon 6/6 ^{red} film sample after submersion in water for 24 h. Sample was reduced at 50 °C for 24 h.

Table 4.3. XPS atomic composition for dewetted regions of nylon 6/6 [red].

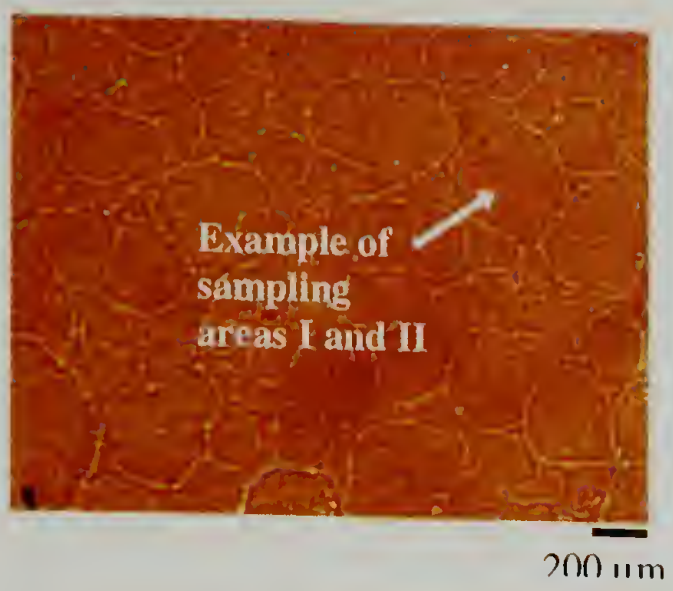

Sampling Area [a]	XPS Atomic Composition (%) [b]		
	C	O	N
I	79.7	11.1	9.2
	74.5	14.8	10.8
II	81.1	11.3	7.3
	77.2	12.7	10.1

[a] Film sample was reduced at 50 °C for 24 h and submerged in water for 24 h. [b] upper rows correspond to 15° take-off angle data and lower rows are 75° take-off angle data.

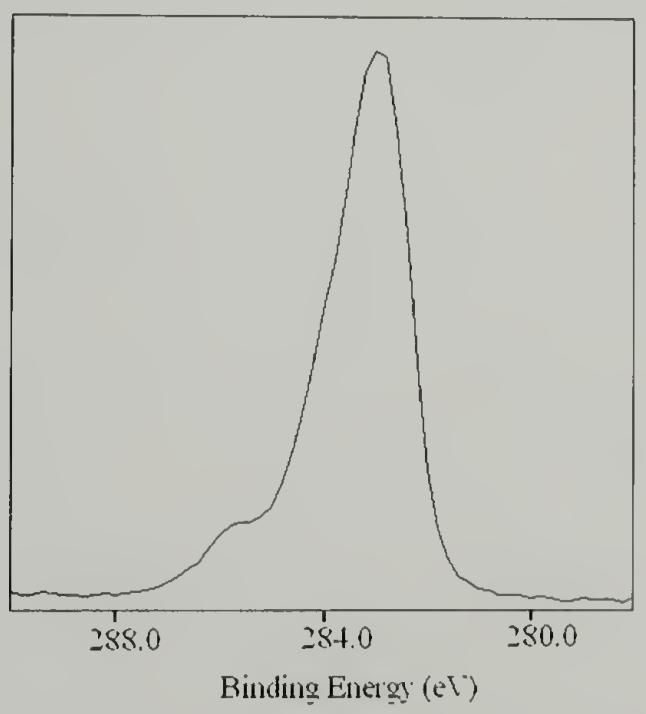

Figure 4.13. C_{1s} high-resolution XPS spectrum of dewetted region of nylon 6/6 [red].

4.3.2. Adsorption of Polyelectrolytes

Formation of polymer multilayers by the electrostatic adsorption of oppositely charged polyelectrolytes is a versatile method commonly used for surface modification.[1] As mentioned in the Introduction of this chapter, surface modification of nylons has been the subject of various studies, however modification through electrostatic adsorption of polyelectrolytes has not been as extensively studied as their covalent modification.[6-11,22-24] The amine-rich surface resulting from the chemical reduction of the amide groups of nylon was further used to modify the films by electrostatic adsorption of poly(4-sodium styrenesulfonate) and alginate (Figure 4.14). The effects of amine surface density, adsorption time, and concentration of the adsorbate are discussed in this section.

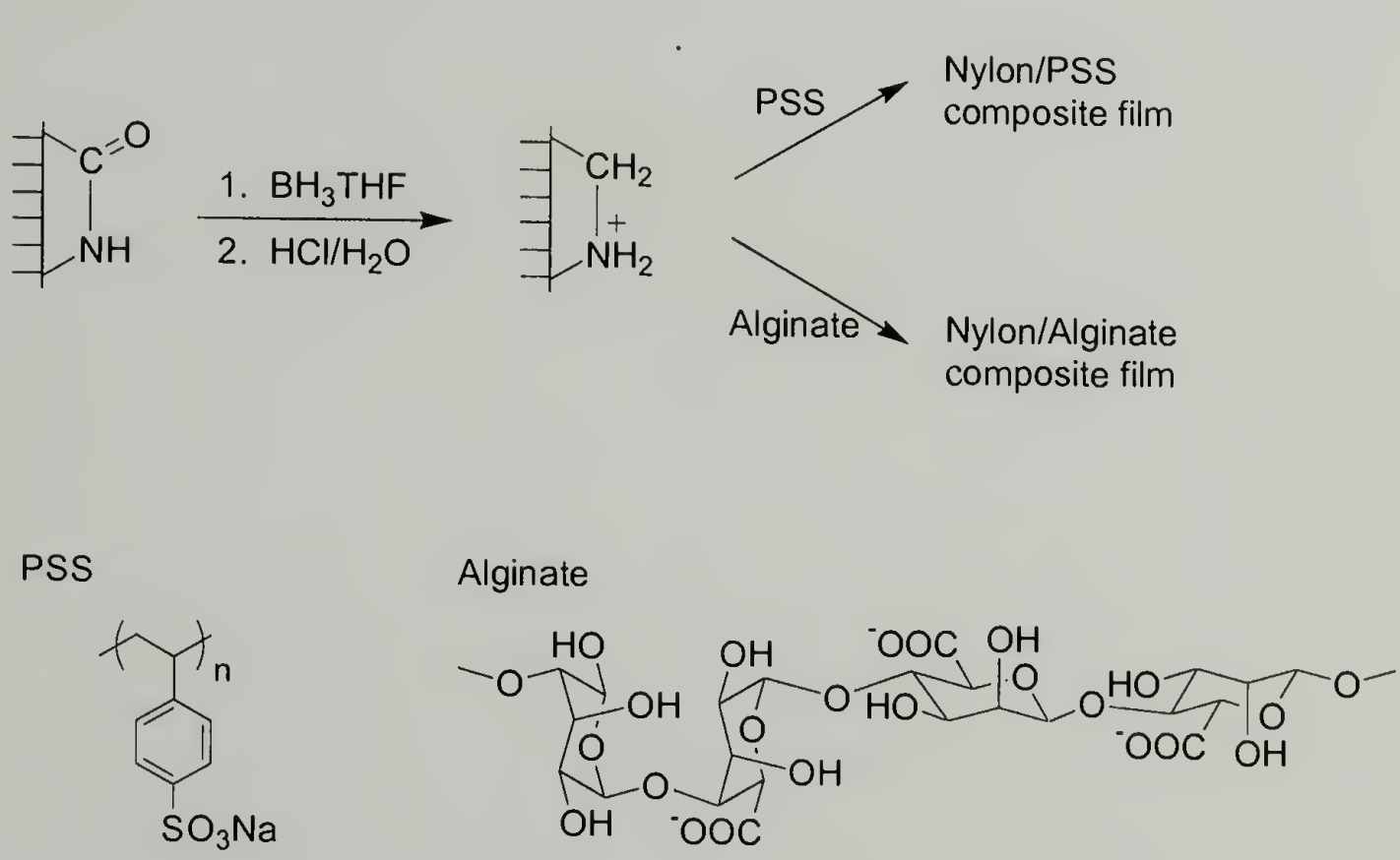

Figure 4.14. Schematic illustrating the electrostatic adsorption of polyelectrolytes onto surface-reduced nylon films samples.

4.3.3. Adsorption of alginate

Alginate, the sodium salt of alginic acid is a naturally occurring polysaccharide consisting of α-(1→4) L-guluronic acid (G) and β-(1→4) D-mannuronic acid (M) residues with a pKa of 3.38 and 3.65, respectively (Figure 4.15). The proportion of each residue is specific to the type of seaweed from which it is extracted, and determines the properties and structure of the macromolecule and its interaction with water. The structure of the polysaccharide is interesting since the mannuronic acid and guluronic acid residues are not randomly distributed throughout the chain, but rather they are found in blocks of M residues (MM), blocks of G residues (GG), and strictly alternating (GM) blocks; this accounts for the conformation of the polymer as either a linear chain (rich in MM blocks) or a more complex structure (rich in GG or GM blocks). Its biocompatibility and low-toxicity allows its use as a thickening agent, emulsifier, stabilizer, encapsulant, and gel-forming agent.

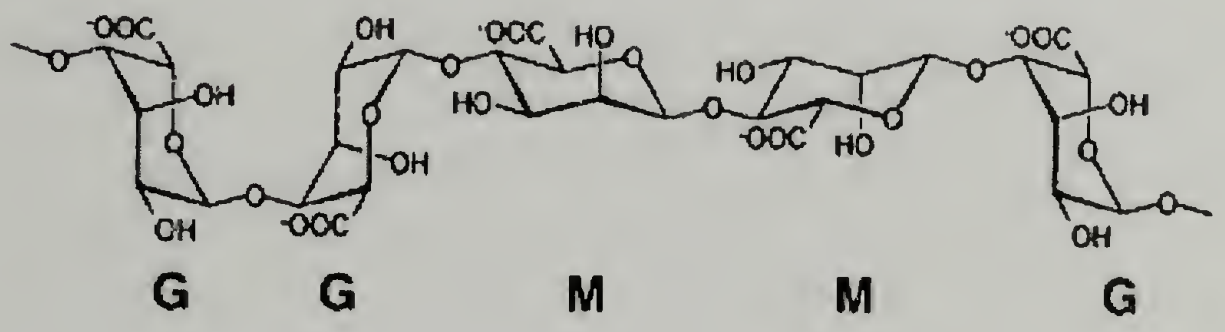

Figure 4.15. Chain conformation of alginate.

XPS results of alginate adsorption onto virgin and reduced nylon 6/6 films are presented in Table 4.4. Alginate adsorption onto virgin nylon films was negligible since no change in the atomic composition was observed; this result is not surprising given the low concentration of amine groups on the original surface. On the other hand, reduced nylon films showed a considerable increase in the concentration of oxygen and a decrease in the concentration of carbon and nitrogen upon adsorption. A higher concentration of oxygen is observed at a higher take-off angle, suggesting that the polysaccharide adsorbed by orientation of the negatively charged carboxylate groups toward the amine-rich surface. High-resolution XPS analysis showed that the carboxylic and glycosidic carbons of alginate broaden the C_{1s} high-resolution signal to higher binding energy (Figure 4.16), which was also the case for the O_{1s} region due to the incorporation of hydroxyl and ether groups. Alginate-coated samples exhibited similar advancing water contact angles and lower receding angles (θ_A/θ_R=32°/7°) compared to the polyamine surface.

Table 4.4. XPS atomic composition for alginate adsorption onto reduced nylon film surfaces.

Sample	XPS Atomic composition (%) [a]		
	C	O	N
Nylon 6/6	77.75	11.52	10.74
	76.04	12.50	11.46
Nylon 6/6 + Alginate (0.05%)	74.50	12.20	13.20
	74.50	12.30	13.10
Nylon 6/6 ^{red}	83.6	5.5	10.4
	80.9	6.5	12.2
Nylon 6/6 ^{red} + Alginate (0.05%)	66.9	24.4	8.7
	65.7	26.2	8.1
Nylon 6/6 ^{red} + Alginate (0.05%) + Ca (1%)	69.1	23.6	7.3
	65.9	25.7	8.4

[a] upper rows correspond to 15° take-off angle data and lower rows are 75° take-off angle data.

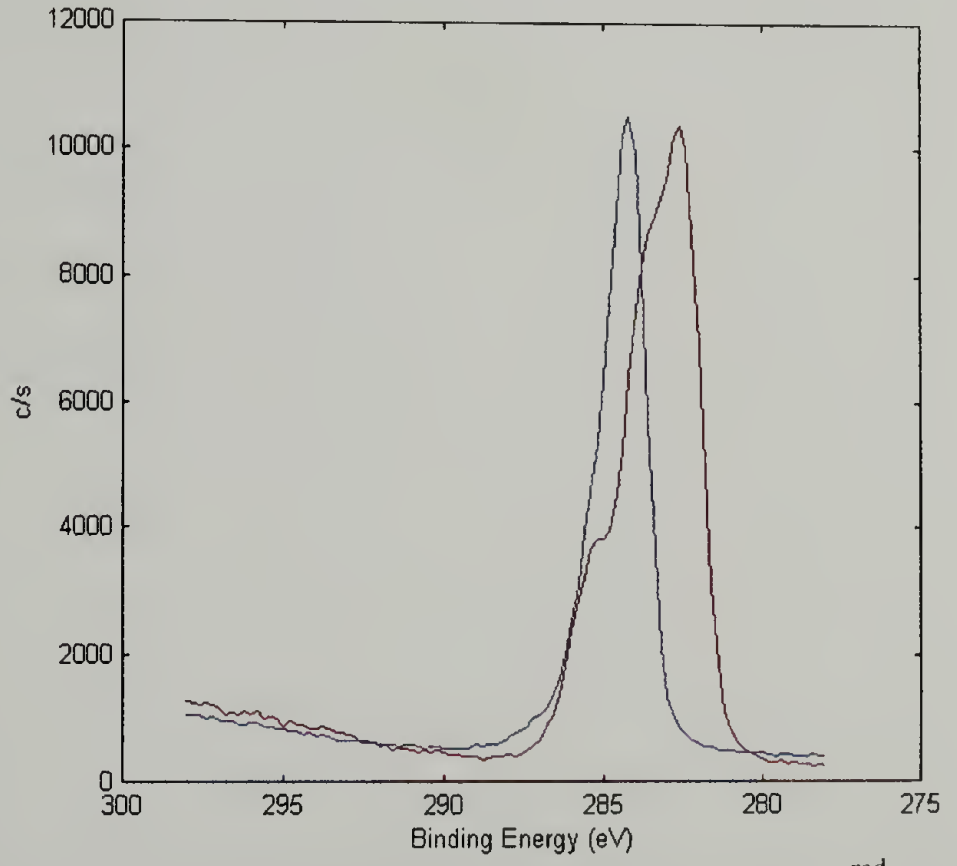

Figure 4.16. C_{1s} high-resolution XPS spectra of nylon 6/6 ^{red} (blue spectrum) and alginate-coated nylon 6/6 ^{red} (red spectrum).

The adsorption isotherm of alginate on 4 h-reduced nylon 6/6 films was determined by varying the adsorbate concentration between 0.01-0.5% (w/v). As presented in Figure 4.17, while a small change in the atomic composition of the surface with respect to the concentration of the polysaccharide exists, for the concentration range here examined, the shape of the isotherm appears to be similar to those observed for high-affinity systems, attributed to the strong interaction of alginate with the amine-enriched nylon surface. Based on these results, further adsorption studies were conducted with a solution concentration of 0.05% (w/v).

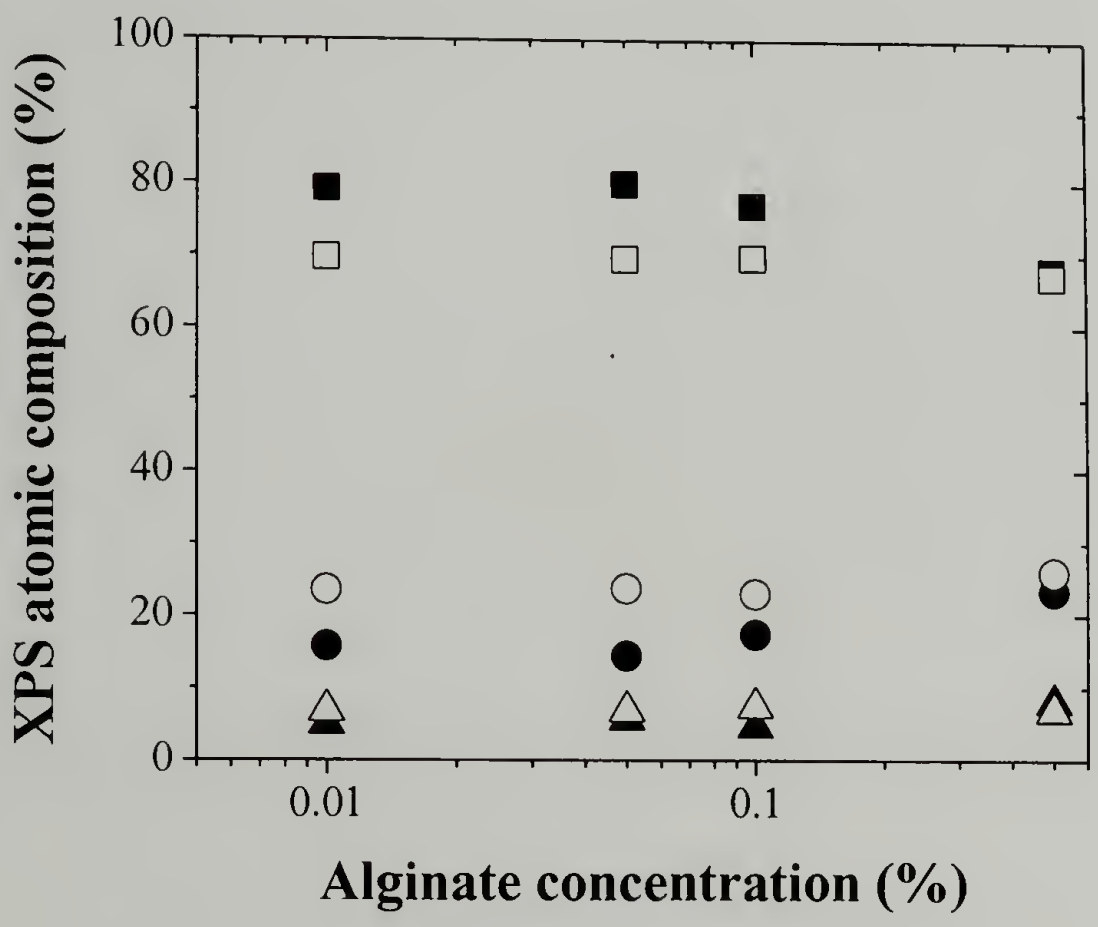

Figure 4.17. Adsorption isotherm of alginate onto nylon 6/6 ^{red} film samples. Surface atomic composition determined by XPS for different take-off angles. Carbon 15° (■) and 75° (□); oxygen 15° (●) and 75° (○); nitrogen 15° (▲) and 75° (△).

Kinetic analysis, done by varying the adsorption time between 0.5 to 3 h showed that the rate of adsorption is fast, reaching the maximum amount of specifically-adsorbed alginate within less than 1 h; longer times did not result in higher surface coverage (Figure 4.18).

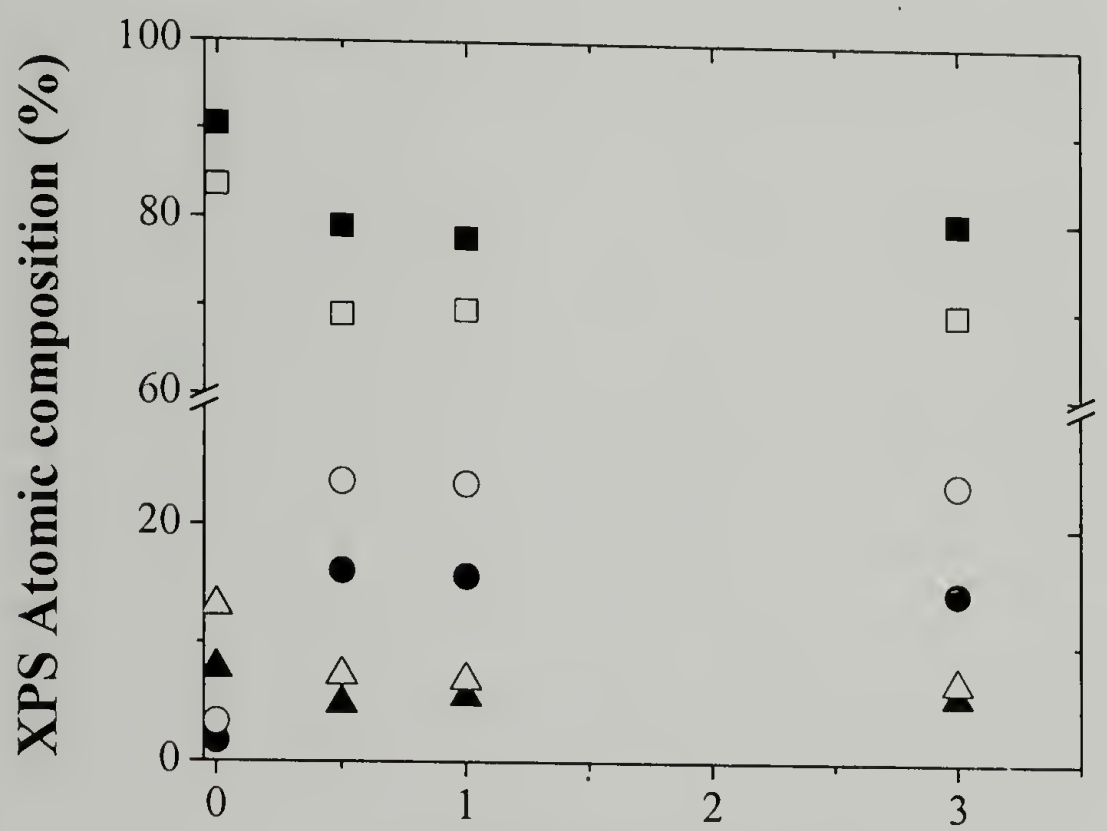

Figure 4.18. Kinetics of adsorption of alginate onto nylon 6/6 ^{red} film samples. Reduction time was 4 h. XPS atomic composition data at different take-off angles. Carbon 15° (■) and 75° (□); oxygen 15° (●) and 75° (○); nitrogen 15° (▲) and 75° (△).

Although primary amine chain-ends are present in a low density on the surface of nylon 6/6 fibers (0.011 $-NH_2/nm^2$),[83] they have been successfully used for grafting reactions. These groups are also liable to undergo electrostatic interactions with anionic species, however, as we found for the adsorption of alginate onto virgin nylon 6/6 films, the end-groups are present is such a low density on the surface that adsorption does not

occur. To determine the effect of the density of cationic sites on adsorption, samples with different reduction times, i.e. different amine group densities, were studied. The results are presented in Figure 4.19 in terms of the atomic composition of the composite film. An increase in the concentration of oxygen and a decrease in the concentration of nitrogen, indicative of adsorption, are observed with reduction time. The fact that the atomic concentration reaches a plateau indicates that a critical concentration of amine groups, corresponding to a reduction yield of ~ 30%, is necessary for significant electrostatic adsorption to occur.

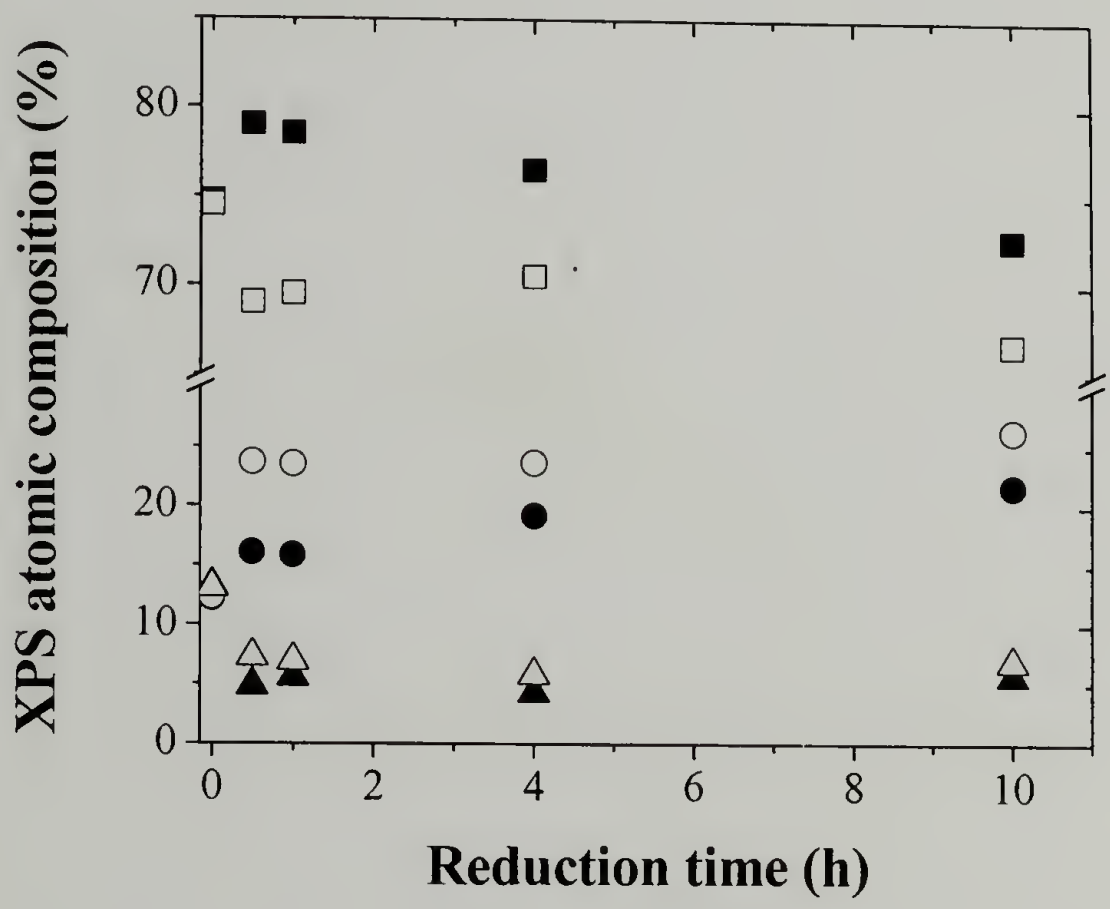

Figure 4.19. Effect of reduction time on the adsorption of alginate onto nylon 6/6 [red]. XPS atomic composition data at different take-off angles: carbon 15° (■) and 75° (□); oxygen 15° (●) and 75° (○); nitrogen 15° (▲) and 75° (△).

Regarding the morphology of the surface after adsorption, AFM results revealed that the polysaccharide coats the surface homogenously, without the formation of large aggregates (Figure 4.20). The thickness of the alginate coating was estimated to be less than 1 μm since ATR-IR spectra of the films before and after adsorption show no change.

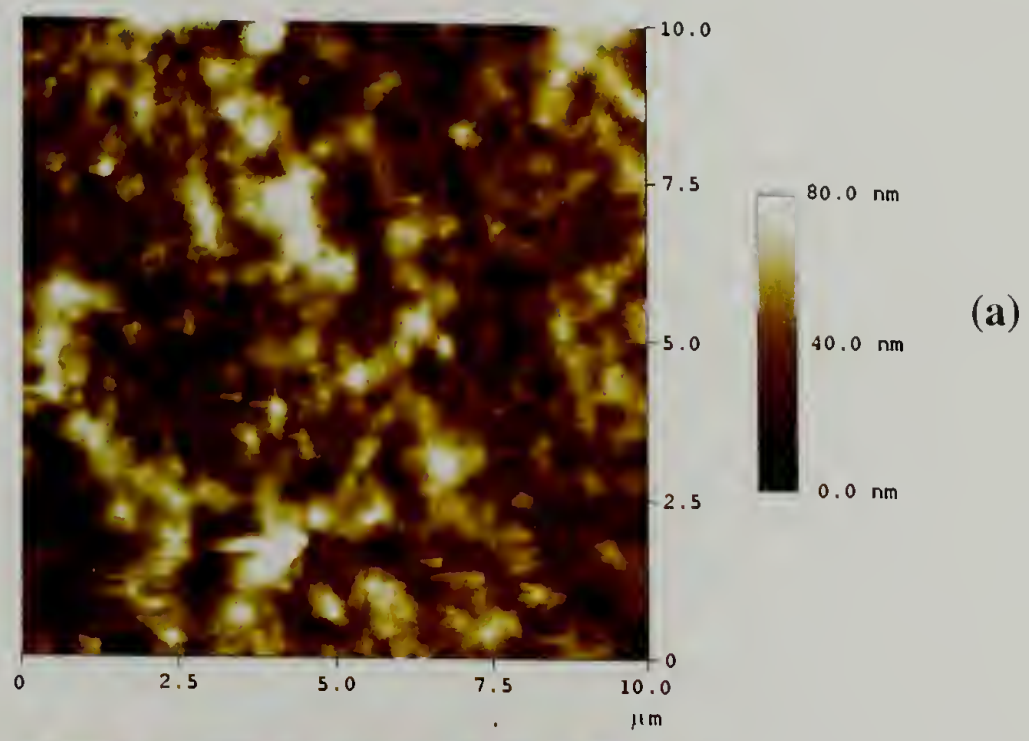

Figure 4.20. Morphology of alginate-coated nylon 6/6 [red]. Film samples were reduced at 50 °C for 10 h; adsorption was done for 3 h from 0.05% (a) and 0.5% (b) w/v solutions of alginate. Images correspond to height plots of a 10 μm x 10 μm sampling area.

Another interesting property of alginate is its capacity to form gels in the presence of divalent ions. This is attributed to the interactions between the divalent ion, commonly calcium, and blocks of guluronic acid, specifically the oxygen atoms of the guluronate segments. Oxygen atoms from the guluronate segments, but not mannuronate, are involved in coordination of the ion, producing a conformation referred to as "egg-box" (Figure 4.21). The adsorption of cross-linked alginate onto amine-rich nylon surfaces was also studied. The atomic composition of cross-linked alginate on reduced nylon surfaces is presented in Table 4.4 and it is very similar to that of alginate at both take-off angles. This difference can be ascribed to the low concentration of calcium used for cross-linking (1% molar with respect to the moles of alginate) and also the cross-linking method. The results suggest that a layer of alginate of a thickness equivalent to that obtained for the non-cross-linked system was adsorbed.

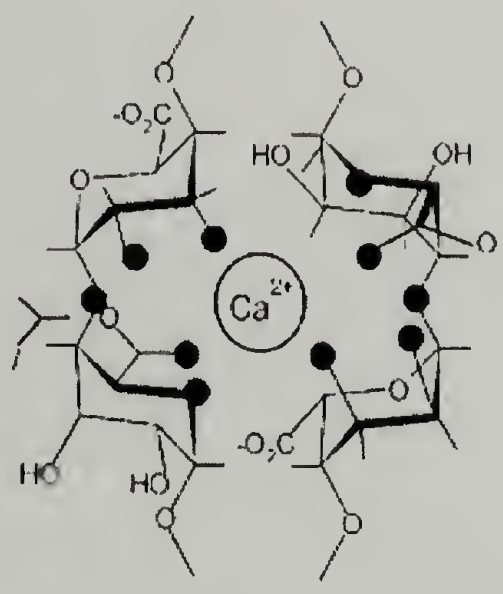

Figure 4.21. Schematic drawing of calcium coordination to guluronate units in the "egg box model". Dark circles represent the oxygen atoms involved in the coordination of the calcium ion.[116]

4.3.4. Adsorption of poly(4-sodium styrenesulfonate)

As proof of concept, the electrostatic adsorption of poly(4-sodium styrene sulfonate), PSS, on reduced nylon films was also studied. PSS is widely used for the formation of polymer multilayers, and since each repeat unit possesses a sulfur atom, which has a high atomic sensitivity factor (0.49 for S_{2p} vs. 0.13 for C_{1s}) it serves as a good label for XPS analysis. The adsorption of PSS on nylon samples reduced for varying periods of time is presented in Figure 4.22. Similar to alginate, a high-affinity isotherm is obtained, and analogous to the previous case, a higher concentration of sulfur was observed at higher take-off angles, confirming the electrostatic nature of the interaction and revealing that the sulfonate groups are buried in the diffuse interface.

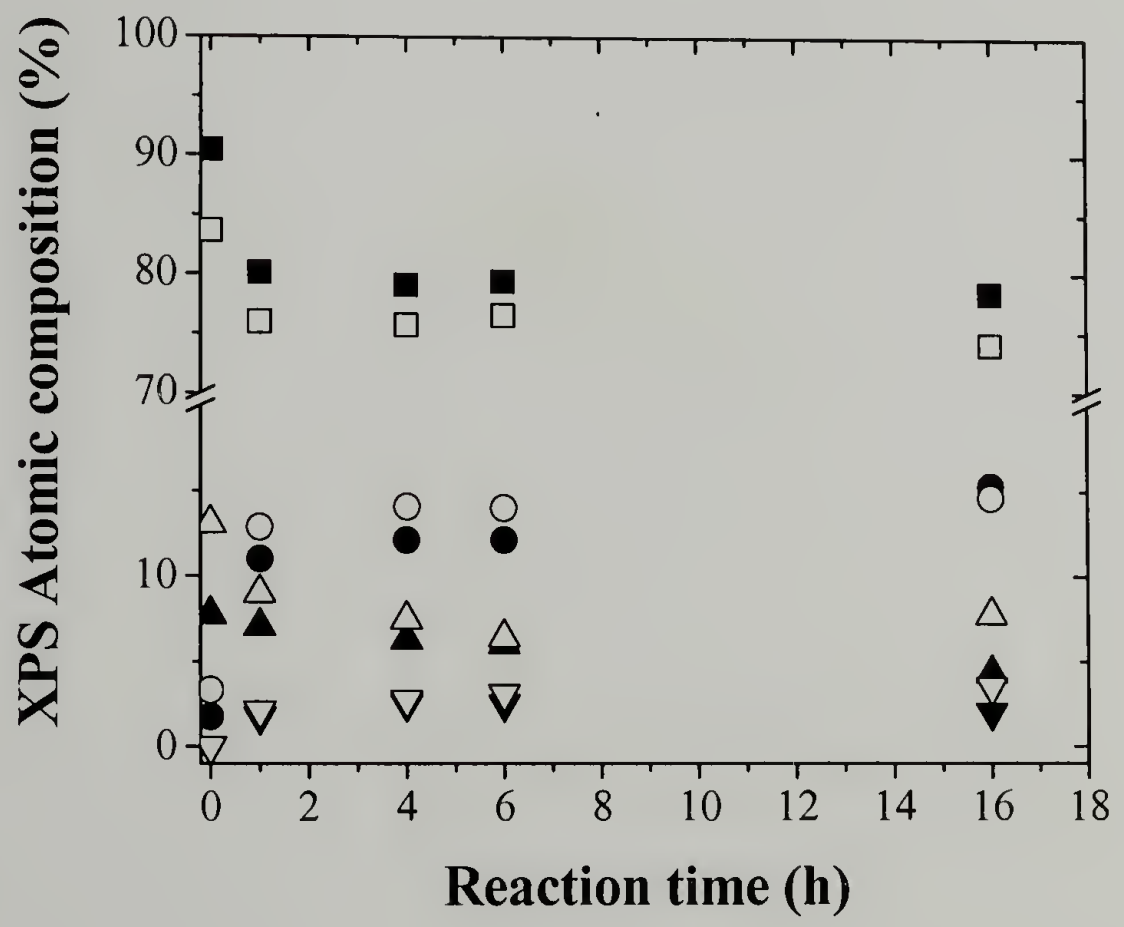

Figure 4.22. Effect of reduction time of nylon 6/6 on the adsorption of poly(4-sodium styrenesulfonate). XPS atomic composition acquired at 15° and 75° take-off angles. Carbon 15° (■) and 75° (□); oxygen 15° (●) and 75° (○); nitrogen 15° (▲) and 75° (△); sulfur 15°(▼) and 75° (▽).

4.4. Conclusions

The chemical reduction of nylon film surfaces by reaction with BH_3THF was studied. While the reaction occurs in high yields, its surface-confinement is highly dependent on the segmental mobility of the polymer, which is in turn determined by the glass transition and/or crystallinity of the polymer. The favorable interaction of the reaction intermediates with the medium produced a change in the surface morphology of the films. With a high concentration of amine groups on the surface, the reduced nylon substrates can now be used as templates for the well-established surface modification through electrostatic adsorption of polyelectrolytes. Composite films were produced by electrostatic adsorption of alginate and poly(4-sodium styrenesulfonate) and the effects of surface charge density and concentration of the adsorbate were discussed.

78. Odian, G. *Principles of Polymerization*; 3rd Ed.; John Wiley and Sons: New York, 1991.

79. Williams, J. C. L. In *Nylon Plastics Handbook*; Kohan, M. I.; Ed.; Hansen Publishers: New York, NY, 1995.

80. Tušek, L.; Nitschke, M.; Werner, C.; Stana-Kleinschek, K.; Ribitsch, V. *Colloid Surface A* **2001**, *196*, 81.

81. Foerch, R.; Hunter, D. H. *J. Polym. Sci. Part A: Polym. Chem.* **1992**, *30*, 279.

82. Weikart, C. M.; Miyama, M.; Yasuda, H. K. *J. Colloid Interface Sci.* **1999**, *211*, 18.

83. Michielsen, S. *J. Appl. Polym. Sci.* **1999**, *73*, 129.

84. Campbell, J.; Hornby, W. N.; Morris, D. L. *Biochm. Biophys. Acta* **1975**, *384*, 307.

85. Thompson, R. Q.; Mandoke, C. S.; Womack, J. P. *Anal. Lett.* **1985**, *18*, 93.

86. Lozano, P.; Iborra, J. L. In *Methods in Biotechnology, Vol. 1: Immobilization of Enzymes and Cells*; Bickerstaff, G. F.; Ed.; Humana Press: Totowa, NJ, 1997.

87. Klein, E.; Feldhoff, P. A. European Patent 0441660A1, 1991.

88. Perry, E.; Savory, J. *J. Appl. Polym. Sci.* **1967**, *11*, 2473.

89. Deng, S.; Bai, R.; Chen J. P. *Langmuir* **2003**, *19*, 5058.

90. Dhamodharan, R.; McCarthy, T. J. *Macromolecules* **1999**, *32*, 4106.

91. Zammateo, N.; Girardeacex, C.; Delforge, D.; Pireaux, J.; Remacle, J. *Anal. Biochem*. **1996**, *236*, 85.

92. Brown, H. C.; Heim, P. *J. Org. Chem.* **1973**, *38*, 912. Brown, H. C.; Choi, Y. M.; Narasimhan, S. *J. Org. Chem.* **1982**, *47*, 3153.

93. Matthiasson, E. *J. Membr. Sci.* **1983**, *16*, 23.

94. Wang, Y.; Kim, J.-H.; Choo, K.-H.; Lee, Y.-S.; Lee, C.-H. *J. Membr. Sci.* **2000**, *169*, 269.

95. Wavhal, D. S.; Fisher, E. R. *Langmuir* **2003**, *19*, 79.

96. Tobiesen, F. A.; Michielsen, S. *J. Polym. Sci. A Polym. Chem.* **2002**, *40*, 719.

97. Kang, M. S.; Chun, B.; Kim, S. S. *J. Appl. Polym. Sci.* **2001**, *81*, 1555.

98. Pieracci, J.; Crivello, J. V.; Belfort, G. *Chem. Mater.* **2002**, *14*, 256.

99. Castilho, L. R.; Anspach, F. B.; Deckwer, W.-D. *J. Memb. Sci.* **2002**, *207*, 253.

100. Beeskow, T.; Kroner, K. H.; Anspach, F. B. *J. Colloid. Interf. Sci.* **1997**, *196*, 278.

101. Castilho, L. R.; Deckwer, W.-D.; Anspach, F. B. *J. Memb. Sci.* **2000**, *172*, 269.

102. Hartley, P. G.; McArthur, S. L.; McLean, K. M.; Griesser, H. J. *Langmuir* **2002**, *18*, 2483.

103. Morra, M.; Cassinelli, C. *Langmuir* **1999**, *15*, 4658.

104. Mason, M.; Vercruysse, K. P.; Kirker, K. R.; Frisch, R.; Marecak, D. M.; Prestwich, G. D.; Pitt, W. G. *Biomaterials* **2000**, *211*, 31.

105. McArthur, S. L.; McLean, K. M.; Kinshott, P.; St John, H. A. W.; Chatelier, R. C.; Griesser, H. J. *Coll. Surf. B: Biointerfaces* **2000**, *17*, 37.

106. Clark, D. T.; Thomas, H. R. *J. Polym. Sci. Polym. Chem. Ed.* **1977**, *15*, 2843.

107. Manku, S.; Laplante, C.; Kopac, D.; Chan, T.; Hall, D. G. *J. Org. Chem.* **2001**, *66*, 874.

108. Chapman, T. M.; Benrashid, R.; Marra, K. G.; Keener, J. P. *Macromolecules*, **1995**, *28*, 331.

109. Chen, W.; McCarthy, T. J. *Macromolecules* **1997**, *30*, 78.

110. Jia, X. Ph. D. Thesis, Polymer Science and Engineering, University of Massachusetts Amherst, **2002**.

111. *High Resolution XPS of Organic Polymers: The Scienta ESCA300 Database;* Beamson, G.; Briggs, D., Eds.; John Wiley & Sons: New York, NY, 1992.

112. Dhamodharan, R.; Nisha, A.; Pushkala, K.; McCarthy, T. J. *Langmuir* **2001**, *17*, 3368.

113. Wamser, C. C.; Gilbert, M. I. *Langmuir* **1992**, *8*, 1608.

114. Perner, T.; Schultz, R. C. *Brit. Polym. J.* **1987**, *19*, 181.

115. Herrera-Alonso, M.; McCarthy, T. J. *Polymer Preprints* **2004**, *45*, 990.

116. Braccini, I.; Pérez, S. *Biomacromolecules* **2001**, *2*, 1089.

CHAPTER 5

FABRICATION OF POLYPROPYLENE/CLAY NANOCOMPOSITES WITH POLYAMINES OF CONTROLLED CHARGE DENSITY AS COMPATIBILIZERS

5.1. Introduction

Recently there has been growing interest in the fabrication of polymer nanocomposites since it was recognized that incorporation of small amounts (< 10% wt) of diverse inorganic materials into engineering polymers produced an enhancement of their properties, such as increased modulus and strength, elevated heat distortion temperatures, enhanced barrier properties, decreased coefficient of thermal expansion, and improved ionic conductivity. Among the inorganic particles used, aluminosilicate clays are the most common, and within this group is montmorillonite with a general structure: $Na^{+}_{0.86}[Mg_{0.86}Al_{3.14}Si_{8.0}O_{20}H_4]^{-}$. The layered structure of montmorillonite consists of two silica tetrahedral sheets and an aluminum octahedral sheet. The clay platelets are approximately 250 nm in length and 10 Å in thickness and possess a net anionic surface charge, countered by the presence of cations. Weak dipolar interactions are responsible for clay stacking, leading to interlayer galleries.

Polymer/clay nanocomposites have been synthesized by three different methods. The first, polymerization intercalation, involves *in-situ* polymerization or cross-linking of monomers in the presence of the clay.[117,118] The second method is polymer solution intercalation, where displacement of solvent molecules from solvent-swollen layered silicates by polymer chains produces an intercalated structure.[119] The last method, which has gained considerable attention in recent years due to its environmentally benign nature, is melt intercalation.[120,121,122,123] In this case, a mixture of polymer and

inorganic particles is annealed above the softening temperature of the polymer, allowing the polymer to diffuse into the clay galleries. Regardless of the method by which they are produced, an important parameter in polymer/clay nanocomposites, which will determine the systems' final properties, is the degree of dispersion of the inorganic phase (Figure 5.1). When the inorganic phase is delaminated and homogenously dispersed throughout the polymer matrix with little or no interaction between individual platelets the system is referred to as being exfoliated. On the other hand, when retention of order within the silicate domain prevails, the system is referred to as being intercalated.

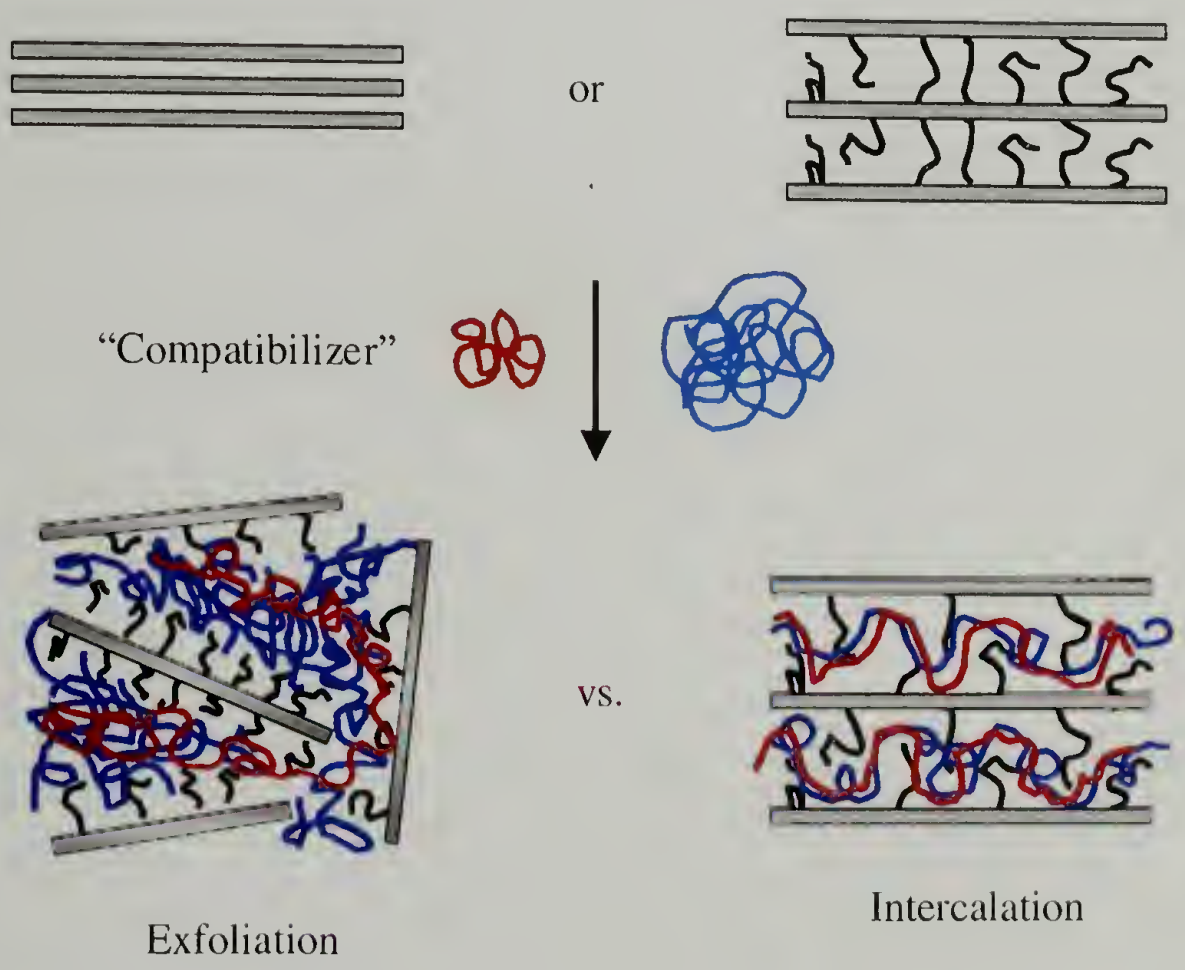

Figure 5.1. Schematic of the intercalation/exfoliation of a system composed of clay/polymer/compatibilizer.

The intercalation/exfolation process in melt intercalation is dependent on the thermodynamic interactions between the polymer chains and the silicate. The entropic loss associated with intercalation must be counterbalanced by favorable energetic interactions between the two phases. For unmodified montmorillonite, this has been accomplished only with hydrophilic and polar polymers such as poly(ethylene oxide)[124,125] and poly(vinyl alcohol).[126] Intercalation in systems where the polymer is non-polar and hydrophobic requires modification of the clay with alkylammonium salts through a cation-exchange reaction, however for systems such as polyethylene and polypropylene, chemical surface modification of the clay is insufficient to allow intercalation/ exfoliation to occur. To enhance the interaction between the polymer and clay, the use of compatibilizers has been proposed, for example with dimethyldioctadecylammonium bromide as a reactive compatibilizer for the melt intercalation of ethylene-vinyl acetate copolymers,[127] or the use of diblock copolymers where one of the blocks has certain affinity for the clay and the other serves to ensure miscibility with the polymer matrix.[128,129] The nature of the interaction between the polymer, or compatibilizer, can be hydrophilic/hydrophilic as is the case for poly(ethylene oxide)-containing copolymers with non-modified clays, or ionic as is the case for long alkylammonium salts. Although polyamines are widely used to study the layer-by-layer assembly of polycations/clay systems in solution, their use as compatibilizers in melt intercalation applications has, to our knowledge, not been studied.

Synthetic polyamines are used in applications involving the electrostatic interactions with anionically charged colloidal particles, for example the flocculation of

particulate matter from turbid natural waters, as aids in pigment retention in the manufacture of paper, sludge dewatering, biocides, for enhanced oil recovery, and for the delivery of DNA to cells (transfection).[130] Synthetic polyamines are generally obtained by reactions on polymer backbones. Poly(N-alkyleneimine)s, or polymeric secondary amines, can be prepared from the ring opening polymerization of N-alkyleneimines, however this reaction is accompanied by a series of side reactions that limit its yield. Among the poly(N-alkyleneimines), the most popular is poly(ethyleneimine) or PEI, which, depending on the method by which it is synthesized, exists either as a highly branched structure or as a linear polymer. Branched amorphous PEI is obtained from the cationic ring opening polymerization of ethylenimine. It contains primary, secondary, and tertiary amino groups, in approximate ratios of 1:1:1 to 1:2:1.[131] Its linear analog is highly crystalline, water-soluble, and depending on its molecular weight, partially soluble in lower alcohols. It is obtained from the cationic polymerization of cyclic iminoethers such as oxazolines, followed by basic hydrolysis of the amide group.[132] Polymerization of six-membered cyclic iminoethers and subsequent hydrolysis has also been reported for the synthesis of poly(trimethyeleneimine). Linear poly(alkyleneimine)s have been applied to metal recovery from dilute solutions by homogenous phase complexation, where it was found that copper (II) forms the most stable complexes with LPEI.[131] Heterogeneous phase complexation has also been studied, and it involves cross-linking the water-soluble polymer with difunctional reagents such as dihalogen derivatives or 2,5-divinylpyridine.

Perner and Schulz found that reduction of polyamide-6 with either lithium aluminum hydride ($LiAlH_4$) or borane-dimethylsulfide (BH_3DMS) produced a new type

of poly(alkyleneimine).[133] Since their discovery, poly(hexaneamine) or poly(iminohexamethylene) has been used in a series of applications: synthesis of semi-fluorinated side-chain ionenes which spontaneously self-organize to expose a uniform $-CF_3$ surface,[134] synthesis of rotaxanes, macromolecular switching devices in which a macrocylic compound (cucurbituril) is threaded, through specific interactions, onto a segment of a polymer chain,[135] as a synthetic carriers for the delivery of therapeutic DNA to cells (transfection) by complexation with polycations.[136,137,138,139,140]

This chapter describes the synthesis of linear polyalkyleneimines with controlled charge density produced by the bulk reduction of nylons, and their application as compatibilizers for the intercalation/exfolation process of polypropylene with modified and unmodified montmorillonite clays. It is speculated that the hydrophilicity and cationic nature of the polyamines will allow them to act as aids in intercalation/exfoliation processes.

5.2. Experimental

5.2.1. Materials

Unless otherwise indicated, all materials were used as received. Nylon 4/6 and nylon 6/9 pellets, anhydrous tetrahydrofuran (THF), borane-THF complex (1.0 M), morpholine (99%), and sodium hydroxide were obtained from Aldrich. Whatman nylon 6/6 membranes (average pore size 0.45 μm), formic acid (88%), and hydrochloric acid (37%) were purchased from Fisher. Polypropylene flakes were supplied by Plastics Distribution Corp. Unmodified montmorillonite (MNa+) and surface-modified montmorillonite (M15A) clays were obtained from Southern Clay Products, Inc. M15A is a surface-modified clay wherein the sodium ion has been replaced with dimethyldi(hydrogenated tallow) ammonium ion by an cation exchange reaction. Both clays were kept inside a vacuum oven at 50 °C to prevent hydration.

5.2.2. Methods

Differential scanning calorimetry (DSC) analysis was conducted with a TA Instruments 2910 DSC thermal analyzer at a heating rate of 10 °C/min. Attenuated total reflectance infrared spectroscopy (ATR IR) was performed on a Bio Rad FTS 175C FT-IR spectrometer with an MCT detector; spectra were recorded using germanium crystals (45°) as the internal reflection element. ^{1}H NMR spectra were obtained on a 300 MHz Bruker DPX spectrometer with D_2O as solvent. MALDI-TOF spectra were recorded on a Bruker REFLEX III mass spectrometer. Potentiometric titrations were done with an Accumet20 pH/conductivity meter. Thermogravimetric analysis was perfomed on a TGA 2950, DuPont Instruments. Scanning electron microscopy (SEM) images were acquired using a JEOL JSM 6320F instrument; a thin layer of gold was sputtered onto

the samples prior to characterization. X-ray photoelectron spectroscopy (XPS) spectra were recorded on a Physical Electronics Quantum 2000 Scanning ESCA Microprobe with MgK_{α} excitation at 15 kV and 50 W for a probing size of 200 μm. Spectra were acquired at 15° and 75° angles with respect to the plane of the sample surface. X-Ray diffraction experiments were performed on a Rigaku RU-200 rotating anode diffractometer. Dynamic mechanical analysis was done on a TA Instruments DMA 2980.

5.2.3. Preparation of nylon membranes

Nylon 4/6 and nylon 6/9 membranes were fabricated by diffusion-induced phase separation. Solutions of the polyamides in formic acid were prepared 12 h prior to casting, 10% wt and 5% wt for nylon 4/6 and nylon 6/9, respectively. The solutions were cast onto clean glass slides with the aid of a 250 μm (~ 10 mil) gap applicator, and immediately submerged into a bath containing a non-solvent, in this case reverse-osmosis treated water (RO water). Coagulation was allowed to proceed for 12 h, after which time the membranes were peeled off the glass slide, allowed to sit in a clean water bath for 12 h and thoroughly rinsed with copious amounts of RO water. Prior to reaction, the membranes were further rinsed with water, ethanol, acetone, tetrahydrofuran, and hexane, and dried at 55 °C under reduced pressure (80 mTorr) for 24 h.

5.2.4. Reduction

Dry membranes (approximately 0.5 g) were rapidly transferred into a round-bottom flask containing a magnetic stir bar inside a nitrogen-purged glove box. Anhydrous THF (25 mL) was cannulated into the flask, followed by the addition of a

borane-THF complex (1 M, 10 equiv with respect to the moles of amide). The solution was heated to reflux (65 °C) and maintained at that temperature for 72 h, after which time it was allowed to cool to room temperature. Isolation of the polyamine was done by addition of morpholine (2 equiv with respect to the moles of borane) to the reaction solution *via* cannula. The solution was heated to 65 °C and allowed to react under reflux for 72 h. THF was then removed under reduced pressure and 35 mL of Milli-Q water were added to dissolve the precipitate. The solution was neutralized (pH = 6) by titration with hydrochloric acid (1 N) and dialyzed from Milli-Q water at room temperature for 72 h. The cutoff molecular weight of the dialysis tube was 17,000 Da. Water was removed using a rotary evaporator, and samples were dried under vacuum in an oven at 50 °C for 12 h, yielding the solid polyamine.

5.2.5. Polyamine/clay nanocomposites

Nanocomposites were prepared by rapidly mixing polypropylene powder (85% wt or 297.5 mg), dry polyamine (10% wt or 35 mg), and dry clay (5% wt or 17.5 mg) in a clean glass scintillation vial. The powder was placed in a steel mold (1.0 cm × 2.0 cm × 0.2 cm) and melt-pressed at 180 °C for 2 h between two sheets of polyimide film to a pressure of 20,000 psi.

5.3. Results and Discussion

5.3.1. Preliminary Results

As discussed in the previous chapter, the chemical reduction of nylon-film surfaces by reaction with BH_3·THF proceeds to high yields with a weak take-off angle dependence observed at the outer 10 Å to 40 Å of the surface and a change in the surface morphology, suggesting that the solvent properties of the medium change upon reaction. A molecular mobility argument, based on the glass transition temperature (Tg) of the polymers, was used to explain the differences in terms of reaction yields for different types of nylons. It was speculated that reactions conducted at temperatures close to, or higher than the Tg of the polymer, would lead to higher penetration depths. To confirm this hypothesis, reduction of nylon 6/6 film surfaces was carried out at 65 ^{o}C, which is 10 ^{o}C higher than the temperature used for the chemical surface modification study. ATR IR analysis revealed a considerable increase in penetration depth (to 500 nm) under these conditions, and the resulting spectra are presented in Figure 5.2. While the absorption bands at 3302 cm^{-1} (N-H stretch), 1635 cm^{-1} (C=O stretch), and 1540 cm^{-1} (N-H bend/C-N stretch), characteristic of amides, were lost upon reaction, new signals appear in the region from 2317-2365 cm^{-1} and 1165 cm^{-1}, attributed to B-H and B-C stretch, respectively. An increase in intensity of the signals associated with the CH_2 group at 2920 cm^{-1} (asymmetric stretch), 2860 cm^{-1} (symmetric stretch), 1460 cm^{-1} (symmetric scissor deformation) was also observed.

A kinetic study of the reduction at 65 ^{o}C (Figure 5.3) between 0 h and 96 h of reaction revealed the gradual decrease of the amide signals and increase of the borane signals, reaching a plateau after 72 h of reaction.

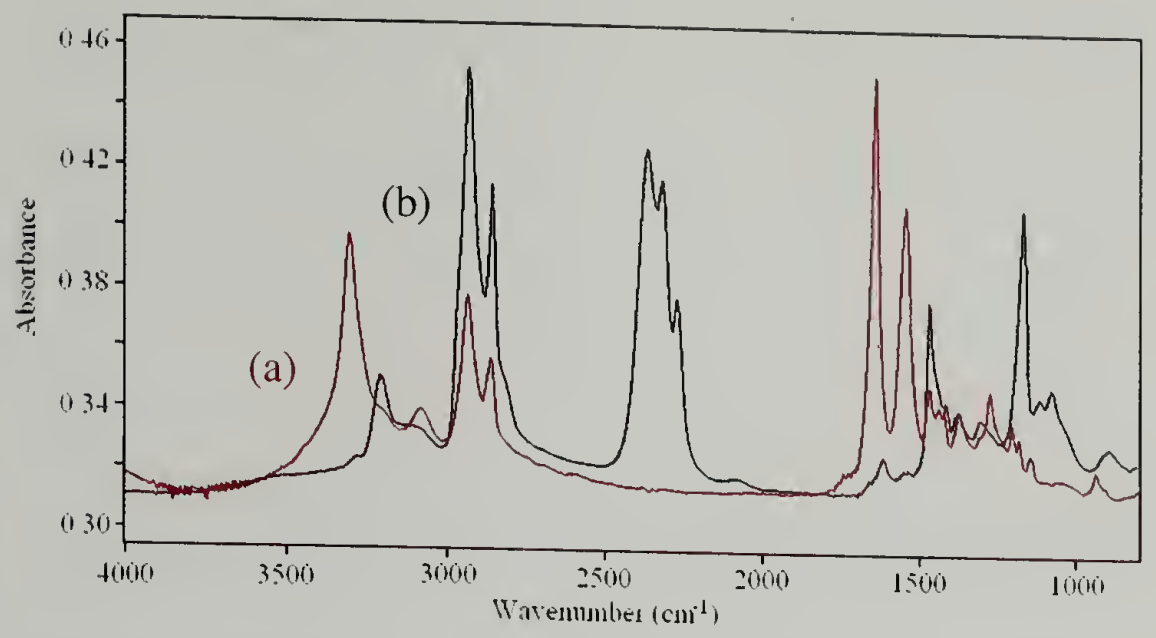

Figure 5.2. ATR IR spectra (RIE Ge 45°) of virgin nylon 6/6 film (a) and $^{BH3THF}nylon_{6/6}$ (b). Reduction was carried out under reflux (65 °C) for 96 h.

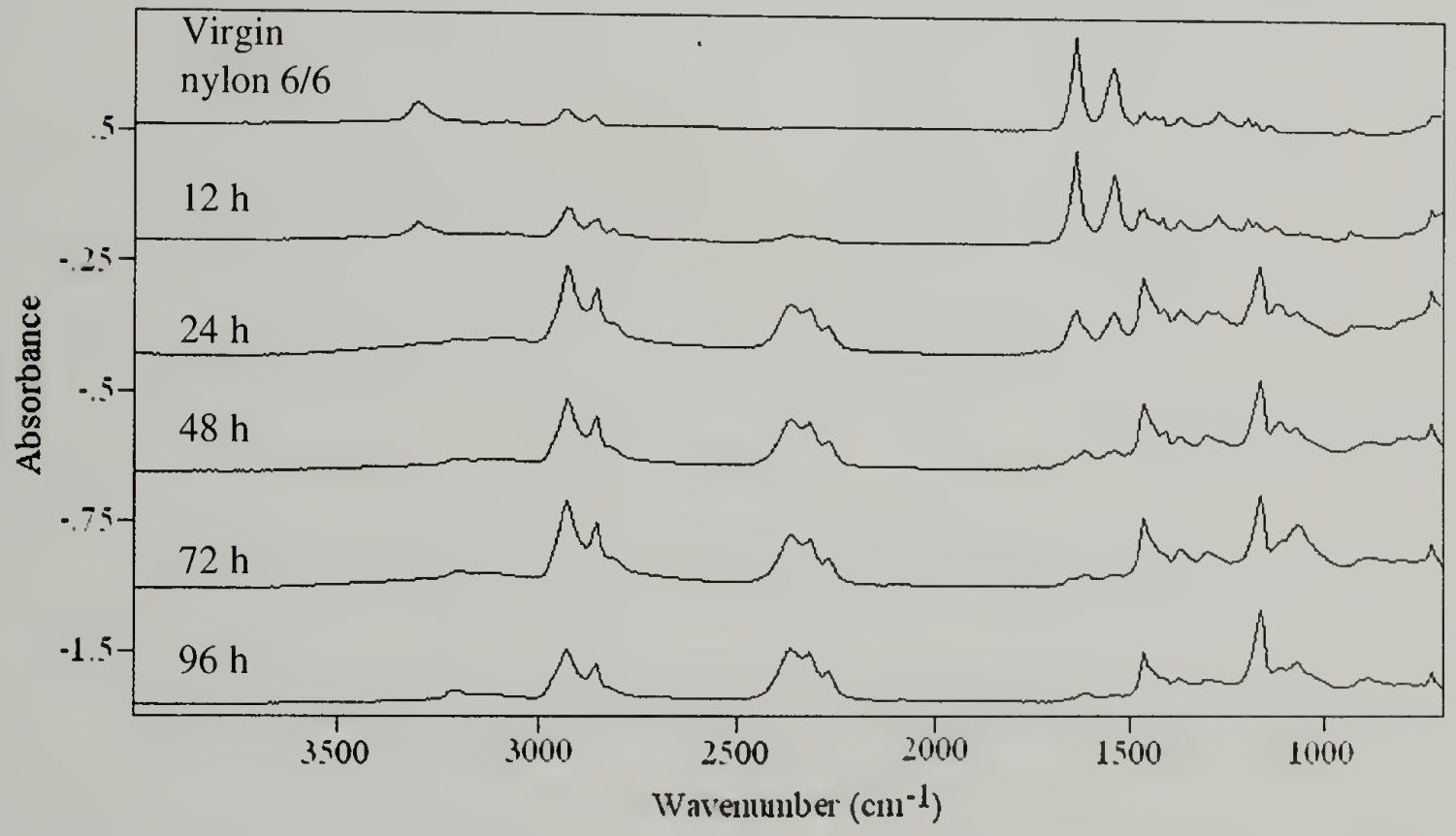

Figure 5.3. ATR IR spectra (Ge 45°) of BH_3·THF-reduced nylon 6/6 films. Reactions were carried out under reflux (65 °C) from 12 h to 96 h.

These results suggest that, given a nylon substrate with high surface area, reduction with BH_3·THF can be carried out in the bulk to synthesize polyalkyleneimines, whose hydrocarbon composition will be dictated by that of the parent polyamide, as shown in Figure 5.4. For the sake of brevity, and not to be confused with the polyamides, the polyamines will be abbreviated as PA46, PA66, and PA69.

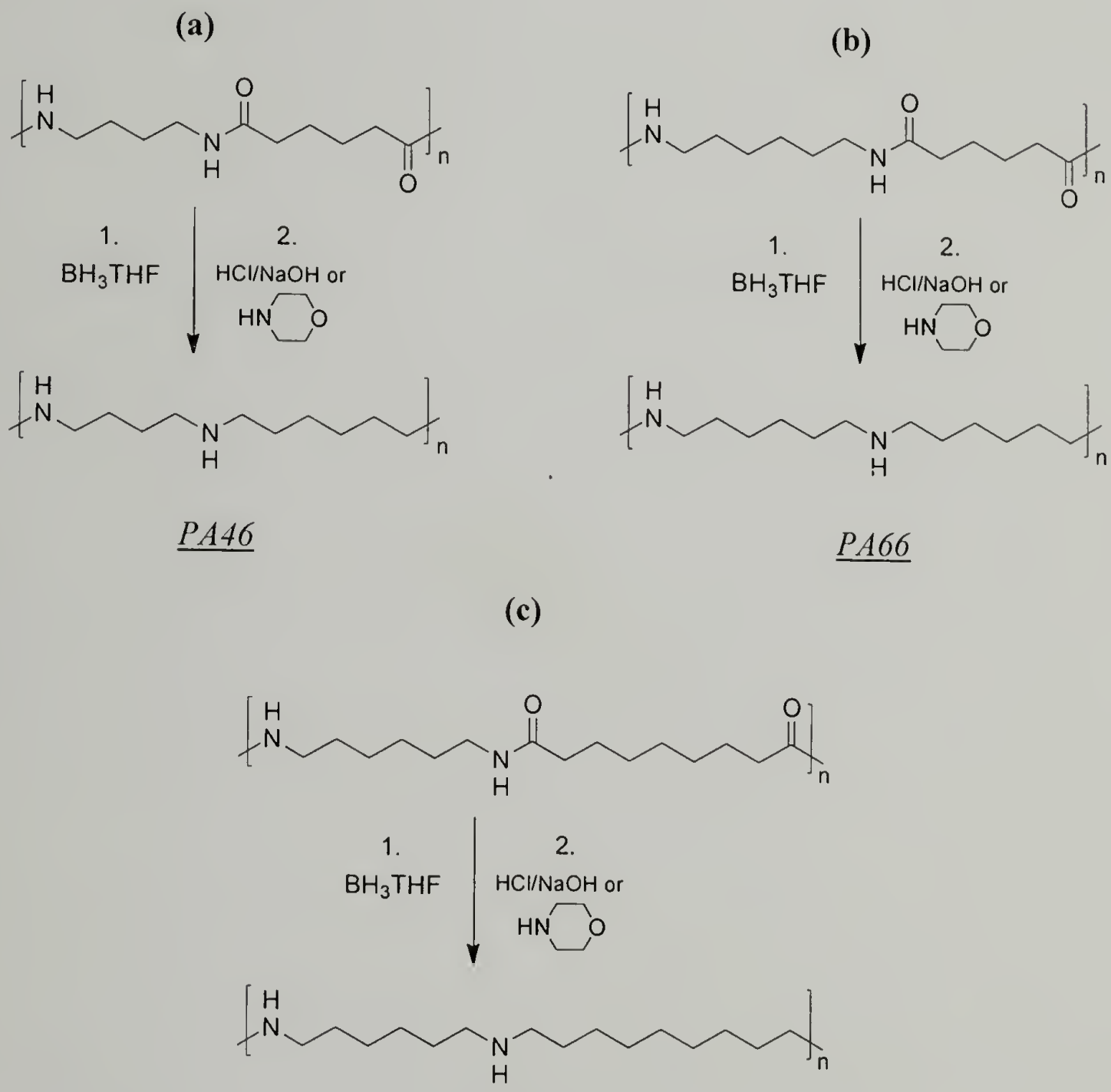

Figure 5.4. Bulk chemical reduction of nylons 4/6 (a), 6/6 (b), and 6/9 (c) with BH_3THF.

5.3.2. Synthesis of polyalkyleneimines

Nylon 4/6 and nylon 6/9 membranes were obtained by diffusion induced phase separation from a ternary system consisting of the polyamide, formic acid, and water. As presented in Figure 5.5, precipitation of nylon 4/6 (a) and nylon 6/9 (c) solutions in water resulted in membranes with a cellular foam-like structure with an average wall thickness of 0.5 μm and 1.7 μm, respectively. Commercial nylon 6/6 membranes (Figure 5.5, b) had an average wall thickness of 1.5 μm. The degree of crystallinity of the membranes was determined by DSC measurements, and the results are presented in Figures 5.6 and 5.7, and Table 5.1. A small endothermic transition was observed at approximately 100 °C, attributed to water. The melting endotherms of nylon 4/6 and nylon 6/6 crystals show two peaks, indicating that two populations of crystals of different sizes were produced during fabrication; nylon 6/9 presented only one melting peak. The second heating cycle, however, showed only one melting peak. The degree of crystallinity was estimated by the ratio of the heat of fusion of the sample to the corresponding theoretical heat of fusion for a perfect crystal. The thermal behavior of nylon membranes is summarized in Table 5.1.

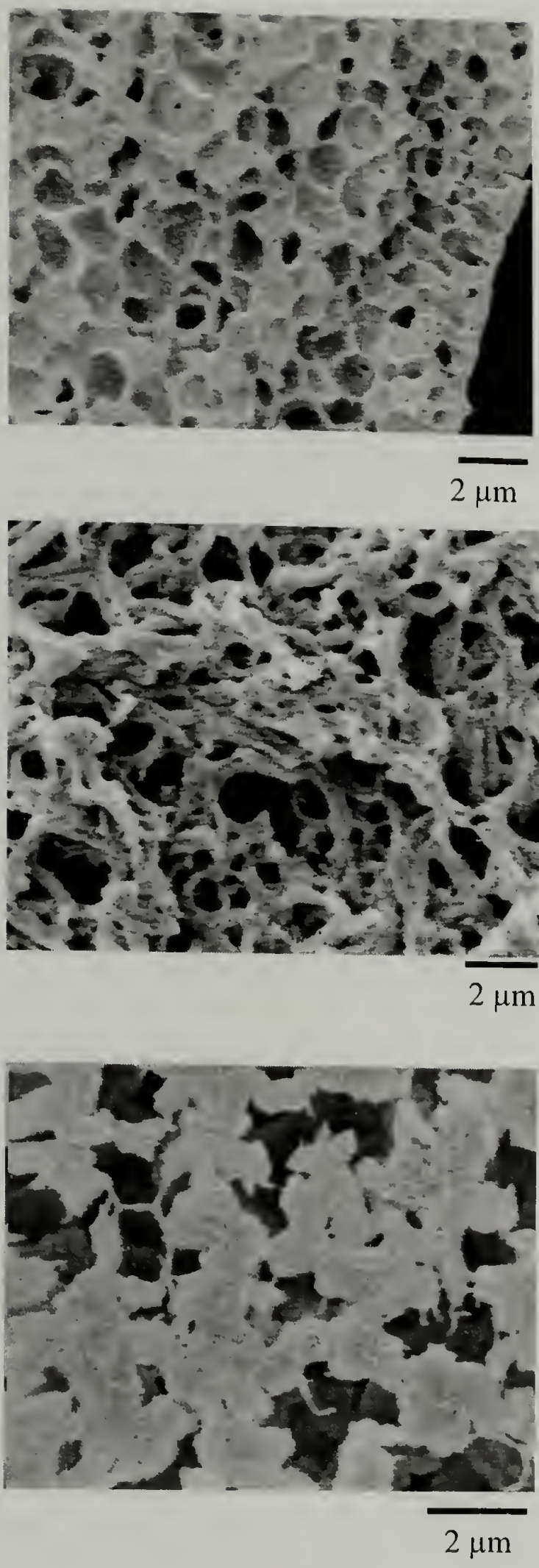

(a)

(b)

(c)

Figure 5.5. Morphology of nylon 4/6 (a), nylon 6/6 (b), and nylon 6/9 (c) membranes.

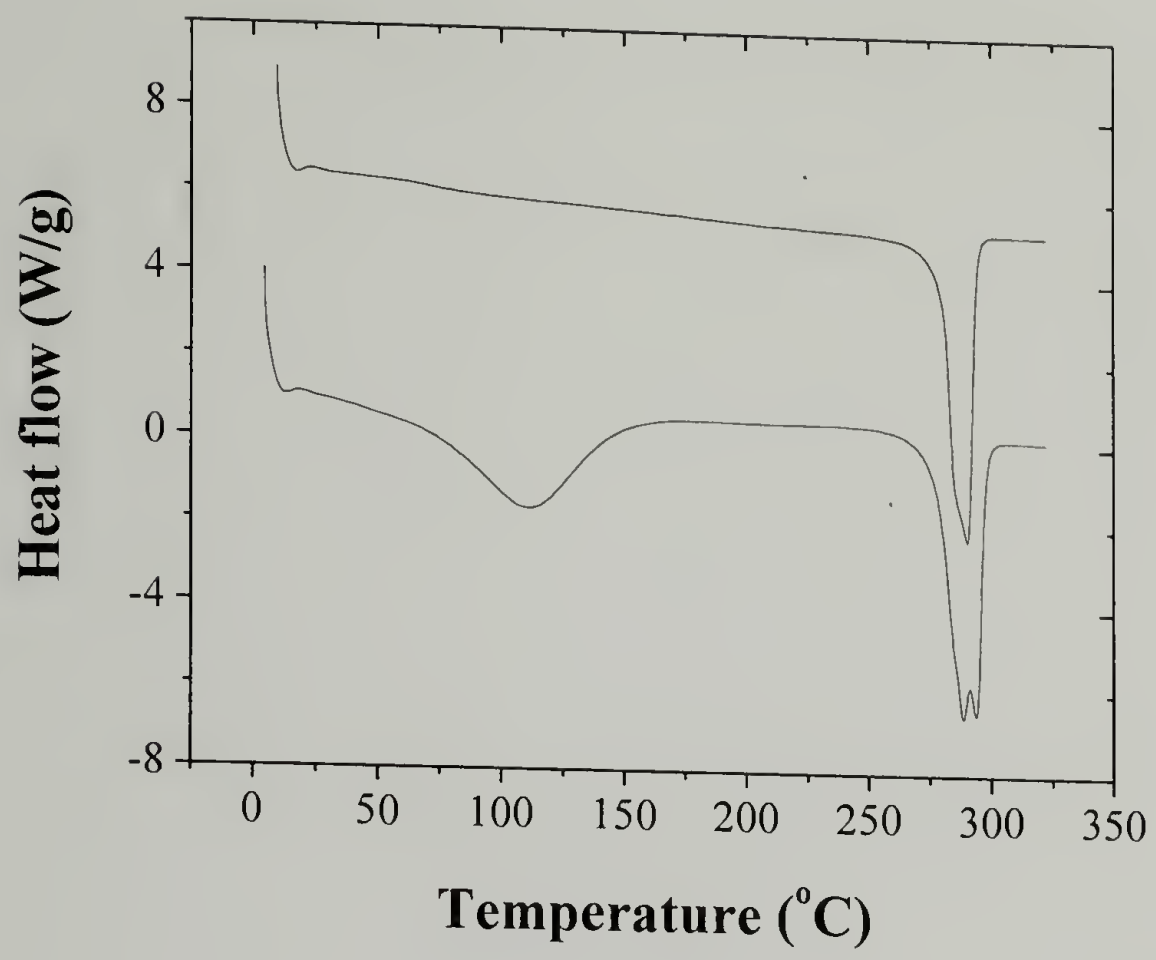

(a)

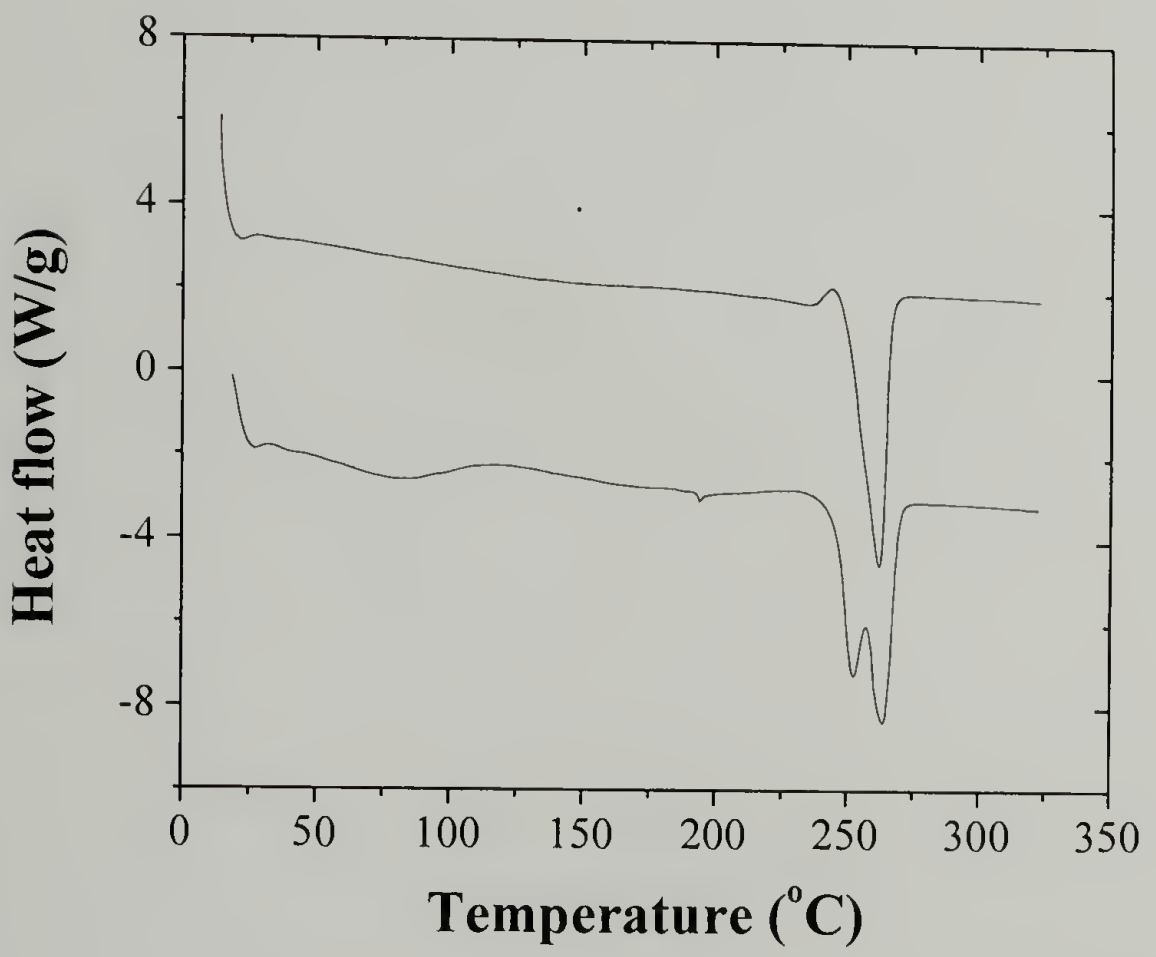

(b)

Figure 5.6. DSC thermograms of nylon 4/6 (a) and nylon 6/6 (b) membranes. The bottom curve corresponds to the first heating cycle and the top curve is the second heating cycle.

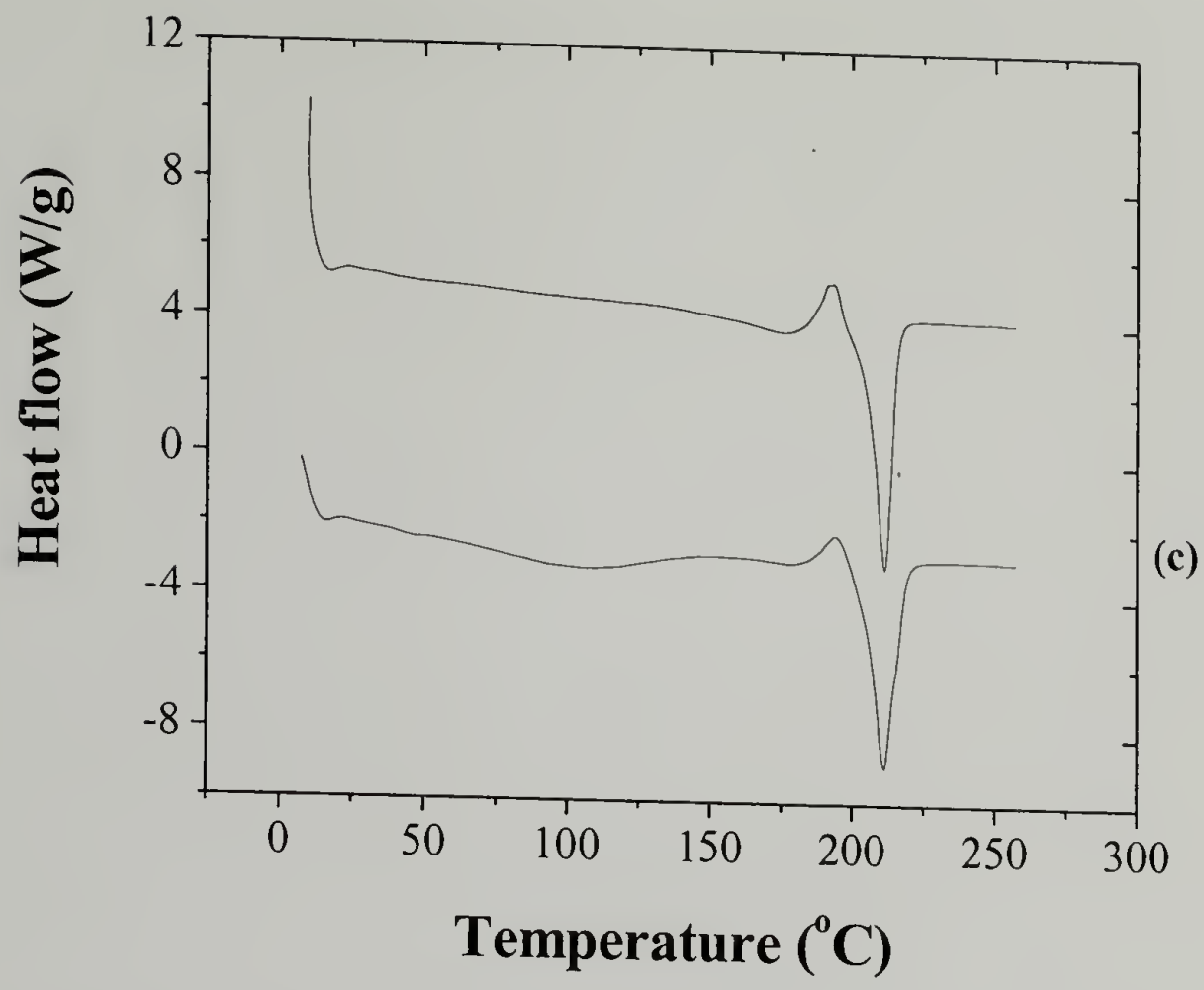

Figure 5.7. DSC thermogram of nylon 6/9 membrane. The bottom curve corresponds to the first heating cycle and the top curve is the second heating cycle.

Membrane samples were reacted with a BH_3·THF complex under reflux for 72 h. THF is neither a known solvent nor plasticizer for nylon, and this was confirmed by exposure of nylon 6/6 membranes to refluxing THF for 24-72 h. The FESEM images showed that the original morphology of the membranes is preserved, although a small increase in the average wall thickness was observed. Reduction with BH_3·THF is therefore a heterogeneous reaction, making the reaction in the bulk surface-controlled. After 24-72 h the medium becomes homogenous, indicating that the amino-borane complex formed (refer to Figure 5.8) is soluble in THF. This is an important result since it explains the high penetration depths and low surface-specificity of the chemical reduction of nylon surfaces.

Table 5.1. Summary of the thermal behavior of nylon membranes.

Sample	Melting temperature (°C)	Heat of fusion (J/g)	Degree of crystallinity (%)
Nylon 4/6 (first run)	288.46 294.09	102.90	49.00
Nylon 4/6 (second run)	290.30	80.79	38.47
Nylon 6/6 (first run)	251.83 263.43	85.82	45.17
Nylon 6/6 (second run)	261.92	64.30	33.84
Nylon 6/9 (first run)	211.19	55.14	21.45
Nylon 6/9 (second run)	211.35	53.35	20.76

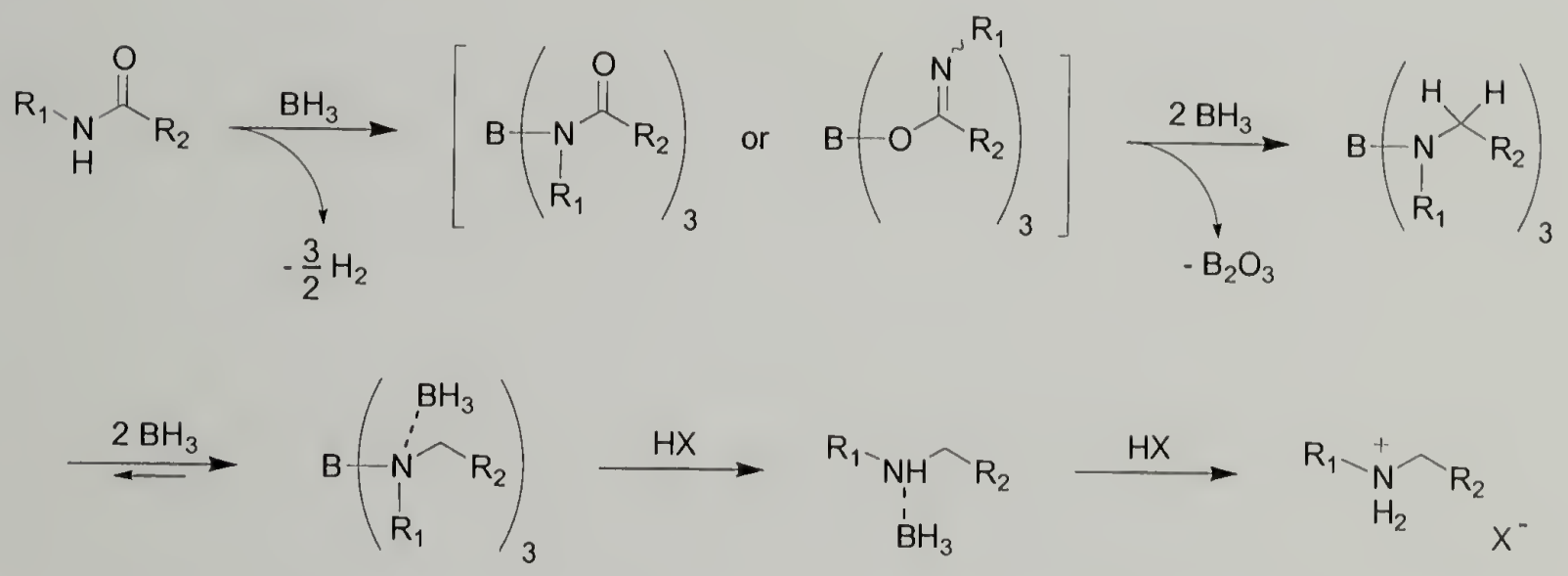

Figure 5.8. Mechanism for the reduction of amides with borane, and subsequent isolation of the free amine by treatment in acidic (1) or basic (2) conditions.

Isolation of the free amine was done by an amine interchange reaction with morpholine, followed by dialysis to remove the morpholine-borane salt, which is highly water-soluble. After workup, the polyamines were collected and analyzed by ATR IR and ^{1}H NMR spectroscopy. It is important to mention that the polyamines were isolated by removal of water from a solution at pH=6, so they are expected to be protonated since the pKa of protonated secondary amines is approximately 10. ATR IR spectra of poly(tetramethylene-*co*-hexamethyleneimine) (PA46) and poly(hexamethylene imine) (PA66) are presented in Figure 5.9. For both cases, absorption bands are observed at 3400 cm^{-1} (NH_2^+ stretch), 2928-2795 cm^{-1} (CH_2-N and CH_2 stretch), 1600 cm^{-1} (NH_2^+ deformation), 1460 cm^{-1} (CH_2 deformation), 1040 cm^{-1} (C-N stretch). The absorption bands observed correlate well with model compounds such as N,N'-diethylhexamethylenediamine and poly(iminohexamethylene).

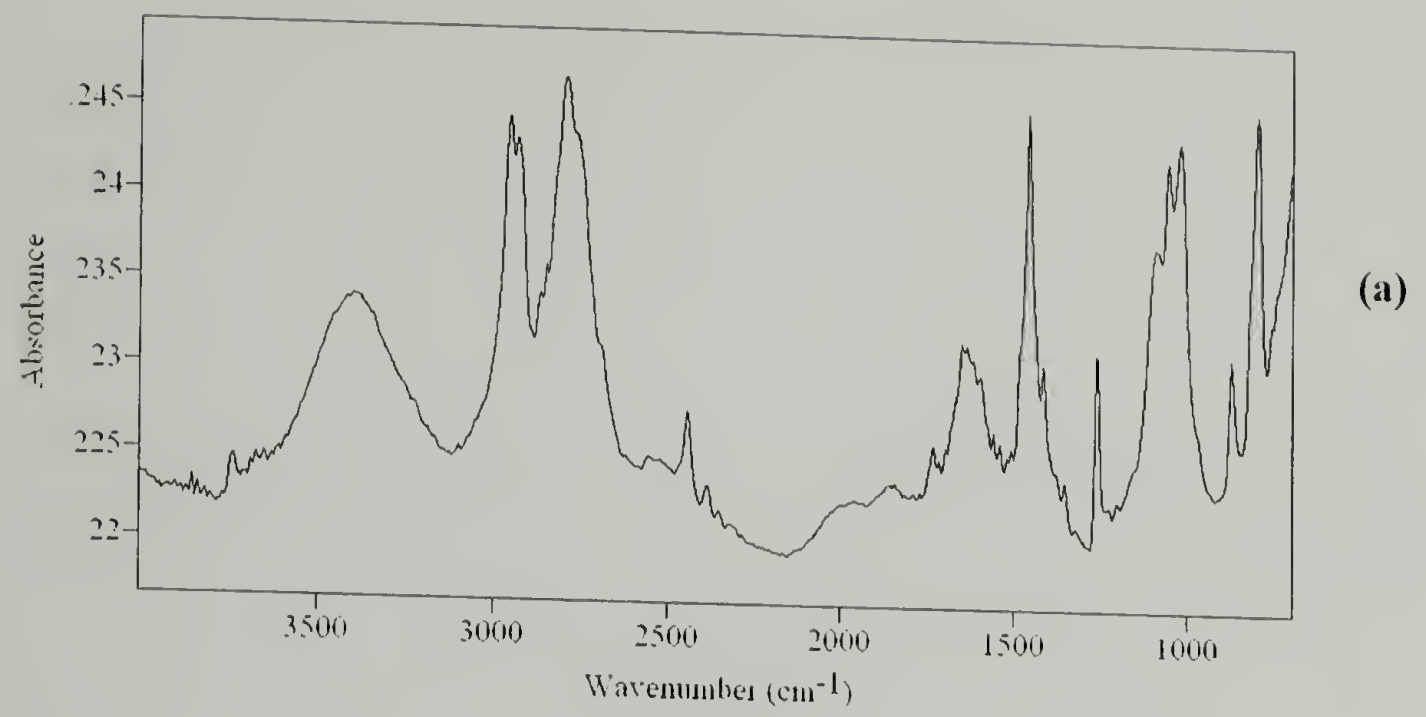

(a)

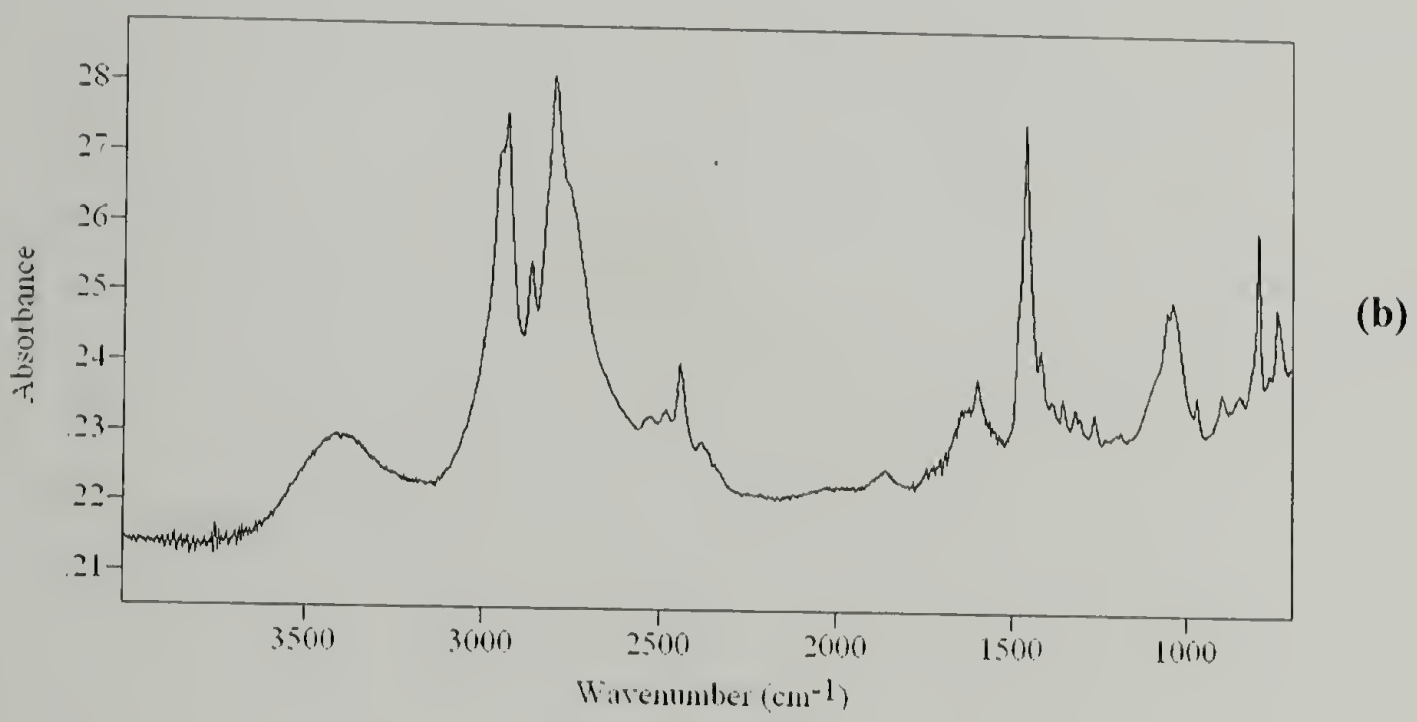

(b)

Figure 5.9. ATR IR spectra of poly(tetramethyleneimine-*co*-hexamethyleneimine) (a) and poly(hexamethyleneimine) (b).

^{1}H NMR spectra (Figure 5.10) indicate the presence of three peaks at 2.9 ppm, 1.6 ppm, and 1.3 ppm. For the case of poly(hexamethyleneimine) a sharp peak was also observed at 2.2 ppm. Peak areas were integrated and compared to the proposed structures (Figure 5.4) and the results are presented in Table 5.2; good correspondence is observed for all cases.

Table 5.2. Summary of ^{1}H NMR data of polyamines.

Sample	α (~ 2.9 ppm)		β (~ 1.6 ppm)		γ + δ + ε (~ 1.3 ppm)	
	Exp.	Theo.	Exp.	Theo.	Exp.	Theo.
Poly(tetramethyleneimine-*co*-hexamethyleneimine)	1.00	1.00	0.98	1.00	0.58	0.50
Poly(hexamethyleneimine)	1.00	1.00	1.00	1.00	1.03	1.00
Poly(hexamethyleneimine-*co*-nonamethyleneimine)	1.00	1.00	0.96	1.00	1.80	1.75

MALDI-TOF was used to determine the molecular weight of the polyamines and also the molecular weight of the repeat unit, however the samples were found to be very sensitive to beam damage. The spectrum of poly(hexamethylene imine) is presented in Figure 5.11. The molecular weight of the repeat unit is approximately 99.5 g/mol, which is close to the theoretical value of 100 g/mol, assuming that the polyamine is protonated.

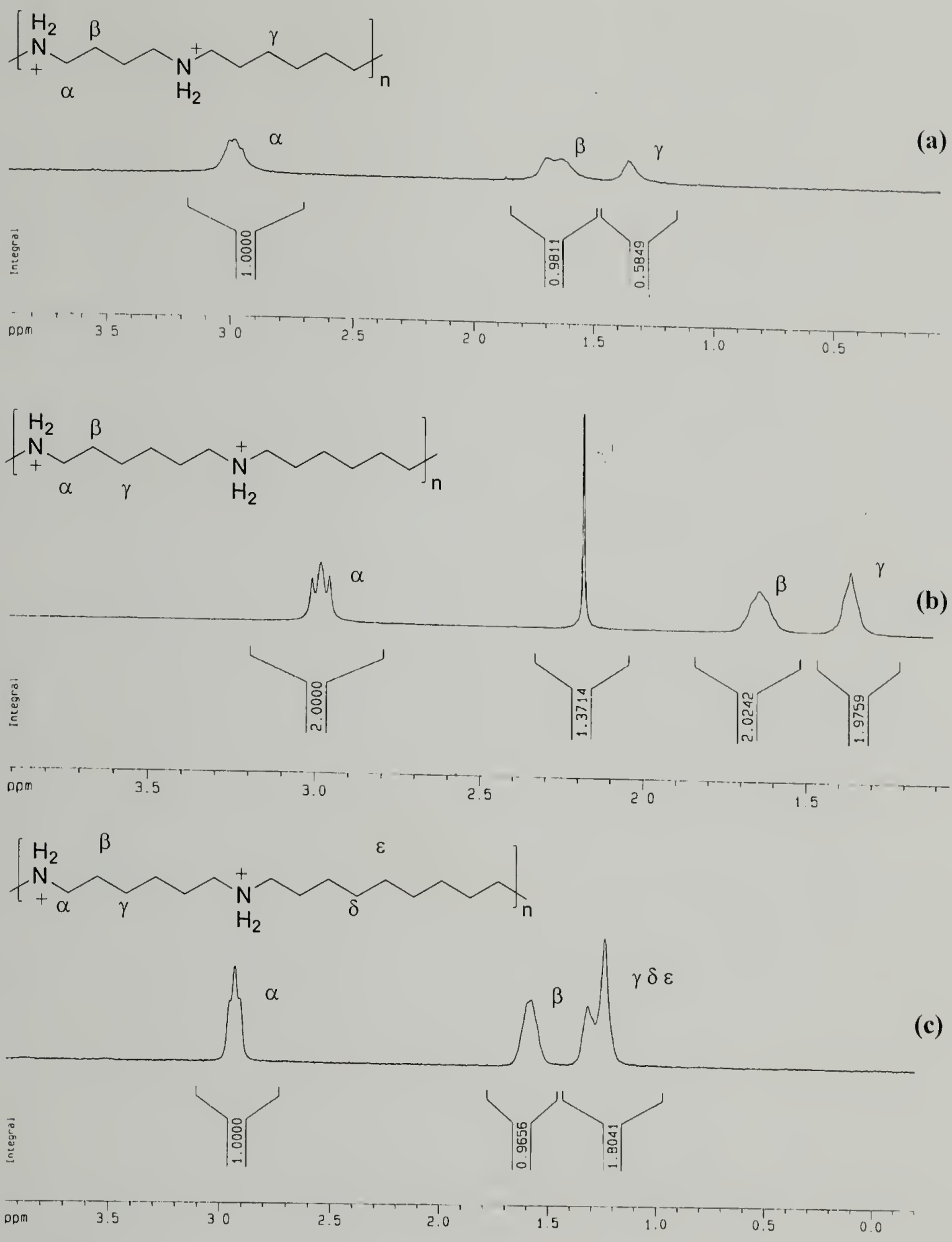

Figure 5.10. ^{1}H NMR of acidic poly(hexamethylene-*co*-tetramethyleneimine) (a), poly(hexamethyleneimine) (b), and poly(hexamethyleneimine-*co*-nonamethyleneimine) (c) showing peak integration. Spectra were acquired in D_2O.

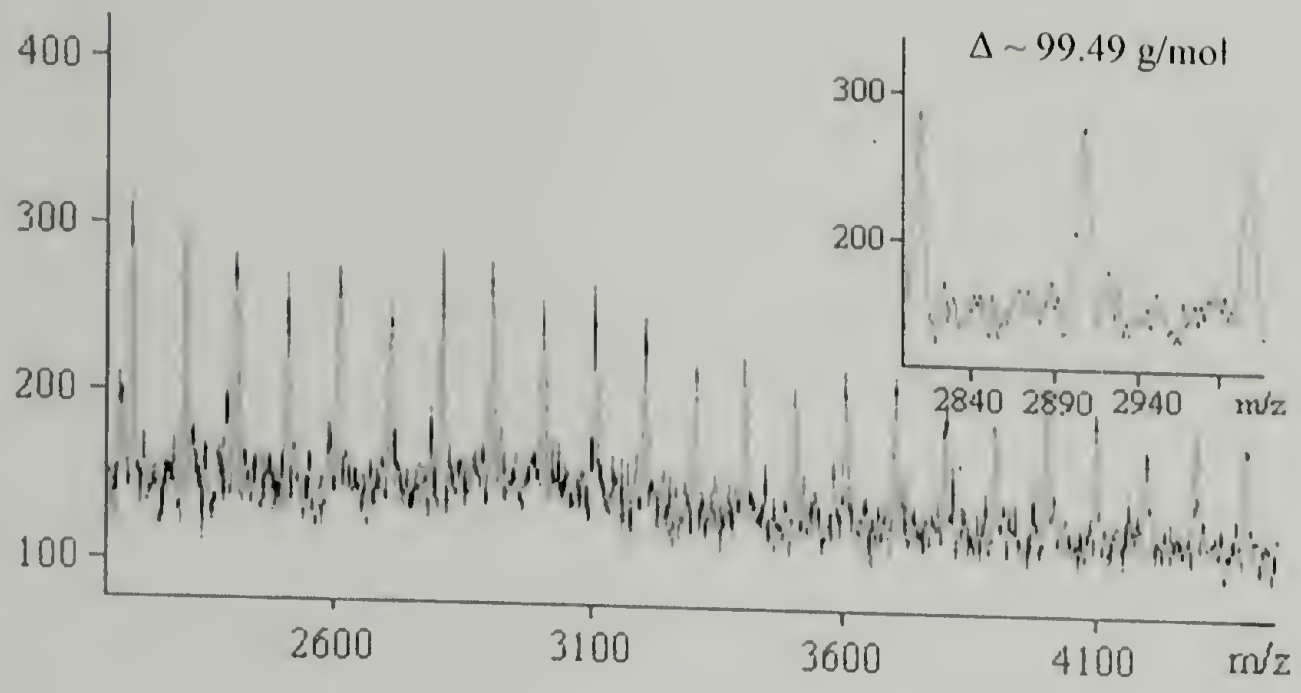

Figure 5.11. MALDI-TOF spectrum of poly(hexamethyleneimine) isolated by cleavage in morpholine. Insert shows the experimental molecular weight of the repeat unit.

The polyamines are soluble in acidic water by formation of salts. Acid/base titrations were made by dissolving the polyamines in water acidified with hydrochloric acid to pH=2 and back-titrating with 0.01 M sodium hydroxide. The acid/base profiles of the potentiometric titration are presented in Figure 5.12. The average pKa of protonated poly(tetramethylene-*co*-hexamethyleneimine) and poly(hexamethyleneimine) are 10.9 and 10.6, respectively.

Analogous to polyethyleneimine, when protonated, the polyamines are amorphous due to charge–charge interactions, while under basic conditions the interactions are no longer present and precipitation occurs to form semicrystalline polymers. DSC thermograms of the polyamines, precipitated from solution at pH=12 are presented in Figure 5.13. A clear trend of increasing melting temperature with the number of methylene groups in the repeat unit is observed, which is opposite to the melting temperatures of the parent polyamides. On the other hand, the heat of fusion,

and possibly the crystallinity, is dependent on the symmetry of the repeat unit, and is therefore higher for poly(hexamethyleneimine) compared to the other two polymers. Table 5.3 summarizes the results from DSC measurements. Thermogravimetric analysis of the samples showed that the polyamines are stable at temperatures lower than 300 °C, the onset temperature of decomposition

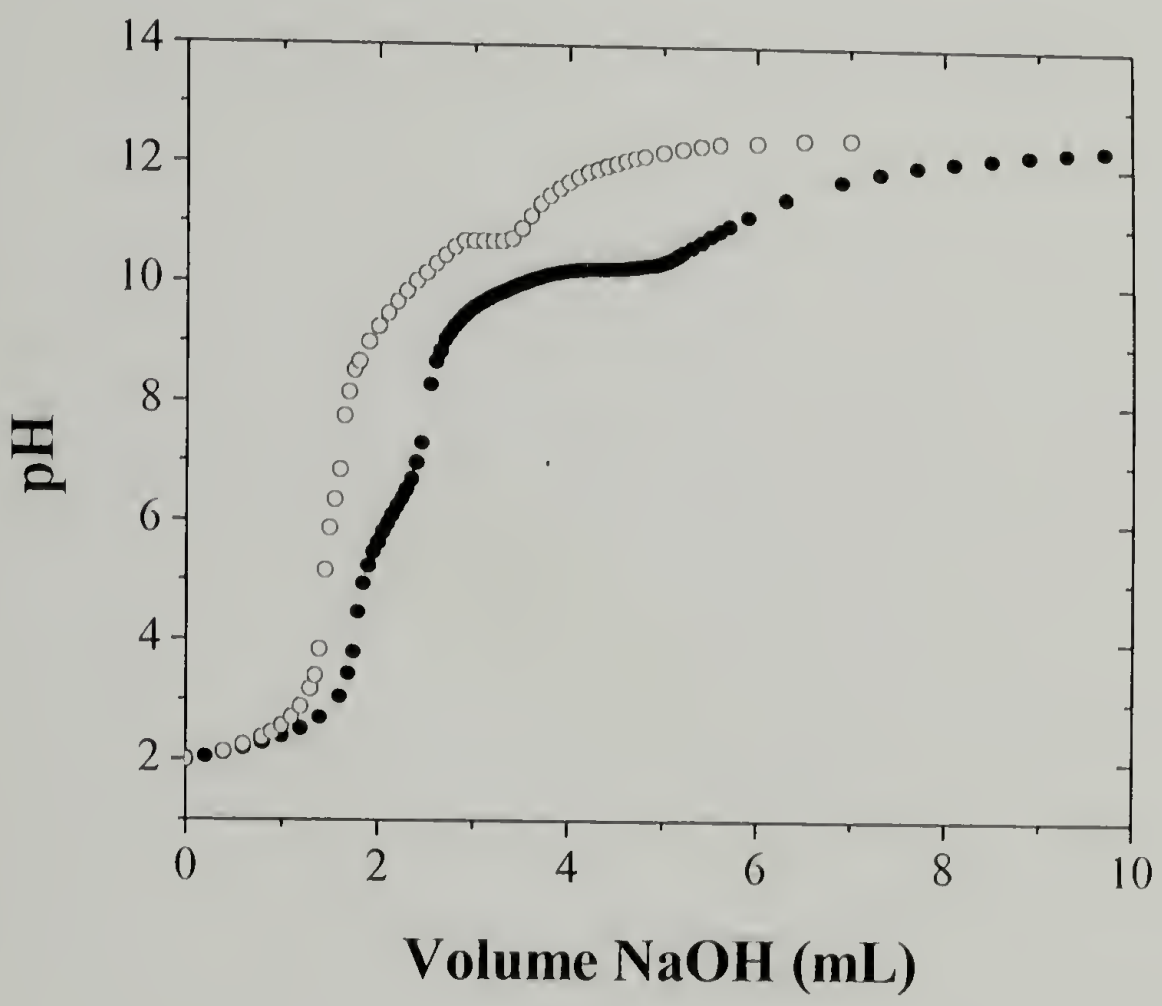

Figure 5.12. Potentiometric titration of acidic solutions of poly(tetramethyleneimine-*co*-hexamethyeleneimine) (○) and poly(hexamethyleneimine) (●) with 0.1 M NaOH as titrant. pH values were recorded 1 min after addition of a given volume of titrant.

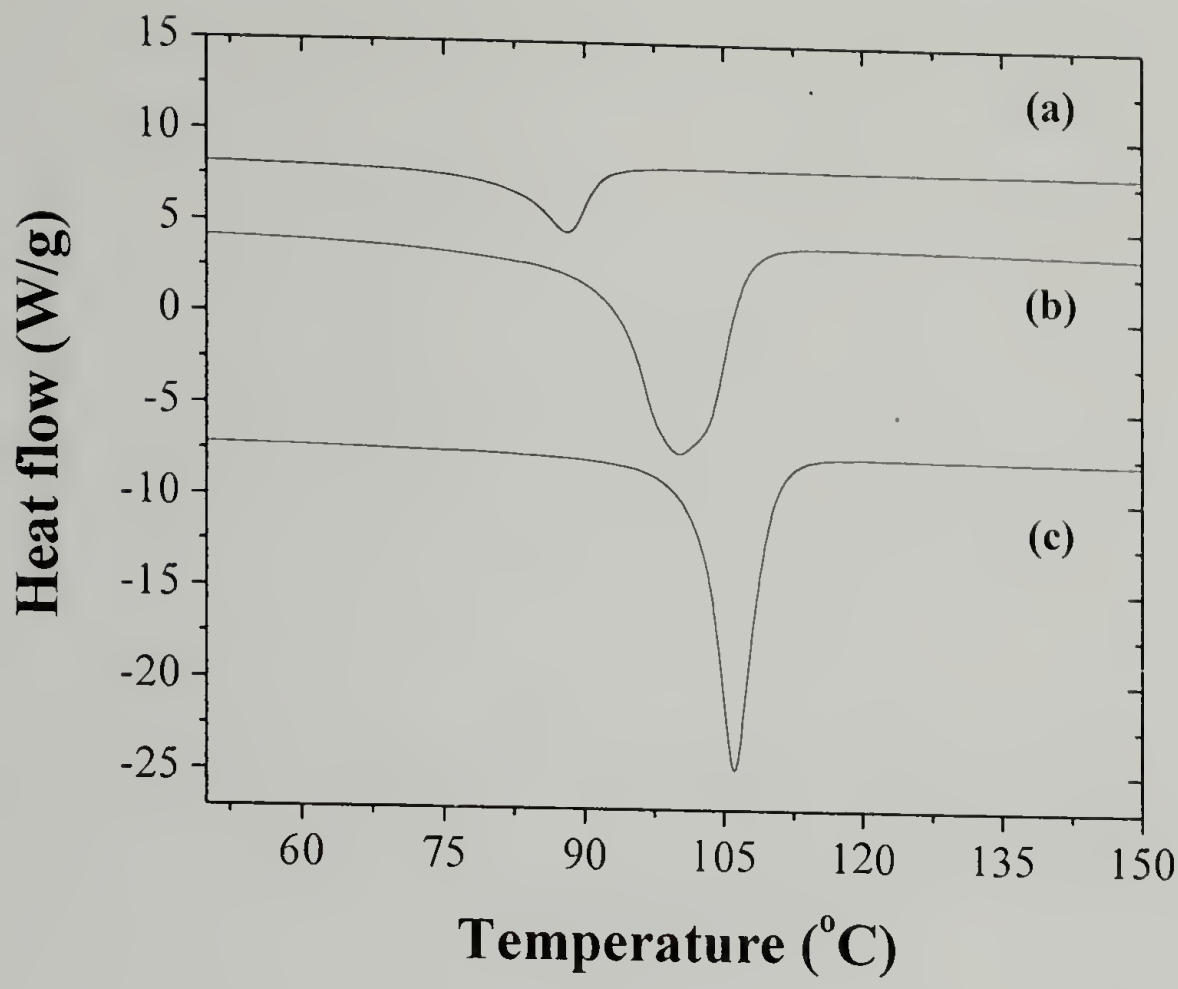

Figure 5.13. DSC thermograms of polyamines precipitated from a solution at pH = 12. (a) poly(tetramethyleneimine-*co*-hexamethyeleneimine); (b) poly(hexamethyeleneimine); (c) poly(hexamethyelene-*co*-nonamethyleneimine).

Table 5.3. Summary of the thermal analysis of polyamines.

Sample	Melting temperature (°C)	Heat of fusion (J/g)
Poly(tetramethyleneimine-*co*-hexamethyleneimine)	88.14	24.90
Poly(hexamethyleneimine)	100.18	117.60
Poly(hexamethyleneimine-*co*-nonamethyleneimine)	106.78	62.45

5.3.3. Fabrication of polymer/clay nanocomposites

Polyamine/clay nanocomposites were produced by melt intercalation under pressure in a conventional melt press. The effects of the type of polyamine, the degree of protonation of the polyamines, and hydrophilicity of the clay on the thermal and mechanical properties of the nanocomposites are discussed. The degree of protonation was varied by isolating the polymer from solutions at two different pH values; the fully protonated polyamines were obtained from a solution at pH=6, while the fully deprotonated polyamines were obtained from a solution at pH=12. It is important to mention that contact with moisture will result in protonation since the pKa of the protonated polyamines is approximately 10.6, however their charge density will still be considerably lower than that of a fully protonated polyamine.

The thermal properties of the nanocomposites were measured by DSC and TGA. Previous studies on the synthesis of nanocomposites by melt intercalation showed that crystallization of semi-crystalline polymers was, on occasions, affected by the presence of clay particles that act as nucleating agents.[141] The results for the systems composed of polypropylene, M15A and MNa^+ clays, and the three types of polyamines (precipitated at pH=12), are presented in Figure 5.14. Regardless of the type of clay, the melting behavior of the polyamines in the nanocomposites displays the same trend of increasing melting temperature with increasing methylene content, as in the case of the pure polymers. Also, as observed for the neat polyamines, the heat of fusion of PA46 is considerably lower than that of the other two polyamines, so its melting peak is not as apparent as for the case of PA66 and PA69, which show evidence of crystallization for both types of clay systems.

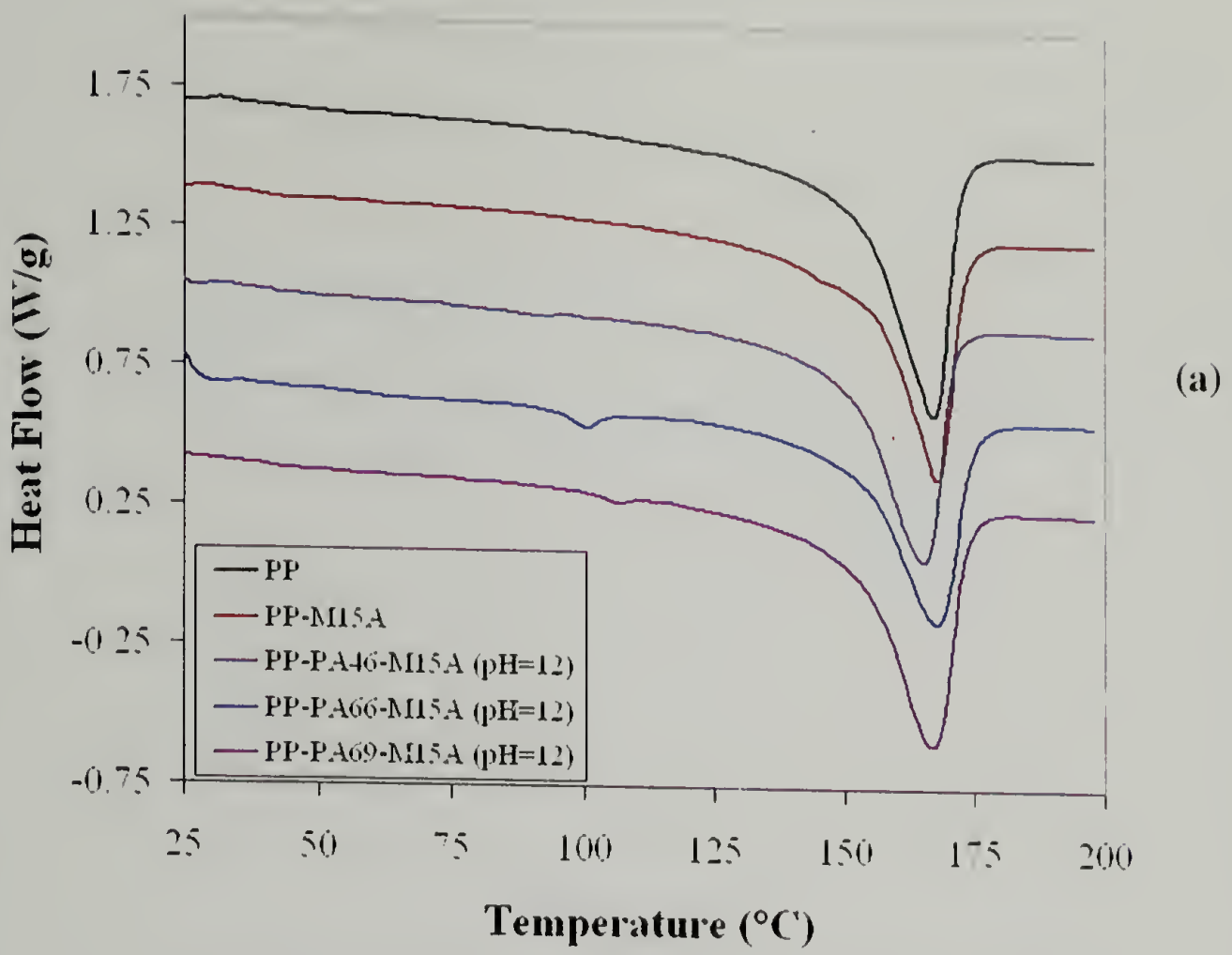

Figure 5.14. Thermal behavior of nanocomposites produced with M15A (a) and MNa^{+} (b) clays.

Regarding the matrix, the results also showed that the melting temperatures of polypropylene crystals in the nanocomposites are similar to that of the pristine polymer, independent of the type of clay or the degree of protonation of the polyamine (Figures 5.15 and 5.16, and Tables 5.4 to 5.6). However, the heat of fusion, and in turn, the crystallinity, decreases in the presence of the clay particles, regardless of the type of clay and the chemical nature or the degree of protonation of the polyamine.

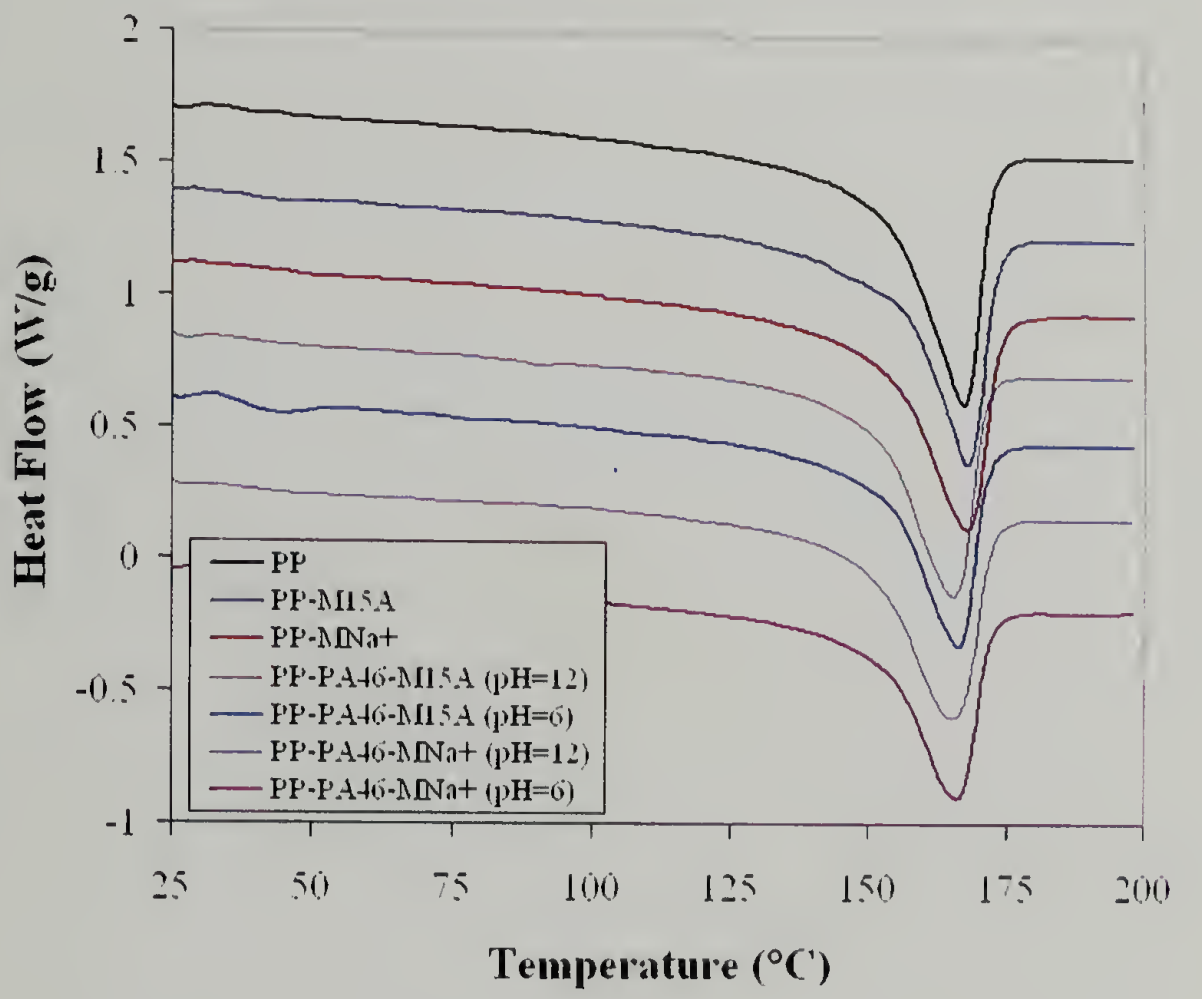

Figure 5.15. Thermal behavior of nanocomposites produced with PA46.

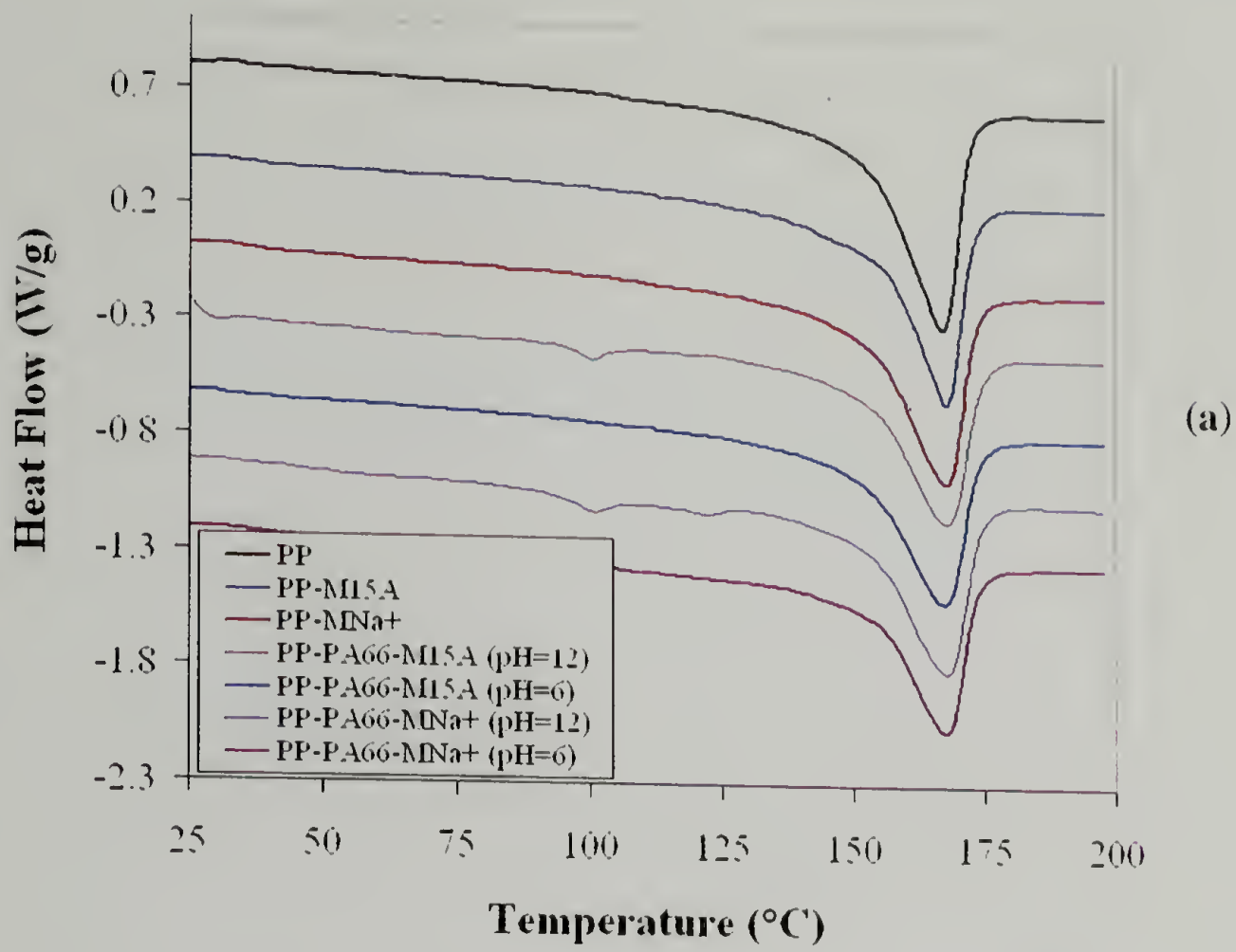

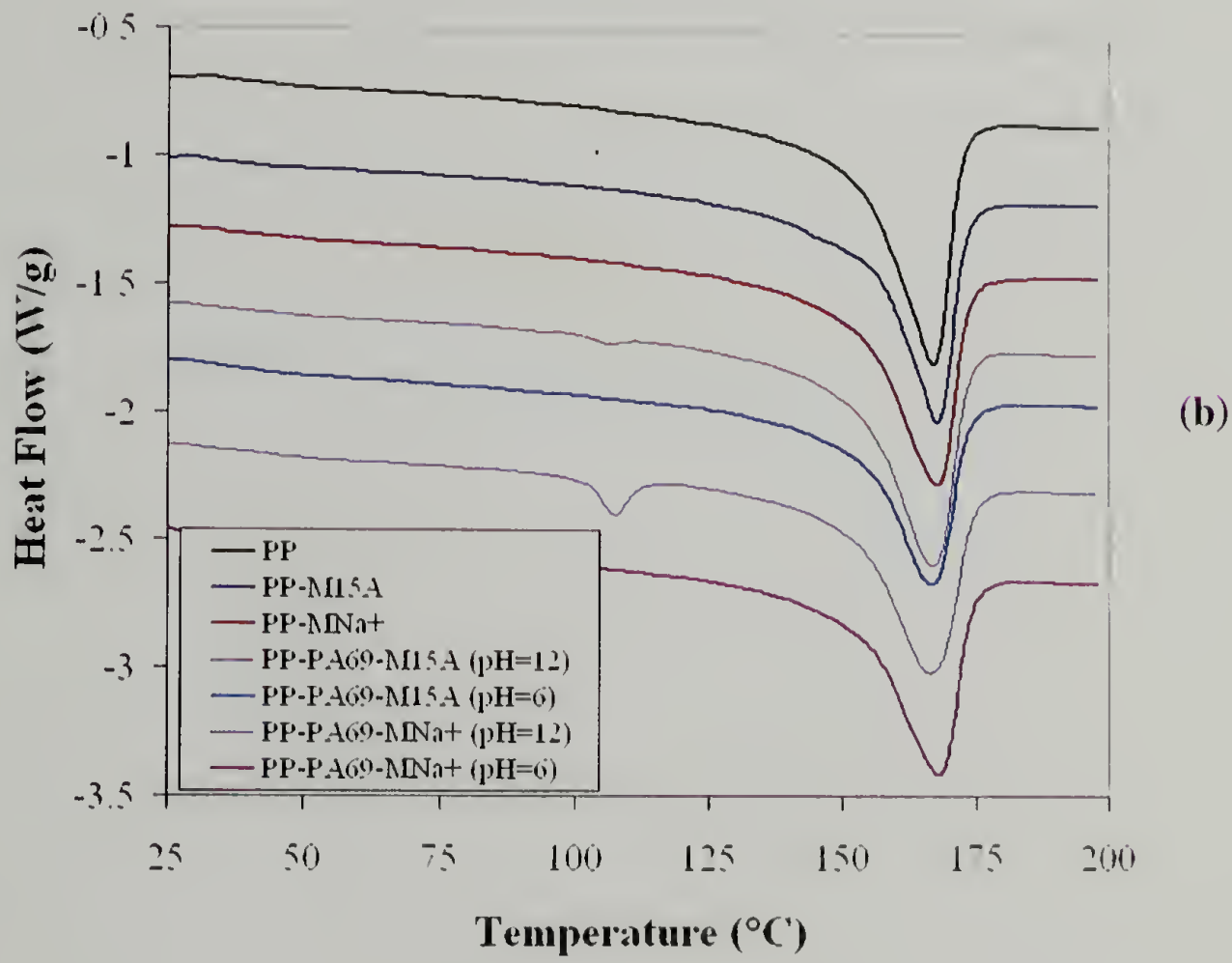

Figure 5.16. Thermal behavior of nanocomposites produced with PA66 (a) and PA69 (b).

Thermal degradation studies revealed that the presence of the polyamine has a detrimental effect on the final thermal stability of the nanocomposite, since degradation temperatures lower than those of the neat polypropylene were observed (Figure 5.17). The decomposition temperatures of the nancomposites are determined by those of the polyamines (~ 300 °C), and the onset of decomposition increases with thermal stability as PA46 < PA66 < PA69. The stability of the polyamine also depended on its degree of protonation and was higher for the fully deprotonated systems (except PA46). Despite there results, it is important to point out that the thermal stability of the overall polypropylene systems were not affected by the presence of the clays nor the polyamines within the typical processing range of the polymer (< 275 °C).

The most revealing results regarding the structure of the nanocomposites were obtained from X-ray diffraction measurements, where changes in the basal spacing of the platelets were indicative of intercalation and/or exfoliation processes. The d-spacing in systems prepared with MNa^+ clay and fully protonated polyamines show no change in the position of the peak (~ 12.6 Å), except for the case of PA69 where a small shift (Δ ~ 1.8 Å) was observed (Table 5.7 and Figure 5.18, a). Since both the polymer and the clay are hydrophilic, and they are oppositely charged, the interactions between the polymer and clay should be favorable and allow intercalation or exfoliation to occur. This, however, is not the case. It is possible that the low mobility of the polyamines, present as salts, limit their diffusion into the clay galleries, except for the case of PA69 which had a smaller particle size and was better dispersed throughout the sample, and/or that systems with lower charge density intercalate more efficiently.

Systems prepared with MNa^+ and non-protonated polyamines show no change in the basal spacing (Table 5.7 and Figure 5.18, b), which is expected due to the disparity of the hydrophobic polyamine and hydrophilic clay that prevent it from diffusing into the galleries.

A more interesting behavior is observed for the case of M15A clays. M15A, relative to MNa^+ is more hydrophobic and, due to the cation exhange reaction, has a larger basal spacing (32.00 Å vs. 12.58 Å). The results for these systems are presented in Figure 5.19 and Table 5.8. Unlike the case for MNa^+ systems, when M15A was used to fabricate the nanocomposites, changes in the basal spacing were evident. In systems where the polyamine is fully protonated, a small change in d-spacing is observed for PA46 and PA66, however PA69 shows a more intercalated structure with an increase of approximately 13 Å. This can, again, be explained in terms of the dispersion of PA69 throughout the sample, so more chains are accessible either to diffuse into the galleries or for the clay particles to intercalate at the surface of the polyamine powder. These results also confirm the possible influence of the polyamine charge density on its ability to promote polymer-clay interactions. The results suggest that systems with lower charge density interact more effectively with the clay particles, confirming the observations made with the MNa^+ clay system.

On the other hand, when the polyamines are non-protonated, dispersion of the clay particles in the polymer occurs due to the favorable interactions between the clay and the polyamines (Figure 5.19,b). In this case, intercalated and exfoliated systems were obtained. PA69 and PA66 show high degrees of intercalation with an increase in basal spacing of approximately 14 Å, and PA46 shows complete exfoliation. Results

suggest that the enthalpie interactions between the polymer systems and the clay dictate the intercalation process. In this regard, as mentioned previously, M15A is considered hydrophilic, and therefore it should be expected to favorably interact with the most hydrophilic of the polyamines, which in this case is PA46, so it is the balance of hydrophilic/hydrophilic interactions that allow for exfoliation to occur.

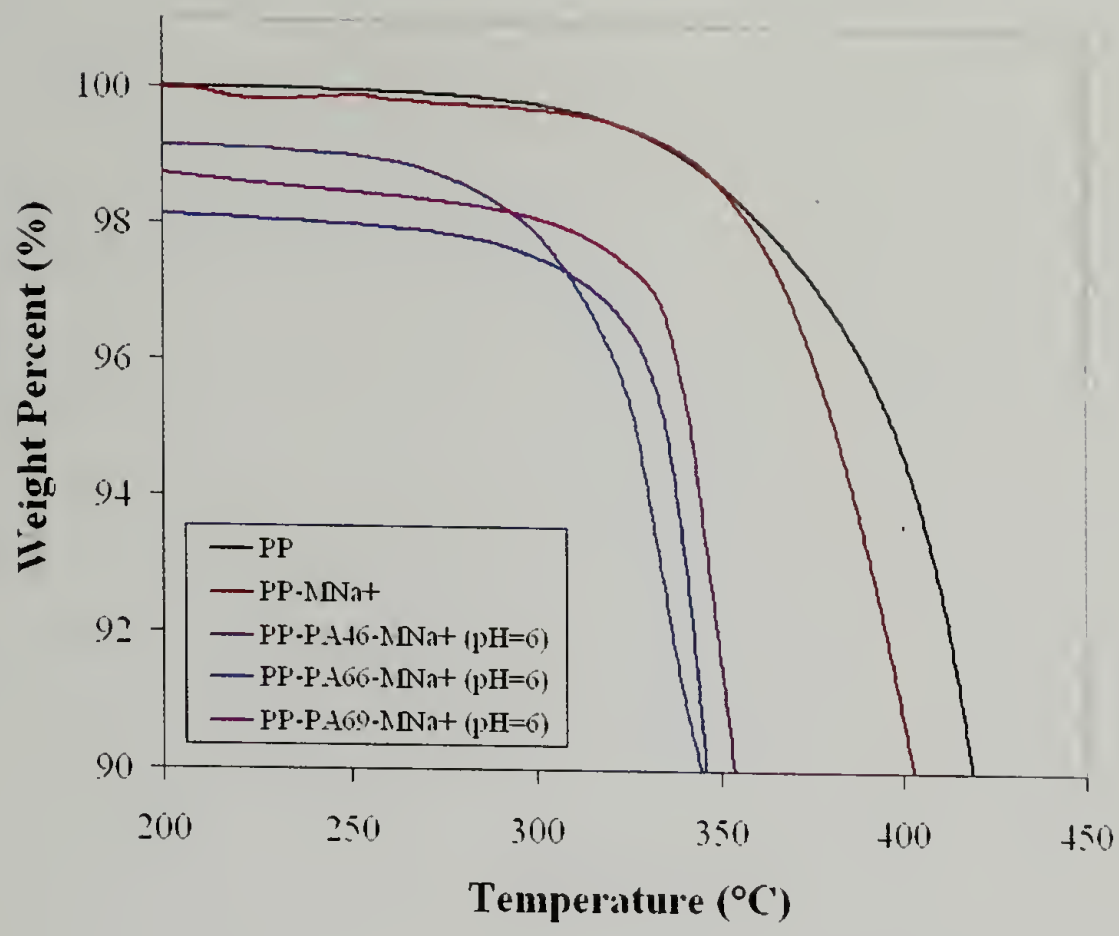

(a)

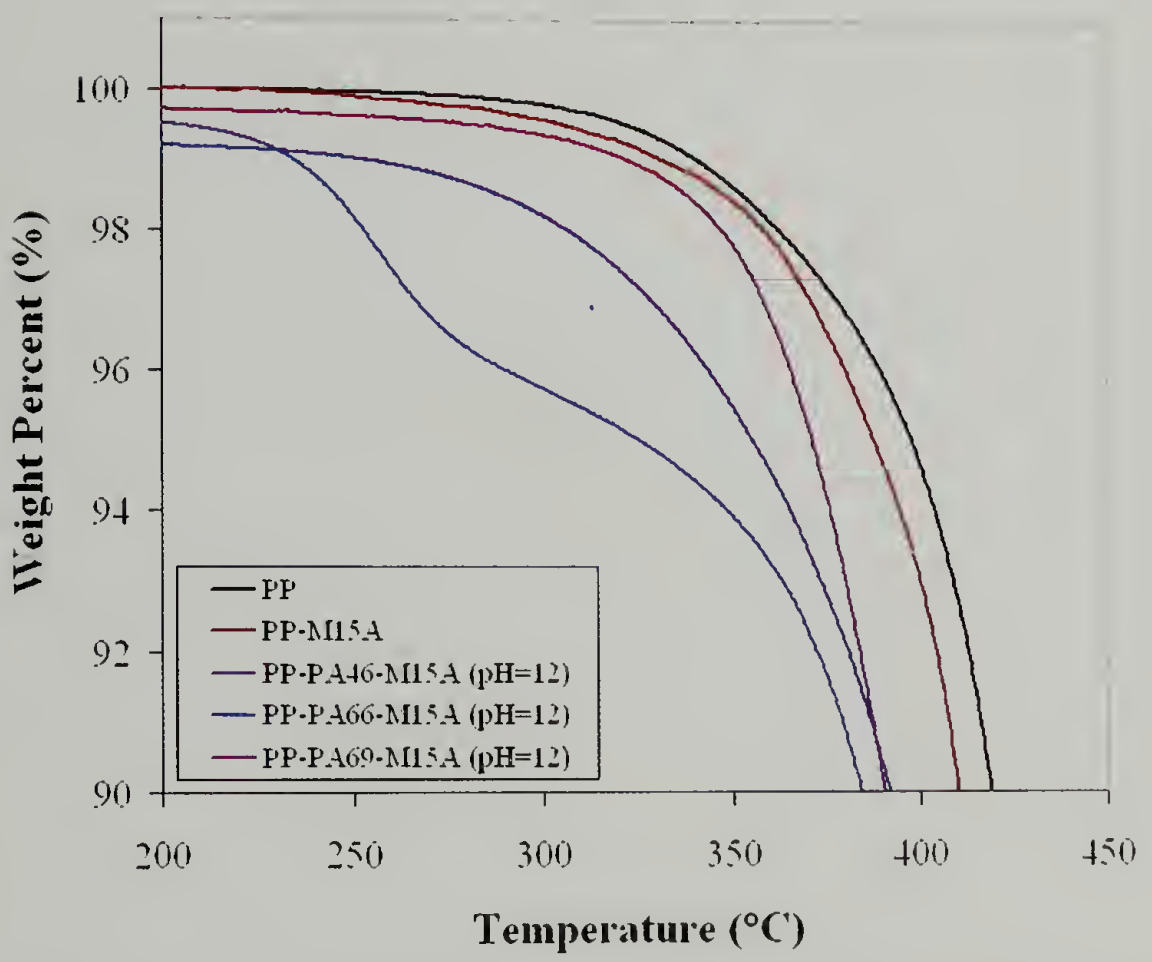

(b)

Figure 5.17. Thermogravimetric results for PP-MNa+ and PP-M15A nanocomposites.

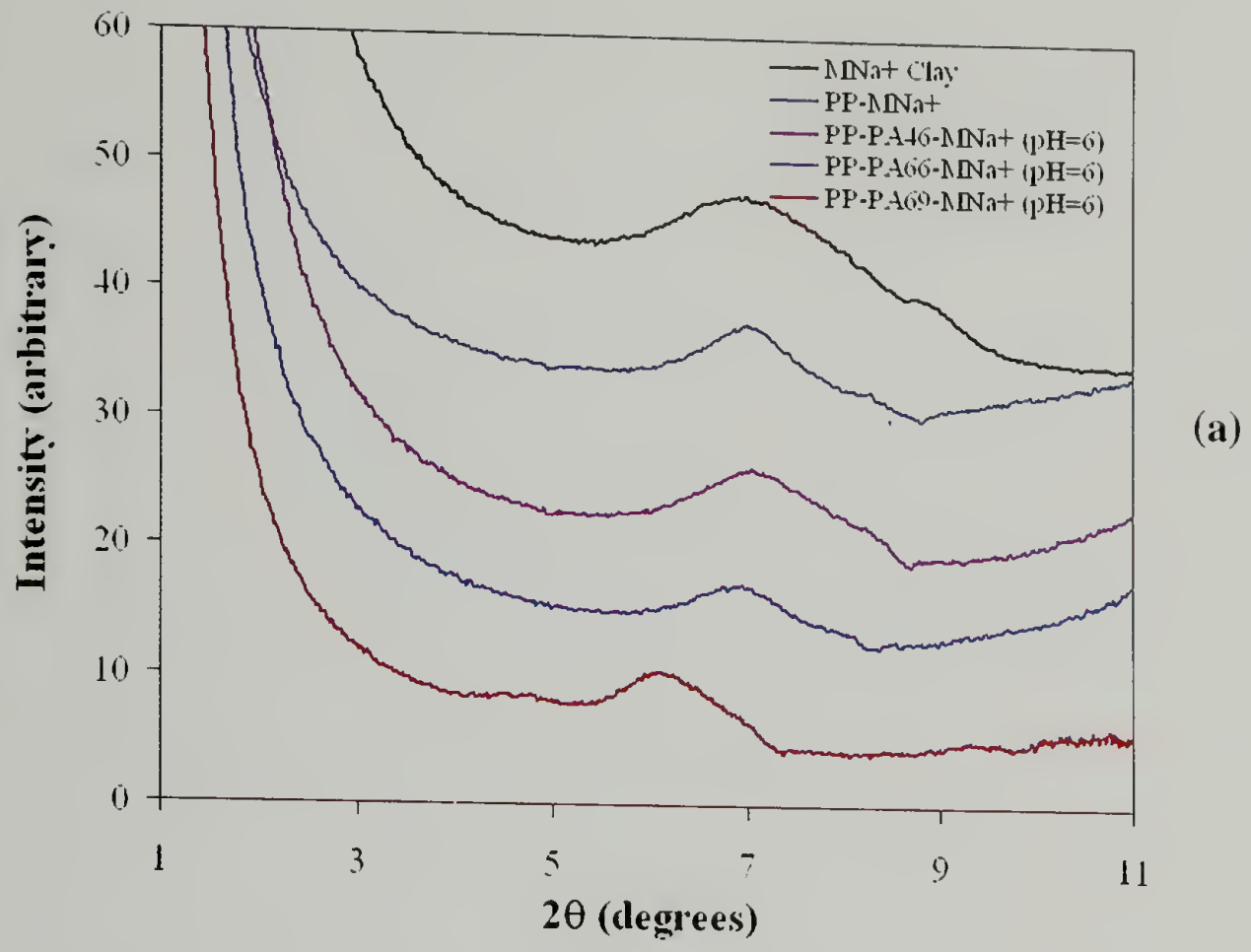

Figure 5.18. WAXS results of MNa^+ nanocomposites for different types of polyamines.

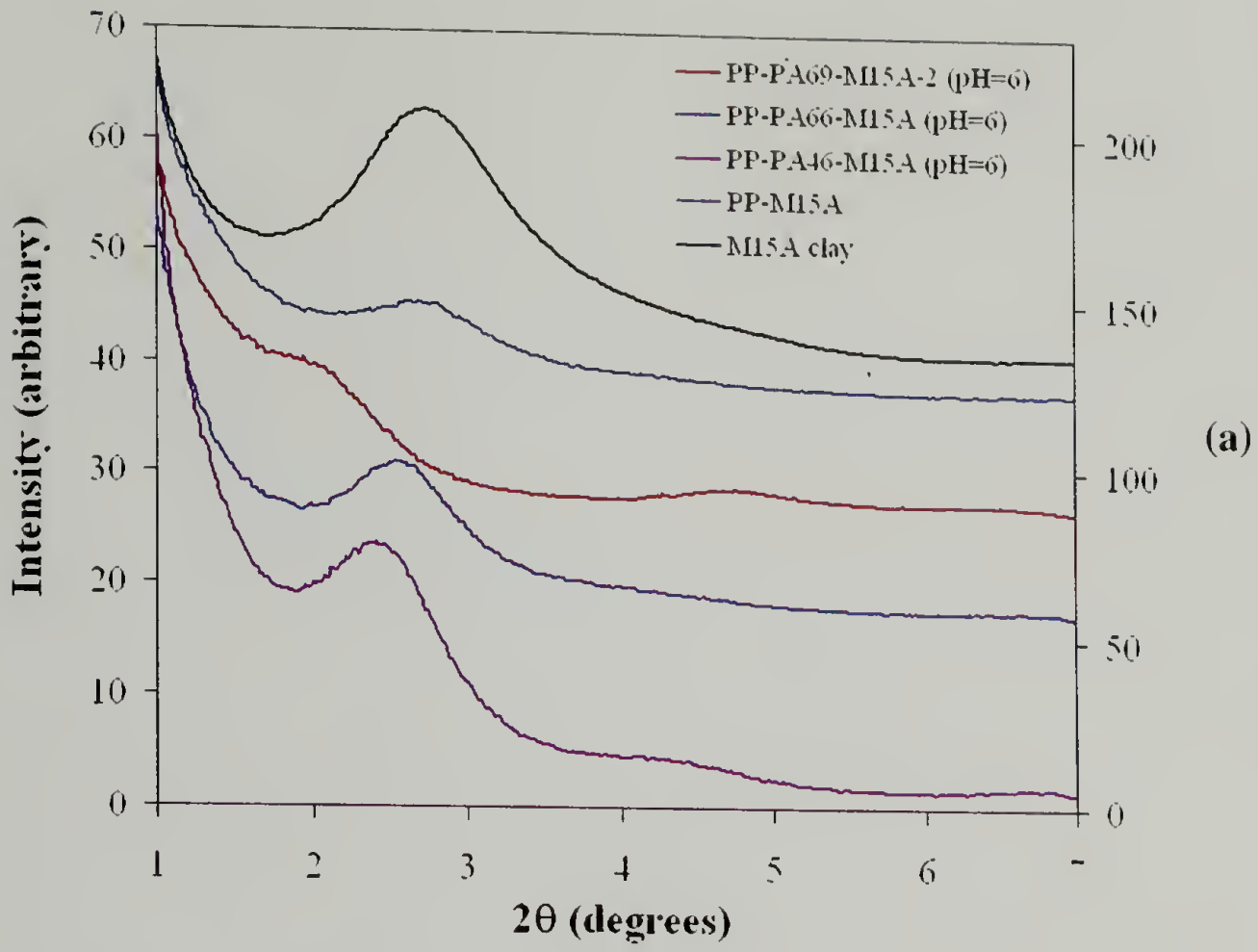

Figure 5.19. WAXS results of M15A nanocomposites for different types of polyamines.

Dynamical mechanical analysis was done for all the samples over a temperature range from –140 °C to 75 °C. Based on the results from DSC and WAXS analysis, the most interesting systems corresponded to those obtained using PA69 and only these results are presented in Figure 5.20. Addition of small amounts of MNa^+ or M15A clays (5% wt) to polypropylene resulted in a considerable increase of the storage modulus at temperatures below 0 °C, with the most pronounced effect for M15A (Δ ~ 698 MPa). Regarding the nanocomposites, those produced with MNa^+ and PA69 exhibited a mechanical behavior similar to the systems containing pure clay, as would be expected given their low degree of intercalation (Figure 5.18). However, more noticeable differences were observed in systems produced from M15A and PA69, where an increase (Δ ~ 457 MPa) in the storage modulus was obtained. This result is in agreement with the results from WAXS, since these systems were found to have the highest degrees of intercalation, particularly those obtained with a fully deprotonated polyamine, confirming that intercalation has a profound effect on the mechanical properties of a polymer.

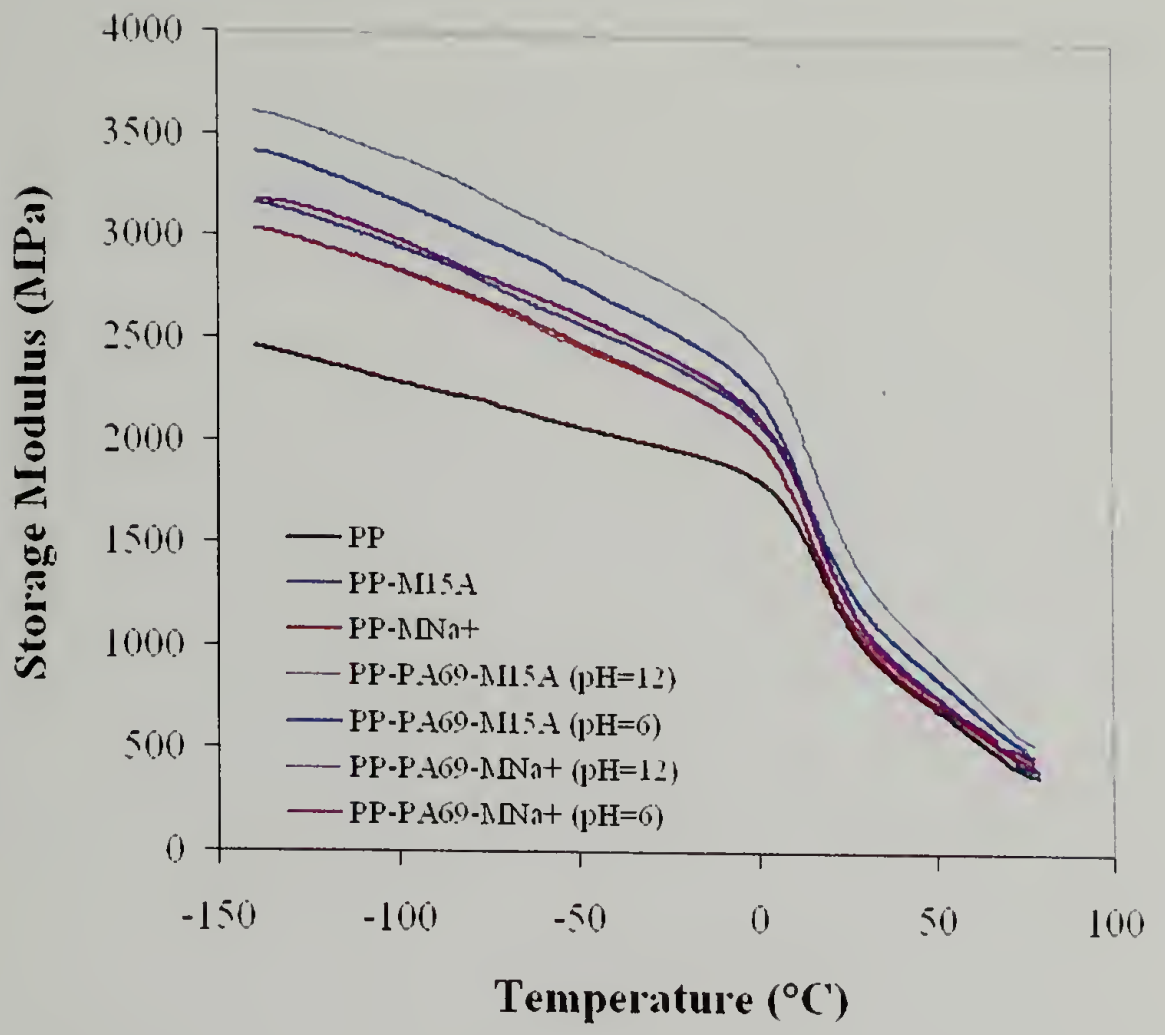

Figure 5.20. Storage modulus of PA69 nanocomposites.

5.4. Conclusions

Linear secondary polyamines, polyalkyleneimines, of different hydrocarbon lengths were synthesized by the surface-mediated reduction of nylons 4/6, 6/6, and 6/9 membranes with a borane-tetrahydrofuran complex. These polyalkyleneimines were further used as compatibilizers for the melt intercalation of montmorillonite clays, modified and unmodified, with polypropylene. While their effect on the thermal properties of the nanocomposites is not evident, they were found to interact favorably with the clays, leading to intercalated and exfoliated systems. The determining factor in controlling the degree of dispersion of the clays and in turn their structure, were the enthalpic interactions, or hydrophilic/hydrophilic interactions, observed for the M15A systems.

Table 5.4. Summary of thermal behavior of PA46 nanocomposites.

Sample	Melting temperature (°C)	Heat of fusion (J/g)	Crystallinity (%)
PP	167.00	82.42	39.43
PP-M15A	167.74	74.70	35.74
PP-MNa^+	167.80	77.07	36.87
PP-PA46-M15A (pH = 12)	165.07	76.40	36.66
PP-PA46-M15A (pH = 6)	166.13	67.44	32.26
PP-PA46-MNa^+ (pH = 12)	164.92	75.12	35.94
PP-PA46-MNa^+ (pH = 6)	165.79	64.97	31.08

Table 5.5. Summary of thermal behavior of PA66 nanocomposites.

Sample	Melting temperature (°C)	Heat of fusion (J/g)	Crystallinity (%)
PP	167.00	82.42	39.43
PP-M15A	167.74	74.70	35.74
PP-MNa^+	167.80	77.07	36.87
PP-PA66-M15A (pH = 12)	167.64	72.69	34.77
PP-PA66-M15A (pH = 6)	167.68	79.38	37.98
PP-PA66-MNa^+ (pH = 12)	167.61	69.59	33.29
PP-PA66-MNa^+ (pH = 6)	167.65	65.07	31.13

Table 5.6. Summary of thermal behavior of PA69 nanocomposites.

Sample	Melting temperature (°C)	Heat of fusion (J/g)	Crystallinity (%)
PP	167.00	82.42	39.43
PP-M15A	167.74	74.70	35.74
PP-MNa^+	167.80	77.07	36.87
PP-PA69-M15A (pH = 12)	166.87	81.42	38.95
PP-PA69-M15A (pH = 6)	166.72	68.52	32.78
PP-PA69-MNa^+ (pH = 12)	166.37	73.52	35.17
PP-PA69-MNa^+ (pH = 6)	168.04	74.72	35.75

Table 5.7. Summary of the WAXS results for MNa^+ nanocomposites.

Sample	2θ (deg)	*d*-spacing (Å)
MNa+	7.01	12.58
PP-MNa^+	7.01	12.58
PP-PA46-MNa^+ (pH=6)	7.05	12.52
PP-N66-MNa^+ (pH=6)	6.97	12.66
PP-N69-MNa^+ (pH=6)	6.12	14.41
PP-N46-MNa^+ (pH=12)	6.95	12.69
PP-N66-MNa^+ (pH=12)	6.79	13.00
PP-N69-MNa^+ (pH=12)	6.87	12.84

Table 5.8. Summary of the WAXS results for M15A nanocomposites.

Sample	2θ (deg)	d-spacing (Å)
M15A	2.75	32.00
PP-M15A	2.74	32.16
PP-N46-M15A (pH=6)	2.43	36.18
PP-N66-M15A (pH=6)	2.59	34.05
PP-N69-M15A (pH=6)	1.94	45.47
PP-N46-M15A (pH=12)	N/A	Exfoliated
PP-N66-M15A (pH=12)	1.87	47.15
PP-N69-M15A (pH=12)	1.94	45.47

117. Fukushima, Y.; Okada, A.; Kawasumi, M.; Kurauchi, T.; Kamigaito, O.; *Clay Miner.* **1988**, *23*, 27.

118. Okada, A.; Kawasumi, M.; Usuki, A.; Koshima, Y.; Kurauchi, T.; Kamigaito, O. *Mater. Res. Soc. Proc.* **1990**, *171*, 45.

119. Greenland, D. G. *J. Colloid Sci.* **1963**, *18*, 647.

120. Lepoittevin, B.; Devalckenaere, M.; Pantoustier, N.; Alexandre, M.; Kubies, D.; Calberg, C.; Jérôme, R.; Dubois, P. *Polymer* **2002**, *43*, 4017.

121. Shen, Z.; Simon, G. P.; Chen, Y.-B. *Polymer* **2002**, *43*, 4251.

122. Liao, B.; Song, M.; Liang, H.; Pang, Y. *Polymer* **2001**, *42*, 10007.

123. Huang, J.-C.; Zhu, Z.-K.; Yin, J.; Qian, X.-F.; Sun, Y.-Y. *Polymer* **2001**, *42*, 873.

124. Vaia, R. A.; Vasudevan, S.; Krawiec, W.; Scanion, L. G.; Giannelis, E. P. *Adv. Mater.* **1995**, *7*, 154.

125. Aranda, P.; Ruiz-Hitzky, E. *Chem. Mater.* **1992**, *4*, 1395.

126. Strawhecker, K. E.; Manias, E. *Chem. Mater.* **2000**, *12*, 2943.

127. Alexandre, M.; Beyer, G.; Henrist, C.; Cloots, R.; Rulmont, A.; Jérôme, R.; Dubois, P. *Chem. Mater.* **2001**, *13*, 3830.

128. Garcia-Leiner, M. A. Ph. D. Thesis, Polymer Science and Engineering, University of Massachusetts Amherst, **2004**.

129. Fischer, H. R.; Gielgens, L. H.; Koster, T. P. M. *Acta Polym.* **1999**, *50*, 122.

130. Mark, H. F.; Kroschwitz, J. I. *Encyclopedia of Polymer Science and Engineering* 2nd ed.; John Wiley: New York, 1990.

131. Rivas, B. L.; Geckeler, K. E. *Adv. Polym. Sci.* **1992**, *102*, 171.

132. Saegusa, T.; Yamada, A.; Taoda, H.; Kobayashi, S. *Macromolecules* **1978**, *11*, 435.

133. Perner, T.; Schultz, R. C. *Brit. Polym. J.* **1987**, *19*, 181.

134. Wang, J.; Ober, C. K. *Macromolecules* **1997**, *30*, 7560.

135. Tuncel, D.; Steinke, J. H. G. *Macromolecules* **2004**, *37*, 288.

136. Tang, M. X.; Szoka, F. C. *Gene Therapy* **1997**, *4*, 823.

137. Zelikin, A. N.; Trukhanova, E. S.; Putnam, D.; Izumrudov, V. A.; Litmanovich, A. A. *J. Am. Chem. Soc.* **2003**, *125*, 13693.

138. Forrest, M. L.; Koerber, J. T.; Pack, D. W. *Bioconjugate Chem.* **2003**, *14*, 934.

139. Jon, S.; Anderson, D. G.; Langer, R. *Biomacromolecules* **2003**, *4*, 1759.

140. Brissault, B.; Kichler, A.; Guis, C.; Leborgne, C.; Danos, O.; Cheradame, H. *Bioconjugate Chem.* **2003**, *14*, 581.

141. Liu, L.; Qi, Z.; Zhu, X. *J. Appl. Polym. Sci.* **1999**, *71*, 1133.

BIBLIOGRAPHY

Alexandre, M.; Beyer, G.; Henrist, C.; Cloots, R.; Rulmont, A.; Jérôme, R.; Dubois, P. *Chem. Mater.* **2001**, *13*, 3830.

Aranda, P.; Ruiz-Hitzky, E. *Chem. Mater.* **1992**, *4*, 1395.

Beeskow, T.; Kroner, K. H.; Anspach, F. B. *J. Colloid. Interf. Sci.* **1997**, *196*, 278.

Bogoczek, R.; Kociolek-Balawedjer, E. *Reactive Polymers* **1986**, *4*, 311.

Braccini, I.; Pérez, S. *Biomacromolecules* **2001**, *2*, 1089.

Brissault, B.; Kichler, A.; Guis, C.; Leborgne, C.; Danos, O.; Cheradame, H. *Bioconjugate Chem.* **2003**, *14*, 581.

Broer, D. J.; Luijks, W. *J. Appl. Polym. Sci.* **1981**, *26*, 2415.

Brown, H. C.; Heim, P. *J. Org. Chem.* **1973**, *38*, 912.

Brown, H. C.; Choi, Y. M.; Narasimhan, S. *J. Org. Chem.* **1982**, *47*, 3153.

Campbell, J.; Hornby, W. N.; Morris, D. L. *Biochm. Biophys. Acta* **1975**, *384*, 307.

Castilho, L. R.; Anspach, F. B.; Deckwer, W.-D. *J. Memb. Sci.* **2002**, *207*, 253.

Castilho, L. R.; Deckwer, W.-D.; Anspach, F. B. *J. Memb. Sci.* **2000**, *172*, 269.

Cepak, V. M.; Martin, C. R. *Chem. Mater.* **1999**, *11*, 1363.

Chapman, T. M.; Benrashid, R.; Marra, K. G.; Keener, J. P. *Macromolecules*, **1995**, *28*, 331.

Chen, W.; McCarthy, T. J. *Macromolecules* **1997**, *30*, 78.

Chilkoti, A.; Ratner, B. D.; Briggs, D. *Chem. Mater.*, **1991**, *3*, 51.

Clark, D. T.; Thomas, H. R. *J. Polym. Sci. Polym. Chem. Ed.* **1977**, *15*, 2843.

Deng, S.; Bai, R.; Chen J. P. *Langmuir* **2003**, *19*, 5058.

Dhamodharan, R.; McCarthy, T. J. *Macromolecules* **1999**, *32*, 4106.

Dhamodharan, R.; Nisha, A.; Pushkala, K.; McCarthy, T. J. *Langmuir* **2001**, *17*, 3368.

Duffy, D. C.; Jackman, R. J.; Vaeth, K. M.; Jensen, K. F.; Whitesides, G. M. *Adv. Mater.* **1999**, *11*, 546.
Encyclopedia of Polymer Science and Engineering, John Wiley and Sons Inc.: New York, 1989; Vol. 17, p 990.

Errede, L. A.; Gregorian, R. S.; Hoyt, J. M. *J. Am. Chem. Soc.* **1960**, *82*, 5218.

Fischer, H. R.; Gielgens, L. H.; Koster, T. P. M. *Acta Polym.* **1999**, *50*, 122.

Foerch, R.; Hunter, D. H. *J. Polym. Sci. Part A: Polym. Chem.* **1992**, *30*, 279.

Forrest, M. L.; Koerber, J. T.; Pack, D. W. *Bioconjugate Chem.* **2003**, *14*, 934.

Fortin, J. B.; Lu, T.-M. *Chem. Mater.* **2002**, *14*, 1945.

Fuertes, A. B. *Carbon* **2002**, *40*, 1597.

Fukushima, Y.; Okada, A.; Kawasumi, M.; Kurauchi, T.; Kamigaito, O.; *Clay Miner.* **1988**, *23*, 27.

Furneaux, R. C.; Rigby, W. R.; Davidson, A. P. *Nature* **1989**, *337*, 147.

Ganguli, S.; Agrawal H.; Wang, B.; McDonald, J. F.; Lu, T.; Yang, G.-R.; Gill, W. N. *J. Vac. Sci. Technol. A* **1997**, *15*, 3138.

Garcia-Leiner, M. A. Ph. D. Thesis, Polymer Science and Engineering, University of Massachusetts Amherst, **2004**.

Gasparac, R.; Kohli, P.; Mota, M. O.; Trofin, L.; Martin, C. R. *Nano Lett.* **2004**, *4*, 513.

Gorham, W. F. *J. Polym. Sci. A-1* **1966,** *4*, 3027.

Gorham, W. F. *J. Polym. Sci., Part A-1* **1966**, *4*, 3027. Beach, W. F. *Macromolecules* 1978, 11, 72.

Göschel, U.; Walter, H. *Langmuir* **2000**, *16,* 2887.

Greenland, D. G. *J. Colloid Sci.* **1963**, *18*, 647.

Grenier, A.; Mang, S.; Schäfer, O.; Simon, P. *Acta Polymer.* **1997**, *48*, 1.

Guest, A.; Hoffman, P. H.; Nugent, M. J. *J. Am. Chem. Soc.* **1972**, *94*, 4241.

Harrick, N. J. Internal Reflection Spectroscopy John Wiley and Sons: New York, 1967.

Hartley, P. G.; McArthur, S. L.; McLean, K. M.; Griesser, H. J. *Langmuir* **2002**, *18*, 2483.

Herrera-Alonso, M.; McCarthy, T. J. *Polymer Preprints* **2004**, *45*, 990.

Herrera-Alonso, M.; McCarthy, T.J. *Langmuir* **2004**, in print.

High Resolution XPS of Organic Polymers: The Scienta ESCA300 Database; Beamson, G.; Briggs, D., Eds.; John Wiley & Sons: New York, NY, 1992.

Hitchman, M. L.; Jensen, K. F. Chemical Vapor Deposition: Principles and Applications; Academic Press: London, 1993.

Hopf, H.; Grahn, W.; Barret, D. G.; Gerdes, A.; Hilmer, J.; Hucker, J.; Okamoto, Y.; Kaida, Y. *Chem. Ber.* **1990**, *123*, 841.

Hou, H.; Jun, Z.; Reuning, A.; Shaper, A.; Wendorff, J. H.; Greiner, A. *Macromolecules*, **2002**, *35*, 2429.

Hsieh, M. C.; Farris, R. J.; McCarthy, T. J. *Macromolecules* **1997**, *30*, 8453.

Huang, J.-C.; Zhu, Z.-K.; Yin, J.; Qian, X.-F.; Sun, Y.-Y. *Polymer* **2001**, *42*, 873.

Hulteen, J. C.; Martin, C. R. *J. Mater. Chem.* **1997**, *7*, 1075.

Hutt, D. A.; Leggett, G. J. *Langmuir* **1997**, *13*, 2740.

Itoh, T. Prog. *Polym. Sci.* **2001**, *26*, 1019.

Iwamoto, R.; Bopp, R.C.; Wunderlich, B. *J. Polym. Sci., Polym. Phys. Ed.* **1975**, *13*, 1925.

Jang, J.; Oh, J. H. *Chem. Commun.* **2004**, 882.

Jia, X. Ph. D. Thesis, Polymer Science and Engineering, University of Massachusetts Amherst, **2002**.

Jon, S.; Anderson, D. G.; Langer, R. *Biomacromolecules* **2003**, *4*, 1759.

Kane, V. K.; Gerdes, A.; Grhan, W.; Ernst, L.; Dix, I.; Jones, P. G., Hopf, H. *Tetrahedron Lett.* **2001**, *42*, 373.

Kang, M. S.; Chun, B.; Kim, S. S. *J. Appl. Polym. Sci.* **2001**, *81*, 1555.

Kim, K.; Jin, J.-I. *Nano Lett.* **2001**, *1*, 631.

Klein, E.; Feldhoff, P. A. European Patent 0441660A1, 1991.

Kohlschütter, H. W.; Sprenger, L. *Z. Phys. Chem.* **1932**, *B16*, 284.

Kozlov, M.; Quarmyne, M.; Chen, W.; McCarthy, T. J. *Macromolecules* **2003**, *36*, 6054.

Kruk, M; Jaroniec, M.; Kim, T.-W.; Ryoo, R. *Chem. Mater.* **2003**, *15*, 2815.

Kubono, A.; Okui, N. *Prog. Polym. Sci.* **1994**, *19*, 389.

Lahann J.; Choi, I. S.; Lee, J.; Jensen, K. F.; Langer, R. *Angew. Chem. Int. Ed.* **2001**, *40*, 3166.

Lahann J.; Höcker, H.; Langer, R. Angew. *Chem. Int. Ed.* **2001**, *40*, 726.

Lahann, J.; Balcells, M.; Rodon, T.; Lee, J.; Choi, I. S.; Jensen, K. F.; Langer, R. *Langmuir* **2002**, *18*, 3632.

Lahann, J.; Klee, D.; Thelen, H.; Bienert, H.; Vorwerk, D.; Hcker, H. *J. Mater. Sci.-Mater. Med.* **1999**, *10*, 443.

Lahann, J.; Langer, R. *Macromolecules* **2002**,*35*, 4380.

Lee, S. B.; Mitchell, D. T.; Trofin, L.; Nevanen, T. K.; Söderlund, H.; Martin, C. R. *Science* **2002**, *296*, 2198.

Lepoittevin, B.; Devalckenaere, M.; Pantoustier, N.; Alexandre, M.; Kubies, D.; Calberg, C.; Jérôme, R.; Dubois, P. *Polymer* **2002**, *43*, 4017.

Leväsalmi, J.-M.; McCarthy, T. J. *Macromolecules* **1997**, *30*, 1752.

Liao, B.; Song, M.; Liang, H.; Pang, Y. *Polymer* **2001**, *42*, 10007.

Liu, L.; Qi, Z.; Zhu, X. *J. Appl. Polym. Sci.* **1999**, *71*, 1133.

Lozano, P.; Iborra, J. L. In *Methods in Biotechnology, Vol. 1: Immobilization of Enzymes and Cells*; Bickerstaff, G. F.; Ed.; Humana Press: Totowa, NJ, 1997.

Lu, Z.; McCarthy, T. J. *Polym. Prepr. (Am. Chem. Soc. Div. Polym. Chem.)* **2004**, *45*, 1051.

Manku, S.; Laplante, C.; Kopac, D.; Chan, T.; Hall, D. G. *J. Org. Chem.* **2001**, *66*, 874.

Mark, H. F.; Kroschwitz, J. I. *Encyclopedia of Polymer Science and Engineering* 2nd ed.; John Wiley: New York, 1990.

Martin, C. R.; Kohli, P. *Nature Rev.* **2003,** *2*, 29.

Martini, D.; Shepherd, K.; Sutcliffe, R.; Kelber, J.; Edwards, H.; San Martin, R. *Appl. Surf. Sci.* **1999**, *141*, 89.

Mason, M.; Vercruysse, K. P.; Kirker, K. R.; Frisch, R.; Marecak, D. M.; Prestwich, G. D.; Pitt, W. G. *Biomaterials* **2000**, *21I*, 31.

Matthiasson, E. *J. Membr. Sci.* **1983**, *16*, 23.

McArthur, S. L.; McLean, K. M.; Kinshott, P.; St John, H. A. W.; Chatelier, R. C.; Griesser, H. J. *Coll. Surf. B: Biointerfaces* **2000**, *17*, 37.

Michielsen, S. *J. Appl. Polym. Sci.* **1999**, *73*, 129.

Moon, S. I.; McCarthy, T. J. *Macromolecules* **2003**, *36*, 4253.

Morra, M.; Cassinelli, C. *Langmuir* **1999**, *15*, 4658.

Nakayama, Y.; Takahagi, T.; Soeda, F.; Hatada, K.; Nagaoka, S.; Suzuki, J.; Ishitani, A. *J. Polym. Sci. A* **1998**, *26*, 559.

Nowlin, T. E.; Smith, D. F. *J. Appl. Polym. Sci.* **1980**, *25*, 1619.

Odian, G. *Principles of Polymerization*; 3rd Ed.; John Wiley and Sons: New York, 1991.

Okada, A.; Kawasumi, M.; Usuki, A.; Koshima, Y.; Kurauchi, T.; Kamigaito, O. *Mater. Res. Soc. Proc.* **1990**, *171*, 45.

Olah, G. "Friedel-Crafts and related reactions", John Wiley and Sons: London, 1963; Vol. 1.

Park, B. D.; Lee, H. I.; Ryoo, S. J.; Lee, Y. S. *Tetrahedron Letters* **1997**, *38*, 591.

Parthasarthy, R. V.; Phani, K. L. N.; Martin, C. R. *Adv. Mater.* **1995**, *7*, 896.

Pastushok, V. N.; Hu, K.; Bradshaw, J. S.; Dalley, N. K.; Bordunov, A. V.; Lukyanenko, N. G. *J. Org. Chem.* **1997**, *62*, 212.

Pelter, A.; Crump, R. A. N. C.; Kidwell, H. *Tetrahedron Lett.* **1996**, *37*, 1273.

Perner, T.; Schultz, R. C. *Brit. Polym. J.* **1987**, *19*, 181.

Perry, E.; Savory, J. *J. Appl. Polym. Sci.* **1967**, *11*, 2473.
Pieracci, J.; Crivello, J. V.; Belfort, G. *Chem. Mater.* **2002**, *14*, 256.

Pierson, H. O. Handbook of Chemical Vapor Deposition, Noyes Publications: New York, 1992.

Plattner, J. J.; Martin Y. C.; Smital, J. R.; Lee, C-M.; Fung, A. K.; Horrom, B. W.; Crowley, S. R.; Pernet, A. G.; Bunnell, P. R.; Kim K. H. *J. Med. Chem.***1985**, *28*, 79.

Polymeric Materials Encyclopedia, CRC Press: New York, 1996; p 7171.

Reich, H. J.; Cram, D. J. *J. Am. Chem. Soc.* **1969**, *13*, 3505. Reich, H. J.; Cram, D. J. *J. Am. Chem. Soc.* **1969**, *91*, 3527.

Reich, H. J.; Cram, D. J. *J. Am. Chem. Soc.* **1969,** *91*, 3505.

Reich, H. J.; Cram, D. J. *J. Am. Chem. Soc.* **1969**, *91*, 3527.

Rivas, B. L.; Geckeler, K. E. *Adv. Polym. Sci.* **1992**, *102*, 171.

Rodgers, S. T.; Jensen, K. F. *J. Appl. Phys.* **1998**, *83*, 524.

Saegusa, T.; Yamada, A.; Taoda, H.; Kobayashi, S. *Macromolecules* **1978**, *11*, 435.

Schaverien, C.J.; Ernst, R.; Schut, P.; Skiff, W.M. *J. Am. Chem. Soc.* **1998**, *120*, 9945.

Schmidt, C.; Stümpflen, V.; Wendorff, J. H.; Hasenhindl, A.; Gronski, W.; Ishaque, M.; Grenier, A. *Acta Polymer.* **1998**, *49*, 232.

Senkevich, J. J.; Yang, G.-R.; Lu, T.-M. *Colloids and surfaces A* **2003**, *216*, 167.

Senkevich, J. J.; Yang, G.-R.; Lu, T.-M. *Colloids and surfaces A* **2003**, *214*, 119.

Shen, Z.; Simon, G. P.; Chen, Y.-B. *Polymer* **2002**, *43*, 4251.

Sochilin, V. A.; Pebalk, A. V.; Semenov, V. I.; Kardash, I. Ye. *Polymer Science* **1991**, *33*, 1426.

Steinhart, M.; Wendorff, J. H.; Grenier, A.; Wehrspohn, R. B.; Nielsch, K.; Schilling, J.; Choi, J.; Gösele, U. *Science* **2002**, *296*, 1997.

Strawhecker, K. E.; Manias, E. *Chem. Mater.* **2000**, *12*, 2943.

Surendran, G.; Gazicki, M.; James, W.J.; Yasuda, H. *J. Polym. Sci., Part A: Polym. Chem.* **1987**, *25*, 1481.

Szwarc, M. *Discuss. Faraday Soc.* **1947**, *2*, 46.

Tang, M. X.; Szoka, F. C. *Gene Therapy* **1997**, *4*, 823.

Teramoto, K. *Reactive Polymers* **1991**, *15*, 89.

Thompson, R. Q.; Mandoke, C. S.; Womack, J. P. *Anal. Lett.* **1985**, *18*, 93.

Tobiesen, F. A.; Michielsen, S. *J. Polym. Sci. A Polym. Chem.* **2002**, *40*, 719.

Tolstopyatov, E. M. *J. Phys. D. Appl. Phys.* **2002**, *35*, 1516.

Tuncel, D.; Steinke, J. H. G. *Macromolecules* **2004**, *37*, 288.

Tušek, L.; Nitschke, M.; Werner, C.; Stana-Kleinschek, K.; Ribitsch, V. *Colloid Surface A* **2001**, *196*, 81.

Vaeth, K. M.; Jensen, K. F. *Chem. Mater.* **2000**, *12*, 1305.

Vaia, R. A.; Vasudevan, S.; Krawiec, W.; Scanion, L. G.; Giannelis, E. P. *Adv. Mater.* **1995**, *7*, 154.

Wamser, C. C.; Gilbert, M. I. *Langmuir* **1992**, *8*, 1608.

Wang, J.; Ober, C. K. *Macromolecules* **1997**, *30*, 7560.

Wang, Y.; Kim, J.-H.; Choo, K.-H.; Lee, Y.-S.; Lee, C.-H. *J. Membr. Sci.* **2000**, *169*, 269.

Wang, Z.; Li, H. L. *Appl. Phys. A* **2002**, *74*, 201.

Wang, Z.; Su, Y.-K.; Li, H.-L. *Appl. Phys. A* **2002**, *74*, 563.

Waters, J. F.; Sutter, J. K.; Meador, M. A. B.; Baldwin, L. J.; Meador, M. A. *J. Polym. Sci. Polym. Chem.* **1991**, *29*, 1917.

Waters, J.F.; Sutter, J.K.; Meador, M.A.; Baldwin, L.J.; Meador, M.A. *J. Polym. Sci., Part A: Polym. Chem.* **1991**, *27*, 1917.

Wavhal, D. S.; Fisher, E. R. *Langmuir* **2003**, *19*, 79.

Weikart, C. M.; Miyama, M.; Yasuda, H. K. *J. Colloid Interface Sci.* **1999**, *211*, 18.

Williams, J. C. L. In *Nylon Plastics Handbook*; Kohan, M. I.; Ed.; Hansen Publishers: New York, NY, 1995.
Wu, C.-G.; Bein, T. *Science* **1994**, *266,* 1013.

Xiang, H.; Shin, K.; Kim, T.; Moon, S. I.; McCarthy, T. J.; Russell, T. P. *Macromolecules* **2004**, *37,* 5660.

Yu, Q.; Deffeyes, J.; Yasuda, H. *Prog. Org. Coatings* **2001**, *41*, 247.

Zammateo, N.; Girardeacex, C.; Delforge, D.; Pireaux, J.; Remacle, J. *Anal. Biochem.* **1996**, *236*, 85.

Zaugg, H. E.; Martin, W. B. Org. React. 1965, 14, 52. van Bommel, K. J. C.; Westerhof, F.; Verboom, W.; Reinhoudt, D. N. *J. Prakt. Chem.* **1999**, *341*, 284.

Zelikin, A. N.; Trukhanova, E. S.; Putnam, D.; Izumrudov, V. A.; Litmanovich, A. A. *J. Am. Chem. Soc.* **2003**, *125*, 13693.